INTERFACIAL PROPERTIES OF ASYMMETRICALLY FUNCTIONALIZED CITRATE-STABILIZED GOLD AND SILVER NANOPARTICLES RELATED TO MOLECULAR ADSORPTION

by

Jong-Won Park

A dissertation submitted to the faculty of
The University of Utah
in partial fulfillment of the requirements for the degree of

Doctor of Philosophy

Department of Chemistry

The University of Utah

May 2013

The University of Utah Graduate School

STATEMENT OF DISSERTATION APPROVAL

The dissertation of **Jong-Won Park**

has been approved by the following supervisory committee members:

Jennifer S. Shumaker-Parry	, Chair	**05/07/2012** Date Approved
Joel M. Harris	, Member	**05/07/2012** Date Approved
John C. Conboy	, Member	**05/07/2012** Date Approved
Michael D. Morse	, Member	**05/07/2012** Date Approved
Steve Blair	, Member	**05/07/2012** Date Approved

and by **Henry S. White**, Chair of the Department of **Chemistry**

and by Donna M. White, Interim Dean of The Graduate School.

ABSTRACT

A detailed understanding of the conformation of adsorbed molecules and regional surface functionalization of metal nanoparticles (MNPs) is challenging for nanometer-size (10 – 100 m) materials and necessary for fundamental studies and applications. The studies are motivated by open questions related to surface chemistry of noble MNPs. Although citrate-stabilized gold NPs (AuNPs) have been widely used, the citrate layer is not well-understood. Thiols have been suggested to displace citrate anions adsorbed on metal surfaces due to strong gold-sulfur interaction, but quantitative experimental evidence of the extent of ligand-exchange has not been reported. Whereas asymmetrically-functionalized AuNPs are utilized for nanoparticle assembly due to the interparticle coupling of localized surface plasmons, the interface between asymmetric nanoparticles in single assemblies has not been studied. Noble MNPs with sizes smaller than citrate-stabilized AuNPs also need to be surface-modified for stability in water for biological applications. The dissertation presents investigations of the chemical and physical properties of gold and silver NPs (AgNPs) related to ligand adsorption at the metal surface. Firstly, self-assembled layers of citrate adsorbed on AuNP (111), (110), and (100) surfaces were proposed, based on geometric considerations and spectroscopic investigations by infrared (IR) and X-ray photoelectron spectroscopy (XPS). Adsorption characteristics of citrate are the unique structure of adsorbed species, intermolecular interactions through hydrogen bonds and van der Waals attractions, bilayer formation,

surface coverage, nanoparticle-stabilization role, and chirality. Secondly, IR and XPS studies showed coadsorption of thiolate on the surface of citrate-stabilized AuNPs. Steric, chelating effects and intermolecular interactions are the origins of the strong adsorption of citrate on AuNP surfaces. Surface coverage was determined from XPS analyses. Thirdly, an exclusive placement of Raman probe molecules (4-nitrobenzenethiol) at junctions (hot-spots) of AuNP dimers was achieved through an asymmetric functionalization approach. The orientation of asymmetric nanoparticles in dimers and the location of Raman probes were investigated using surface-enhanced Raman scattering (SERS). A linear correlation of SERS signal with hot-spot population and a SERS enhancement factor are presented. Lastly, AuNPs and AgNPs of small sizes (< 5 nm) were synthesized in water using poly(allylamine). Ligand-exchange by thiols was demonstrated by IR spectroscopy and transmission electron microscopy analyses.

To my parents.

To my wife.

TABLE OF CONTENTS

LIST OF TABLES

LIST OF SYMBOLS

A	Absorbance or surface area
e	Electron
I	Intensity
pK_a	Acid dissociation constant
q	Particle charge
R	R enantiomer
S	S enantiomer

Greek Letters

δ	Bending vibration
ε	Extinction coefficient
η	Hapticity
λ_{max}	Wavelength at absorbance maximum
ν	Stretching vibration
σ	Standard deviation
χ	Fractional ratio

LIST OF ABBREVIATIONS

1-D	One-dimensional
2-D	Two-dimensional
AFM	Atomic force microscopy
AgNPs	Silver nanoparticles
AuNPs	Gold nanoparticles
alch	Alcohol
asy	Asymmetric
ATR	Attenuated total internal reflectance
BE	Binding energy
Citrate-AgNPs	Citrate-stabilized silver nanoparticles
Citrate-AuNPs	Citrate-stabilized gold nanoparticles
C_n	$(CH_2)_n$
COOH	Carboxylic acid group
COO^-	Carboxylate group
cts	Counts
D	Deuterium
DFT	Density functional theory
EG	Ethylene glycol
EM	Electromagnetic

fs	Femto-second
FT-IR	Fourier transform-Infrared
FWHM	Full width at half maximum
$H_2Citrate^-$	Dihydrogen citrate
LSPR	Localized surface plasmon resonance
LSPs	Localized surface plasmons
M	Metal
MEA	2-Mercaptoethylamine
MHA	16-Mercaptohexadecanoic acid
ML	Monolayer
MUOH	Mercapto-1-undecanol
N.A.	Numerical aperture
$Na_3Citrate$	Trisodium citrate
NBT	Nitrobenzenethiol
NMR	Nuclear magnetic resonance
NPs	Nanoparticles
PAAm	Poly(allylamine)
Ph	Phenyl
Py	Pyridine
R-SH	ω-terminated alkanethiol
SAMs	Self-assembled monolayers
SEIRA	Surface enhanced infrared absorption
SEM	Scanning electron microscopy

SERS	Surface enhanced Raman scattering
SQRT	Square root
STM	Scanning tunneling microscopy
sym	Symmetric
UV-Vis	UV-visible absorption spectroscopy
XPS	X-ray photoelectron spectroscopy
ZnSe	Zinc selenide

ACKNOWLEDGEMENTS

I would like to express my sincere gratitude to my advisor, Dr. Jennifer Shumaker-Parry, for not only the patient guidance and mentorship in the dissertation research but also the thoughtful consideration of another side of my graduate life, which she allowed for numerous times of travel past years for me to keep a long-distance relationship with my fiancée, now wife.

My deep appreciation is also to my committee members, Drs. Joel Harris, John Conboy, Michael Morse, and Steve Blair for thought-provoking questions, suggestions, comments, and careful proofreading of the original dissertation.

I thank my fellow Ph.D. students, Ai-Xiang Liu for some parts in the experiment in Chapter 4, Patrick Shem, Cindy Cooper, Cara Barnes, and Mark Swartz for valuable feedback, and former Ph.D. students, Rostislav Bukasov for help in IR measurements in the beginning, and Jianping Liu for comments. I also thank Rajesh Sardar, a former post-doctoral fellow, for providing experimental guidance in Chapter 5. I appreciate that Seung Hei Cho in Chemical Engineering handled the dissertation for me during the editing process while I have been staying in Boston.

I thank Nancy Chandler at the HSC Core Research Facilities for help in TEM, Randy Polson at the Physics Department for teaching me to operate the SEM, and Dr. Michael Granger at the Nano Institute for guide to using the SERS microscope. I greatly appreciate that Dr. Brian van Devener at Nanofab discussed XPS experiments with me.

CHAPTER 1

DISSERTATION INTRODUCTION

1.1 Citrate-stabilized gold nanoparticles

Citrate-stabilized gold nanoparticles (Citrate-AuNPs) have been used as nanomaterials for various studies and applications including nanoparticle assembly,[1] optical, photothermal[2] and electrochemical studies,[3] biological imaging,[4] sensing,[5] and medical[2,6-8] applications including drug delivery. Citrate is the conjugate base of citric acid (2-hydroxypropane-1,2,3-tricarboxylic acid), which reduces gold ions to atoms and stabilizes formed gold nanoparticles (AuNPs) during a solution-based synthesis (Figure 1.1). A size-controlled method of the citrate-AuNP synthesis was developed in the early 1970's, which is called the standard Turkevich-Frens method,[9,10] although AuNPs have been used since ancient times.[11] Through this method, citrate-stabilized AuNPs can be obtained with sizes between 10 - 100 nm diameter by adjustment of the ratio of the Au^{3+} and citrate concentrations used in the reaction. Oscillation of conduction electrons in the AuNPs, which is called a localized surface plasmon resonance (LSPR), produces a strong visible absorbance and scattering, and the size-dependent optical properties and assemblies of individual AuNPs are primary topics relating to manipulation of the LSPR behavior.

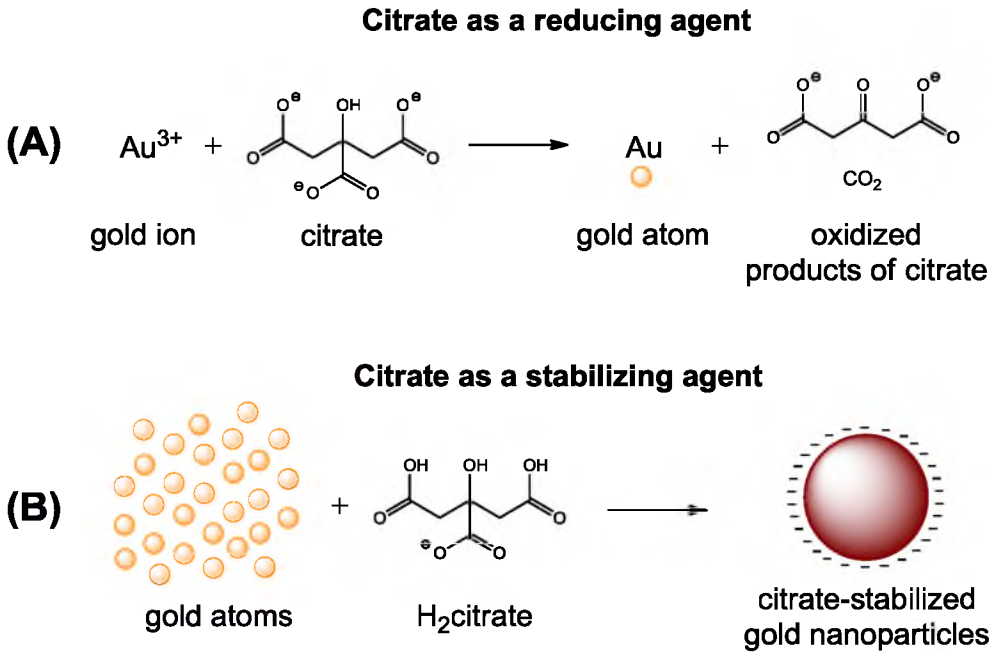

Figure 1.1. Roles of citrate during synthesis of gold nanoparticles (Turkevich-Frens method). (A) reducing agent; (B) stabilizing agent. Protonation depends on pH.

1.2 Citrate conformation on the AuNP surface

In contrast to the large number of investigations focused on utilizing citrate-AuNPs for various applications, the details of the conformation of citrate on the AuNP surface are still unknown. Figure 1.2A and B illustrate two examples of the coarse configurations of citrate layers on AuNPs in recently published articles. In these reports, a multilayer of surface citrate was proposed[12] (illustration A) and in the second article, a more general picture is presented without depicting the coordination of adsorbed citrate[13] (illustration B). Although the citrate structure generally has been neglected, understanding of the conformation of the adsorbed citrate layer can have a significant influence on answering questions related to a number of interfacial phenomena observed for citrate-AuNPs such as particle aggregation,[14] surface charge,[15] linker conjugation,[16] particle growth mechanism,[17] nanoparticle catalytic activity,[18] and ligand exchange reactions.[19] For

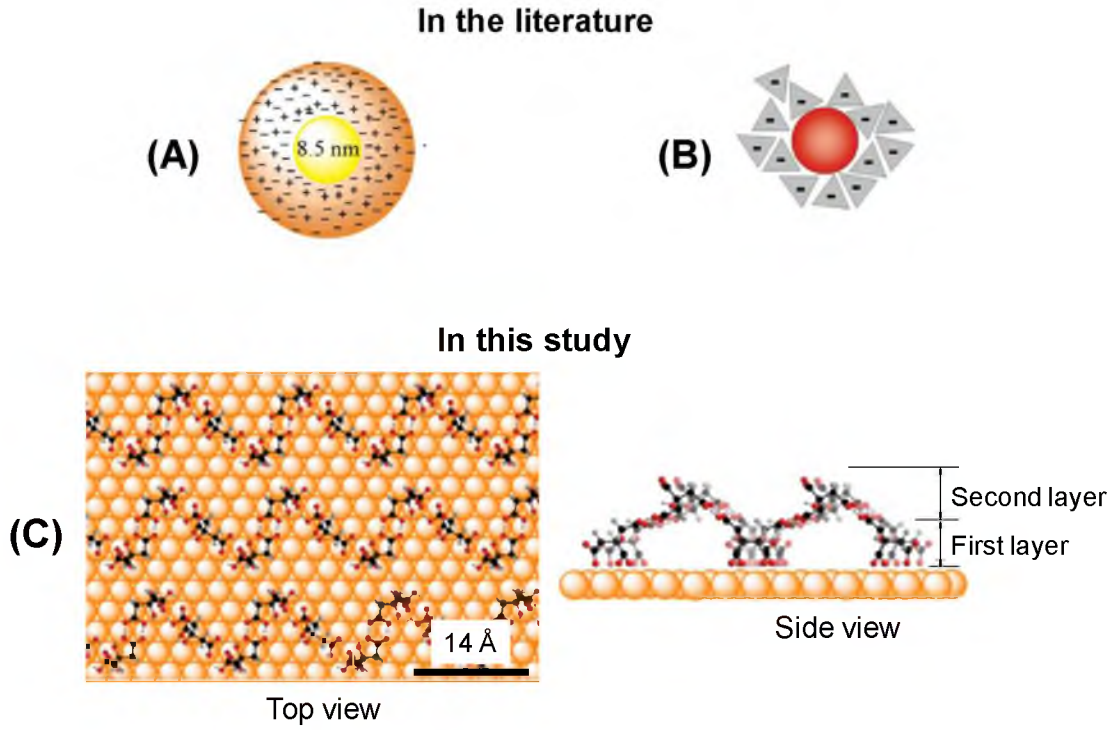

Figure 1.2. Comparison of understandings of citrate layers on citrate-AuNPs. (A, B) Examples of the coarse understanding found in the literature; (C) a molecular-level understanding proposed in this study, which shows a significant development of the understanding of the citrate layer on AuNP surfaces. In (A and B), yellow and red spheres are AuNPs, and surface citrates are represented as negative signs. In (C), surface gold atoms (orange spheres) on a gold (111) surface are depicted as a space-filling model whereas citrate molecules are shown as a ball-and-stick model. ((A): Reprinted with permission from Dahl, J. A.; Maddux, B. L. S.; Hutchison, J. E. *Chem. Rev.* **2007**, *107*, 2261, Figure 31. Copyright 2007 American Chemical Society, (B): Reprinted with permission from Ivanov, M.; Bednar, H. R.; Haes, A. J. *ACS Nano* **2009**, *3*, 388, Scheme 1. Copyright 2009 American Chemical Society)

instance, the entire citrate layer as stabilizer can be incorporated into mechanism studies of the particle formation. A detailed study of the coordination of carboxylate and hydroxyl groups of the adsorbed citrate on AuNP surfaces also can provide insights for the binding interactions of biomolecules[20] on metal surfaces, including amino acids and other small organic molecules[21] possessing carboxylic and/or hydroxyl functional groups. In this dissertation, citrate self-assembly on AuNP surfaces is proposed at a molecular

level including detailed intermolecular interactions of surface citrates (Figure 1.2C), which were studied by Fourier transform infrared spectroscopy (FTIR), X-ray photoelectron spectroscopy (XPS), and geometry-based modeling on the surfaces of AuNPs. The proposed pattern of the citrate organization is consistent with atomic-resolution transmission electron microscopy (TEM) images of the citrate bilayer on AuNPs[22] and published scanning tunneling microscopy (STM) images of an ordered citrate layer on a Au(111) surface.[23] This research is an example of a detailed study of organic layers on metal NPs, which is generally challenging to investigate due to the curvature and size of NPs.

Researchers have investigated citrate conformation on a planar gold surface, but the previously proposed structure is not accurate and needs to be modified. Nichols and co-workers proposed the coordination of all three carboxylate groups of adsorbed citrates on a gold (111) surface. Based on the citrate structure proposed by Nichols and co-workers (inset in Figure 1.3A), Bai and co-workers interpreted a citrate adsorption image from STM on a gold (111) surface,[23] but the interpreted molecular configuration displayed on the STM image is about twice as large as the actual one (Figure 1.3A). Moreover, the patterned STM image of citrate adsorption cannot be explained by the citrate structure proposed by Nichols and co-workers since there is no functional group of the adsorbed citrate available for lateral interaction on the surface. Atomic-resolution TEM analysis indicates a bilayer formation of surface citrate on AuNPs,[22] but interpretation of the citrate layer at a molecular level was not attempted due to the lack of information about citrate structure (Figure 1.3B). The previously proposed conformation of citrate on the planar gold (111) surface[24] can neither suggest intermolecular interaction[25] nor explain the long-range ordered assembly of citrate molecules revealed by the STM image[23] as

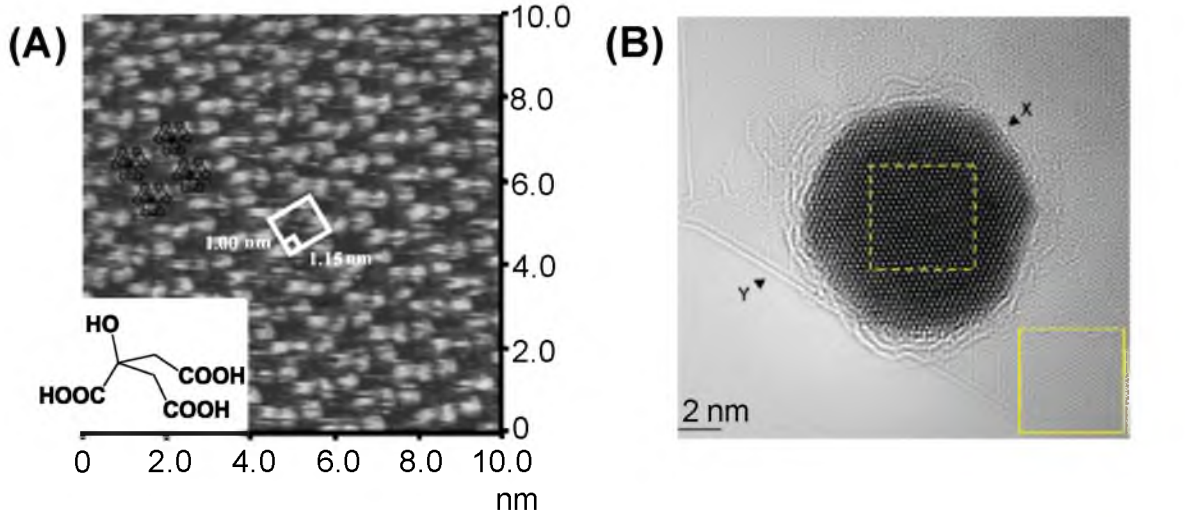

Figure 1.3. Two important images for this study relating to a citrate layer on gold surfaces. (A) A STM image of citrate adsorption on a gold (111) surface and (B) an atomic-resolution TEM image of citrate layers on citrate-AuNPs. In (A), white dots represent citrate molecules. In (B), white curved lines around the particle indicate citrate layers. (A: Reprinted with permission from Lin, Y.; Pan, G.-B.; Su, G.-J.; Fang, X.-H.; Wan, L.-J.; Bai, C.-L. *Langmuir* **2003**, *19*, 10002, Figure 2. Copyright 2003 American Chemical Society, B: Reprinted with permission from Lee, Z.; Jeon, K.-J.; Dato, A.; Erni, R.; Richardson, T. J.; Frenklach, M.; Radmilovic, V. *Nano Lett.* **2009**, *9*, 3367, Figure 3. Copyright 2009 American Chemical Society)

well as the formation of citrate layers.[22] Therefore, the previously proposed citrate conformation on the gold surface needs to be revised. The previous STM and TEM images of citrate layers on the gold surface were used to aid the analysis of the data from the study described in this dissertation (Figure 1.3).

1.3 Importance of the citrate conformation for citrate-to-thiol ligand exchange of citrate-AuNPs

Due to the important role of surface chemistry of AuNPs, it is often desirable to modify the surface functional groups to tailor the surface and chemical properties for specific applications. The most commonly used approach for surface modification is to

exchange the adsorbed ligands which are incorporated during the synthesis with another type of incoming ligand through a process called ligand exchange. Because thiols (R-SH) have a strong affinity for metals such as Au and Ag and form organized self-assembled monolayers (SAMs) on flat 2-D Au and Ag surfaces, ω-terminated thiols are often used for ligand exchange for the formation of robust ligand shells on metal NPs. One of the most common ligand exchange processes used is the replacement of citrates with functionalized thiols on AuNPs. The common perspective has been that adsorbed citrates are spontaneously replaced by incoming thiols,[26] but direct evidence for initially adsorbed citrate species to be desorbed from the surface of AuNPs has not been reported. Considering the abundant examples in the literature of assuming or relying on complete displacement of adsorbed citrate by thiols and the impact of residual citrates on surface coverage,[27] particle stability,[28] linker conjugation on NP surface,[5,16,29] particle-molecule interaction, [30] particle-ion interaction, [31] intracellular activity, [32, 33] and other biological/medical applications,[5,7,8,34] it is important to investigate the citrate-to-thiol ligand exchange.

Most experimental data indicate a decrease in the negatively-charged surface potential on AuNPs[19] or planar gold surfaces[35] after ligand exchange, but these data do not necessarily prove complete replacement of citrate. Other surface ions, rather than citrate molecules, may be replaced. It has been believed that the strong Au-S lattice interaction leads to the spontaneous displacement of citrates by thiols, but other factors in ligand exchange reactions on a metal surface including steric, chelating, solvent, and kinetic effects, need to be considered. Due to the spectroscopic indications of the adsorbed citrate species, direct spectroscopic evidence of the citrate desorption can be obtained. Adsorption of thiols[36] on the surface of citrate-AuNPs has been investigated,

which showed strong resistance of citrate to desorption by thiols. The ratio between the amount of surface citrates and coadsorbed thiols, which was determined by XPS analysis, is in good agreement with a calculated surface ratio based on the citrate model on a Au(111) surface.

1.4 Asymmetric functionalization of metal NPs for specific placement of molecules at assembly junctions

Assemblies of noble metal nanoparticles (NPs) give rise to localized electromagnetic (EM) field enhancements in NP junctions by coupling of localized surface plasmons (LSPs). This EM field enhanced region is often called a *hot spot*.[37,38] Due to the strong electric field enhancement at hot spots, NP assemblies including dimers, trimers, and 1-D chains have been utilized as plasmonic nanomaterials[39,40] especially for surface enhanced Raman scattering (SERS) applications.[41] Many SERS studies have been based on random NP aggregates which often result in irreproducible SERS responses from the uncontrollable distribution[42] and/or the minute population[43] of hot spots, which hamper systematic studies. In this regard, gold and silver NP dimers have been investigated as SERS platforms, due to the generation of enhanced SERS signals from molecules located in the junction hot spot.[44-48] A challenge of using NP assemblies in SERS studies is the rational attachment of Raman probe molecules at hot spot interfaces which are well-defined in terms of the gap spacing as well as the location and surface coverage of Raman probes. Probe placement is especially important in assemblies because of the strong influence of the local fields. Placing Raman probes in a well-defined position even in a single assembly[42] enables fundamental understanding as well as helps to develop a quantitative approach for SERS.

In order to understand the interface of the NP hot spot, it is desirable to utilize asymmetrically functionalized metal NPs as building blocks for formation of well-defined assembly junctions. Previously, Shumaker-Parry and co-workers demonstrated that the asymmetric AuNPs acted as building blocks for NP assemblies including dimers [49] and 1-D chains[1] (Figure 1.4). This approach allows for controlled functionalization in a spatially-localized region of individual NPs. The asymmetrically-functionalized NPs are assembled in solution through covalent bond formation [50] or attractive interactions between spatially localized ligands present on different particles. During the NP assembly process, target molecules are exclusively adsorbed in this NP region. In this study, positively charged ligands was used to stabilize NPs in solution while using hydroxyl ligands[51,52] to induce formation of AuNP dimers through hydrogen bonds and incorporating Raman-active molecules, 4-nitrobenzenethiol. Through the dimer formation by the asymmetric functionalization method Raman probes are directed to the junctions where field enhancements are expected leading to SERS from hot spots. In this dissertation, a SERS study of AuNP dimers is presented with Raman probe molecules directed to hot spots by the asymmetric functionalization approach. A linear

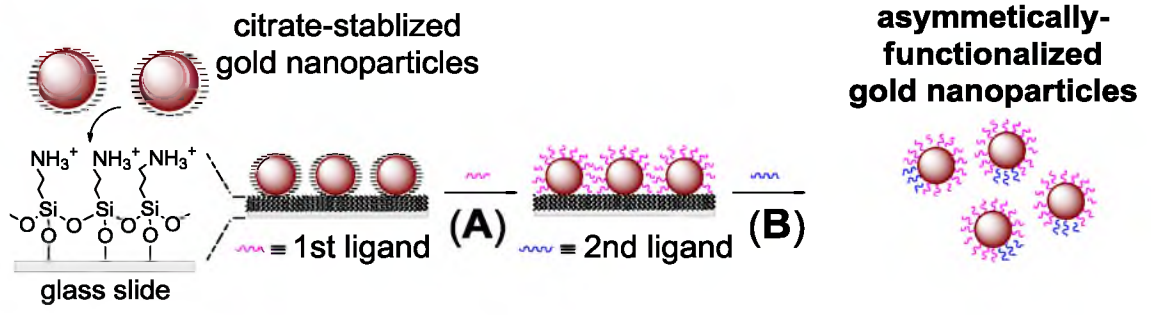

Figure 1.4. Asymmetric functionalization approach prior to formation of AuNP dimers. Using a silanized glass substrate to mask a region of the AuNP surface (Step A), asymmetrically functionalized AuNPs (Step B) are produced.

relationship between SERS intensities and dimer formation yields has been observed, which experimentally demonstrates the role of hot spots in generating SERS.

1.5 Synthesis of small AuNPs and silver nanoparticles using polymer*

Gold nanoparticles have received wide attention for application in photonics,[53,54] electronic and optical detection systems,[5,55] device development,[56] therapeutics,[57] and catalysis.[58] Due to the requirements for control of nanoparticle size and surface functionalization for this broad range of applications, different synthetic methods have been developed to generate monodisperse AuNPs. The Brust method[59] and various modifications[60] are useful for the generation of AuNPs having core sizes ranging from 1 to 4 nm. In the Brust method, the transfer of $AuCl_4^-$ into toluene or chloroform is performed using tetraalkylammonium bromide followed by reduction with sodium borohydride in the presence of alkylthiols. Disadvantages of this method include contamination of the synthesized particles with boride[61] and potential presence of impurities introduced by the use of capping ligands which also hinder the surface modification and functionalization of particles for particular applications. In addition, reduction of gold salt to form AuNPs using amine-containing organic molecules has been investigated,[62] but most of the amine compounds used in those AuNP syntheses are soluble only in organic solvents, and the reduction reactions must take place in an organic solvent or in a biphasic system. As a result, the nanoparticles prepared using those methods are not easily dispersed in aqueous solution. To use the AuNPs in aqueous-based or biological systems, it is necessary to functionalize the particles with ligands, which

*Reproduced in part from Sardar, R.; Park, J.-W.; Shumaker-Parry, J. S. *Langmuir* **2007**, *23*, 11883-11889. Copyright 2007 American Chemical Society

facilitate phase transfer from an organic to an aqueous medium.

Alternative synthetic strategies based on using polymers as both the reducing and stabilizing agent for the generation of stable metal nanoparticles without the use of an additional stabilizing agent have been developed. Some polymers can fulfill the required dual role as a reducer and stabilizer, which examples include poly(N-vinyl-2-pyrrolidone),[63] poly(ethylene oxide),[64] and poly(vinyl alcohols).[65] However, even in the syntheses using those polymers, either the reduction reaction was carried out in organic solvents or produced polydisperse nanoparticles. The major advantage of using a polymer as a stabilizing agent is that it can be used to tailor the nanocomposite properties and also to provide long-tem stability of the nanoparticles by preventing particle agglomeration.[66] Although monodisperse particles may be synthesized using a thiolated polymer,[67] the surface modification of those nanoparticles by nonthiolated ligands would be difficult due to the strong sulfur-gold interaction and complete displacement by even thiolated ligands would be difficult to achieve. On the other hand, an amine group has a weak interaction with metal nanoparticles and can be easily replaced by a thiolated ligand.[68]

In this context, a suitable synthetic approach is desirable where the nanoparticles could be stabilized by polymer-containing amine functional groups which can undergo ligand exchange with a variety of thiolated ligands for specific nanoparticle applications. Although poly(allylamine) (PAAm) was previously studied for its stabilizing ability,[69] the polymer's dual character both as reducing and stabilizing agent for the generation of stable metal nanoparticles has not been reported yet. A simple, inexpensive, single-step synthesis of gold nanoparticles was investigated with PAAm used both as a reducing and a stabilizing agent (Figure 1.5). The synthetic method and ligand exchange are applied to

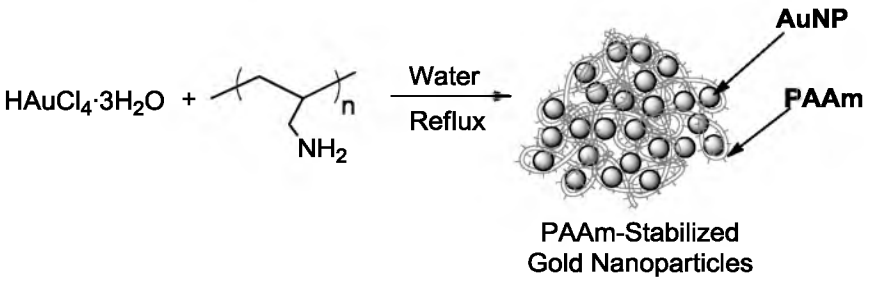

Figure 1.5. PAAm-induced synthesis and stabilization of gold nanoparticles in water (Reprinted with permission from Sardar, R.; Park, J.-W.; Shumaker-Parry, J. S. *Langmuir* **2007**, *23*, 11885, Scheme 1. Copyright 2007 American Chemical Society)

generate AuNPs and silver nanoparticles (AgNPs) in aqueous solution

1.6 Main goal of the dissertation research

The main goals of the dissertation research were 1) investigation of the conformation of citrate layers on citrate-AuNPs, 2) study of citrate-to-thiol ligand exchange for citrate-AuNPs, 3) specific placement of Raman probe molecules at the junction of AuNP dimers for hot-spot-based SERS studies, and 4) development of a new synthetic method of AuNPs and AgNPs using polymers in water and subsequent ligand exchange reactions.

Firstly, the coordination of adsorbed citrate has been characterized by using attenuated total reflectance infrared spectroscopy (ATR-IR) and XPS. After a specific configuration of the adsorbed citrate was determined, intermolecular interactions between surface citrates were identified, and a geometry-based model was used to propose self-assembled layers of citrate adsorbed on (111), (110), and (100) surfaces of AuNPs. These results are expected to provide insights about various interfacial phenomena of citrate-AuNPs, including a NP shape-formation mechanism as well as interparticle interactions between individual NPs. Secondly, with aid of spectroscopic evidence of the adsorbed

citrate on AuNPs, the desorption of citrate by incoming thiols was investigated, and the origins of the strong resistance of the adsorbed citrate to desorption were suggested. The resultant low surface coverage of thiols and remaining carboxylate/hydroxyl functional groups on the metal surface will impact the popular approach for modifying the metal NP surface by thiols. Thirdly, the asymmetric functionalization approach was used to place Raman probes exclusively at the hot spots of AuNP dimers, and a relationship of the SERS intensities with the hot-spot populations has been elucidated. This approach can be used as a protocol for systematic SERS studies on NP assembly. Lastly, a new synthetic method for poly(allyl)amine-coated AuNPs and AgNPs has been developed. Facile ligand exchange reactions by various ω-terminated alkanethiols were demonstrated.

1.7 Outline of the dissertation

Chapter 2 presents an investigation of the conformation of surface citrates on AuNPs using ATR-IR, XPS, and geometry-based modeling on AuNP surfaces. A specific conformation of adsorbed citrate is proposed. The geometrical modeling and the spectroscopy data are used to consider lateral and vertical interactions of adsorbed citrates on AuNP (111), (110), and (100) surfaces. Intermolecular/interlayer spacing of the adsorbed citrates, driving forces for citrate self-assembly, citrate bilayer formation, chirality of the self-assembled layer of citrate, surface coverage, NP-stabilizing role, as well as similar citrate adsorption on AgNPs and other metal NPs are discussed.

Chapter 3 describes ligand-exchange reactions of citrate-stabilized AuNPs by thiols. From the IR and XPS spectroscopic characteristics of the adsorbed citrate, residual citrate molecules adsorbed on AuNPs are probed after addition of thiol to the solution of AuNPs. Coadsorption of incoming thiols on citrate-AuNPs, rather than a facile ligand exchange,

is demonstrated regardless of NP aggregation that is generally induced due to a decrease in electrostatic repulsion. Surface coverage between thiol and citrate molecules is quantitatively determined using XPS analysis. The strong resistance of surface citrate to desorption is explained by steric and chelating effects as well as intermolecular interactions.

Chapter 4 describes a method of a specific placement of Raman probe molecules in the junctions (hot-spots) of AuNP dimers, characterized by Raman scattering spectroscopy. An asymmetric functionalization approach is used to direct Raman probes to a small region of the AuNP surface. It is shown that the asymmetric NPs are aligned in the dimers generating large SERS signals. Relationship between Raman intensities and hot-spot populations are proposed. Correlation of the Raman intensities with change of interparticle spacing and a SERS enhancement factor are presented.

Chapter 5 presents an investigation of a new simple method of synthesis of AuNPs and AgNPs using poly(allylamine) in water. It is demonstrated that the polymer acts as both reducing and stabilizing agents, and ligand exchange of the polymer by incoming thiols is discussed with IR and TEM analyses.

1.8 References

(1) Sardar, R.; Shumaker-Parry, J. S. *Nano Lett.* **2008**, *8*, 731-736.

(2) Jain, P. K.; Huang, X.; El-Sayed, I. H.; El-Sayed, M. A. *Acc. Chem. Res.* **2008**, *41*, 1578-1586.

(3) Brust, M.; Gordillo, G. J. *J. Am. Chem. Soc.* **2012**, *134*, 3318-3321.

(4) El-Sayed, I. H.; Huang, X.; El-Sayed, M. A. *Nano Lett.* **2005**, *5*, 829-834.

(5) Katz, E.; Willner, I. *Angew. Chem., Int. Ed.* **2004**, *43*, 6042-6108.

(6) Jain, P. K.; El-Sayed, I. H.; El-Sayed, M. A. *Nano Today* **2007**, *2*, 18-29.

(7) El-Sayed, I. H.; Huang, X.; El-Sayed, M. A. *Cancer Lett.* **2006**, *128*, 2115-2120.

(8) Grainger, D. W.; Castner, D. G. *Adv. Mater.* **2008**, *20*, 867-877.

(9) Turkevich, J.; Stevenson, P. C.; Hillier, J. *Discuss. Faraday Soc.* **1951**, 55-75.

(10) Frens, G. *Nature Phys. Sci.* **1973**, *241*, 20-22.

(11) Freestone, I.; Meeks, N.; Sax, M.; Higgitt, C. *Gold Bulletin* **2007**, *40*, 270-277.

(12) Dahl, J. A.; Maddux, B. L. S.; Hutchison, J. E. *Chem. Rev.* **2007**, *107*, 2228-2269.

(13) Ivanov, M.; Bednar, H. R.; Haes, A. J. *ACS Nano*, **2009**, *3*, 386-394.

(14) Storhoff, J. J.; Elghanian, R.; Mirkin, C. A.; Letsinger, R. L. *Langmuir* **2002**, *18*, 6666-6670.

(15) Kunze, J.; Burgess, I.; Nichols, R.; Buess-Herman, C.; Lipkowski, J. *J. Electroanal. Chem.* **2007**, *599*, 147-159.

(16) Choi, Y.; Park, Y.; Kang, T.; Lee, L. P. *Nat. Nanotechnol.* **2009**, *4*, 742-746.

(17) Polte, J.; Ahner, T. T.; Delissen, F.; Sokolov, S.; Emmerling, F.; Thünemann, A. F.; Kraehnert, R. *J. Am. Chem. Soc.* **2010**, *132*, 1296-1301.

(18) Xu, W.; Kong, J. S.; Yeh, Y.-T.; Chen, P. *Nat. Mater.* **2008**, *7*, 992-996.

(19) Weisbecker, C. S.; Merritt, M. V.; Whitesides, G. M. *Langmuir* **1996**, *12*, 3763-3772.

(20) Forster, M.; Dyer, M. S.; Persson, M.; Raval, R. *J. Am. Chem. Soc.* **2009**, *131*, 10173-10181.

(21) Tomba, G.; Ciacchi, L. C.; De Vita, A. *Adv. Mater.* **2009**, *21*, 1055-1066.

(22) Lee, Z.; Jeon, K.-J.; Dato, A.; Erni, R.; Richardson, T. J.; Frenklach, M.; Radmilovic, V. *Nano Lett.* **2009**, *9*, 3365-3369.

(23) Lin, Y.; Pan, G.-B.; Su, G.-J.; Fang, X.-H.; Wan, L.-J.; Bai, C.-L. *Langmuir* **2003**, *19*, 10000-10003.

(24) Nichols, R. J.; Burgess, I.; Young, K. L.; Zamlynny, V.; Lipkowski, J. *J. Electroanal. Chem.* **2004**, *563*, 33-39.

(25) Teobaldi, G.; Zerbetto, F. *J. Phys. Chem. C* **2007**, *111*, 13879-13885.

(26) Weitz, D. A.; Oliveria, M. *Phys. Rev. Lett.* **1984**, *52*, 1433-1436.

(27) Hill, H. D.; Millstone, J. E.; Banholzer, M. J.; Mirkin, C. A. *ACS Nano*, **2009**, *3*, 418-424.

(28) Zhang, S.; Leem, G.; Srisombat, L.-O.; Lee, T. R. *J. Am. Chem. Soc.* **2008**, *130*, 113-120.

(29) Yang, J.; Lee, J. Y.; Ying, J. Y. *Chem. Soc. Rev.* **2011**, *40*, 1672-1696.

(30) Gourishankar, A.; Shukla, S.; Ganesh, K. N.; Sastry, M. *J. Am. Chem. Soc.* **2004**, *126*, 13186-13187.

(31) Yu, C.-J.; Tseng, W.-L. *Langmuir* **2008**, *24*, 12717-12722.

(32) Mahmoudi, M.; Azadmanesh, K.; Shokrgozar, M. A.; Journeay, W. S.; Laurent, S. *Chem. Rev.* **2011**, *111*, 3407-3432.

(33) Glusker, J. P. *Acc. Chem. Res.* **1980**, *13*, 345-352.

(34) Graham, D.; Faulds, K. *Chem. Soc. Rev.* **2008**, *37*, 1042-1051.

(35) Dagastine, R. R.; Grieser, F. *Langmuir* **2004**, *20*, 6742-6747.

(36) Love, J. C.; Estroff, L. A.; Kriebel, J. K.; Nuzzo, R. G.; Whitesides, G. M. *Chem. Rev.* **2005**, *105*, 1103-1169.

(37) Stockman, M. I.; Pandey, L. N.; George, T. F. *Phys. Rev. B* **1996**, *53*, 2183-2186.

(38) Aravind, P. K.; Nitzan, A.; Metiu, H. *Surf. Sci.* **1981**, *110*, 189-195.

(39) Halas, N. J.; Lal, S.; Chang, W.-S.; Link, S.; Nordlander, P. *Chem. Rev.* **2011**, *111*, 3913-3961.

(40) Jones, M. R.; Osberg, K. D.; Macfarlane, R. J.; Langille, M. R.; Mirkin, C. A. *Chem. Rev.* **2011**, *111*, 3736-3827.

(41) Otto, A. *J. Raman Spectrosc.* **2006**, *37*, 937-947.

(42) Camargo, P. H. C.; Rycenga, M.; Au, L.; Xia, Y. *Angew. Chem., Int. Ed.* **2009**, *48*, 2180-2184.

(43) Camden, J. P.; Dieringer, J. A.; Wang, Y.; Masiello, D. J.; Marks, L. D.; Schatz, G. C.; Van Duyne, R. P. *J. Am. Chem. Soc.* **2008**, *130*, 12616-12617.

(44) Wustholz, K. L.; Henry, A.-I.; McMahon, J. M.; Freeman, R. G.; Valley, N.; Piotti, M. E.; Natan, M. J.; Schatz, G. C.; Van Duyne, R. P. *J. Am. Chem. Soc.* **2010**, *132*, 10903-10910.

(45) Li, W.; Camargo, P. H. C.; Lu, X.; Xia, Y. *Nano Lett.* **2009**, *9*, 485-490.

(46) Chen, G.; Wang, Y.; Yang, M.; Xu, J.; Goh, S. J.; Pan, M.; Chen, H. *J. Am. Chem. Soc.* **2010**, *132*, 3644-3645.

(47) Talley, C. E.; Jackson, J. B.; Oubre, C.; Grady, N. K.; Hollars, C. W.; Lane, S. M. Huser, T. R.; Nordlander, P.; Halas, N. J. *Nano Lett.* **2005**, *5*, 1569-1574.

(48) Ringler, M.; Klar, T. A.; Schwemer, A.; Susha, A. S.; Stehr, J.; Raschke, G.; Funk, S.; Borowski, M.; Nichtl, A.; Kürzinger, K.; Phillips, R. T.; Feldmann, J. *Nano Lett.* **2007**, *7*, 2753-2757.

(49) Sardar, R.; Heap, T. B.; Shumaker-Parry, J. S. *J. Am. Chem. Soc.* **2007**, *129*, 5356-5357.

(50) Hofmann, A.; Schmiel, P.; Stein, B.; Graf, C. *Langmuir* **2011**, *27*, 15165-15175.

(51) Li, M.; Johnson, S.; Guo, H.; Dujardin, E.; Mann, S. *Adv. Funct. Mater.* **2011**, *21*, 851-859.

(52) Matsunaga, M.; Aizenberg, M.; Aizenberg, J. *J. Am. Chem. Soc.* **2011**, *133*, 5545-5553.

(53) Burda, C.; Chen, X.; Narayan, R.; El-Sayed, M. A. *Chem. Rev.* **2005**, *105*, 1025-1102.

(54) Thomas, K. G.; Kamat, P. V. *Acc. Chem. Res.* **2003**, *36*, 888-898.

(55) Taton, T. A.; Mirkin, C. A.; Letsinger, R. L. *Science* **2000**, *289*, 1757-1760.

(56) Feldheim, D. L.; Keating, C. D. *Chem. Soc. Rev.* **1998**, *27*, 1-12.

(57) Jain, P. K.; Lee, K. S.; El-Sayed, I. H.; El-Sayed, M. A. *J. Phys. Chem. B* **2006**, *110*, 7238-7248.

(58) Enache, D. I.; Edwards, J. K.; Landon, P.; Solsona-Espriu, B.; Carley, A. F.; Herzing, A. A.; Watanabe, M.; Kiely, C. J.; Knight, D. W.; Hutchings, G. J. *Science* **2006**, *311*, 362-365.

(59) Brust, M.; Walker , M.; Bethell, D.; Schiffrin, D. J.; Whyman, R. *J. Chem. Soc., Chem. Commun.* **1994**, 801-802.

(60) Collier, C. P.; Saykally, R. J.; Shiang, J. J.; Henrichs, S. E.; Heath, J. R. *Science* **1997**, *277*, 1978-1981.

(61) Bonnemann, H.; Brijoux, W.; Brinkmann, R.; Fretzen, R.; Joussen, T.; Koppler, R.; Korall, B. K.; Neiteler, P.; Richter, J. *J. Mol. Catal.* **1994**, *86*, 129-177.

(62) Kumar, P. S.; More, A. S.; Shingte, R. D.; Wadgaonkar, P. P.; Sastry, M. *Adv. Mater.* **2004**, *16*, 966-971.

(63) Hoppe, C. E.; Lazzari, M.; Pardines-Blanco, I.; Lopez-Quintela, M. A. *Langmuir* **2006**, *22*, 7027- 7034.

(64) Sakai, T.; Alexandridis, P. *J. Phys. Chem. B* **2005**, *109*, 7766-7777.

(65) Longenberger, L.; Mills, G. *J. Phys. Chem.* **1995**, *99*, 475-478.

(66) Balaza, A. C.; Emrick, T.; Russell, T. P. *Science* **2006**, *314*, 1107-1110.

(67) Wuelfing, W. P.; Gross, S. M.; Miles, D. T.; Murray, R. W. *J. Am. Chem. Soc.* **1998**, *120*, 12696-12697.

(68) Hiramatsu, H.; Osterloh, F. E. *Chem. Mater.* **2004**, *16*, 2509-2511.

(69) (a) Lee, J.; Yang, B.; Li, R.; Seery, T. A. P.; Papadimitrakopoulos, F. *J. Phys. Chem. B* **2007**, *111*, 81-87. (b) El-Khoury, J. M.; Caruntu, D.; O'Connor, C. J.; Jeong, K.U.; Cheng, S. Z. D.; Hu, J. *J. Nanopart. Res.* **2007**, *9*, 959-964. (c) Hong, Y.; Sen, A. *Chem. Mater.* **2007**, *19*, 961-963.

CHAPTER 2

CONFORMATION OF CITRATE MOLECULES ADSORBED ON GOLD NANOPARTICLES

2.1 Introduction

One of the most common synthetic methods for preparation of gold nanoparticles (AuNPs) is based on citrate reduction and stabilization. Citrate typically serves a dual role in the variations developed based on the standard Turkevich-Frens method.[1-4] Citrate-stabilized AuNPs (citrate-AuNPs between 10 - 100 nm diameter) can be obtained by adjustment of the ratio of the Au^{3+} and citrate concentration used in the reaction. The importance of controlling the nanoparticle size is related to the dependence of the optical properties of citrate-AuNPs on the size of the nanoparticle core.[5,6] The outer surface of the citrate-capped AuNPs is composed of citrate coordinating to the Au NP surface atoms by inner-sphere complexation of the carboxylate groups of the citrate as well as trace amounts of $AuCl_4^-$, Cl^-, and OH^- on the metal surface.[7,8] Citrate-AuNPs are commonly employed as the materials for a wide range of metal nanoparticle based studies and applications including nanoparticle assembly,[9,10] optical,[11] photothermal[12] and electrochemical studies,[13] biological imaging,[14] sensing,[15,16] and medical[13,17,18] applications including drug delivery.

In contrast to the large number of investigations focused on utilizing citrate-AuNPs

for various applications, the details of the conformation of citrate on the AuNP surface are still unknown due to the challenges[19] of studying the buried metal/organic interfaces at a molecular level. Although the citrate structure has been generally neglected, understanding of the conformation of the adsorbed citrate layer can have a significant influence on answering puzzling questions related to a number of interfacial phenomena observed for citrate-AuNPs such as particle aggregation,[20-22] surface charge,[23-25] linker conjugation,[15,21,22,26-31] particle growth mechanism,[32-39] nanoparticle catalytic activity,[40-42] and ligand exchange reactions.[43-46] A detailed study of the coordination of carboxylate and hydroxyl groups of the adsorbed citrate on AuNP surfaces also can provide insights for the binding structures of biomolecules[47-55]on metal surfaces, including amino acids and other small organic molecules[56-63] possessing carboxylic and/or hydroxyl functional groups.

Despite the importance of the citrate structure and coordination, there have been only a few studies of the conformation of citrate on a planar gold surface, and the conformation on AuNPs is still in question. Nichols and co-workers proposed the tridentate coordinations of all three carboxylate groups of adsorbed citrates on a gold (111) surface by using in-situ subtractively normalized interfacial Fourier transform infrared spectroscopy (SNIFTIR).[64, 65] Observation of one type of carboxylate coordination, which is through two oxygen atoms (η^2-COO^-), led to a proposed citrate conformation, but the IR spectra exhibit an indication of other types of carboxylate coordinations, e.g., η^1-COO^-. Based on the citrate structure proposed by Nichols and co-workers, Bai and co-workers interpreted scanning tunneling microscopy (STM) images on citrate adsorbed on a gold (111) surface.[66] However, after analyzing the data from both investigations, a discrepancy in lengths exists. The interpreted lateral length of the

citrate molecular configuration determined by STM was about 10 Å, which is not an acceptable molecular size for the tridentate citrate. Moreover, the pattern in the STM image of citrate adsorption cannot be interpreted using the isolated citrate configuration as a building block since possible moieties, i.e., $-CH_2-$ and -OH, of the adsorbed citrate for intermolecular interactions point outward from the surface, and thus there is no moiety available for lateral interaction on the surface. Teobaldi and Zerbetto pointed out that the carboxylate-Au interaction is not the driving force for the adsorption of citrate, which was studied by computer simulation using the same conformation of citrate on a flat gold (111), and they suggested that intermolecular interaction plays a role in formation of the citrate layers.[63] As a result, the previously proposed conformation of citrate on a planar gold (111) surface[64] can neither suggest intermolecular interaction[63] as a necessary force for adsorption nor explain the long-range ordered citrate adsorption revealed in the STM image.[66] Consequently more investigations are needed to obtain a detailed understanding of the conformation of adsorbed citrate on a gold surface.

One aspect to be considered for the study of the conformation of adsorbed citrate is coordination of the alcoholic hydroxyl group and protonation of carboxylate groups. Although a hydroxyl group of adsorbed hydroxycarboxylate on metal surfaces is often neglected in the investigation of the adsorbed molecules, coordination of the hydroxyl group of citrate on the metal surface needs to be considered.[67,68] The α-hydroxyl group of citrate and other hydroxydicarboxylates[69-71] are well-known for five-membered chelating coordination to metal atoms,[72] and alkoxide species adsorbed on a metal surface have been reported in the literature.[73-84] While computational simulations for citrate and citric acid[85] have been carried out to investigate optimized citrate conformations on metal surfaces, most of the calculations do not include the possibility of binding of the hydroxyl

group as well as the degree of protonation of citrate[63,86-88] although di- and tri-hydrogen species of citrate are the most populated in solution (pH ~3.2) after AuNP synthesis.

In this chapter, a study of the orientation of surface-adsorbed citrates on AuNPs is presented by using attenuated total reflectance infrared spectroscopy (ATR-IR) and X-ray photoelectron spectroscopy (XPS) combined with geometry-based modeling on AuNP surfaces. Studies in this research reveal that a specific conformation of adsorbed citrate is dominant.[89] The adsorbed citrate coordinates to the Au surface by bidentate binding through the central carboxylate and one terminal carboxylate. This conformation of individually adsorbed citrate species is similar to what Smith and co-workers proposed for silver nanoparticles (AgNPs), which was studied by surface-enhanced Raman spectroscopy (SERS).[90] More importantly, a model was developed to explain the presented data and intermolecular interactions. Based on this, a citrate trimer, consisting of two adsorbed species interacting with a dangling species through hydrogen bonds of carboxyl groups, is proposed as a building block on AuNP (111), (110), and (100) surfaces. The configuration of the citrate trimer is consistent with spacing of citrate layers on AuNPs[91] obtained on a graphene sheet by atomic-resolution imaging using transmission electron microscopy (TEM) and published STM images of an ordered citrate layer on a Au(111) surface,[66] which suggest formation of a citrate bilayer, rather than a monolayer or multilayers. More detailed analyses of the intermolecular interactions between the citrate trimers lead to the suggestion that polymeric citrate chains are assembled on AuNP surfaces. Detailed features of citrate self-assembly on AuNPs are discussed, including the intermolecular/interlayer spacing of citrate molecules, the driving forces for the citrate self-assembly, the surface coverage of citrate, and the chirality of adsorbed citrate as well as possible citrate self-assembly on AgNPs. This

detailed conformational study of organic layers on large metal NPs is unprecedented. A detailed description of citrate conformation on AuNPs may offer an important perspective for research involving various interfacial phenomena on citrate-AuNPs.

2.2 Experiments

2.2.1 Materials

All chemicals are of reagent grade and used without further purification unless otherwise stated. Tetrachloroaurate ($HAuCl_4 \cdot 3H_2O$), trisodium citrate ($Na_3C_6H_5O_7 \cdot 2H_2O$), sodium deuteroxide (NaOD, 30 wt% solution in D_2O), ethanol-d (CH_3CH_2OD, EtOD), ethanol-d_6 (CD_3CD_2OD, EtOD-d_6, 99 atom % D), 4-mercaptobenzoic acid (90%), 1-dodecanethiol (98%), and 1-butanethiol (99%), 1,3-propanedithiol (99%), 1,4-butanedithiol (97%), 1,5-pentanedithiol (96%), and 1,6-hexanedithiol (96%) were purchased from Sigma-Aldrich. 1,9-nonanedithiol (99%) and 1,11-undecanedithiol (99%) were purchased from Asemblon. Ethanol (EtOH, 200 proof, Pharmco-Aaper or Decon Labs), sodium hydroxide (NaOH, Mallinckrodt Chemicals), deuterium oxide (D_2O, Cambridge Isotope Labs), lead perchlorate ($Pb(ClO_4)_2 \cdot 3H_2O$, GFS Chemicals were obtained from aforementioned companies. Water was used after purification (Barnstead Nanopure Diamond UV-UF, 17.8 MΩ/cm). All glassware was washed with aqua-regia (3:1, HCl/HNO_3) to remove gold particles and organic contaminants, and glassware contaminated heavily with organic materials and silicon wafers (Silicon Inc.) were cleaned with piranha solution (5:1, H_2SO_4/30% H_2O_2). *Caution! The piranha solution and the aqua-regia solution are highly corrosive and mixing the solution is very exothermic. It should be handled with extreme care and appropriate safety precautions*. The aqua-regia or piranha treated glassware was rinsed

thoroughly with water and dried in an oven at 120 ^{o}C at for 2 h.

2.2.2 Citrate-AuNP synthesis

AuNPs were synthesized by the Frens method.[2] Briefly, $HAuCl_4 \cdot 3H_2O$ (0.0232 g) was dissolved in water (200 mL), and the gold ion solution was refluxed. $Na_3Citrate \cdot 2H_2O$ (0.0227 g) was dissolved in water (1 mL) and added to the boiling gold ion solution all at once with vigorous stirring. Heating continued for an additional hour, and the resulting AuNP solution was allowed to slowly cool to room temperature with continuous stirring. The average AuNP size was 39 nm in diameter with a ~25% deviation. The AuNP solution exhibits a localized surface plasmon resonance peak maximum (λ_{max}) at 535 nm.

2.2.3 Purification of citrate-AuNPs

AuNPs were purified using a centrifugation method. Typically, 10 mL of citrate-AuNP solution was centrifuged at 4000 rpm, and the supernatant solution was discarded. The concentrated AuNPs were sonicated to redisperse the particles in 5 mL of water that was adjusted to pH ~10. This is to reduce formation of citrate layers due to hydrogen bonding between adsorbed citrates and free citrates in solution. At this pH, the carboxylic acid groups are deprotonated, interrupting hydrogen bonding in citrate layers and reducing loss of AuNPs by irreversible aggregation during centrifugation. The centrifugation and dispersion steps were repeated three times. For a fourth purification step, water adjusted to pH 9 was used due to incompatibility of the ZnSe crystal used for IR measurements with solutions with pH > 9. When the citrate-AuNPs were purified with $NaOD/D_2O$, the same procedures and conditions were applied. The spectrum of pure

trisodium citrate was obtained by dissolving solid trisodium citrate in trace amounts of water and drying the resultant solution on a ZnSe crystal.

2.2.4 Addition of lead ions in a solution of purified citrate-AuNPs

A solution of 4.5 μL of 7.6 mM $Pb(ClO_4)_2$ solution was added to an aliquot of purified citrate-AuNPs (< 20 μL) on the ZnSe crystal, and the AuNPs aggregated immediately as observed by film formation on the crystal surface. The ATR-IR spectra were collected after the solution evaporated.

2.2.5 Alkanethiol adsorption on citrate-AuNPs

To preserve the original citrate layers during purification of AuNPs, adsorption of alkanethiols was utilized. The thiol layer prevents AuNPs from aggregating irreversibly under centrifugation. Ten mL of citrate-AuNP solution were centrifuged, and the concentrated AuNP solution (< 100 μL) was added to 10 mL of 1 mM 11-undecanethiol solution in ethanol. After 2 h the functionalized AuNPs were purified by the centrifugation and dispersion method with ethanol three times. For the partial functionalization of AuNPs by thiols, the stoichiometric amounts of thiols were calculated based on the surface area of a 35-nm AuNP (3.85×10^{-11} cm^2), an estimated surface coverage of alkanethiols (4.8×10^{14} molecules/cm^2),[92] the measured absorbance (A = 1.33), and the molar absorptivity coefficient for 34.5-nm citrate-AuNPs[93] ($\varepsilon = 6.1 \times 10^9$ $M^{-1}cm^{-1}$). For example, 50 μL of 0.38 mM 1-dodecanethiol solution in ethanol was added to 10 mL of redispersed citrate-AuNPs in ethanol, obtained after a single centrifugation of 10 mL of as-prepared citrate-AuNP solution. For the functionalization of AuNPs by dithiols, the concentrated citrate-AuNP solution (10 mL to < 100 μL) was

added to 10 mL of 1 mM dithiol solution.

2.2.6 UV-Vis absorption spectroscopy

Absorbance spectra of citrate-AuNP solution were collected for a spectral range of 400 - 800 nm using a PerkinElmer Lambda 19 UV/vis/NIR spectrophotometer.

2.2.7 ATR-FTIR spectroscopy

A MIRacle ATR (ZnSe crystal, PIKE Technologies) was used with a PerkinElmer spectrum 100 FT-IR (Fourier transform-infrared) spectrometer. An aliquot of centrifuged AuNP solution was transferred to the crystal surface and dried with nitrogen gas. Spectra were collected at 4000 - 550 cm^{-1}. Four consecutive scans were done for most measurements, but only one scan was done when monitoring spectral changes of citrate-AuNPs with the degree of drying.

2.2.8 Transmission FTIR spectroscopy

Transmission mode was used to obtain FTIR spectra at a high pH due to the incompatibility of the ZnSe ATR crystal at pH > 10. The AuNP solution in ethanol or ethanol-d_6 after functionalization and purification steps was adjusted to pH ~11 by dissolving a NaOH pellet directly in the solution or adding NaOD/D_2O solution, and the pH was measured using pH paper. The pH-adjusted AuNP solution was centrifuged once. The concentrated AuNPs were spread on a KBr IR card (International Crystal Laboratories, NJ) and dried under nitrogen gas. Spectra were collected using a PerkinElemer Spectrum 100 FT-IR spectrometer.

2.2.9 X-ray photoelectron spectroscopy

X-ray photoelectron spectra were collected using a monochromatic Al Kα source (1486.6 eV) with a power of 144 W on a Kratos Axis Ultra DLD instrument (Chestnut Ridge, NY) and a 300 × 700 μm spot size. A drop-cast film of the AuNPs was prepared on a piranha-cleaned silicon wafer, and an aqueous solution of trisodium citrate was dried on another silicon wafer. The dense coverage of the AuNP film was assured by absence of Si peaks. Survey spectra were recorded with a pass energy of 160 eV (1 eV steps, 200 ms dwell), and high-resolution spectra at energy ranges of interest were recorded with a pass energy of 40 eV (0.1 eV, 400 ms dwell). The base pressure was 2×10^{-9} Torr. The incidence angle of the incoming X-ray was 54.7°, and the electron take-off angle was 90°. The binding energies shifted by substrate charging were corrected by referencing the C 1s peak of adventitious carbon to 284.8 eV. The background was subtracted by Shirley's method, providing a baseline for determining peak areas. Spectra were fitted using Gaussian/Lorentzian type functions.

2.2.10 Citrate conformation studies on AgNPs

AgNPs were synthesized using reported methods.[40,94] Briefly, 27 mg of $AgNO_3$ was dissolved in 150 mL water (1.0 mM), and the solution was refluxed. With vigorous stirring 61.7 mg of $Na_3Citrate{\cdot}2H_2O$ in 6 mL water was added to the silver ion solution (35 mM, 1% by weight). A milky yellow-greenish solution was obtained, and the pH was ~6.6. The samples for ATR-IR, transmission IR, and XPS were prepared by the same methods as described above for AuNPs.

2.2.11 TEM for AuNP size analysis

TEM images were obtained using an FEI Company Tecnai T-12 transmission electron microscope operating at 100 KV accelerating voltage. One drop of AuNP solution was deposited on a 150-mesh Formvar-coated copper grid. The particle size was analyzed with 56 particles in the TEM images using Scion Image Beta 4.02 software.

2.2.12 Geometric modeling of citrate on gold surfaces

3-D structures of citrate were generated on ChemBio3D Ultra (version 11.0) program. The conformations of adsorbed citrates were obtained from citrate-Au_3 clusters (Au-Au: 2.72Å). Accurate citrate sizes on Au(111) surface were adjusted based on a Au-Au lattice spacing of 2.88 Å. For modeling on Au(110) and Au(100) surfaces, citrate-Au_4 clusters were generated in ChemBio3D. Exact orientations of free carboxylate groups of adsorbed citrates on gold surfaces were determined with the aid of a CPK model. The minimum energy of each conformation was obtained using MM2 at 300 K in ChemBio3D.

2.3 Results and discussion

The approach to a conformational study of citrate layers on AuNP surfaces is based on characterization of coordination of adsorbed citrate species directly in contact with the metal surface, followed by identification of intermolecular interactions between the adsorbed citrates and/or citrate species that were not in contact with the metal surface. The results and discussion of the studies in Chapter 2 are presented as organized in the Scheme 2.1. The first step of the investigation of the citrate adsorption on AuNPs was to probe the coordination of the citrate functional groups using IR spectroscopy and XPS. The spectroscopic studies focus on the binding nature of carboxylate groups of adsorbed

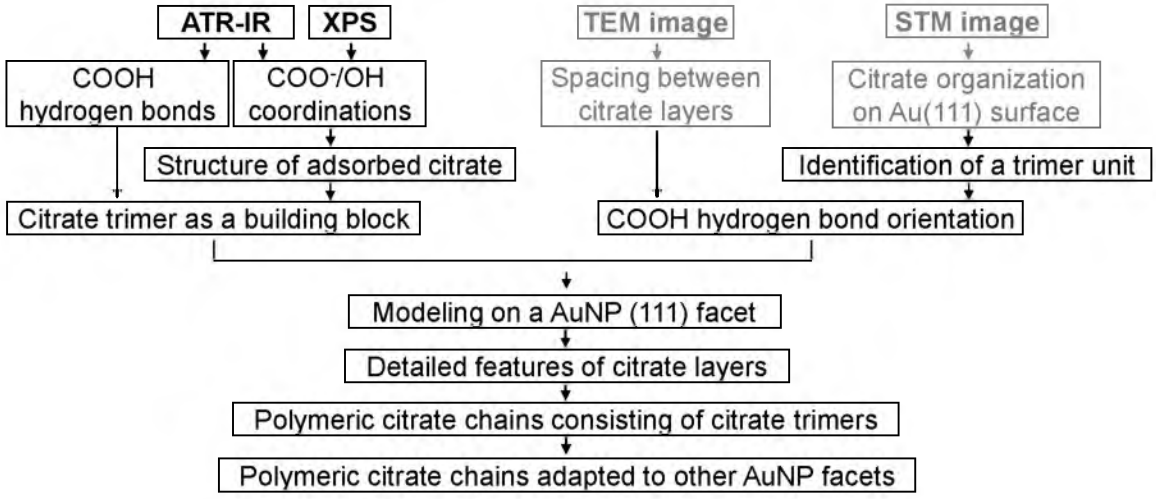

Scheme 2.1. Methods for structure analysis of the citrate layer on AuNPs in this study. TEM/STM images were obtained from literature.

citrate species and the characteristics of the citrate hydroxyl group. After the structure of the adsorbed citrate is determined from the IR and XPS analyses, intermolecular interaction of citrate layers on AuNP surfaces are characterized.

Typically, STM and AFM (atomic force microscopy) analyses are used for detailed structure determination and intermolecular interaction of adsorbed organic layers on atomically flat surfaces, but these analytical techniques are difficult to employ on AuNPs due to the intrinsic curvature of NPs. From the STM image on a gold (111) surface, however, the orientation of the intermolecular interaction of the adsorbed citrate was inferred. Also, interlayer spacing of the citrate layer on AuNPs, which was obtained from atomic-resolution TEM images by others, was attributed to the orientation of citrate functional groups involving interlayer interaction between the adsorbed layer in contact with the gold surface and the additional layer. The TEM and STM data used for determination of the orientation of -COOH hydrogen bonds were obtained from literature.

Finally, geometry-based modeling is used to propose a self-assembly of surface

citrates using the citrate trimer as a building block. Evidence of the adsorption of polymeric citrate chains on AuNP surfaces, which are broken into the citrate trimers as a stabilized formation of the citrate adsorption, is considered.

2.3.1 Structure determination of adsorbed citrate species

2.3.1.1 Investigation of stretching vibrations of carboxylate groups of the citrate monolayer on AuNPs

First, interactions of citrate molecules with a AuNP surface were investigated. IR analysis leads to identification of the binding nature of the carboxyl groups of citrate molecules on a metal surface that are directly correlated to the geometry of the adsorbed hydroxypropane tricarboxylic acid. The vibration frequencies of carboxylate groups are highly dependent on coordination modes, such as η^1-COO^-, η^2-COO^- bridging, and η^2-COO^- chelating[i] while the characteristic hydrogen bonds between protonated carboxylic groups are indicative of intermolecular interactions of the adsorbed molecules. The IR analysis of the characteristic carboxyl groups was used to investigate structural features of citrate species adsorbed on AuNPs. The IR spectral features originated from coordinated citrate species. Prior to the characterization, excess citrate layers on AuNPs were removed by interrupting the intermolecular interaction of COOH hydrogen bonds in a basic condition of pH ~10 where deprotonated COO^- groups repel each other.

Figure 2.1 presents IR spectra measured using an ATR-IR approach. A film of citrate-capped AuNPs gave rise to intense carboxylate peaks of the adsorbed citrate molecules indicative of asymmetric/symmetric COO^- stretching vibrations. Other researchers also

[i] η^1-COO^-: one oxygen atom of COO^- binds to a metal atom, η^2-COO^- bridging: both oxygen atoms of COO^- bind to each adjacent metal atom, and η^2-COO^- chelating: both oxygen atoms of COO^- bind to a same metal atom.

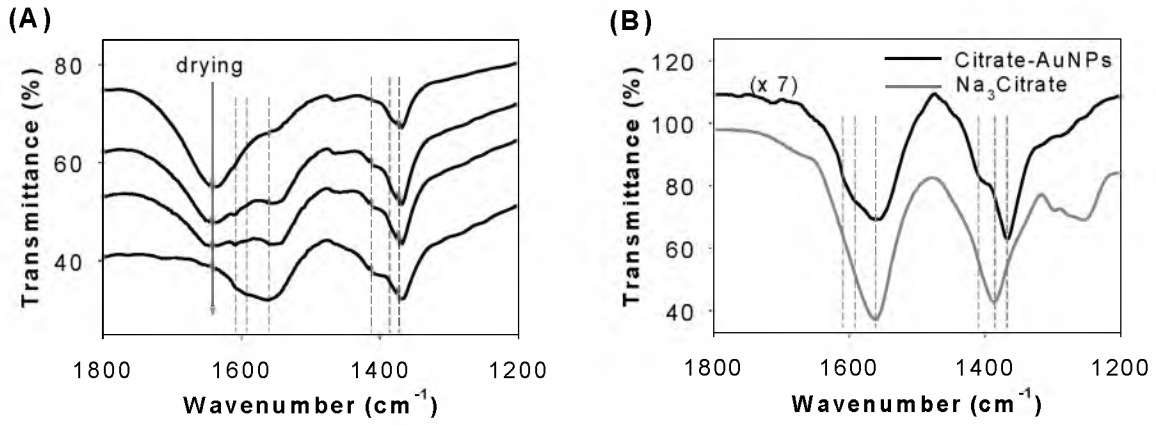

Figure 2.1. ATR-IR spectra of purified citrate-AuNPs. (A) Each spectrum was collected at different time periods after dispersing the AuNPs on the ATR crystal, which shows changes due to water evaporation. Peaks of the $\nu_{asy}(COO^-)$ at 1611, 1593, 1558 cm^{-1} and $\nu_{sym}(COO^-)$ at 1405, 1394, 1370 cm^{-1} appear (dotted lines). The broad band at 1630 cm^{-1} is a water bending vibration. (B) Comparison of ATR-IR spectra of the citrate-AuNPs and trisodium citrate. Note that peak positions are different.

reported that intense peaks of adsorbates on metal nanoparticles were produced with ATR-IR measurements on a ZnSe crystal,[95] rather than with transmission-based IR measurements. In the transmission mode on a KBr card, carboxylate vibrational peaks were too weak to be assigned whereas the water bending vibration at a similar position of 1630 cm^{-1} was dominant.[96] In order to gain information about the orientation of the citrate molecules, surface selection rules must be considered. In the case of molecules adsorbed on a 2-dimensional metal surface, this is more straightforward.[97-101] According to the surface selection rule, only vibrational modes with dipoles oscillating perpendicular to a metal surface are IR-active, and thus only symmetric COO^- stretching vibrations are expected to be IR-active and give rise to an observable IR peak on a metal surface. From IR measurements for adsorbed citrates on AuNPs, however, asymmetric COO^- stretching vibrations were observed, and these vibrational modes are parallel to the AuNP surface assuming that the surface is atomically flat where the molecules are

adsorbed. A dipole moment still exists on metal nanoparticles,[102,103] but the surface selection rule is not valid for the AuNP film in this study,[ii] possibly due to surface-enhanced infrared absorption (SEIRA).[104,105] More specifically, the coupling of charge transfer to the molecular vibration may be responsible for the enhanced IR peaks of the asymmetric COO^- stretching vibrations. For example, a charge-transfer induced dipole moment oscillation may couple with molecular vibrations resulting in activation of symmetric molecular modes that are considered to be IR-inactive by surface selection rules.[106-110]

The ATR spectra of the citrate monolayer on AuNPs show three distinct peaks, the asymmetric COO^- stretching vibrations ($\nu_{asy}(COO^-)$) at 1611, 1593, and 1558 cm^{-1} and three other peaks assigned to symmetric COO^- stretching vibrations ($\nu_{sym}(COO^-)$) at 1405, 1394, and 1370 cm^{-1} (Figure 2.1). Typically, the carboxylate group exhibits an asymmetric and a symmetric stretching vibration around 1500 - 1630 cm^{-1} and 1305 - 1415 cm^{-1}, respectively.[111-114] Spectra collected at different time periods to probe the spectra as water evaporated from AuNPs dispersed on a ZnSe crystal show COO^- stretching vibrations, which are relatively sharp and distinguishable (Figure 2.1A). The vibrational peaks broaden once the film of AuNPs is completely dried, but the positions remain constant. While two $\nu_{asy}(COO^-)$ at 1611 and 1558 cm^{-1} and two $\nu_{sym}(COO^-)$ at 1405 and 1370 cm^{-1} are pronounced, the $\nu(COO^-)$ at 1593 and 1394 cm^{-1} are resolved at the end and beginning of the drying step, respectively. A peak at 1540 cm^{-1} can be another type of $\nu_{asy}(COO)^-$, which may result from binding to Au(110) and/or Au(100)

[ii]The orientation of the molecules on the faceted surfaces of metal NPs may not be well-defined with respect to the electromagnetic fields of the evanescent wave. On a planar surface, there is only one face parallel with the crystal face. However, the particles have faces with different orientations with respect to the ATR crystal face.

facets of AuNPs. The IR peaks of the carboxylate stretching vibrations of pure trisodium citrate on the ZnSe crystal[114] are consistent with those collected on a diamond crystal,[115] and thus a peak shift of citrate carboxylate groups due to direct contact with a ZnSe surface is negligible. In this study, the majority of the probed region is a stack of AuNPs placed above the ATR crystal surface. Although these spectral features are similar to those for pure trisodium citrate possessing the COO^- stretching vibrations at 1575 and 1385 cm^{-1} (Figure 2.1B; see the Appendix for peak positions and related references in the entire spectral region)[116] due to ionic coordination with Na^+,[117,118] the peak positions of the carboxylate stretching vibrations are different from each other. Two additional $\nu_{asy}(COO^-)$ stretching vibrations at 1610 and 1555 cm^{-1} as well as the asymmetric shape of the $\nu_{sym}(COO^-)$ peak with a shoulder centered at ~1390 cm^{-1} indicates presence of at least three types of $\nu_{sym}(COO^-)$ stretching vibrations. This correlates well with literature reports of IR analysis of adsorbed citrate on a planar gold (111) surface.[64] As a result, the IR spectra indicate that the COO^- vibrational frequencies are split into three distinct peaks for the adsorbed citrate.

Typically, the bending vibrations of adsorbed water on metal surfaces[100,101,119-123] are observed at 1610 - 1670 cm^{-1}, which is in the regime of one of the asymmetric COO^- vibrations at 1611 cm^{-1}. Thus, the sharp peak at 1611 cm^{-1} often is assigned to the bending vibration of water[121,124,125] free from hydrogen bonding. However, lack of the corresponding sharp O-H stretching around 3440 cm^{-1}[119,126] excludes the possibility of the water bending mode for the 1611 cm^{-1} peak. Instead, the water bending vibration was observed at ~1635 cm^{-1}, which was supported by the change in amplitude during water evaporation[96] (Figure 2.1A). In order to confirm the spectral contribution from water at ~1635 cm^{-1}, $NaOD/D_2O$ was used to rinse the AuNPs. In this deuterated condition, the

asymmetric COO^- vibration still appears at 1620 cm^{-1}, which confirms that the peak does not originate from water (Figure 2.2). The different interaction of D_2O with the η^1-COO^- group by hydrogen bond[114,127,128] may cause the shift in the carboxylate peak to a higher wavenumber at 1620 cm^{-1}. Typically, upon change of H_2O solvent to D_2O the $\nu_{asy}COO^-$ of deprotonated carboxylate groups shifts to higher frequency by 5 - 13 cm^{-1},[129,130] while the carbonyl stretching vibration of protonated carboxylic acid groups[131] and amide groups of amino acids[130] shifts to lower frequency.[iii]

As mentioned previously, the purification procedure with OH^- ions leads to removal of excess citrate. This indicates that the remaining citrate molecules on the AuNPs are expected to be a monolayer, evidenced by absence of intermolecular interaction through the COOH hydrogen bonds and by deprotonation of all carboxylic groups (Figure 2.1). The hydroxide ions did not replace adsorbed citrates since the IR peaks of citrate were

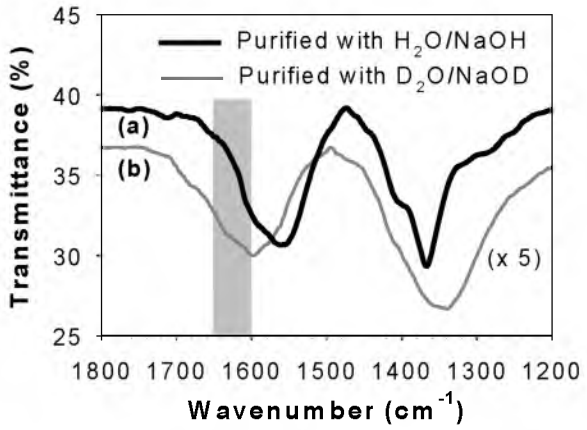

Figure 2.2. ATR-IR spectra of citrate-AuNPs purified by (a) H_2O/NaOH and (b) D_2O/NaOD at the frequency regions of carboxylate stretching vibrations. The typical frequencies of water (H_2O) bending vibrations are highlighted in the grey region. The $\nu_{asy}(\eta^1$-$COO^-)$ is still observed at 1620 cm^{-1} under the deuterated condition.

[iii]On the contrary, it was reported that the $\nu_{asy}COO^-$ shifts to higher frequency by less than 4 cm^{-1}. See ref. 129: Norén, K.; Loring, J. S.; Persson, P. *J. Colloid Interface Sci.* **2008**, *319*, 416-428.

still observed after the purification step. Also, the hydroxide is known to compete with citrate in binding on Ag nanorods,[132] but significant hydroxide adsorption on the AuNPs was not observed, which is evidenced by absence of a Au-OH vibration at 520 - 580 cm^{-1} under the high pH condition.[88, 133] The purified AuNPs exhibit the same absorbance and NP shape with AuNPs as prepared (see UV-Vis absorbances and TEM images of citrate-AuNPs in the Appendix), which implies the AuNPs are not impacted by the hydroxide treatment. Although there might be an orientation change of the adsorbed citrate due to deprotonation [134] of the free carboxylic acid as well as changes of the adsorbate concentration[135] and ionic strength,[136] the binding geometry of the adsorbed citrate is not altered significantly under the purification condition (see Section 2.3.8).

2.3.1.2 Identification of free carboxylate groups

In order to distinguish between surface-coordinated and free carboxylate groups on a Au surface, Pb^{2+} was added to the solution of purified citrate-AuNPs (Figure 2.3). The asymmetric COO^- stretching vibration of the free carboxylate is expected to shift away from the broadened region of the asymmetric COO stretches to about 1515 cm^{-1} (η^2-COO^- chelating[137]) or 1540 cm^{-1} (η^2-COO^- bridging[138]) upon coordination with Pb^{2+} while the frequency of the bound carboxylate should remain at the same position. It was observed that the peak at 1593 cm^{-1} is significantly attenuated with introduction of the Pb^{2+}. In addition, new broad peaks centered at 1540 cm^{-1} and 1417 cm^{-1} appear, which are assigned to the asymmetric and symmetric COO^- stretching vibrations of the free carboxylate due to η^2-COO^- bridging coordination with the Pb^{2+} (Figure 2.3a).[138] The symmetric COO^- vibration around 1390 cm^{-1}, with the asymmetric COO^- vibration appears at 1593 cm^{-1}, is difficult to resolve due to other strong symmetric COO^-

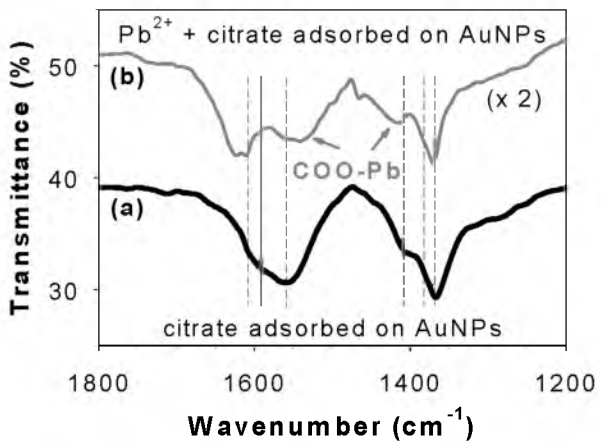

Figure 2.3. ATR IR spectra of (a) purified citrate-AuNPs and (b) Pb^{2+} treated citrate-AuNPs. Note that the peak around at 1593 cm^{-1} disappears (a solid line in the region of the $\nu_{asy}COO^-$), and new peaks at 1541 cm^{-1} and 1417 cm^{-1} appears upon Pb^{2+} addition (arrowed). The $\nu_{sym}COO^-$ does not show a significant decrease in peak intensities.

vibrations. The peak at ~1630 cm^{-1} is the water bending vibration. Thus, the peak at 1593 cm^{-1} is assigned to an asymmetric COO^- stretching vibration of a free carboxylate group of the adsorbed citrate.[139] The presence of this band indicates that the adsorbed citrate exhibits a free carboxylate group.

2.3.1.3 Coordination character of the binding carboxylate groups

AuNPs have facets, and the Au(111) surface typically is the most populated facet in a large AuNP.[140] Since the spectral difference of the distinct COO^- stretches with respect to the crystal facet is known to be less than 15 cm^{-1} as observed for single crystal electrodes of Pt(hkl)[141] and negligible for Au(hkl),[120,142] the measured wavenumbers of the COO^- stretches result from the unique binding modes of carboxylate rather than from varied AuNP facets. In Figure 2.1A, the peaks at 1611 and 1370 cm^{-1} are attributed to a η^1-COO^- binding[68,139,143-152] on a Au surface[119] whereas the peaks at 1558 and 1405 cm^{-1} are

associated with a η^2-COO^- coordination[68,72,123,126,150-159] on a Au [160] surface.[57,64,65,88,101,119,120,122,134,147,149,161-166] These observed vibrational frequencies of the adsorbed carboxylate groups also match with computational results for two-dimensional planar gold single crystal surfaces.[88,119] In general, the $\Delta\nu$, $\nu_{asy}(COO^-) - \nu_{sym}(COO^-)$, is indicative of the binding character of a carboxylate group with a metal ion.[167-170] The $\Delta\nu$ values of the η^1- and η^2-COO^- groups of the adsorbed citrate are 241 cm^{-1} and 153 cm^{-1}, respectively. These values are in good agreement with the coordination nature of carboxylate groups with a metal. Some of the gold acetate complexes exhibit the η^1-COO^- coordination to gold ions in solution.[171-175] Lackovic et al. identified dominant binding modes between the η^1- and η^2-COO^- species for adsorbed citrate on a FeOOH surface at different pH values.[116] The coordination of citrate molecules on metal oxide surfaces such as goethite α-FeOOH[116] and hydroxyapatite[176] and intercalation in layered double hydroxides such as hydrotalcite $Mg_6Al_2[(OH)_{16}|CO_3]\cdot 4H_2O$ have been investigated.[177] However, these results cannot be simply translated to other metal surfaces without considering specific surface interactions in assigning -COO(H) peaks.

The deuterium exchange also was consistent with the nature of the carboxylate coordination on the gold surface relating to interaction with water. Comparing with the carboxylate stretching vibrations of citrate on AuNPs under the normal condition, the η^2-COO^- carboxylate stretching vibrations at ~1558/1405 cm^{-1} did not shift, and the ν_{asy}COO- of the free carboxylate group appeared at the same frequency at ~1593 cm^{-1}, due to the lack of interaction with water. The former is associated with the coordination of both oxygen atoms to metal surfaces, and the latter is related to the intramolecular interaction with the hydroxyl group of the adsorbed citrate (see Section 2.3.1.4). However, the η^1-COO^- carboxylate group has one oxygen atom likely available for interaction with

water, which hydrogen bonding of the oxygen atom with D_2O[178] may shift the $\nu_{sym}(COO^-)$ to higher frequency[129,130] at 1620 cm^{-1} (Figure 2.2). The peak broadening of the asy/sym carboxylate stretching vibration by use of D_2O also is consistent with various hydrogen-bond configurations.[178]

2.3.1.4 Features of the free carboxylate group

The assignment made for the vibrational frequencies of the free carboxylic acid and deprotonated carboxylate group of the adsorbed citrate were investigated. The purified citrate-AuNP solution was adjusted to pH ~9 which is relatively high compared to the highest pK_a value (6.4) among three carboxylic groups of citric acid in bulk solution. Under this strong basic condition, free carboxylic acids at 1764 cm^{-1},[100,157,179] as well as hydrogen-bonded carboxylic acids at 1711 cm^{-1} were still observed (see the Appendix for the magnified spectrum of citrate-AuNPs in Figure 2.1B) probably through interactions with the hydroxyl group via intramolecular hydrogen bonds.[127,180] The surface pKa of the citrate molecules should be dependent on the presence of hydrogen bonds. For example, it has been shown that the surface pK_a of self-assembled monolayers (SAMs) on a metal surface is higher than in solution where intermolecular interactions[181-186] are more favorable for the molecules confined to the surface. However, the SAMs of short chain carboxylic acids have exhibited a decreased pK_a upon adsorption on a metal surface where the intermolecular hydrogen bonds are weak.[187,188] The peak at 1711 cm^{-1} does not originate from common hydrogen bonds by carboxylic acid acyclic/cyclic dimers.[100,189-192] The peaks at1734 and 1700 cm^{-1} have been assigned as due to citrate dimer formation as discussed in Section 2.3.3. The possibility of interparticle hydrogen bonding between free carboxylic acids of citrate on different citrate-capped AuNPs was ruled out because a

characteristic blue-shift of the surface plasmon band was not observed, which would be expected if the AuNPs were in close proximity (see UV-Vis absorbances of citrate-AuNPs in the Appendix).

In comparison with an asymmetric COO^- stretching vibration of common aliphatic carboxylate groups[111,120] at ~1550 cm^{-1}, the relatively high $\nu_{asy}(COO^-)$ of the free carboxylate[139,189] at 1593 cm^{-1} also may originate from an interaction with the hydroxyl group.[144,193] For some metal-citrate complexes, $\nu_{asy}COO^-/\nu_{sym}COO^-$ of the free terminal carboxylate are reported at higher positions, e.g., 1586/1372 cm^{-1},[148] 1586/1386 cm^{-1},[194] 1596/1397 cm^{-1},[194] and 1587/1363 cm^{-1}.[72,153] It is interesting that there are negatively-charged carboxylate groups of surface citrate which do not bind on the positively-charged AuNP surface, and this may be due to the charge balance on the surface[195] or the presence of counterions. Moreover, the free carboxylate groups on AuNPs may not coordinate to the lead ions by *interparticle-type* interaction because gaps between some aggregated NPs are present (see TEM image of purified citrate-AuNPs after addition of lead ions in the Appendix). Although it has been suggested that citrate-AgNPs are aggregated by *interparticle-type* interactions through the free carboxylate groups of adsorbed citrates on different AgNPs mediated by added metal ions,[196] experimental results from this study indicate that the interaction of the free carboxylate groups with metal ions may occur primarily on the surface of same AuNPs.

2.3.1.5 Coordination of the alcoholic OH group

Coordination of the alcoholic group of the adsorbed citrate was studied. In most previous studies of citrate conformations on a metal surface, the binding of the citrate hydroxyl group was neglected. Since the hydroxyl group of citrate and other

hydroxydicarboxylates[69-71] is well-known for 5-membered chelating coordination to metal atoms, such as Al(III),[143, 197] Ga(III),[143] W(VI),[139, 198] Mo(VI),[144, 199] U(VI),[167, 200] Fe(III),[148] Ti(IV),[193, 201 - 204] Mn(II),[194] Cu(II),[72] V(V),[205] Zn(II),[206] and Cd(II),[207] the hydroxyl group of citrate to the metal nanoparticle surface needs to be considered.[67,68] Alkoxide species on a metal surface have been reported[73-84] while methanol and/or ethanol coordinate to small noble metal clusters ($n \leq 15$) without O-H bond cleavage.[208-214] The crystal structures of various citrate-metal complexes revealed that the hydroxyl group acts as a supporting donor group for the central carboxylate coordinate. A hydroxyl group of small organic molecules, such as methanol,[77] ethanol,[75] butanol,[76,81] ethylene glycol,[74] and 2-haloethanol,[78,79] has been reported to be cleaved during alkoxide formation on a metal surface, and it was suggested that ethoxide adsorbed on a Au surface is not stable.[75]

$\nu(C\text{-}O)_{alch}$[68b,88,112-114,127,187,200,215-220] at 1137, 1111, and 1076 cm^{-1} for pure trisodium citrate and the shift of those peaks to 1070 cm^{-1} for the citrate-AuNPs were observed (see ATR-IR spectra and IR band assignments for purified citrate-AuNPs and trisodium citrate in the Appendix). The shift of $\nu(C\text{-}O)_{alch}$ has been used as evidence for alcohol coordination to gold clusters.[209-213, 221] Depending on the size and charge of the gold cluster as well as the type of the alcohol (e.g., methanol or ethanol), the $\nu(C\text{-}O)_{alch}$ of a gold-alcohol complex decreases by 25 - 60 cm^{-1} compared to a free alcohol in the gas phase. For larger nanoparticles or a planar surface, the $\nu(C\text{-}O)_{alch}$ shift also has been employed as a probe to determine the alcohol group coordination. Cornell et al. showed examples of the involvement of the alcoholic OH in coordination on a FeOOH surface for various hydroxycarboxylic acids where the alcohol $\nu(C\text{-}O)_{alch}$ of citrate decreases from 1125 cm^{-1} to 1070 cm^{-1} upon surface coordination.[217,222] Ha et al. monitored the shift of

the $\nu(C\text{-}O)_{alch}$ peak at 1126 cm^{-1} for investigating coordination of lactate $CH_3CH(OH)COO^-$ on hematite (α-Fe_2O_3) nanoparticles,[223] and Awatani et al. proposed the hydroxycarboxylate-type coordination of lactate and glycolate to a TiO_2 surface evidenced by shift of the $\nu(C\text{-}O)_{alch}$ to a higher wavenumber and characteristic η^1-COO^- coordination.[68] Lindegren et al. proposed coordination of adsorbed citrate to α-FeOOH surfaces at a high pH as one η^1-COO^-, one η^2-COO^- (outer-sphere complex), and one free carboxyl group with the involvement of the hydroxyl group in surface coordination,[115] but the diagnostic peak of the bending vibration of the hydroxyl group is not clearly distinguished from the determination of the hydroxyl group coordination in their study. In this study, a new $\nu(C\text{-}O)_{alch}$ at 1070 cm^{-1} was observed, but it was not concluded that the shift of the $\nu(C\text{-}O)_{alch}$ was due to be the coordination of the OH group to the Au surface since γCH_2 and $\nu(C\text{-}C)$ are probably shifted around the $\nu(C\text{-}O)_{alch}$ region simultaneously upon citrate adsorption on the AuNP surface due to the resultant conformational change.[187] This vibration band may be associated with a C-C-C skeletal vibration,[224,225] which also appears for alcohol-free alkanethiolates. Therefore, more experimental evidence is required for determination of the involvement of the citrate hydroxyl group in coordination on the AuNP surface.

In order to probe the coordination of the citrate hydroxyl group, the IR spectrum of purified citrate-AuNPs was investigated using a deuterium exchange experiment (Figure 2.4). NaOD and D_2O in the purification step of the citrate-AuNP were used instead of NaOH and H_2O, and the pH was adjusted to ~ 9 where protonated carboxylic species are present at a minute level and a spectral change is expected from hydroxyl groups. The most distinct features of the spectrum are the appearance of a strong $\delta(OD)_{alch}$[80,226,227] peak of the citrate hydroxyl group at 877/833 cm^{-1} as well as the disappearance of the

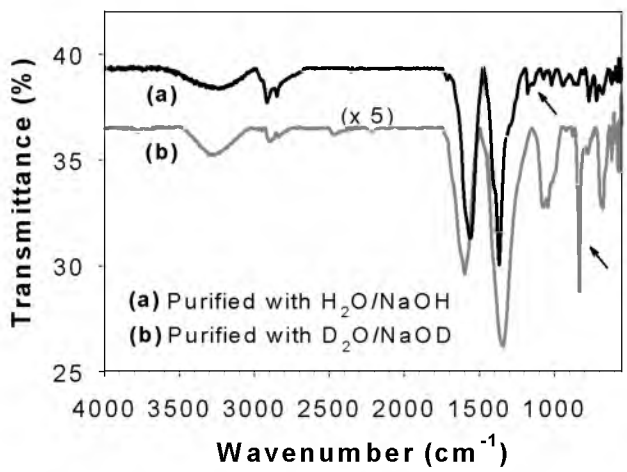

Figure 2.4. ATR-IR spectra of citrate-AuNPs purified by (a) H_2O/NaOH and (b) D_2O/NaOD. Note that the $\delta(OH)_{alch}$ at 1175/1146 cm^{-1} is shifted to $\delta(OD)_{alch}$ at 877/833 cm^{-1} upon deuteration (arrow).

counterpart peak of the $\delta(OH)_{alch}$[228] located at 1175/1145 cm^{-1}.[78,79,81,229,230] The intensities of the peak at 833 cm^{-1} for the deuterated citrate-AuNPs and the peak at 1175 cm^{-1} for the citrate-AuNPs do not change significantly as samples are dried (see ATR-IR spectra of purified citrate-AuNPs taken during water evaporation in the Appendix), which this consistent vibrational feature indicates those vibrational bands stem from an identical vibration mode. This observation verifies the existence of a free hydroxyl group that does not participate in metal complexation. Max et al. monitored vibrational bands of malic acid $HOOCCH_2CH(OH)COOH$, monosodium malate $HOOCCH_2CH(OH)COONa$, and disodium malate $NaOOCCH_2CH(OH)$ $COONa$, and observed a peak at 1184 - 1195 cm^{-1} for all species.[127] Taking into consideration this observation in the literature, it also is expected that the 1175/1145 cm^{-1} peaks are not associated with a $\delta(OH)$ vibration from -COOH groups. Note that most of carboxylic acid groups in this experiment are deprotonated. The bending vibrations of H_2O, HOD, and D_2O in a liquid phase appear at 1640, 1442, 1202 cm^{-1}, respectively.[231]

On the other hand, the hydroxide of NaOH may be adsorbed on the Au surface,[232] but the characteristic peaks of metal hydroxides,[233] which are νMO-H at 3650 - 3850 cm^{-1} (νMO-D at 2650 - 2800 cm^{-1}), νAu-OH at 529 cm^{-1},[234] and δMOH at 575 - 890 cm^{-1} (δMOD at 470 - 660 cm^{-1}), are not overlapped with the $\delta(OH)_{alch}$. Thus, monitoring $\delta(OH)_{alch}$ is a successful protocol to determine the involvement of the hydroxyl group of citrate in coordination to a metal surface. In addition, a slight shift of the $\nu(C\text{-}O)_{alch}$ of citrate-AuNPs from 1062 to 1070 cm^{-1} was observed as water evaporated (see ATR-IR spectra of purified citrate-AuNPs taken during water evaporation in the Appendix). The shift by degree of solvation also indicates the hydroxyl group is not coordinated to the surface. The $\nu(C\text{-}O)_{alch}$ of the deuterated citrate-AuNPs typically was shifted between1085 - 1020 cm^{-1} (not shown), which indicates that the hydroxyl group of the adsorbed citrate is subject to hydrogen bonding with water that may be influenced by the amount of H_2O/OH^- and D_2O/OD^- present. Note that H_2O from air is adsorbed into the deuterated sample during the sample purifications and IR measurements. The strong peaks at 1041 and 690 cm^{-1} are assigned to an in-plane OD bending (δOD_{COOD}[235] + νCO_{COOD}) and an out-of-plane OD bending (γOD_{COOD}), which are observed upon deuteration with disappearance of the in-plane OH bending (δOH_{COOH} + νCO_{COOH}) at 1283 cm^{-1} and γOH_{COOH} at 938 cm^{-1}.[236-239] The carbonyl stretching vibrations of COOH and COOD are located at identical frequencies.[235,237-240]

2.3.1.6 XPS characterization of adsorbed citrates

XPS has been extensively employed for surface analysis. The binding energy (BE) of electrons on an atom is sensitive to the local electronic state of adjacent atoms. XPS was measured for both of a drop-cast film of the purified citrate-AuNPs and trisodium citrate

molecules on silicon wafer, respectively. The binding energy of the C 1s for adventitious carbon as reference is 284.8 eV. The deconvoluted C 1s spectrum consists of four distinct binding energies[241] at 284.8, 285.9, 287.6, and 289.4 eV, which are attributed to adventitious carbons (C-C or C-H), the free hydroxyl ($C\text{-}OH_{alch}$)[242-245] and/or the α-carbons (CH_2),[246] the coordinated carboxylates (COO-Au),[242, 247-250] and free carboxyl moieties (COOH[251] or COO^-),[246] respectively (Figure 2.5 and Table 2.1). Two carboxylate peaks can be identified depending on coordination to a Au surface, which is consistent with IR analysis in this study. Since a coordinated alcohol group by O-H cleavage is expected to be undetectable under the deuterated IR analysis, the regions of the XPS C 1s were analyzed to distinguish the binding alcohol species. It is known that

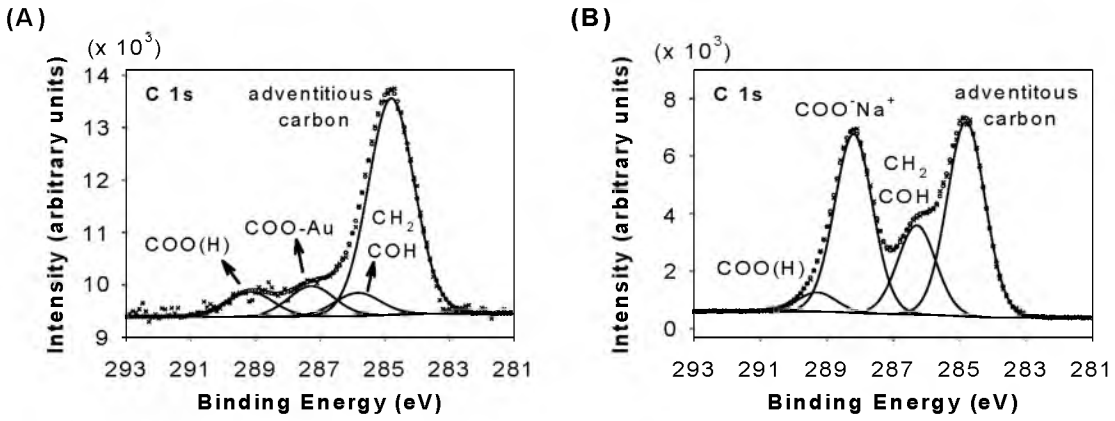

Figure 2.5. XPS spectra of C 1s binding energy of (A) purified citrate-AuNPs and (B) pure trisodium citrate.

Table 2.1. C 1s binding energy of purified citrate-AuNPs and pure trisodium citrate.

C 1s BE (eV)	Adventitious C	COH/CH_2	$Au\text{-}COO^-$	COO^-Na^+	free COO(H)
Na_3Citrate	284.8	286.3	-	288.2	289.3
Citrate-AuNPs	284.8	285.9 (0.1)	287.6 (0.3)	-	289.4 (0.2)

the C 1s of coordinated propanoxide on $Cu_2O(100)$ is placed at a higher binding energy by 1.5 eV compared to that of an aliphatic carbon.[244] On the other hand, it has been reported that the C 1s of hydroxyl groups shift to a lower energy by ~0.5 eV upon coordination.[242] Although the C 1s binding energy of the C-OH regime in the measurement in this study is located within the C-OH coordinate, a conclusion cannot be made about the C-OH binding on the Au surface because the CH_2 binding energy is overlapped and appears as one peak which cannot be deconvoluted into two components due to the intrinsic low concentration of the adsorbed citrate.[iv] However, the peak for pure trisodium citrate can be split into two components (C-OH and CH_2, data not shown). As a result, the hydroxyl group coordination on the surface cannot be excluded by XPS analysis as well as the IR study. Two peaks for the pure trisodium citrate also were assigned, which are the Na^+-coordinated and the peaks associated with the free carboxylates. This assignment confirms that the free carboxylate group of the adsorbed citrate interacts with other functional groups rather than Na^+ ions.

Binding energy of the Au(I) $4f_{7/2}$ is larger by more than 0.60 eV whereas in the case of the thiolated SAMs on AuNPs, the shift is less than 0.36 eV.[252-255] This implies that the binding nature of the carboxylates on the Au surface is more ionic than that of the Au-S bond (see the XPS spectrum of Au 4f binding energy of citrate-AuNPs in the Appendix).

2.3.1.7 Conformation of the adsorbed citrate on AuNPs

Based on the two distinct binding modes of carboxylate groups with the hydroxyl group intact and one carboxylate group freely exposed to solution, it can be proposed that

[iv]The O 1s binding energy is not as distinct as in the literature due to the presence of water and hydroxide ions in this study. For O 1s binding energy of carboxylate groups: Lin, N.; Payer, D.; Dmitriev, A.; Strunskus, T.; Wöll, C.; Barth, J. V.; Kern, K. *Angew. Chem.* **2005**, *117*, 1512-1515.

the citrate is adsorbed on a AuNP surface by the η^2-COO^- bridging coordination of the central carboxylate group and the η^1-COO^- coordination of the terminal carboxylate group as a dominant species (Figure 2.6, conformation I). This adsorption geometry through the binding of the central and one terminal carboxylate groups of citrate, rather than the two terminal carboxylate groups, is consistent with the proposed citrate conformation on AgNPs[90] as well as the suggested preferential binding of citrate to Ag(111) of silver nanoplates.[256] Although it is not possible to distinguish between bridging and chelating coordinations of carboxylate groups from IR data,[120] Rodes and co-workers concluded that bridging coordination dominates based on DFT calculations for adsorption of glycolate anions ($OHCH_2COO^-$) on a Au(111) surface.[88] The DFT results indicate that chelate η^2-COO^- coordination is not stable, transforming to a η^1-coordination.[88,257] Wandlowski and co-workers also suggested the bridging coordination of carboxylate groups, rather than the chelating coordination, on gold surfaces.[57,122] From the geometry-based modeling of the adsorption of surface citrates on the Au(111) surface,

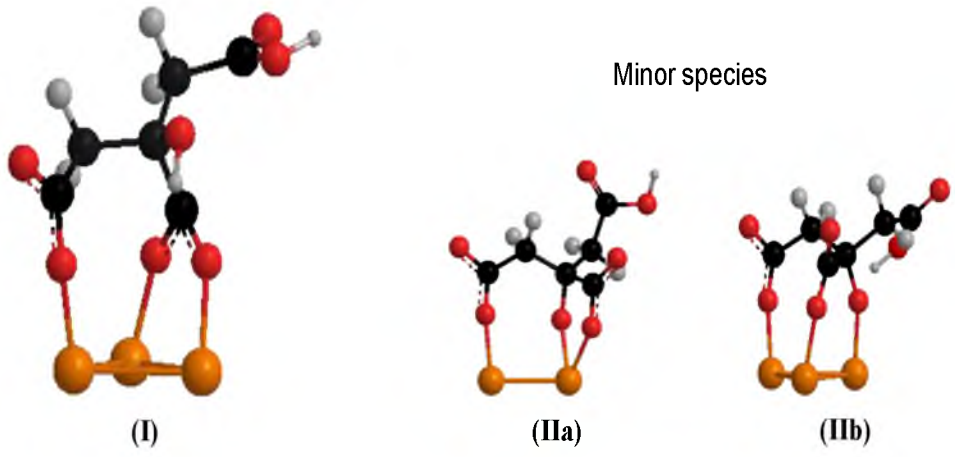

Figure 2.6. Proposed conformation of adsorbed citrate on AuNPs. Conformation (**I**) is consistent with the IR analysis, but the mixture of conformation (**I**) and (**II**) also is possible. Orange: gold (representative of the Au(111) surface), red: oxygen, black: carbon, grey: hydrogen.

it also was found that the bridging configuration of the central carboxylate group of adsorbed citrate led to generation of the identical pattern of the STM image of citrate adsorption while the chelating conformation failed to produce the assembled pattern of surface citrates (see Section 2.3.6).

Due to the intrinsic ensemble nature of IR measurements, the mixture of various conformations of the adsorbed citrate may produce three characteristic carboxylates, but the least probable citrate species was ruled out based on the protonation trend of citrate. Martin has reported that the dihydrogen citrate species ($H_2Citrate^-$) with the central carboxylic group deprotonated is the most populated species at the beginning of deprotonation processes of citric acid.[258] The central carboxylate group has the lowest pK_a,[259] and it probably binds on the Au surface preferentially at the beginning of citrate adsorption.[260, 261] Although citric acid ($H_3Citrate$) and dihydrogen citrate species ($H_2Citrate^-$) are expected to be dominant at pH ~3.2 condition[25] of as-prepared citrate-AuNP solution, the protonated carboxylic groups of citric acid can be adsorbed on a Au(111) surface by an anodic reaction associated with oxidation of the Au surface,[262] and/or the purification procedure by hydroxide ions may promote the binding of free carboxylic acid groups. The coordination of the central carboxylate group also is supported by the formation of acetone-1,3-dicarboxylate that is generally accepted as an oxidized form of citrate in the synthesis of AuNPs[1,263,264] and AgNPs.[40] Moreover, a lattice match between spacing of the surface gold atoms and molecular length of adsorbed moieties may prevent citrate adsorption through the two terminal carboxylate groups on the Au(111) surface. Yin and co-workers[256] suggested that dicarboxylic acids having more than two methylene ($-CH_2-$) units do not selectively bind to the Ag(111) surface (the silver lattice spacing: 2.89 Å) due to the size mismatch. In this study, the

central and a terminal carboxylate group are spaced apart by two carbon atoms (distance between two carbons of the carboxylate groups: 3.3 Å), and this length of the molecular moiety for adsorption is commensurate with the lattice spacing of 2.88 Å for Au(111). Possible adsorption of citrate through a terminal-carboxylate coordination also was excluded based on the reported spacing of citrate layers on AuNPs.[91] The adsorbed citrate by the terminal-carboxylate coordination can be stretched away from surface at a height of up to 9.2 - 9.4 Å from the surface, and this would result in the citrate layer spacing larger than ~6 Å since the distance between α-carbons of carboxylic acid dimers is ~6.2 Å. However, the spacing of citrate layers on AuNPs is 3.0 - 3.5 Å,[91] and this relatively short spacing cannot be produced with the stretched citrate conformation only by the one terminal-carboxylate coordination.

Conformation II (IIa: chelating, IIb: bridging) also is proposed as minor species (Figure 2.6) since the possibility of the presence of a mixture of conformations I and II cannot be ruled out based on the IR and XPS results (A brief discussion of energy for each conformation is in the Appendix). Both of the conformations II are associated with a coordination of the hydroxyl group. The detection of $\delta(OH)_{alch}$ does not necessarily mean that all of the hydroxyl groups are uncoordinated, and the C 1s binding energy of the hydroxyl group is not sensitive to coordination due to the low citrate concentration. However, conformation II itself does not explain the IR results because the intact hydroxyl group has been detected. The coordination of the hydroxyl group and the central carboxylate group to a Au (III) ion via five-membered ring formation was suggested as an intermediate structure during AuNP synthesis,[264] which also is common for citrate-metal complexes (conformation IIa).

For the citrate conformation involving the central and terminal dicarboxylate

coordination, characteristic peaks include a CH_2 rocking[265,266] at 771 cm^{-1} overlapped with a COO scissoring[49,135,265,267] mode at 771 cm^{-1} and 721[v] cm^{-1} (see Section 2.5.1 IR bands of purified citrate-AuNPs and Na_3Citrate in the Appendix). The CH_2 rocking band of citrate appears at a higher wavenumber compared to that of long alkanes exhibiting typically at 720 cm^{-1}.[156,225,268] The strained CH_2 bending at a decreased wavenumber (1453 cm^{-1}) has been detected[269] whereas the CH_2 bending at 1465 cm^{-1} is assigned for the α-carbon from the free carboxylate group. The peak of $\nu_{asy}COO^-$ at 1593 cm^{-1} is relatively high, and this can be explained by COO^--OH hydrogen bond (see possible configurations of citrate molecules adsorbed on AuNPs in the Appendix). There is a weak band of $\nu(C=O)_{COOH}$ at 1711 cm^{-1}, which is neither a free carboxylic acid (1764 cm^{-1}) nor a cylic/acylic dimer (1704/1734 cm^{-1}) of the carboxylic acid group of citrate. Lindegren et al.[115] pointed out the carboxylic acid COOH of citrate at 1708 cm^{-1} is correlated to the free deprotonated carboxylate COO^- on the FeOOH surface. They also observed that under a deuterated condition at pD 3.4, the intensity of the peak at 1708 cm^{-1} increases, which was concluded as an unidentified citrate surface complex. Considering the IR results and the observation from literature for the FeOOH surface, it is concluded that the peaks at 1711/1593 cm^{-1} originate from an OH_{alch}-HOOC/OH_{alch}-OOC interaction.[270]

Nichols et al. proposed a citrate structure with all three carboxylate groups coordinated on a Au (111) surface as a η^2-COO^- mode.[64] They claimed that there was only one symmetric COO^- stretching vibration of a η^2-COO^- coordination at 1385 cm^{-1}, which led to the proposed citrate conformation. Contrary to the aforementioned

[v]An alternative assignment for the 721 cm^{-1}: $\nu(O\text{-}H)_{alch}$ for a low barrier hydrogen bond of the O-O distance 2.45 Å. The O-O distance between the hydroxyl group and the terminal carboxylic acid group of citrate molecules is about 2.65 Å, which suggests the possibility of the OH---HOOC interaction. The peak at 721 cm^{-1} disappears upon deuteration: (a) Bertolasi, V.; Gilli, P.; Ferretti, V.; Gilli, G. *Chem. Eur. J.* **1996**, *2*, 925-934. (b) Häggman, L.; Lindblad, C.; Oskarsson, H.; Ullström, A.-S.; Perrson, I. *J. Am. Chem. Soc.* **2003**, *125*, 3631-3641.

observation there also were the small but noticeable peaks at 1610 and 1555 cm^{-1} as well as a broad peak of $\nu_{sym}(COO^-)$ with a shoulder, which is indicative of a different COO^- coordination and thus possibly disparate structures. It was found that there are a couple of examples of contradictory explanations using the tridentate citrate binding (η^2-COO^- coordination) to gold surfaces in the literature. One example is that interpretation of the STM image of citrate organization on Au(111) by Bai and co-workers[66] is not plausible. The estimated lateral length of the citrate based on the STM scale bar is about 10 Å, but the actual size of the tridentate citrate molecule is about 5 Å. Moreover, the proposed citrate conformation is not achievable as a building block for the 2-D citrate self-assembly on Au(111), due to the unfeasible orientation of possible moieties of the adsorbed citrate, i.e., $-CH_2-$ and -OH, pointing outward from the surface. Thus, there is no molecular moiety available for lateral intermolecular interactions on the surface that should play a role in the patterned assembly of citrate. In another study, Teobaldi and Zerbetto conclude that adsorption of citrate molecules on a Au(111) surface through three η^2-COO^- coordinations may not occur. They suggested that the carboxylate-Au interaction is not the driving force for citrate adsorption, which was studied by computer simulation using the same conformation of citrate on a flat gold (111).[63] These contradictory results imply that the previously proposed citrate conformation needs to be altered. In addition, it has been proposed that the conformational change of surface citrate on AuNPs is induced by charge transfer,[86, 271] but the resistance of a single citrate molecule (three η^1-COO^- coordinations) for a single AuNP[271] is large by a factor of 10^5 than the measured and calculated value for citrate-AuNP film.[86] This inconsistency also indicates that the assumed conformation of the tridentate citrate binding (three η^1-COO^- coordinations) is not feasible.

2.3.2 Surface binding of free carboxylate groups of citrate

The binding of carboxylate has been demonstrated by change of pH[134] and electric field.[195,272] The proposed citrate conformation on a AuNP surface via the terminal and the central carboxylate groups is further supported by the binding of the free carboxylate group. The binding of the terminal carboxylate group of citrate adsorbed on the AuNP surface was induced through an increase of pH (Figure 2.7). First, the surface of citrate-AuNPs was functionalized with ω-terminated alkane or aryl thiols. The pH was adjusted to above 11 through addition of NaOH solution into the functionalized AuNPs. The thiol layer at each particle surface prevents an interparticle-type interaction of the free carboxylate group of the adsorbed citrate. The pH condition can lead to formations of either tridentate carboxylate coordinations (conformation IIa in Figure 2.7) or tetradentate hydroxyl/carboxylate coordinations (conformation IIb in Figure 2.7). Those structures were proposed based on IR analysis. New IR peaks at 2985, 2976, 1614, 1371, 1349, 1310, 1108, 1077, 825, and 583 cm^{-1} appear when the pH is higher than 11 for partially functionalized AuNPs with ω-terminated HOOC-Ph-SH and CH_3-C_{11}-SH thiols, respectively (Figure 2.8). Those peaks are not related to the thiols and should be associated with citrate molecules.

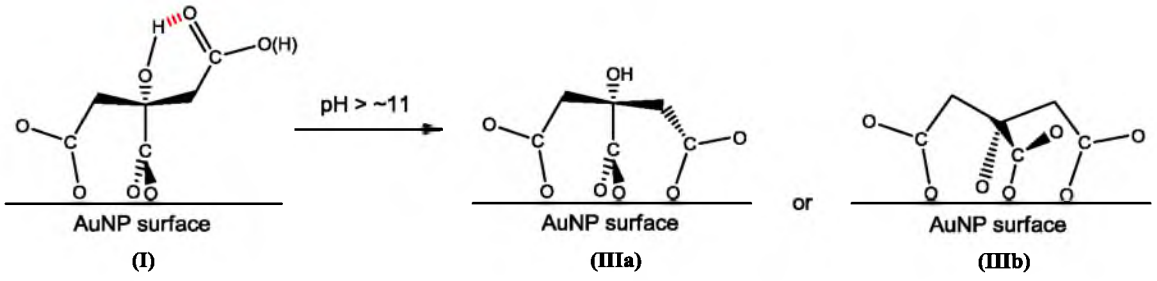

Figure 2.7. Binding of the free carboxylate group of adsorbed citrate on the Au surface when pH is higher than 11. Two different binding geometries are possible.

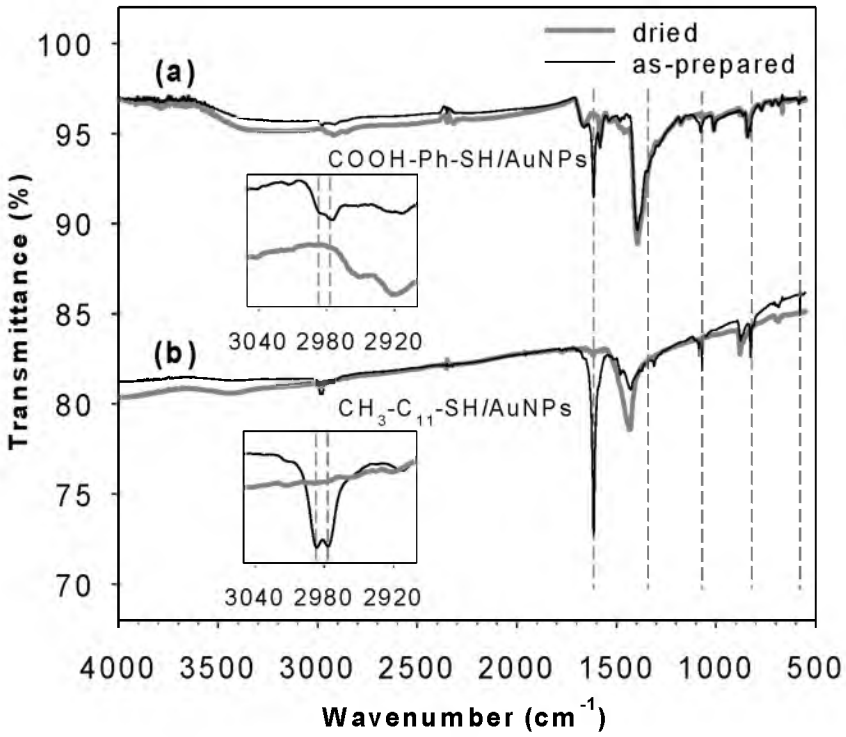

Figure 2.8. Transmission IR spectra of partially functionalized citrate-AuNPs by (a) HOOC-Ph-SH and (b) CH_3-C_{11}-SH thiols. The labeled bands (dotted lines) appear when the pH $> \sim 11$, which can be explained by the binding of the free carboxylate group of the adsorbed citrate.

IR data in this study is consistent with the proposed citrate configuration for the binding of the terminal carboxylate group. The CH_2 stretching is located at 2985/2976 cm^{-1}.[114,273] The peaks at 1108 and 1077[vi] cm^{-1} can be assigned to a C-C stretching[274] and/or a CH_2 wagging vibration,[73] which are newly exhibited after the pseudo-ring formation of the adsorbed citrate on the Au surface. The asymmetric/symmetric COO^- stretching vibrations at 1614/1371 cm^{-1} indicate a η^1-COO^- coordination. The relatively strong in-plane COO^- rocking[150,265,275-278] at 583 cm^{-1} can be correlated to the terminal COO^- coordination combined with an in-plane COO^- scissoring[277] at 825 cm^{-1}. When the

[vi]If this peak is assigned to $\nu_{(C-O)alch}$, the conformation IIIb is more plausible for the free COO^- binding. Note that $\nu(\eta^1\text{-}COO^-)$ at 1614/1371 cm^{-1} 1have been observed, but the central $\nu(\eta^2\text{-}COO^-)$ at 1558/1405 cm^{-1} were not detected.

other terminal carboxylate group binds to the AuNP surface, the adsorbed citrate may face a strain on the 2, 3-carbon skeleton with a larger C-C-C bond angle due to a surface-induced binding geometry limit between the carboxylate group and the surface gold atom. Conformation IIIa is a direct structural transformation from Conformation I via adsorption of the terminal carboxylate group, and Conformation IIIb also is possible after deprotonation of the hydroxyl group, which results in a common 5-ring formation with the hydroxyl and the central carboxylate groups. Both configurations are consistent with the assignments of the IR peaks shown under conditions of high pH. It was observed that the citrate-AuNPs prior purification and functionalization aggregate suddenly beyond pH 11 to pH 12. This is consistent with the report by Weisbecker et al.,[44] indicating the free COO^- binding likely occurs between pH 11 and 12. Overall, the intensities of the vibrational frequencies have been significantly enhanced upon coordination of all carboxylate groups.

The ethanol/ethoxy adsorbed on metal surfaces has a similar vibrational feature with the new peaks from citrate under conditions of high pH.[75] To eliminate possible contribution from adsorption of hydroxide, ethanol and/or its oxidative species in the peak assignments of the free carboxylate binding, ethanol-d_6 (CD_3CD_2OD) and NaOD were used in the functionalization and pH-adjustment procedure. New peaks of -OD, -OCD_2CD_3, and/or any oxidative species[279,280] including acetaldehyde -$OCCD_3$ and acetic acid -$OOCCD_3$ were expected after the deuteration step, but the peak shift was not observed (see transmission IR spectra of CH_3-C_{11}-SH functionalized citrate-AuNPs by use of EtOD-d_6/NaOD in the Appendix). Therefore, it was confirmed that the new peaks under the OH^- treatment were generated from the adsorbed citrate. The mechanism of the IR enhancement is not clear at this point.[281]

2.3.3 Configuration of surface citrate on AuNPs by intermolecular interactions

It is known that on a flat Au surface ω-carboxylalkenthiol forms a double layer by formation of carboxylic acid dimers.[100,282,283] Also, the studies of diacids by ^{1}H solid-state NMR revealed a formation of multilayers on zirconia and titania surface.[284] It is likely that the protonated citrate exhibits similar layer formation on AuNPs. Lee, Jeon and Dato et al. estimated a 2 - 3 molecular layer thickness of citrate on AuNPs with a spacing of 3.0 - 3.5 Å between layers by atomic-resolution TEM analysis.[91] The free carboxylic acid group plays an important role in a citrate 2-D monolayer by hydrogen bond.[57,87,251,285] In this study, a characteristic peak of the hydrogen bond by the carboxylic acid dimer centered at 1710 cm^{-1} was observed (Figure 2.9; see the Appendix for the entire spectral region). This verifies the presence of the intermolecular interaction between surface citrates.

Citrate-AuNPs were functionalized with ½ - ¼ stoichiometric amounts of alkanethiols relative to a monolayer coverage so that adsorbed citrate would be preserved on the remaining ½ - ¾ of the surface area on AuNPs. Purification of the citrate-AuNPs under

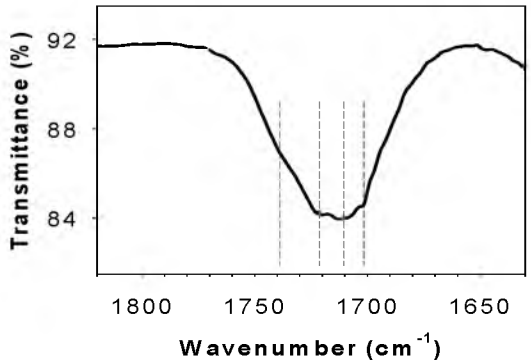

Figure 2.9. ATR-IR spectrum of citrate-AuNPs as prepared. Dotted lines act as guides for relevant peak positions of ν(C=O) frequencies from carboxylic acid dimers.

basic condition destroys the intermolecular hydrogen bond by deprotonation of the carboxylic acid of the citrate layers while use of ethanol or acidic water in purifying citrate-AuNPs results in irreversible aggregation of the AuNPs during repeated centrifugations and particle dispersion steps. In order to retain the original structure of the citrate layer under the rinsing step with EtOH, the adsorption of the alkanethiols on the citrate-AuNPs was used. Carboxylic acids are not deprotonated in ethanol in the absence of a base,[60] so the carboxylic acid dimers can maintain their hydrogen bonds during the EtOH rinsing step. Relatively long alkanethiols (CH_3-C_{11}-SH) were used, which do not interact with the carboxylic group of citrate and are long enough to protect the adsorbed citrate overlayers involving intermolecular hydrogen bond. By this purification method, physisorbed citrates and other decomposed species from the AuNP synthesis were removed, and the intermolecular interaction of the citrate layer on the AuNPs was investigated. Characteristic COOH dimer peaks at 1734 and 1704 cm^{-1} were observed in the partially alkanethiol-functionalized AuNPs, which verifies the formation of acylic and cylic COOH dimers,[138,192,286] respectively (see ATR-IR spectra of partially functionalized citrate-AuNPs by the alkanethiol molecules in the Appendix). It has been observed that addition of thiols leads to phase separation between the citrate layers and the adsorbed thiols rather than citrate displacement, and this leads to observation of original citrate layers. IR data in this study indicate that there are both thiol layers and hydrogen-bonded citrate layers. A detailed mechanism of ligand-exchange reaction on citrate-AuNPs will be discussed in Chapter 3 and another article.[287]

The AuNPs functionalized with ½ surface-stoichiometric amounts of thiols exhibit a relatively strong peak of the free $\nu_{asy}COO^-$ at 1593 cm^{-1} (inset, Figure 2.10A) with a peak of the -COOH hydrogen bond at 1704 cm^{-1}. The $\nu_{asy}COO^-$ at 1593 cm^{-1} is pronounced for

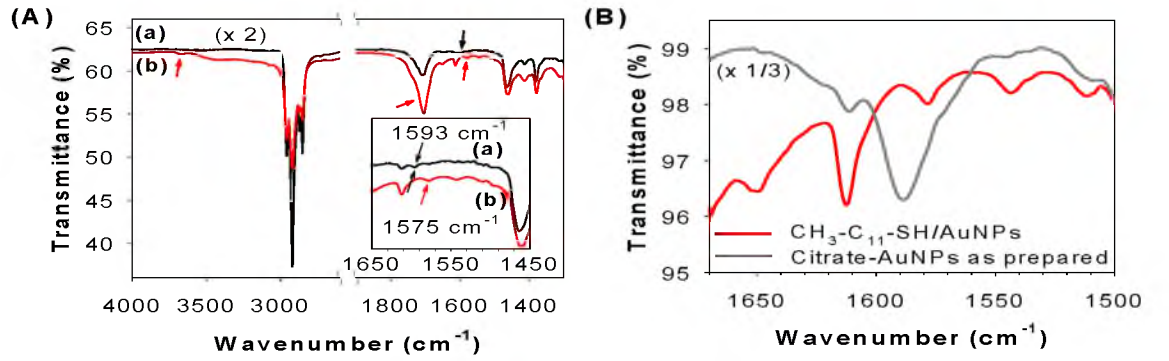

Figure 2.10. ATR-IR spectra of partially functionalized citrate-AuNPs by methyl-terminated alkanethiol (CH_3-C_{11}-SH thiol). (A) The amount of thiol added to the AuNP solution is adjusted to functionalize (a) half of the total surface area on AuNPs and (b) excess. The red-arrowed peaks at 3672, 1704, and 1575 cm^{-1} originate from organized citrate overlayers. (B) Comparison of as-prepared citrate-AuNPs before and after functionalization with CH_3-C_{11}-SH thiol at the frequency region of $\nu_{asy}COO^-$ vibrations.

as-prepared citrate-AuNPs before the addition of thiols (Figure 2.10B). On the other hand, when excess thiols were added to the AuNP solution, the peak of the COOH hydrogen bond at 1704 cm^{-1} became stronger, and the peak intensity of $\nu_{asy}COO^-$ at 1575 cm^{-1} was much enhanced (Figure 2.10A), which the latter can be associated with the dihydrogen citrate ($H_2Citrate^-$) that is deprotonated on the central carboxylic group. The $\nu_{asy}COO^-$ of monosodium malate, $HO_2CCH_2CH(OH)CO_2^-Na^+$, is observed at 1579 cm^{-1}.[114] The first deprotonation of citric acid occurs at the central carboxylic acid. However, the free terminal carboxylate group at 1593 cm^{-1} became indistinguishable by addition of excess thiols. Interestingly, a non-hydrogen-bonded $\nu(O\text{-}H)_{alch}$[288-290] at 3672 cm^{-1} has been detected (arrowed, Figure 2.10A). This correlation between the terminal carboxylate and the hydroxyl groups implies possible interaction by hydrogen bonds. Although the interaction of the α-hydroxyl group (e.g., the central hydroxyl group of citrate) the α-carboxylate group (e.g., the central carboxylate group of citrate) in α-hydroxycarboxylic acids is favorable,[291] the hydroxyl group of citrate probably interacts with the terminal

carboxyl group (see possible configurations of citrate molecules adsorbed on AuNPs in the Appendix). The $\nu(O\text{-}H)_{alch}$ peak does not originate from trapped EtOH in the AuNP sample. Other thiol-functionalized AuNPs did not exhibit this peak when EtOH was used as solvent. The alkanethiol layer may promote the formation of non-hydrogen-bonded hydroxyl groups of surface citrates through removing any contaminant of hydroxycarboxylate molecules from the surface during functionalization. The small peak at 3076 cm^{-1} is $\nu(O\text{-}H)_{COOH}$ resulting from interaction between carboxylic acid groups,[114] whereas the absence of the $\nu(O\text{-}H)_{COOH}$ of a free carboxylic acid typically at ~3520 cm^{-1},[61,292] is consistent with a lack of the carbonyl stretching of a free carboxylic acid at 1764 cm^{-1}. The characteristic $\nu_{asy}COO^-$ peaks indicative of the adsorbed citrate species still appear at 1611 and 1558 cm^{-1} regardless of the amount of the thiol used in functionalization. The $\nu_{sym}COO^-$ bands between 1410 and 1370 cm^{-1} are buried by strong CH_2 vibrations as well as C-O-H bending vibrations.

Figure 2.10B shows a comparison of the asymmetric COO^- stretching vibrations before and after addition of alkanethiols to the solution of citrate-AuNPs as prepared. The acidic pH condition was maintained during thiol functionalization due to the thiol proton, which leads to estimation of the nature of $COOH/COO^-$ interactions without deprotonation by NaOH. Notably, the peak at ~1590 cm^{-1} for citrate-AuNPs disappeared after the thiol addition. This indicates that the peak originates from the uncoordinated COO^- functional groups of surface citrates, because it was influenced by H^+ uptake from the formation of thiolates on the surface. The previous peak assignment in this study for the peak at 1593 cm^{-1} with $\nu_{asy}COO^-$ of the terminal carboxylate group of the adsorbed citrate is consistent with the intensity attenuation of that peak as the amounts of thiols for the functionalization of citrate-AuNPs increase. The $\nu_{asy}(\eta^1\text{-}COO^-)$ at 1611 cm^{-1} and

$\nu_{asy}(\eta^2\text{-}COO^-)$ at 1545 cm^{-1} remain constant since those COO^- are coordinated groups. The peaks at 1650 [293, 294] and 1510 [295] cm^{-1} are probably related to COOH-OOC interactions due to various hydrogen bond configurations since those peaks were not observed in the deprotonated condition for carboxyl groups at high pH.

The correlation between the 3672 cm^{-1} band of free $\nu(O\text{-}H)_{alch}$, the 1575 cm^{-1} band of $\nu_{asy}COO^-$, the 1593 cm^{-1} band of $\nu_{asy}COO^-$, and the 1704 cm^{-1} band of $\nu(C{=}O)_{COOH}$, indicates the presence of additional layer(s) interacting with the adsorbed citrate species. The incorporation of the second citrate species into the adsorbed citrate leads to the appearances of the liberated non-hydrogen-bonded $\nu(O\text{-}H)_{alch}$ at 3672 cm^{-1} and the noninteracting central $\nu_{asy}COO^-$ of the second citrate species at 1575 cm^{-1}. The terminal carboxyl group of adsorbed citrate at 1593 cm^{-1}, exhibiting the intramolecular hydrogen bond with the hydroxyl group, turns into the intermolecular hydrogen bond with the terminal carboxylic group of citrate in the additional citrate-layer. This results in the formation of the hydrogen-bonded -COOH at 1704 cm^{-1}, as well as the liberation of the hydroxyl group into non-hydrogen-bonded one at 3672 cm^{-1}. Thus, the intermolecular interaction of the citrate layer is mediated through the hydrogen bonds of carboxyl groups rather than hydroxyl groups. The hydroxyl group of citrate involves only the intramolecular hydrogen bond.

This correlation analysis for those IR bands is consistent with the proposed unit of a citrate trimer, consisting of two adsorbed and one dangling dihydrogen species (Figure 2.11A). The formation of the citrate trimer is associated with the ordered orientation of hydroxyl groups from the adsorbed and second citrate layers, which can generate the distinct peaks of the free $\nu(O\text{-}H)_{alch}$ at 3672 cm^{-1}. The citrate configuration in Figure 2.11A likely represents ideal building blocks of surface citrates on AuNPs. Figure 2.11B

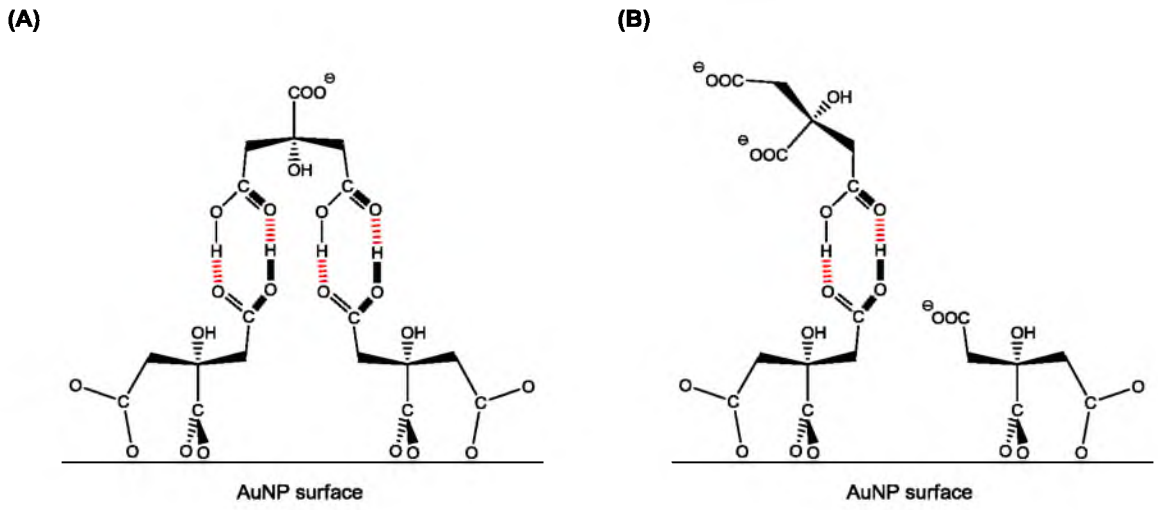

Figure 2.11. Proposed configuration of a unit of citrate trimer consisting of two adsorbed and one dangling species as building blocks of surface citrate on AuNPs. Intermolecular interactions are mediated by hydrogen bonds between terminal carboxylic acids. (A) Ideal organization leads to formation of a citrate bilayer; (B) A disrupted citrate trimer is associated with deprotonated terminal COO^- groups. Note that the terminal COO^- groups can interact with -OH groups through intramolecular hydrogen bonds.

illustrates a transition from the well-ordered citrate organization into disordered configuration, resulted from breakage of the intermolecular interaction between the terminal carboxylic groups by OH^- ions (see Section 2.3.1) or physisorbed alkanethiol layers. Not only can the alkanethiols be a source of protons during adsorption, but also can be a suppressor against -COOH hydrogen bonding between the surface citrates. This is consistent with the observation in that the peak 1593 cm^{-1} of the terminal carboxylate group is intense compared to the peak 1575 cm^{-1} of the central carboxylate group when the amount of added alkanethiol is less than a monolayer coverage on AuNPs. The citrate configuration in Figure 2.11B shows deprotonated terminal COO^- groups from both of the adsorbed and second citrate layers, which are accompanied with less pronounced hydrogen bonds between -COOH groups and possible interactions of the hydroxyl groups with the terminal COO^-. Complete removal of the second citrate layer by OH^- ions would

leave only the adsorbed citrate layer with deprotonated terminal COO^- groups behind on the surface, and related IR spectral features indicating this adsorbed citrate species were observed. Therefore, the proposed citrate configurations in Figure 2.11 are consistent with the IR bands of surface citrates, observed from addition of OH^- ions and alkanethiols to citrate-AuNPs.

An interesting consequence of the citrate trimer is the formation of a citrate bilayer. The citrate bilayer on AuNPs is different from that on gold nanorods with the cationic surfactant.[296] The former consists of the citrate trimer, i.e., two adsorbed species linked by one dangling citrate, whereas the latter forms through one closed-packed adsorbed monolayer interacting with the other outer layer. The outer negative charge from the central carboxylate of the second citrate layer may be the origin of the well-known electrostatic repulsion of the citrate-capped AuNPs.

2.3.4 Citrate trimers as building blocks on AuNP (111) surface

The citrate trimer was proposed as the building block on AuNP surface based on the IR analysis, but determination of the spacing between the two adsorbed species and organization of the citrate trimer on AuNPs are beyond the capability of analytical tools in this study. From the sharp C-H stretching of the adsorbed citrate, however, it was speculated that the surface citrate is well-organized on AuNP surface (see the C-H stretching vibration regions of ATR-IR spectra of citrate-AuNPs and trisodium citrate in the Appendix). Lee, Jeon and Dato et al. measured the citrate spacing of 3.0 - 3.5 Å on AuNPs by atomic-resolution TEM (see Figure 1.3B in Chapter 1).[91] Taking into account the distance between the α-carbons of carboxylic acid dimers (~6.2 Å), the angle of the COOH hydrogen bond plane from the AuNP surface is not steep. The layer spacing can

provide for an accurate direction of the terminal carboxyl groups. In this study, the spacing of the proposed citrate bilayer is defined as the distance between the central carbon of the adsorbed citrate on the Au surface and the central carbon of the second citrate layer because the electron density is expected to be the highest at the center carbons. Given spacing of the citrate layer to be 3.2 Å and the distance between the center carbons to be 7.4 Å, the COOH plane is oriented at an angle of ~25° from surface (Figure 2.12A). Furthermore, the full width at half maximum (FWHM) of the adsorbed citrate and the second citrate layer is approximately 1.5 - 1.7 nm in the intensity profile along a citrate-AuNP, which indicates that the conformations of both citrate species are not stretched out from the surface even though the FWHM values (1.5 - 1.7 nm) do not reflect directly the height of citrates due to less electron density on an edge of the small organic molecule. By using the conformation I as the adsorbed citrate (Figure 2.6), with the 25° angle of the terminal COOH orientation, specific directions of the terminal

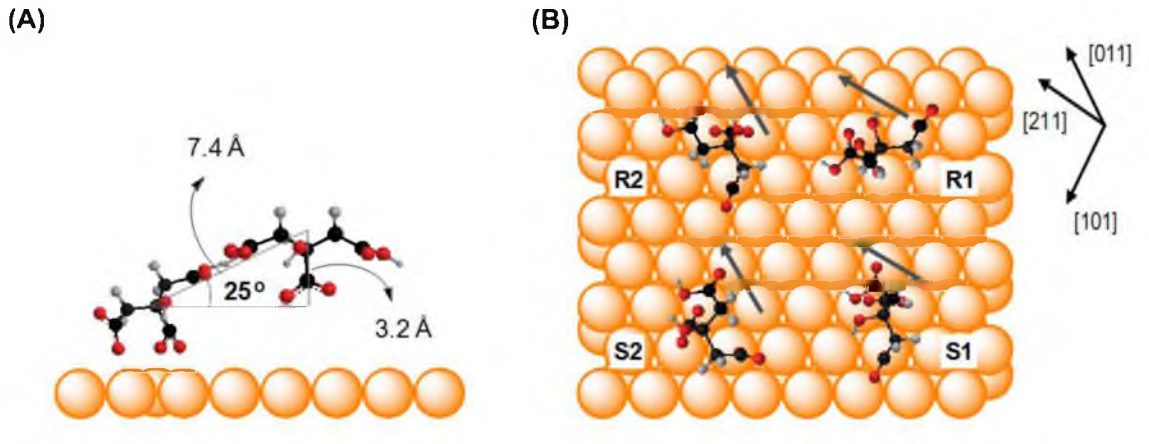

Figure 2.12. Geometric configurations of citrate adsorbed on Au(111). (A) Given a 25° angle of the terminal COOH from surface, (B) specific directions of the terminal COOH (grey-arrowed) are determined on Au(111) due to carboxylate coordination to the surface. R: R-enantiomers, S: S-enantiomers; there are two types of conformers of each enantiomer (1 and 2). Surface gold atoms are depicted as a space-filling model.

COOH are determined on Au(111) due to carboxylate coordinates to the surface, and four possible conformations were generated (Figure 2.12B; see a ruled-out conformation of adsorbed citrate due to van der Waals repulsion between the free carboxylic acid group and the CH_2 moiety in the Appendix). Although citrate is not a chiral molecule, R- and S-enantiomers, relative to the center carbons, are formed upon adsorption. The terminal COOH is oriented to the [211] direction for the R1 and S1 conformers whereas the [011] direction for the R2 and S2 conformers. Each conformer can rotate by 60^{o} on Au(111) surface.

On the other hand, citrate adsorption has been investigated on 2-D planar Au(111) surface by IR,[64,65] electrochemical,[25] simulation,[63] and STM[66] methods. The conformation of adsorbed citrate used for those studies on the Au(111) surface is based on the structure proposed by Nichols and co-workers,[65] for which all three carboxylate groups coordinate on surface. It can be pointed out that the experimental results associated with the citrate adsorption on the Au(111) surface do not contradict data in this study, and the proposed citrate conformation by Nichols and co-workers resulted from considering one symmetric COO^- stretch to be dominant. Floate et al. have observed the increased intensity of the COOH peak of citric acid at 1720 cm^{-1} on a Au (111) surface as the deprotonated citrates are adsorbed on the surface, but they realized that the COOH peak does not originate from an adsorbed citrate species.[65] This may suggest intermolecular interactions between the adsorbed citrate and the second citrate layer by COOH hydrogen bonds. Also, the small peaks around at 1611 and 1555 cm^{-1} have not been assigned,[64] but these peaks were observed in ATR-IR measurements in this study and the peaks were assigned to the η^1-COO^- and the η^2-COO^- coordinates, respectively. Kunze et al. determined that the electroadsorption valency number (formal partial charge

number) of citric acid adsorption, interpreted as the surface dipole, ranged from -1.5 to -2.5 at the most positive potential,[25] and this probably implies the binding of the free carboxylate groups of the adsorbed citrate. Teobaldi et al. mentioned that the carboxylate-Au interaction for the adsorption of citrate is not the driving force and the intermolecular interaction plays a role in formation of the citrate layers.[63] Lin et al. interpreted the bright spots as each carboxylate group of the adsorbed citrates,[66] but the resultant lateral size of the proposed citrate structure on the STM image is about twice as large as the real molecular dimension (see Figure 1.3A in Chapter 1). It is difficult to image carboxylate groups of one citrate molecule separately and unambiguously since they are close each other.[297] The STM image of the adsorbed citrate on Au(111) was interpreted in a different way and assumed the bright spot is an individual adsorbed species. Based on this assumption, a trimer unit can be identified as a building block for the organization of citrates. As a result, it is concluded the conformation of the citrate layer on 2-D flat Au(111) surface is identical to that found through spectroscopic studies for AuNP (111) surface.

The R1 conformer is best described with the STM image of the adsorbed citrates[66] in terms of the orientation of the hydrogen-bonded COOH groups (Figure 2.13). From the STM image on Au(111), a trimer unit was defined as a building block, which consists of three bright spots aligned to the [211] direction on Au(111) surface. The proposed citrate trimer in this study has been determined to match it with the orientation of the identified citrate unit of the STM image. The configuration of dangling citrate species ($H_2Citrate^-$) in the second citrate layer was obtained from one of the most stable conformations by ChemBio3D, having both terrminal COOH be parallel to each other. However, the orientation of the central COO^- group, i.e., pointing toward the metal surface or pointing

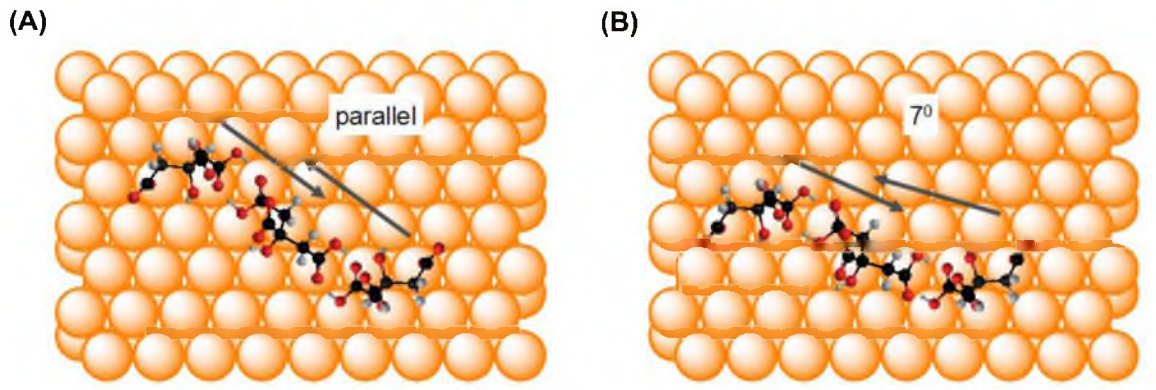

Figure 2.13. Proposed adsorption structures of citrate trimers on Au(111) surface. (A) The configuration having both hydrogen-bonded COOH parallel to each other is dominant in the STM image (B) whereas the one with the orientation of both COOH groups slightly off from the parallel configuration is minor. The grey arrows represent the orientations of -COOH hydrogen bonds at the terminal carboxylic acids.

outward, is not clear. The direction of both hydrogen-bonded COOH is parallel each other in most trimers of the STM image (Figure 2.13A), but a slight deviation from this orientation also was observed, which leads to determination about the angle difference of the hydrogen-bonded COOH as ~7° (Figure 2.13B).

In the proposed formation of the citrate trimer that is consistent with the STM image, the dangling citrate species interacts with two adsorbed citrates. Although glutamic acids stabilized at ~4.6 Å above a silver surface without being in direct contact with the surface have been imaged in STM,[298] it is not straightforward to determine whether a dangling citrate species is visible in STM imaging, and thus calculations and/or simulations are necessary.[299] From the geometry-based modeling, an additional citrate adsorbed between the two adsorbed citrates was found (R1 configurations), which binds to the surface through η^2-COO^- coordination, cannot interact through hydrogen bonds between the terminal carboxylic acid groups due to a surface-induced limitation of carboxylic acid orientation (see configurations of the mediating citrate species and two adsorbed citrate

molecules in the Appendix). While the orientation of the two carboxylic acid groups of the adsorbed citrates is parallel each other (Figure 2.13A), the direction of two terminal carboxylic groups of the mediating citrate species is deviated by ~60° from a parallel configuration (see the Appendix). This combination for a citrate trimer, i.e., three adsorbed citrates, is not commensurate on the surface. The only configuration of a mediating citrate species, whose terminal carboxylic acid groups are oriented parallel to each other, is through a η^1-COO^- binding with OH-coordination, but this conformation is not feasible due to van der Waal repulsion between the terminal COOH and the uncoordinated oxygen atom of the central η^1-COO^- group (see the Appendix). Therefore, the presence of the dangling citrate species is plausible in the formation of the citrate trimer. Notably, the interaction of the two hydrogen bonds of the free carboxylic acids is far stronger (total ~28 kcal/mol; ~7 kcal/mol per hydrogen bond of carboxylic acid dimers at room temperature) [300 - 303] than the single carboxylate-Au interaction (~2 kcal/mol).[304] In this case, the intermolecular interaction predominates the molecule-metal interaction.

2.3.5 Assembly of citrate trimers on a Au(111) surface

In order to assess the feasibility of the assembly of the citrate trimer, a geometric modeling was used. From the STM image of the surface citrates on the 2-D Au(111) surface,[66] the periodicity of the imaged pattern was adapted and adsorption of the citrate trimers on Au(111) was simulated based on geometrical consistency. Heinz and co-workers concluded that molecular adsorption is governed by molecular size and geometry rather than specific interfacial chemistry, investigated by molecular dynamics simulation for adsorptions of single amino acids and surfactant molecules on Au(111).[19] In this

modeling, the geometric coordination of the adsorbed citrate species also was considered with respect to the direction and spacing of the top lattice of the Au(111) surface, and other parameters including water solvent, additional anions/cations,[vii] surface stress,[305] and surface charges could not be taken into account.

The citrate trimers (Figure 2.13A) were used as building blocks for the citrate assembly on Au(111) surface with the gold atom spacing of 2.88 Å.[306] The surface reconstruction that is usually generated by adsorption of molecules,[307,308] as well as possible effects of the second/third atomic metal layer on molecular adsorption[19] were not considered. Lin et al. determined the unit cell parameter with 1.00 nm, 1.15 nm, and 90°, but the actual angle is 84° - 86° with deviation on the [110] direction as ±2°. The angle deviation probably indicates the surface reconstruction. On an ideal Au(111) surface, building the assembly of the citrate trimers was successful (Figure 2.14; see the model of citrate assembly overlapped on the STM image of adsorbed citrates on the gold surface in the Appendix), with all unit cell parameters consistent with the STM image except the length parameters are increased by one gold atom distance. The cell parameter (a) on the [110] direction is defined as the number of gold atoms. For the model of the adsorbed citrate on Au(111) there are five gold atoms along the perimeter (a), which results in a length of 1.44 nm ($5a_o$ = 14.4 Å where a_o = 2.88 Å). It was tried reducing the perimeter (a) by the dimension of one gold atom to 1.15 nm, but the angle parameter (γ) changes to 90° and the CH_2 moieties encounter each other (see the organized pattern of the citrate trimers with the identical cell parameters to the reported values in the Appendix). It may be possible that the scale bar in the STM image of the citrate organization may be

[vii] Bridged interactions between Na^+ ions and COO^- groups on surfaces: Heinz, H.; Farmer, B. L.; Pandey, R. B.; Slocik, J. M.; Patnaik, S. S.; Pachter, R.; Naik, R. R. *J. Am. Chem. Soc.* **2009**, *131*, 9704-9714.

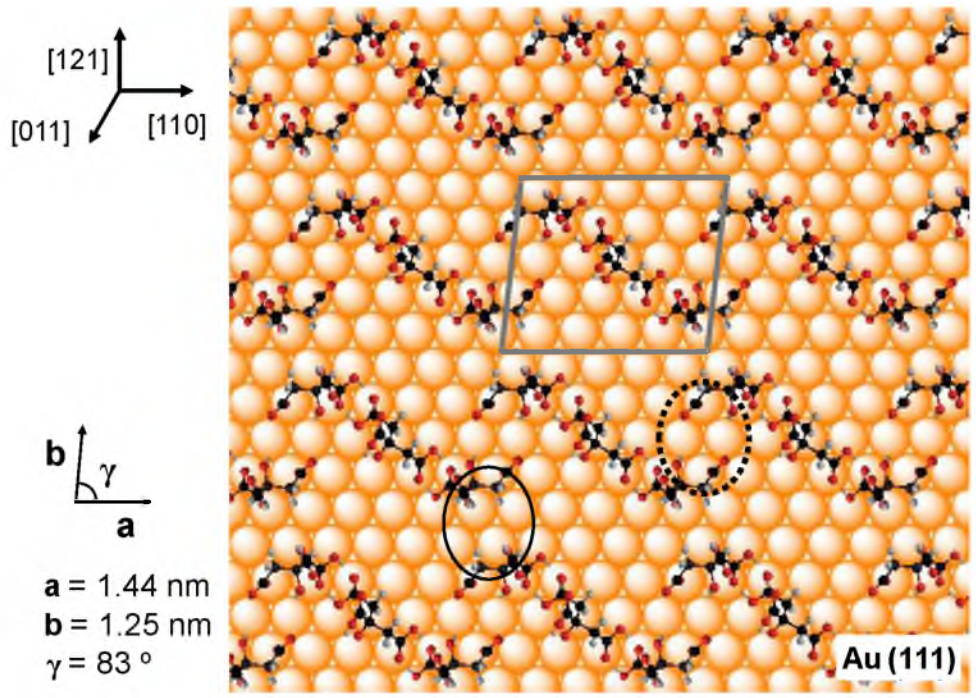

Figure 2.14. Assembly of the citrate trimers on (111) surface of AuNPs. The circle and the dotted circle represent van der Waals interactions of CH_2 moieties and possible hydrogen bonds, respectively. The parallelogram represents a unit cell (area: 179 $Å^2$).

inaccurate. The other length parameter (b) of the unit cell is 1.25 nm ($\sqrt{19}a_o$ = 12.5 Å), and the angle (γ) of the unit cell is 83°. The area of this unit cell is 179 $Å^2$. The distance of the adjacent adsorbed citrate involving possible hydrogen bonds is 7.0 Å ($1.4\sqrt{3}a_o$ = 7.0 Å), whereas the distance between two adsorbed citrates in the trimer unit is 12.9 Å. Interestingly, it was found from the model that the CH_2 moieties are close with a spacing of 5.5 Å ($1.1\sqrt{3}a_o$ = 5.5 Å), which probably implies a contribution of van der Waals interactions as a driving force of the citrate assembly. Due to the citrate-Au surface interaction, the spacing of the CH_2 moieties of the adsorbed citrates is larger than that of the optimized van der Waals interaction (4.2 - 4.6 Å).[306,309-312] Glutamic acdis on Ag(100) can be separated by 5.4 Å in a upstanding configuration.[313] It was reported that there is a net attractive force between two methane molecules in water for separated distances

between 4.2 and 7.8 Å, investigated by molecular dynamics simulations.[314] Thus, van der Waal attraction of the citrate CH_2 moieties can occur in the distance of 5.5 Å.

2.3.6 Preferential bridging coordination of carboxylate groups predicted by simulation

The binding of the central carboxylate group of the adsorbed citrate binds to the gold surface through bridging coordination rather than chelating coordination was investigated with aid of similar modeling of the citrate assembly on Au(111). When the bridging configuration of the adsorbed citrate changes to the chelating configuration, the direction of the free carboxylic acid group of the adsorbed citrate is deviated by ~15° from that of the bridging conformation with respect to the lattice direction of the Au(111) surface (see citrate conformations and assembly with chelating η^2-$COO^-_{central}$ coordination of adsorbed citrate in the Appendix). The 15°-rotated R2 conformer in Figure 2.12B exhibits the orientation of the free carboxylic group close to the [211] direction that represents the orientation of the intermolecular hydrogen bonds between surface citrates. Based on the assembly modeling with the same unit cell on Au(111), it was found that adsorbed citrate species are located within van der Waals repulsion and intermolecular interactions between adsorbed citrates are not feasible (see the Appendix). Oxygen atoms of the uncoordinated η1-COO^- conflict with the CH_2 fragments, and the hydroxyl groups that are the only available moieties for hydrogen bonds are too far to interact with each other (O···O: ~4 Å). Therefore, it was demonstrated that the binding geometry of the central carboxylate group of the adsorbed citrate is bridging coordination, rather than chelating coordination. The preferred bridging coordination was also suggested by others.[57,88,122.257] Recently, the structures of single molecules adsorbed on metal surfaces have been

investigated using DFT calculations, but these computational approaches may not be accurate to predict molecular conformation governed by strong intermolecular interactions. Under certain circumstances in which intermolecular interactions significantly affect molecular assembly on metal surfaces having high surface energy, the simple simulation without computation can be an effective method to understand the configuration of molecular adsorption. Not only can the geometry-based simulation suggest detailed intermolecular interactions, but also it can predict specific coordination of adsorbed molecules with being influenced by intermolecular interactions since there is a direct correlation between molecular assembly and molecular conformation on a metal surface.

2.3.7 Formation of citrate bilayers on AuNPs

Bilayer formation of surface citrate on AuNPs was suggested by the modeling and results from the literature. Figure 2.15 shows the citrate bilayer formation consisting of

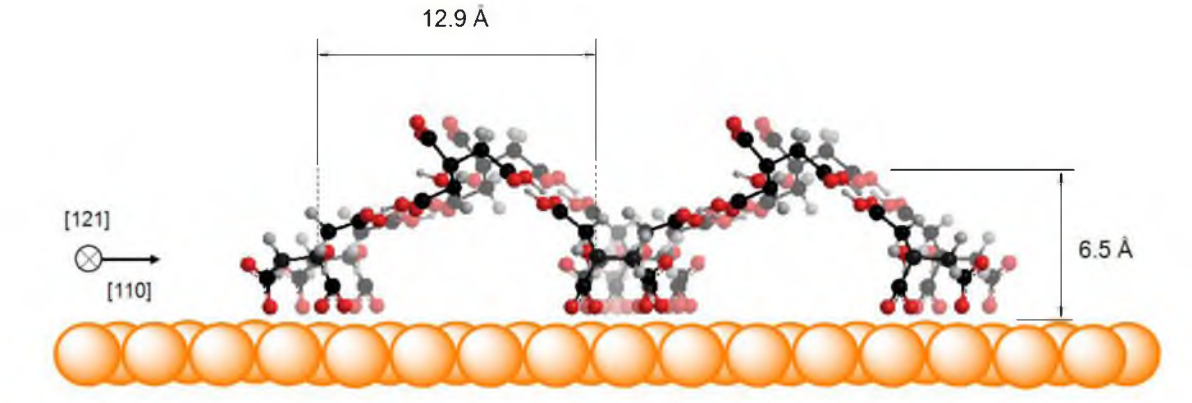

Figure 2.15. Formation of citrate bilayers on (111) surface of AuNPs. Citrates in direct contact with the surface are the first layer whereas dangling citrates between two adsorbed citrates are the second (outer) layer. Bilayer thickness is ~6.5 Å, and the spacing of the adsorbed citrate is 12.9 Å.

the citrate trimers. It is considered that the adsorbed citrate species in direct contact with the AuNP surface are parts of the first layer and the dangling citrate species hydrogen-bonded with two adsorbed citrates of the first layer are parts of the second (outer) layer. Projection of electron beams for TEM onto this side likely provides enough contrast between the two layers (with spacing of ~3.2 Å), due to regular molecular orientation and low electron density in the hydrogen-bonding terminal carboxylic groups, as was imaged by TEM and subsequent image process for atomic resolution.[91] This bilayer configuration is unexpectedly unique, because multilayer formation can be predicted for hydroxyl triacid citrate molecules. Mulvaney and Giersig[315] estimated the thickness of the citrate layer on AuNPs as ~5 Å with directly measuring the interparticle spacing of the closely-packed NP 2-D array at a positive voltage. This value is comparable with the thickness of the citrate bilayer in this study, measured from the top metal surface to the center carbon atom in the second citrate layer (~6.5 Å). The applied potential may contract the citrate bilayer. The simulation for the assembly of surface citrates suggests not only the bilayer formation and its thickness but also specific orientations of the central hydroxyl and carboxylate groups in the outer layer. This proposed layer configuration at the molecular level may open detailed studies about the effects of molecular conformation and adsorption in the electrical double layer on AuNP surfaces. In addition, the behavior of the central carboxylic group in the outer layer may play an important role in interparticle-type interactions between citrate-AuNPs in solution.

2.3.8 Self-assembled layers of polymeric citrate chains on AuNP (111) surface

The distance for the van der Waals interaction of the citrate CH_2 groups is 5.5 Å on Au(111), which is not optimized, so it is speculated that the hydrogen-bonds involving

the carboxylic group and water form to stabilize the adsorbed citrate species. However, O-H stretching vibrations from cluster-like water have not been observed, which might be located at the regions indicating possible hydrogen-bonds. This led to a proposal for another basis for self-assembled layers of citrate molecules, in which the terminal carboxylate groups form -COOH hydrogen-bonds instead of binding to the surface by η^1-COO^- coordination (Figure 2.16A). The distance (7.0 Å) between the two carboxylic acids of the adjacent adsorbed citrates is optimized for hydrogen bonds through dimeric COOH groups (6.9 Å).[viii]

The configuration of two adjacent adsorbed citrates interacting through the -COOH hydrogen bond may imply the presence of possible ionic hydrogen bonds, i.e., COOH···OOC interactions. The peak at 1611 cm^{-1} previously assigned as $\nu_{asy}(\eta^1\text{-}COO^-)$

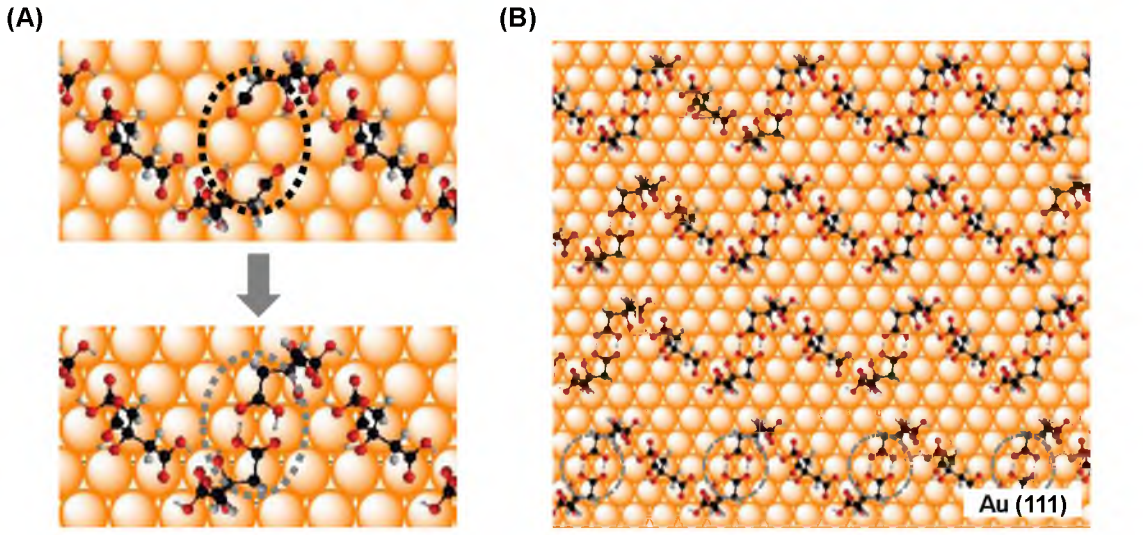

Figure 2.16. Polymeric citrate chains mediated by COOH hydrogen-bonds. (A) Configuration of noninteracting adsorbed citrates (top) is modified to hydrogen-bonded ones (bottom). Note that the positions of citrates are identical, but the terminal η^1-COO^- changed to hydrogen-bonded COOH (dotted circles). (B) Proposed citrate self-assembly through the resulting configuration of polymeric 1-D chains on Au(111) surface.

[viii]The length was determined for a dimer of acetic acids by ChemBio3D.

can also be an asymmetric stretching vibration of carboxylate groups from COO···H···OOC interactions.[316] For this ionic hydrogen bond, the length between the two oxygen atoms interacting with the hydrogen atom is reduced by 1.5 - 2.0 Å from normal carboxylic acid dimers,[317,318] and this subtle bond contraction is difficult to be determined from this modeling. In the deuterated complexes having COO···D···OOC interactions, the carboxylic acid (-COOD) shifts to higher frequencies[319] and the carboxylate species ($^-$OOC-) shifts to lower frequencies since the deuterium is bonded to the oxygen atom more closely than the hydrogen.[317] In the deuterated condition in this study, however, the $\nu_{asy}(COO^-)$ shifted to the higher frequency at 1620 cm^{-1}, and the carbonyl stretching vibration of -COOD at a higher frequency has not been observed. Therefore, it was concluded that the peak at 1611 cm^{-1} originated from the η^1-COO^- coordination as previously assigned in this study.

In general, hydrogen bonds are not observed in STM imaging due to low electron density,[320] and the STM image analysis cannot confirm this hydrogen-bonded citrate molesules. However, Nichols and co-workers[64,65] observed the strong $\nu_{sym}(\eta^2\text{-}COO^-)$ and $\nu(C{=}O)_{COOH}$ peaks for citrate adsorption on gold surfaces, and this probably represents the configuration of polymeric citrate chains shown in Figure 2.16B since only the central carboxylate groups bind to the surface by the η^2-COO^- bridging coordinate (i.e., dihydrogen citrate $H_2Citrate^-$) and terminal carboxylic groups participate in the -COOH hydrogen bonds. AFM force measurements demonstrated the presence of a citrate network on a planar gold surface, possibly due to intermolecular hydrogen bonding.[23] Another AFM force measurement for citrate layers between a AuNP and a planar gold substrate suggested a neutral hydrogen-bonded network consisting of dihydrogen citrate molecules due to the low charge density and possible multilayer adsorption on the

surface.[321] Consequently, the building block of the self-assembly of surface citrates can be the citrate 1-D chain formed by hydrogen bonds between terminal carboxylic acid groups. Pseudo-polymeric behavior of citric acid was observed in aqueous solution.[322] The assembly of the citrate chains is driven by van der Waals interactions between the methylene fragments of the adsorbed citrate species.

The formation of the 1-D chain network of the surface citrate during the synthesis of the NPs is probably favorable due to the configurational versatility[317,318] of the carboxyl-based hydrogen bonds. Ionic hydrogen bonds through COOH-OOC interaction are also possible, and the strength of this type of hydrogen bonds (low barrier hydrogen bonds) is very strong.[323] It was reported that carboxylic groups of benzenetricarboxylic acids are deprotonated at 420 K and the COOH-OOC hydrogen bonds are formed.[324] The surface citrates may possess the ionic hydrogen bonds of carboxylic groups during the synthesis of AuNPs at ~100 ^{o}C (see Figure 2.10B). Formations of carboxylic acid dimers[325,326] and clusters[327] in aqueous solution were demonstrated although there were opposed results reported.[328,329] Due to adsorbed citrate species on surfaces during the synthesis of AuNPs, the transformation to the citrate network within the electrical double layer[330] on the AuNP surfaces is feasible. The driving forces for molecular assemblies[331] of citrate were proposed as van der Waals interactions (-CH_2-···-CH_2- interaction: 0.8 kcal/mol, determined for alkanethiols on gold surfaces)[332] and hydrogen bonds of carboxylic acid groups. Due to the weak nature of carboxylate-Au interaction, it is plausible to conclude that the citrate adsorption is driven by the intermolecular interactions and the molecule-surface interaction is of secondary importance.[63] In order to promote the intermolecular interactions of the surface citrates, it is necessary for the citrates to diffuse on Au surfaces since the carboxylate group does not readily adsorb on Au as it does on silver and

copper.[262] The nature of the COO-Au is partly ionic,[262] and COO^{-}[333] rather than -COOH[334] binds on Au(111). The adsorption of trimethylacetic acids (TMAA) on TiO_2(110) surface has been studied in detail at a molecular level. TMAA diffuses on the surface with physisorbed state by COOH binding, and the chemisorbed TMMA species after O-H cleavage do not diffuse at room temperature and form a long-range ordering.[335] A similar mechanism can be applied for the adsorption of the surface citrates on Au surfaces. The adsorbed citrates prior to the central COO^{-} binding to surface probably diffuse on surface for maximum intermolecular interactions, and the central COO^{-} binds to the surface once the favorable molecular interactions are achieved. It was reported that diffusion plays an important role in SAMs of cystein adsorbed on Au(111).[336]

2.3.9 Citrate polymeric chains as building blocks on other facets of AuNPs

The Au(111) surface is the most populated facet in a large AuNP[140] due to having the lowest surface energy,[337] and there are other facets including Au(110) and Au(100) for the face-centered cubic structure in the truncated octahedron of large-sized AuNPs (> 10 nm).[140,338] The 1-D citrate chain unit was adapted to Au(100) surface to investigate the possibility of the citrate chain as a building block on Au(100), and the same configuration of the citrate chain on Au(110) was used since it can be assumed that the geometry deviation of the adsorbed citrate is negligible between Au(110) and Au(100). Surprisingly, the citrate configuration was also fit to these crystal lattice surface of Au(110) and Au(100) with the same van der Waals and hydrogen bond interactions (Figure 2.17). The two oxygen atoms of the central carboxylate group likely bind to two adjacent gold atoms on the [110] direction on Au(110) as was demonstrated by DFT calculation for malic acid on Cu(110).[339] Intervals between adjacent adsorbed citrates are

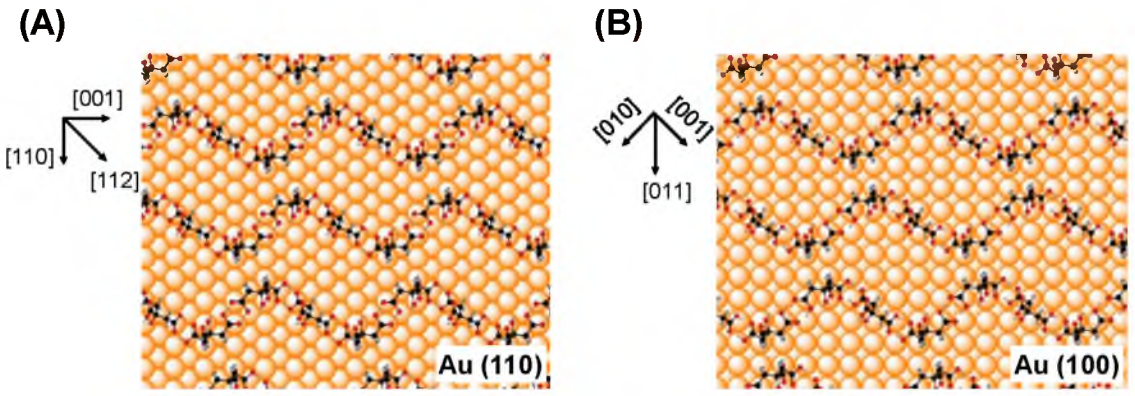

Figure 2.17. Proposed self-assemblies of citrate on (110) and (100) surfaces of AuNPs.

identical between Au(110) and Au(100) surfaces due to the adsorption onto the direction of the same lattice spacing of gold atoms. In other words, the adsorbed citrates with the same molecular symmetry are aligned along the [110] direction on Au(110) and the [011] direction on Au(100), and the spacing of gold atoms for both directions is 2.88 Å. The distance of the CH_2 moieties between the adjacent adsorbed citrates ($2 \times a_o$ = ~5.8 Å; a_o = 2.88 Å) can bring about van der Waals attraction. The distances between the two α-carbons of the dimeric COOH groups in the adjacent adsorbed citrates are ~6.6 Å for the Au(110) surface and ~7.1 Å for the Au(100) surface, and the angles of unit cells are ~70° for Au(110) and ~62° for Au(100). Interestingly, the distance of the dimeric COOH groups is more commensurate on Au(111) (7.0 Å) than on Au(100) (7.1 Å), and this size match may be related to the stronger adsorption of citrate on Ag(111) than on Ag(100).[340] The adsorption configurations, which the COOH hydrogen bonds between adjacent adsorbed citrates are broken and the terminal carboxylic acid groups bind to the gold atoms through η^1-COO^- coordination, are also commensurate on the gold surfaces (see proposed citrate adsorptions on Au(110) and Au(100) surfaces in the Appendix). Obtaining STM images of citrate adsorptions on the Au(110) and Au(100) surfaces

would verify the self-assembly through the polymeric chain network. This is an example of a building block on one facet fitting to another. It has been reported that the self-assembled uracil on Au(111) exhibits the identical packing model on Au(100).[341] In addition, the estimated thickness of the citrate bilayer in Figure 2.15 (~6.5 Å) is expected to be uniform on entire AuNP surfaces.

From the simulation of the citrate self-assembly on the two facets of Au(111) and Au(100) surfaces, it was concluded that the stabilizing effect of citrate on AuNPs is more pronounced on (111) surface than (100) surface due to the size commensurate with the hydrogen-bonded network of the molecular adsorption. This led to suggestions of a facet-depended stabilizing role of citrate adlayers for irregular-shaped nanoparticles including nanorods, nanoplates, branched and pentagonal/hexagonal-shaped nanoparticles. Previously, only the reducing role of citrate[342] has been discussed in the proposed growth mechanisms for nanorods,[343,344] branched[345] or pentagonal/hexagonal[346] nanoparticles produced by seed-mediated growth approaches as well as nanoplates[347] prepared by a conventional synthetic method. In those mechanisms, the stabilizing role of citrate depending on different facets has been neglected, probably due to lack of understanding detailed configuration of surface citrate. Instead, preferential bindings of other surfactants such as CTAB (cetyltrimethylammonium bromide), SDS (sodium dodecyl sulfate), and PVP (poly(vinyl pyrrolidone)) on Au(100) or Au(110) surfaces were suggested as main driving forces, leading to nanocrystal growths onto Au(111) surface. The simulation result of the weaker adsorption of citrate on Au(100) is consistent with the surfactant bindings on the Au(100). Citrate adsorption through hydrogen-bonded self-assembly is strongest on Au(111) among AuNP facets, and this cannot be explained by the previous growth mechanism onto the (111) lattice. Herein, it can be proposed that the high

crystalline interface of the citrate/Au(111) lead to the crystal growth onto this surface. The better organized interface likely induces a metal crystallite surface. It should be mentioned, however, that more complicated factors may govern the nanocrystal growths, including a pH-effect[4] by ascorbic acid added additionally in the seed-mediated synthetic methods above. Chloride ions, which are introduced during the AuNP syntheses, are known to have a little effect on the shape of growing nanoparticles.[348,349]

2.3.10 Thickness measurement of the citrate bilayer on AuNP surfaces

Experimental measurement of the thickness of the citrate layer was attempted. Alkanedithiols (HS-$(CH_2)_n$-SH, n = 3, 4, 5, 6, 9, 11) were used as molecular linkers for AuNP aggregation. Since one thiol group of dithiols bind to a metallic surface of a single AuNP and the other thiol can bind to that of another AuNP, dithiols can act as molecular linkers to connect two different AuNPs.[350] When the hydrocarbon length of a dithiol is long enough for both sulfur atoms to adsorb on two different AuNPs, NPs are expected to be aggregated in solution beyond van der Waal repulsion from the citrate layers of two different NPs (interparticle-type adsorption). When the hydrocarbon length of a dithol is too short for both sulfur atoms to bind surfaces of different NPs simultaneously due to van der Waals repulsion from the citrate layer, AuNPs can remain as single NPs in solution without aggregation (intraparticle-type adsorption). Although both sulfur atoms of alkanethiols can bind to a surface (lying-down configuration),[351] there are some populations of dithiols with only one sulfur atom adsorbed on the surface (upright configuration) at a high concentration of the dithiol.[352] Interestingly, the length-dependent stability of AuNPs was observed as predicted. Figure 2.18 shows dispersion stability of AuNPs in solution upon addition of dithiols with varied alkane chain lengths. When the

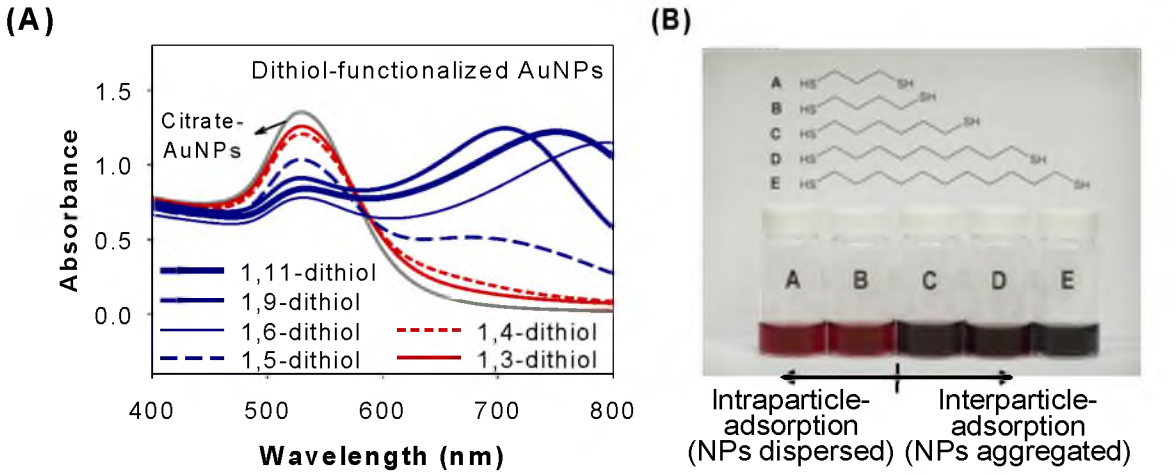

Figure 2.18. Molecular length-dependent stability of citrate-AuNP upon addition of alkane-dithiols with varied hydrocarbon length. (A) UV-Vis absorbance spectrum of citrate-AuNP in solution by addition of dithiols, and (B) pictures of the AuNP solutions showing a drastic change of AuNP stability due to dithiol length-dependent interparticle interactions. NP aggregation is governed by interparticle-type connection through dithiol adsorption.

length of alkanedithiols is short (for n = 3, 4), NPs are not aggregated and remain dispersed in solution. This produces the characteristic reddish color of stable AuNPs. When the length of alkanedithiols is long (for n = 5, 6, 9, 11), however, NPs exhibit aggregation characterized by the bluish color of aggregated AuNPs. Possible effect of alkanedithiol concentration on AuNP aggregation [353] was excluded by a control experiment, which the same result was observed upon reducing the concentrations of long dithiols (n = 5, 6, 9, 11) by half. This confirms that direct adsorption of alkanedithiols on AuNPs through the Au-S interaction govern the stability of AuNPs upon addition of the linker molecule.

Based on the length-dependent interparticle interaction, thickness of the citrate layer in solution could be estimated. It was assumed that the electrostatic repulsion from the citrate layer becomes shielded completely under the high concentration of dithiol solution

(1 mM) and only van der Waals repulsion from the outer layer of surface citrate plays a role in the NP stability. The length of the citrate layer falls between the lengths of 1,4-dithiol and 1,5-thiols. Given the Au-S bond length to be 2.85 Å and the tilt angle of adsorbed alkanethiols to be 30^{o} to normal with respect to a AuNP surface, calculated interparticle spacing is 11.6 Å for 1,4-dithiol (n = 4) whereas 12.5 Å for 1,5-dithiol (n = 5), which this measured thickness of each citrate layer (~6 Å) is in excellent agreement with estimated thickness of the citrate layer based on the model (~6.5 Å). Therefore, the measured thickness is consistent with the model of the citrate bilayer conformation in AuNP solution. Grieser and co-workers demonstrated the existence of uncharged surface species on citrate-AuNPs, and they also measured the barrier size for surface citrates to be 10 ± 2 Å in acidic pH and 7 ± 2 Å in basic pH, respectively.[8] This can be related to the formation of citrate bilayer proposed in this study, adding the size of hydrated sodium ions above the thickness of the citrate layer. In basic pH, the dangling citrates are removed from the adsorbed citrates, which can have the layer thickness of 7 Å, i.e., the sum of the thicknesses of the adsorbed citrate and the hydrated sodium ion. A similar analysis is also possible for the barrier value of 10 Å in acidic pH with the model of the citrate bilayer.

2.3.11 Coordination of oxygen atoms of carboxylate groups at bridged sites

In most cases, atop locations[88,119,120,123] of oxygen atoms of carboxylate groups are considered for bridging coordination on gold surfaces, but the binding of oxygen atoms in bridged sites[126] has been suggested by STM studies of benzoate adsorption on Au(111). Also, Heinz and co-workers proposed that the oxygen atoms of carboxylate groups in amino acids are located at bridged sites on Au(111) where the polarizable atoms are

drawn into the bridged sites (attractive epitaxial sites) having deep potential wells due to the high surface energies of the metal.[19] For the modeling of citrate adsorption, it is not possible to distinguish binding locations of oxygen atoms between atop and bridged sites (see the Appendix) since the entire adsorption pattern can be translocated from atop positions to bridged ones. Nonetheless, it was demonstrated from this study that the COO^--coordination at the bridged sites of gold surfaces are feasible for citrate molecules.

2.3.12 Chirality of the self-assembled layer of citrate on AuNP surfaces

In general, the adsorption of molecules on solid substrates is governed by molecule-surface and intermolecular interactions.[354] It has been reported that organic molecules are self-assembled on a surface by maximizing intermolecular van der Waals interaction[354] whereas carboxylic acids are stabilized through hydrogen-bonds.[355] Interestingly, only the R conformation (R1 in Figure 2.12B) can generate the self-assembled pattern that describes the STM image. This observation does not necessarily mean that the S conformers do not participate in the self-assembled citrate layer on AuNPs. The mirror-imaged pattern on Au(111) with only S conformers also can be built (S1 in Figure 2.12B; see chiral self-assembly of surface citrates on Au(111) with R and S enantiomers in the Appendix). The similar chiral assembly of achiral molecules upon adsorption on a metal surface was reported.[251,356,357] It has been demonstrated that adsorption of one chirality induces the adsorption of homo-chirality,[ix,354,358,359] and intermolecular hydrogen-bond interactions play an important role in chiral self-assemblies[360] on Au(111).[361] In this study, it also can be suggested that there are strong intermolecular interactions on the

[ix]The organization of racemic malic acids on Cu(110) leads to heterochiral 2D phases. See: Roth, C.; Parschau, M.; Ernst, K.-H. *ChemPhysChem* **2011**, *12*, 1572-1577.

chiral self-assembly of citrate molecules.

2.3.13 Surface coverage of citrate adsorbed on AuNPs

The area of the adsorbed citrate on AuNPs was estimated, based on the proposed model. The unit cell area is 179 $Å^2$ on Au(111), and the dimension of one adsorbed citrate is ~28 $Å^2$, so the surface coverage by the adsorbed citrates is 1.86×10^{-10}mol/cm^2. Note that the pattern of the citrate adsorptions are similar to Au(110) and Au(100), which are the most populated facets along with Au(111) on AuNPs. With including the free citrates in the second layer, the surface coverage by the citrate trimers is ~2.8×10^{-10}mol/cm^2 (~45% coverage). This relatively low coverage of surface citrate on AuNPs is consistent with the speculation by Nelson and Rothberg, based on their investigation of DNA adsorptions on citrate-AuNPs.[362] Using an electrochemical method, Kunze et al. determined citrate coverage at pH 3 on Au(111) as 4.6×10^{-10}mol/cm^2,[25] which probably one more citrate molecule is adsorbed in a unit area due to the electric potential. The surface coverage determined by elemental analysis for citrate-AuNPs (diameter: 17 - 20 nm) is 5.2×10^{-10}mol/cm^2,[363] and this value was likely overestimated because the carbon-based determination of citrate molecules also included oxidized by-products of citrate formed during the gold ion reduction.

2.3.14 Extension of the proposed conformation of citrate layers to silver and other NPs

The IR bands of the silver nanoparticles exhibit similar COO^- stretching vibrations except the incorporation of NO^{3-} ions on surface (see the ATR-IR spectrum of purified citrate-AgNPs in the Appendix). Nonequivalent symmetric COO^- vibrations have been

reported by SERS measurements.[153] Munro et al.[90] indentified three $\nu_{sym}(COO^-)$ vibration peaks of surface citrate on AgNPs at 1412, 1400, and 1370 cm^{-1}, and the proposed adsorption geometry of citrate through binding of the central and one terminal carboxylate groups is consistent with the proposed citrate conformation on AuNPs in this study. Yin and co-workers[256] suggested the similar configuration of adsorbed citrate on Ag(111), which is the preferential binding of citrate to Ag(111) of silver nanoplates through the central and one terminal carboxylate groups rather than the two terminal carboxylate groups. Since the lattice parameter of surface silver atoms (2.89 Å) is almost identical to that of gold atoms (2.88 Å) for (111) surfaces,[19] the same pattern of the citrate self-assembly can be applied to the silver nanoparticles. Also, the free carboxylate peaks under the high pH are the same as for AuNPs. The interaction force measured by AFM suggested multiple layers of the citrate ions on the silver surface, and the thickness of the citrate layer was estimated to 5 – 6 Å.[24] This thickness is comparable with that of the citrate bilayer on AuNP (Figure 2.15).

The stabilization of the multi-surfaces of citrate-AuNPs by the single fashion of the citrate adsorption may be related to the isotropic shape,[364] i.e., spherical, of the AuNP. The role of citrate as a stabilizer has been demonstrated for spherical silver,[365] gold, platinum,[366,367] and palladium[368] nanoparticles in water. The lattice spacing of the (111), (110), and (100) surfaces is deviated within 5% between the largest (silver) and the smallest (palladium) metal.[19] Interestingly, the lattice spacing of copper is smaller than that of silver by more than 11%,[19] and this may be related to the instability of copper nanoparticles in water synthesized by citrate reduction method.[369] Given the same pattern of citrate adsorption on those nanoparticles, the surfaces of copper nanoparticles may not be able to accommodate the citrate self-assembly with optimized intermolecular

interactions due to the size mismatch between the molecular building block and the metal surfaces. Surface citrate can act as stabilizer on the surfaces of the special silver, gold, platinum, and palladium NPs while the molecular framework of the self-assembled layer of citrate on the surfaces swells or contracts within 5% deviations, depending on the lattice sizes of the metal surface. Size match between molecules and metal surfaces, rather than specific surface chemistry, is the most important factor for molecular adsorption on metal surfaces having high surface energy.[19] The role of the citrate adsorption for stabilizing metal NPs is consistent with the experiment results in the literature above, likely suggesting the proposed pattern of the citrate self-assembly in this study as a ubiquitous configuration on the metal NPs.

2.3.15 Application of the proposed conformation of the adsorbed citrate for NP assembly

Due to the detailed ligand structure[370] hydrogen bonds of the interfacial citrate layers can be proposed as a driving force in the metal NP assembly, opposed to the adsorbate-induced electric dipole interaction of entire NPs.[371] A specific orientation of the central carboxylic acid group of dangling citrate species may influence the NP interaction, because the COOH groups are located at the very outer layer of the AuNPs. The interactions between NPs may depend on the chirality of the citrate layer on each surface. In the electric dipole driven mechanism, a nonuniform adsorption of molecules generates eventually the electric dipole formation. On the other hand, the dipolar interaction is responsible for the assembly of semiconductor NPs[370,372] due to the permanent dipole moment on the semiconductor,[373] but there is no such a strong dipole moment on bare metal NPs.[374] Moreover, the dephasing time of surface plasmon resonances (gold: < 5

fs,[375],[376] silver: < 7 fs[377]) is much faster than the time scale of the molecular/ionic rearrangements in the Stern layer and the diffuse layer on metal surfaces of the plasmonic metal NPs, and thus the temporal charge accumulation of the dipolar formation is unrealistic for the interparticle interaction in solution. On the contrary, the roles of interfacial molecular interactions [378] and facet-dependent assemblies [379] have been demonstrated for NP interactions. A temporal transition of the short range repulsive forces[8] into attraction may be a key factor for the aggregation of the citrate-AuNPs. The orientation of the central COOH groups of the dangling citrate molecules may play a critical role in the attractive forces for the facet-dependent assembly of AuNPs.

2.4 Conclusion

The conformation and self-assembly of citrate layers on AuNP surfaces were investigated. This is one of a few examples of a detailed spectroscopic study of organic layers on the surface of metal NPs.[380] ATR-IR, transmission FT-IR, XPS as well as a geometry-based simulation were employed, and those results are consistent with TEM and STM images of the citrate layer obtained from literature. Di-hydrogen citrate ($H_2Citrate^-$) is adsorbed on the Au surface by η^2-COO^- coordination of the central carboxylate group with the hydroxyl group intact. The adsorbed citrate interacts with an adjacent adsorbed species and a dangling citrate species through hydrogen bonds between the terminal carboxylic acid groups. This hydrogen-bonded surface citrates produce 1-D polymeric citrate chains, which interact each other through van der Waals attraction between adjacent CH_2 moieties, leading to formation of the self-assembled layer of citrate molecules adsorbed on AuNP facets including (111), (110), and (100) surfaces. When the hydrogen bonds between the terminal carboxylic acid groups of adjacent

adsorbed species are broken and bind to the surfaces by η^1-COO^- coordination, the polymeric citrate configuration turns into a repeated unit of citrate trimers, consisting of two adsorbed species interacting with a dangling citrate, as alternative building blocks on AuNP (111), (110), and (100) surfaces. The proposed configuration between adsorbed and dangling citrates suggests a bilayer formation on AuNPs. The estimated thickness of the citrate bilayer is 6.0 – 6.5 Å. From the pattern of the citrate adsorption on AuNP surfaces, molecular chirality was predicted. The surface coverage only by the adsorbed citrates is 1.86×10^{-10}mol/cm^2. With including the dangling citrates, the surface coverage becomes ~2.8×10^{-10}mol/cm^2. The IR data of citrate-stabilized AgNPs also indicate the similar coordination of the carboxylate groups of surface citrate. With applying the same driving forces for the citrate self-assembly, the identical adsorption conformation of surface citrate for AgNPs was proposed. The detailed study of the citrate layer on AuNPs is expected to provide new explanatory approaches for experimental observations from citrate-AuNP based studies as well as possibly for other citrate-stabilized metal NPs, including surface modification, particle growth,[35,381] NP assembly,[382] nanoelectronics, and catalysis.

2.5 Appendix: Conformation of citrate molecules adsorbed on gold nanoparticles

2.5.1 IR bands of purified citrate-AuNPs and Na_3Citrate

The ATR-IR measurements on a ZnSe crystal show intense vibrational peaks from organic molecules adsorbed on metal nanoparticles.[95] The peaks of purified citrate-AuNPs are located at 2971, 2918, 2898, 2848, 1764, 1711, 1611, 1593, 1558, 1543, 1465,[100,146, 383] 1453,[384] 1405, 1383, 1369, 1284,[112, 385] 1221,[200,277, 386] 1177,[387] 1146, 1070,[217] 1022,[388] 938, 908, 875, 846, 786, 770, 721, 692, 674, 618 cm^{-1} whereas the peaks of Na_3Citrate[114,115,217,273] are located at 1598, 1578, 1560, 1436, 1388, 1341,[134] 1294, 1279, 1258, 1188, 1137, 1111, 1076, 1056, 943, 911, 896, 839 cm^{-1}.

2.5.2 Binding energy of citrate molecules on gold clusters

The binding energy of each conformation in Figure 2.6 was estimated using ChemBio3D program by MM2 at 300 K although the gold-citrate clusters do not reflect accurately citrate molecules on a gold surface. The distance of Au-Au is 2.72 Å for Au_3 and 2.70 Å for Au_2. Conformation I results in ~240 kcal/mol whereas conformation IIa ~190 kcal/mol and conformation IIb ~340 kcal/mol. For comparison, the binding energy through only central carboxylate and/or hydroxyl groups was estimated. A bridging COO-Au_2 cluster shows ~20 kcal/mol, and a bridging COO/OH-Au_2 exhibits similar energy (~20 kcal/mol). This indicates that additional coordination through the terminal carboxylate group significantly increases the binding energy. Interestingly, the energy of conformation I, which represents citrate adsorbed on the Au(111) surface, decreases to 135 – 140 kcal/mol for citrate-Au_4 clusters. The latter represents citrate adsorbed on the Au(100) surface. This suggests there may be a favorable conformation on each surface.

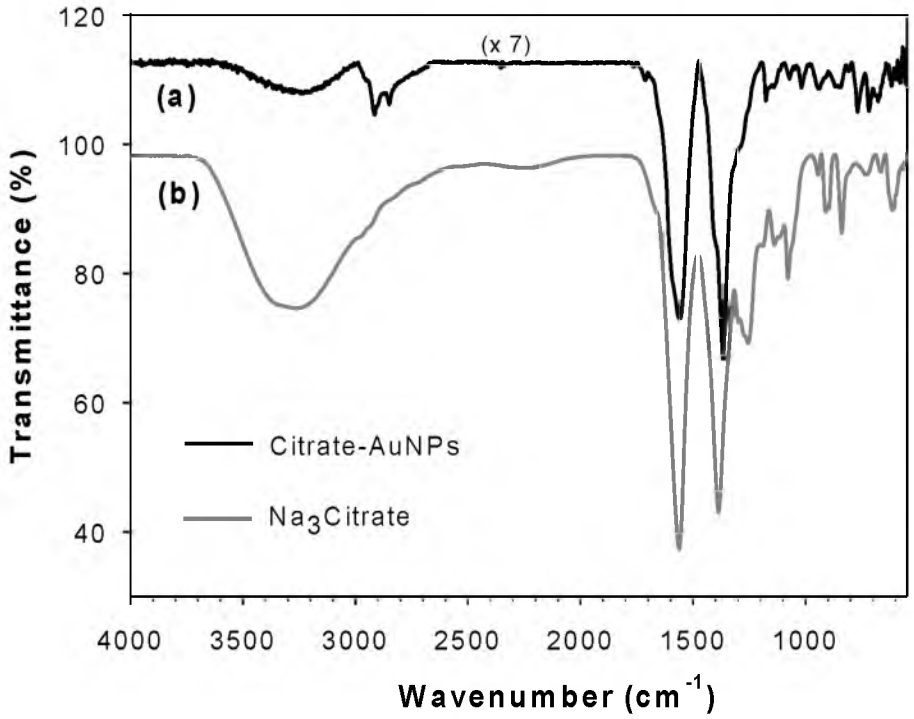

Figure 2.19. ATR-IR spectra of purified citrate-AuNPs and pure trisodium citrate.

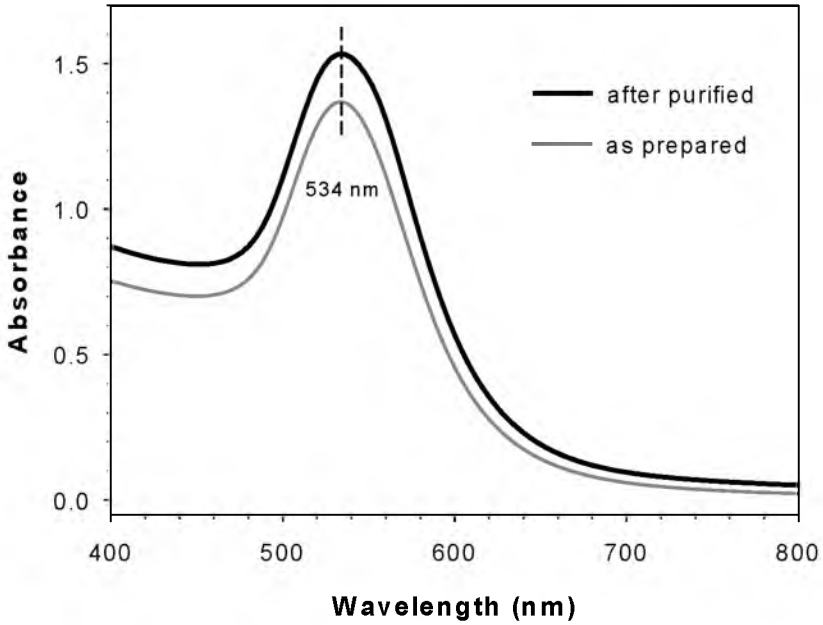

Figure 2.20. UV-Vis absorbances of citrate-AuNPs before and after purified with pH ~10 water. The dotted line guides λ_{max} at 534 nm for both samples.

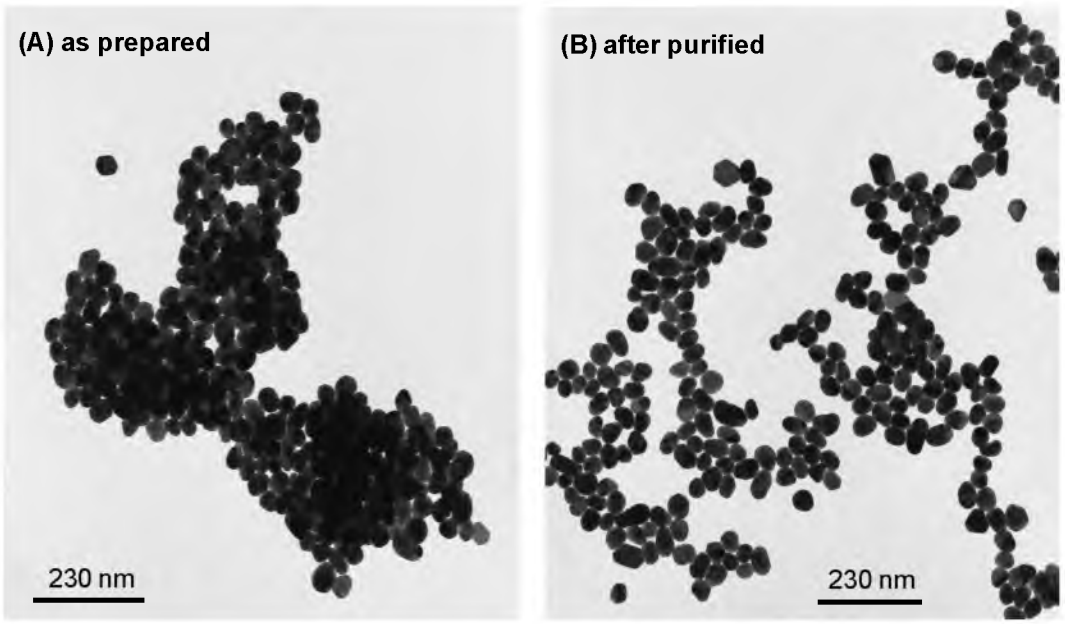

Figure 2.21. TEM images of citrate-AuNPs (A) before and (B) after purified with pH ~10 water.

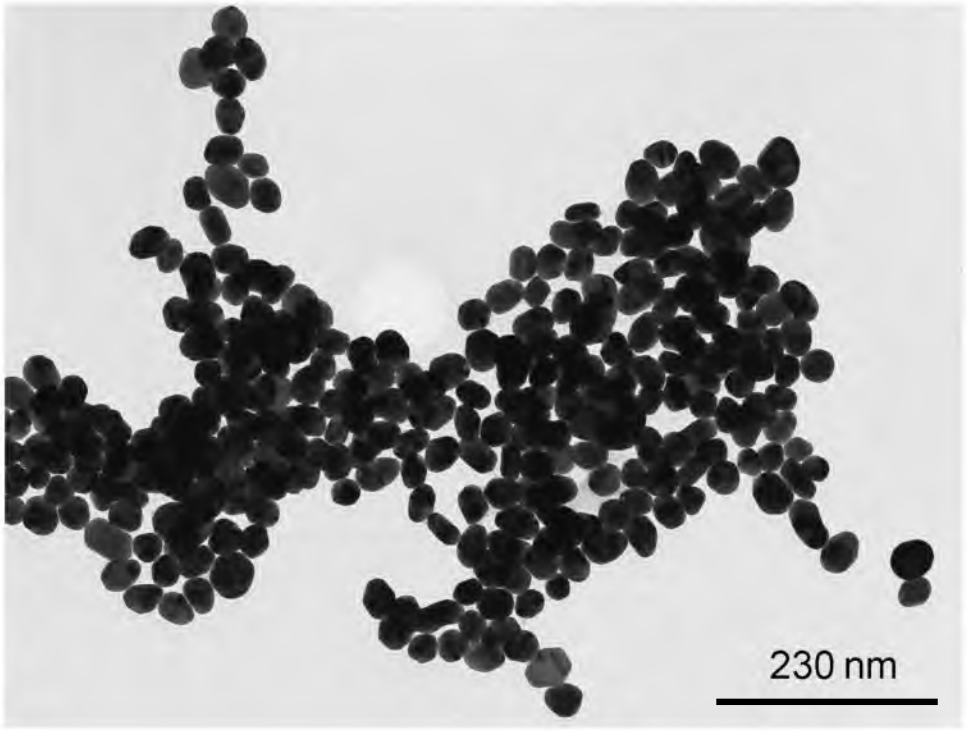

Figure 2.22. TEM image of purified citrate-AuNPs after addition of lead ions.

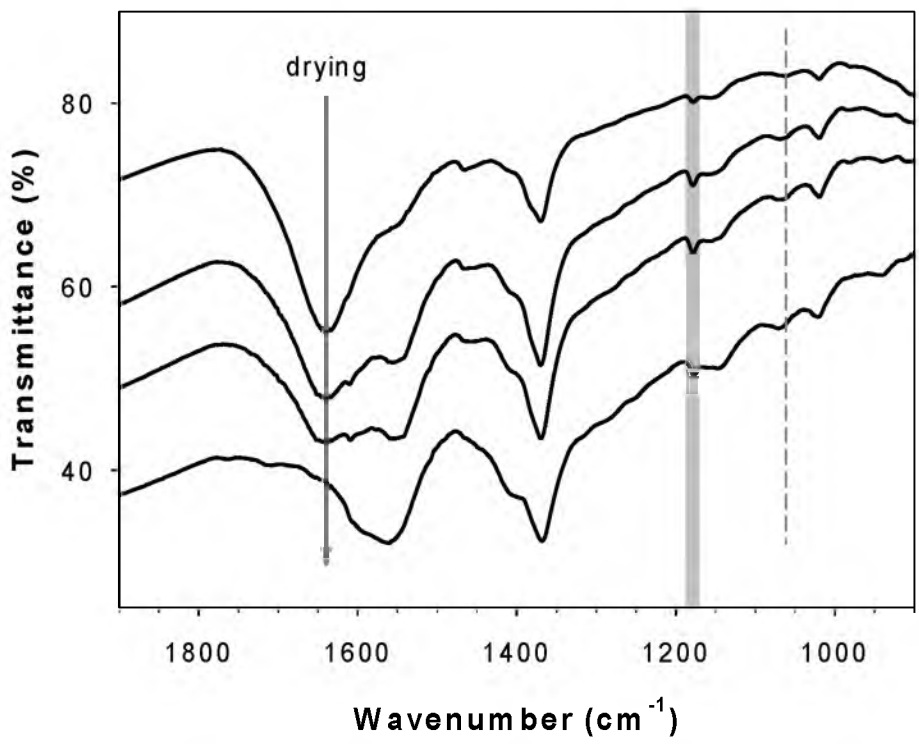

Figure 2.23. ATR-IR spectra of purified citrate-AuNPs taken during water evaporation. The shift of $\nu(C\text{-}O)_{alch}$ from 1062 to 1070 cm^{-1} as drying implies that the hydroxyl group is subject to solvation and does not coordinate to the surface (dotted line). Note that the intensities and positions of $\delta(OH)_{alch}$ at 1175 cm^{-1} do not change significantly (grey background).

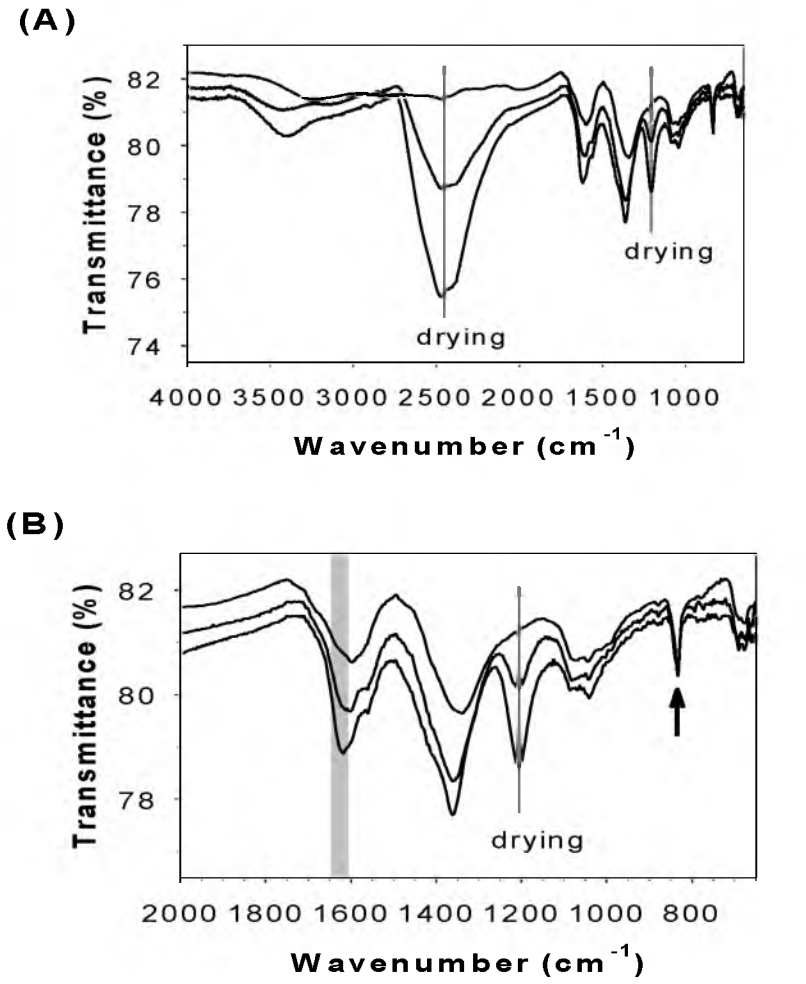

Figure 2.24. ATR-IR spectra of purified citrate-AuNPs after deuterated with D_2O/NaOD. (A): spectra at the frequency region of 4000 - 550 cm^{-1}, (B): zoomed region. The intensities of $\nu(O\text{-}D)_{D_2O}$ at ~2400 cm^{-1} and $\delta(OD)_{D_2O}$ at ~1200 cm^{-1} decrease, respectively, as D_2O evaporates (grey arrows in A). The intensities of $\delta(OD)_{alch}$ at 833 cm^{-1} do not change significantly (black arrow in B). The peak of $\nu_{asy}COO^-$ at 1620 cm^{-1} is still observed in the deuterated condition (grey background in B).

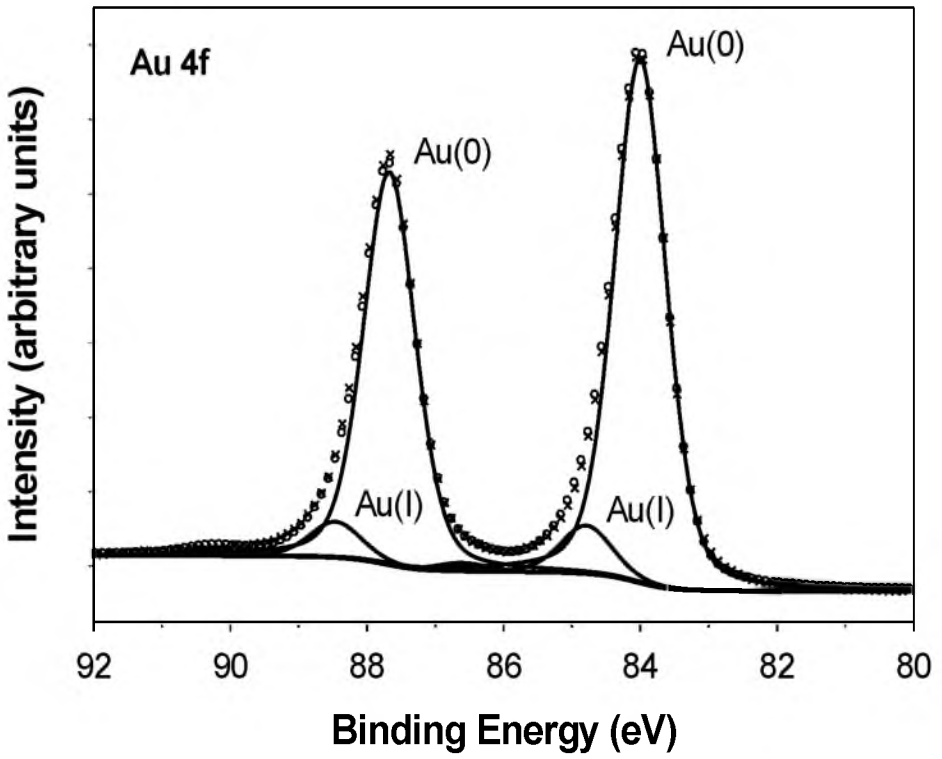

Figure 2.25. XPS spectrum of Au 4f binding energy of purified citrate-AuNPs. A surface Au(I)[389,390] species appears due to Au-carboxylate coordination.

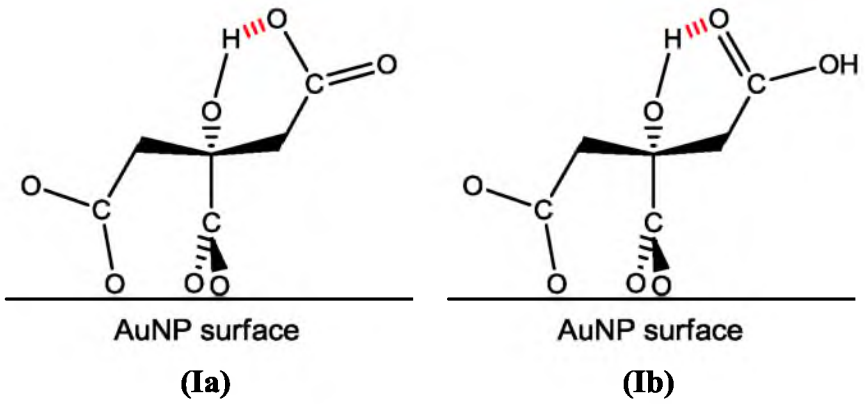

(Ia) **(Ib)**

Figure 2.26. Possible interactions between the hydroxyl group and the carboxylic acid group of citrate adsorbed on the surface of AuNPs.

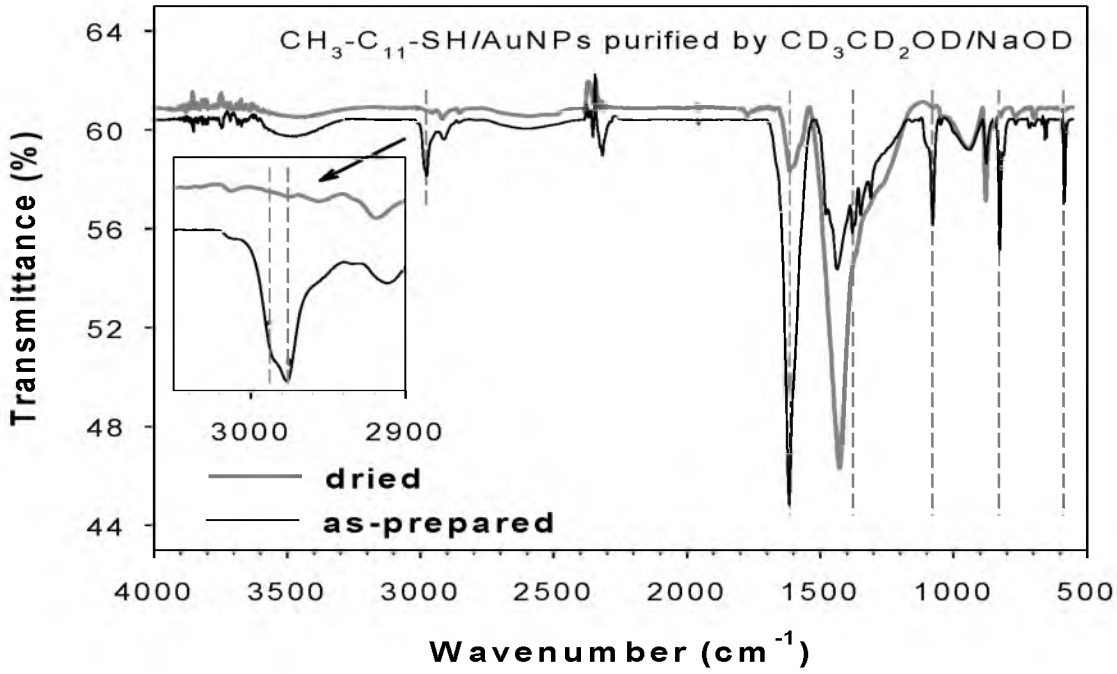

Figure 2.27. Transmission IR spectra of CH_3-C_{11}-SH functionalized citrate-AuNPs under the basic condition by use of EtOD-d_6/NaOD. The new peaks are still observed at the same frequencies (dotted lines), which verify that the peaks originate from preadsorbed organic molecules (i.e., citrate).

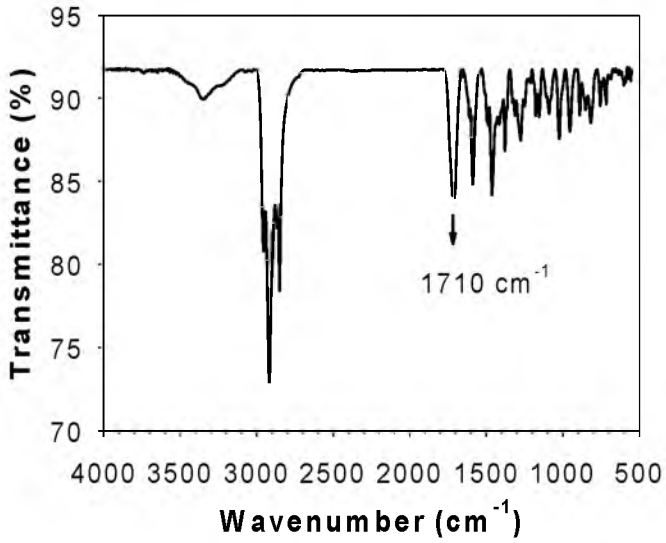

Figure 2.28. ATR-IR spectrum of citrate-AuNPs as prepared. The peak at 1710 cm^{-1} (arrowed) indicates the presence of hydrogen bonds between carboxylic acid groups of citrate molecules.

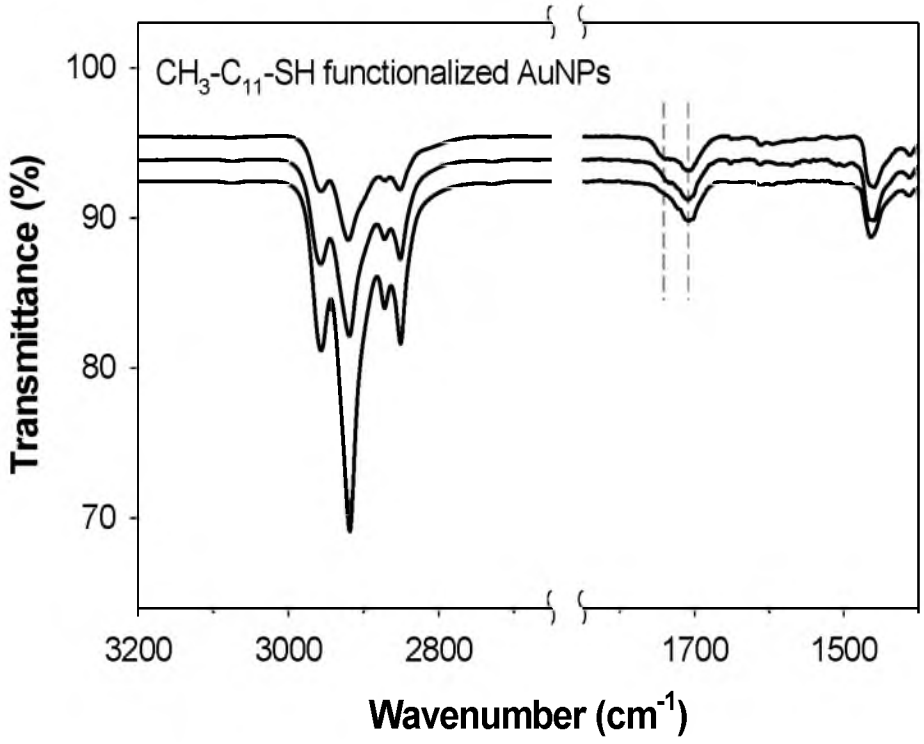

Figure 2.29. ATR-IR spectra of partially functionalized citrate-AuNPs by CH_3-C_{11}-SH. The thiol molecules can be adsorbed only in limited surface areas on AuNPs (1/4, 1/3, and 1/2 from top to bottom; note that the intensity changes of ν(C-H) around 2900 cm^{-1}), which was determined based on the amounts of the thiol added to citrate-AuNP solutions. The dotted lines act as guides for the peaks located at 1734 cm^{-1} (acylic dimers of carboxylic groups) and 1704 cm^{-1} (cylic dimers of carboxylic groups), respectively.

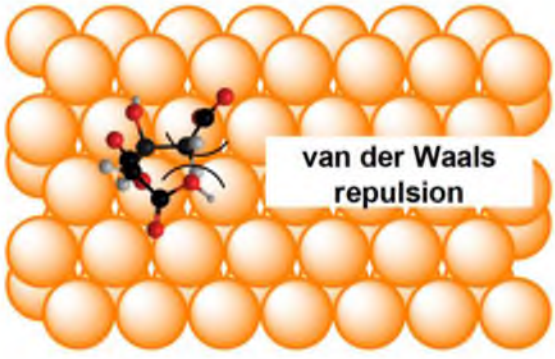

Figure 2.30. Ruled-out conformation of adsorbed citrate due to probable van der Waals repulsion between the free terminal carboxyl group and the CH_2 moiety.

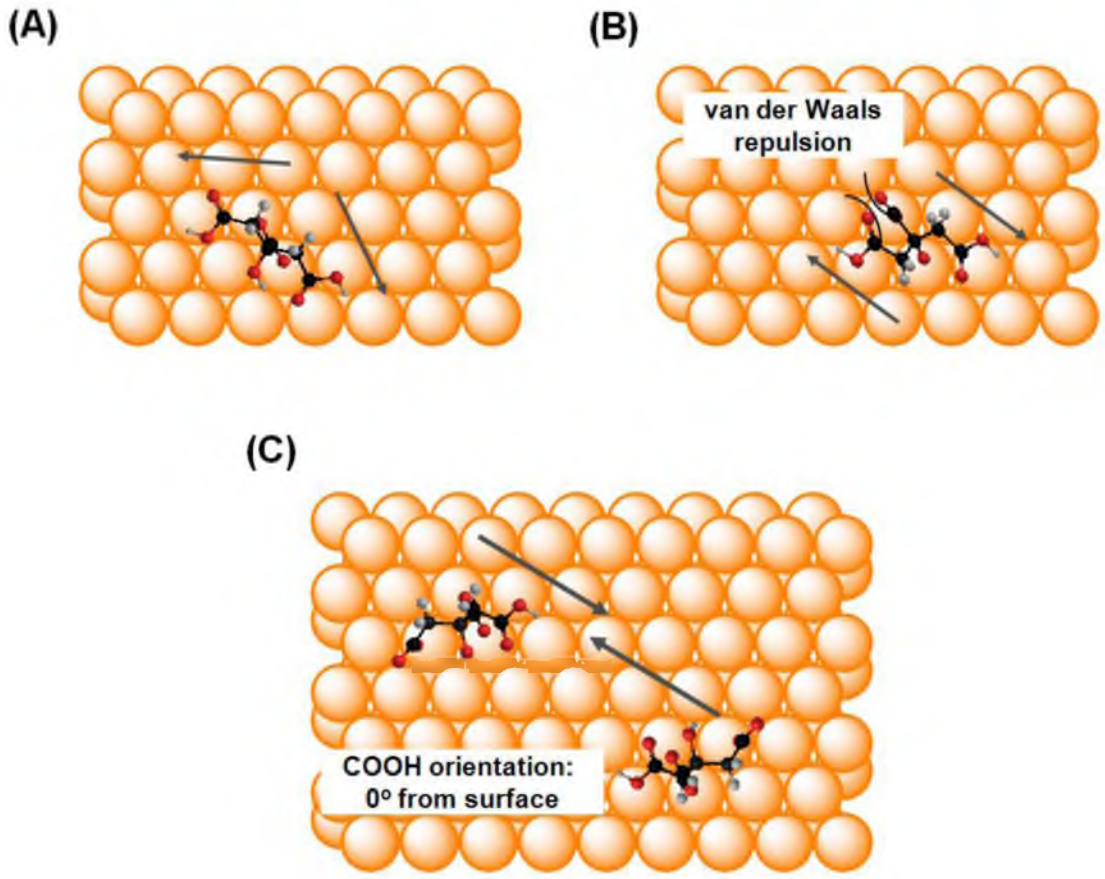

Figure 2.31. Configurations of the mediating citrate species and two adsorbed citrate molecules. Orientations of the terminal -COOH groups of (A and B) the mediating citrate adsorbed on the surface and (C) two adsorbed citrate molecules at both ends of the mediating citrate (grey arrows). The vertical orientations of all -COOH groups for potential hydrogen bonds are parallel to the surface.

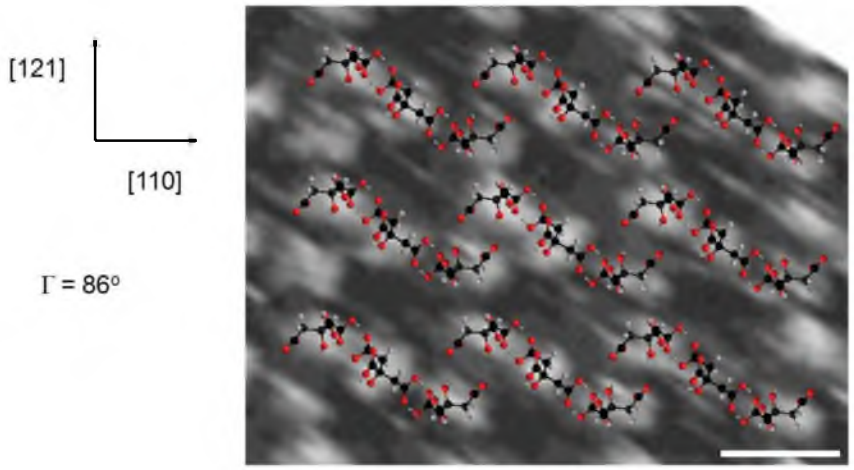

Figure 2.32. Interpretation of the STM image of citrate molecules adsorbed on Au(111) based on the model of citrate assembly in this study. STM image: adapted with permission from Lin, Y.; Pan, G.-B.; Su, G.-J.; Fang, X.-H.; Wan, L.-J.; Bai, C.-L. *Langmuir* **2003**, *19*, 10002, Figure 2. Copyright 2003 American Chemical Society. The model of citrate assembly is overlapped on the STM image. The scale bar is 10 Å, which was determined from the STM image shown in Figure 2b in the literature.

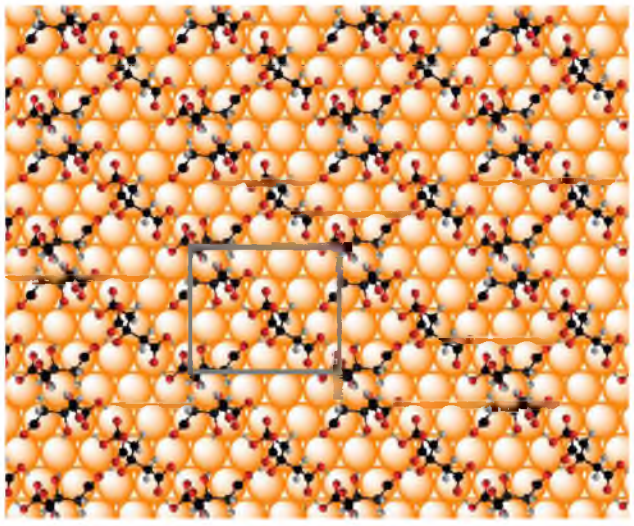

Figure 2.33. Organization of the citrate trimers with the identical cell parameters to the reported values (1.15 nm, 1.00 nm, 90°). Note that the CH_2 moieties encounter each other. To prevent this van der Waals repulsion, the gold spacing should be contracted to 2.30 Å, which is not an acceptable value. The Au atom spacing of large AuNPs with a radius of 25.7 nm is 2.88 Å[391] and of ~1 nm is 2.82 Å,[392] respectively.

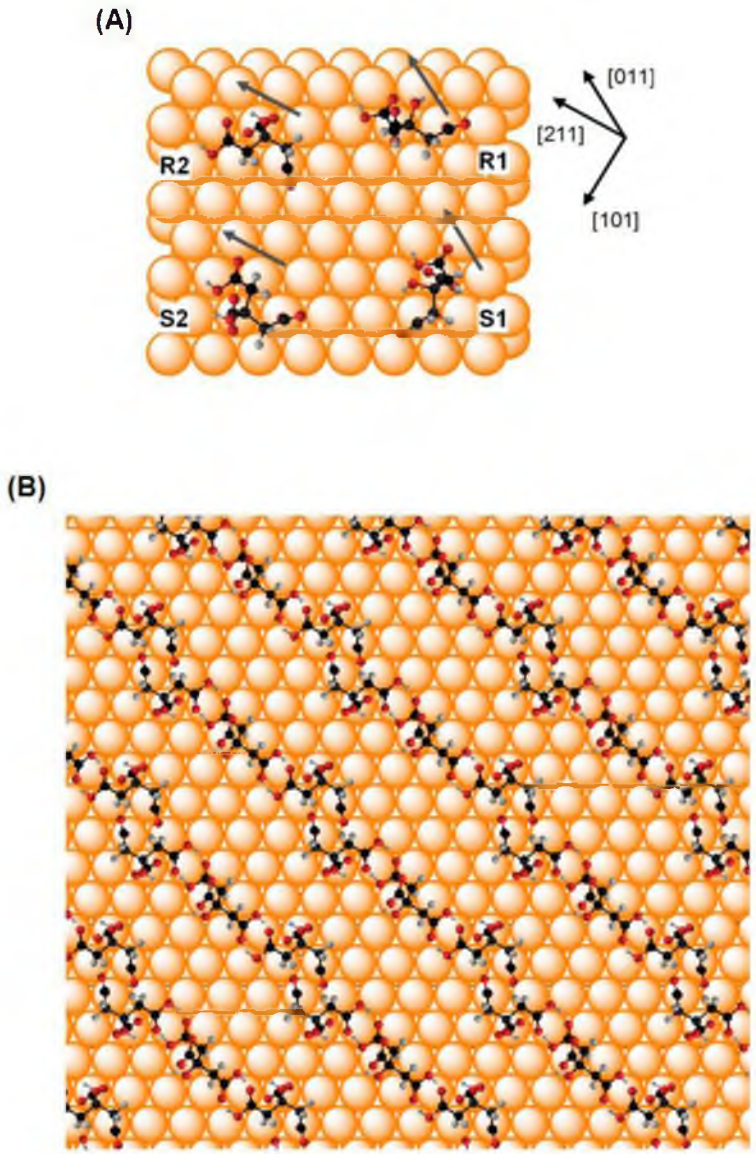

Figure 2.34. Citrate conformations and assembly with chelating η^2-$COO^-_{central}$ coordination of citrate molecules adsorbed on the Au(111) surface. (A) The carbon atoms of the coordinated central COO^- groups are located on top of gold atoms. In bridging coordination, the carbon atoms are located in between two adjacent gold atoms. (B) In the assembly with the chelating citrate molecules, which the model was generated in agreement with the STM image, there is van der Waals repulsion between the CH_2 moieties and the terminal coordinated COO^- groups.

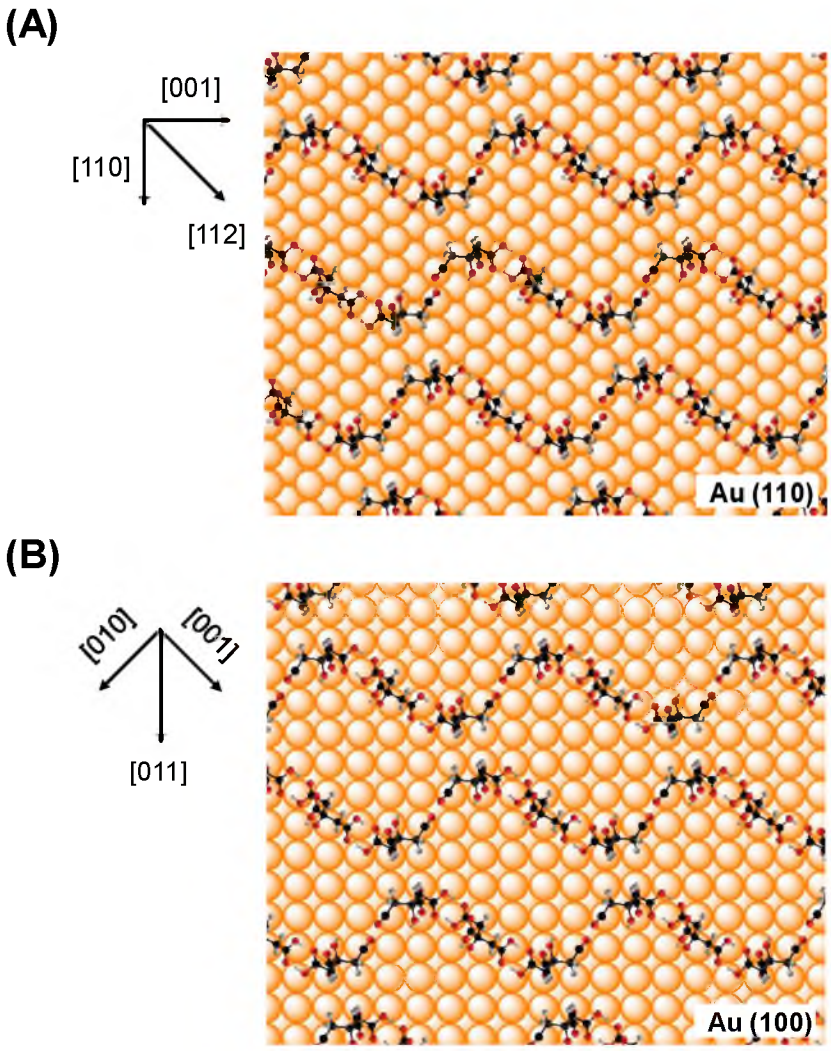

Figure 2.35. Proposed citrate adsorptions on Au(110) and Au(100) surfaces after the COOH hydrogen bonds between adsorbed citrate species are broken.

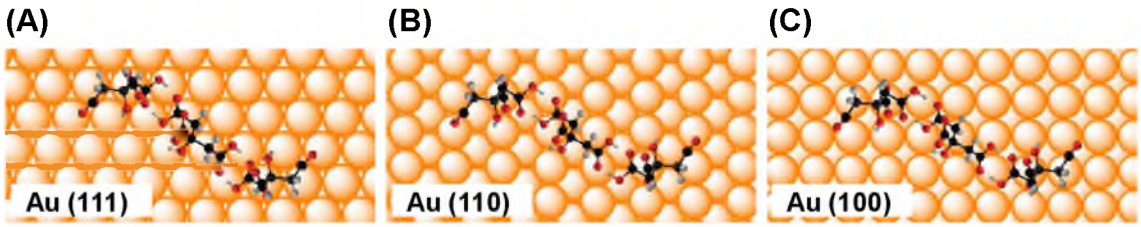

Figure 2.36. Units of the citrate trimer on different gold surfaces. Adsorbed citrate species bind to gold atoms at bridged sites through oxygen atoms of carboxylate groups.

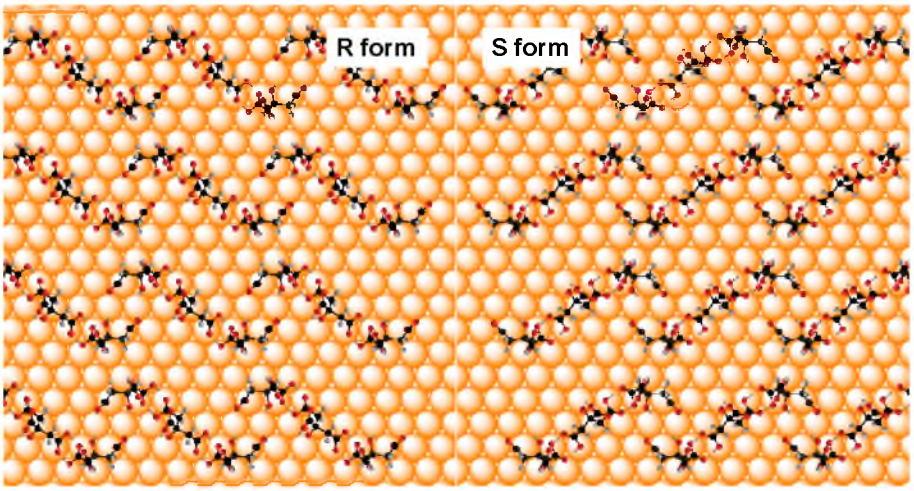

Figure 2.37. Chiral self-assembly of surface citrates on Au(111) with R and S isomers. Two types of stereoisomers are associated only with adsorbed citrate species.

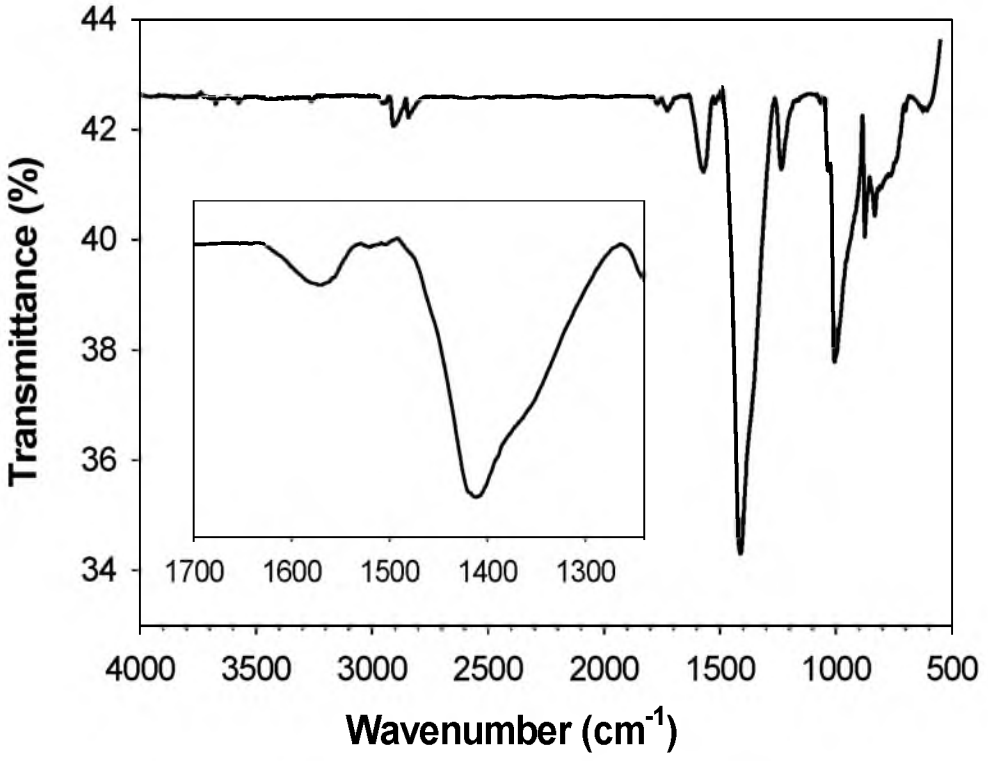

Figure 2.38. ATR-IR spectrum of purified citrate-AgNPs (Inset: the frequency region of COO^- stretching vibrations).

2.6 References

(1) Turkevich, J.; Stevenson, P. C.; Hillier, J. *Discuss. Faraday Soc.* **1951**, 55-75.

(2) Frens, G. *Nature Phys. Sci.* **1973**, *241*, 20-22.

(3) Kimling, J.; Maier, M.; Okenve, B.; Kotaidis, V.; Ballot, H.; Plech, A. *J. Phys. Chem. B* **2006**, *110*, 15700-15707.

(4) Ji, X.; Song, X.; Li, J.; Bai, Y.; Yang, W.; Peng, X. *J. Am. Chem. Soc.* **2007**, *129*, 13939-13948.

(5) Kreibig, U.; Vollmer, M. *Optical Properties of Metal Clusters*; Springer: Berlin, Germany, 1995.

(6) Links, S.; El-Sayed, M. A. *Annu. Rev. Phys. Chem.* **2003**, *54*, 331-366.

(7) Biggs, S.; Mulvaney, P.; Zukoski, C. F.; Grieser, F. *J. Am. Chem. Soc.* **1994**, *116*, 9150-9157.

(8) Chow, M. K.; Zukoski, C. F. *J. Colloid Interface Sci.* **1994**, *165*, 97-109.

(9) (a) Sardar, R.; Heap, T. B.; Shumaker-Parry, J. S. *J. Am. Chem. Soc.* **2007**, *129*, 5356-5357. (b) Sardar, R.; Shumaker-Parry, J. S. *Nano Lett.* **2008**, *8*, 731-736.

(10) Mirkin, C. A.; Letsinger, R. L.; Mucic, R. C.; Storhoff, J. J. *Nature* **1996**, *382*, 607-609.

(11) Haiss, W.; Thanh, N. T. K.; Aveyard, J.; Fernig, D. G. *Anal. Chem.* **2007**, *79*, 4215-4221.

(12) Jain, P. K.; Huang, X.; El-Sayed, I. H.; El-Sayed, M. A. *Acc. Chem. Res.* **2008**, *41*, 1578-1586.

(13) Li, Y.; Cox, J. T.; Zhang, B. *J. Am. Chem. Soc.* **2010**, *132*, 3047-3052.

(14) El-Sayed, I. H.; Huang, X.; El-Sayed, M. A. *Nano Lett.* **2005**, *5*, 829-834.

(15) Katz, E.; Willner, I. *Angew. Chem. Int. Ed.* **2004**, *43*, 6042-6108.

(16) Lee, K.-S.; El-Sayed, M. A. *J. Phys. Chem. B* **2006**, *110*, 19220-19225.

(17) (a) Jain, P. K.; El-Sayed, I. H.; El-Sayed, M. A. *Nano Today* **2007**, *2*, 18-29. (b) El-Sayed, I. H.; Huang, X.; El-Sayed, M. A. *Cancer Lett.* **2006**, *128*, 2115-2120.

(18) Grainger, D. W.; Castner, D. G. *Adv. Mater.* **2008**, *20*, 867-877.

(19) Feng, J.; Pandey, R. B.; Berry, R. J.; Farmer, B. L.; Naik, R. R.; Heinz, H. *Soft Matter* **2011**, *7*, 2113-2120.

(20) Yu, C.-J.; Tseng, W.-L. *Langmuir* **2008**, *24*, 12717-12722.

(21) Storhoff, J. J.; Elghanian, R.; Mirkin, C. A.; Letsinger, R. L. *Langmuir* **2002**, *18*, 6666-6670.

(22) Xie, H.; Tkachenko, A. G. Glomm, W. R.; Ryan, J. A.; Brennaman, M. K.; Papanikolas, J. M.; Franzen, S.; Feldheim, D. L. *Anal. Chem.* **2003**, *75*, 5797-5805.

(23) Citrate desorption on a planar gold surface: Larson, I.; Chan, D. Y. C.; Drummond, C. J.; Grieser, F. *Langmuir* **1997**, *13*, 2429-2431.

(24) Citrate desorption on a flat silver surface: Dagastine, R. R.; Grieser, F. *Langmuir* **2004**, *20*, 6742-6747.

(25) Kunze, J.; Burgess, I.; Nichols, R.; Buess-Herman, C.; Lipkowski, J. *J. Electroanal. Chem.* **2007**, *599*, 147-159.

(26) Gearheart, L. A.; Ploehn, H. J.; Murphy, C. J. *J. Phys. Chem. B* **2001**, *105*, 12609-12615.

(27) Gourishankar, A.; Shukla, S.; Ganesh, K. N.; Sastry, M. *J. Am. Chem. Soc.* **2004**, *126*, 13186-13187.

(28) Lèvy, R.; Thanh, N. T. K.; Doty, R. C.; Hussain, I.; Nichols, R. J.; Schiffrin, D. J.; Brust, M.; Fernig, D. G. *J. Am. Chem. Soc.* **2004**, *126*, 10076-10084.

(29) Choi, Y.; Park, Y.; Kang, T.; Lee, L. P. *Nat. Nanotech.* **2009**, *4*, 742-746.

(30) Cárdenas, M.; Barauskas, J.; Schillén, K.; Brennan, J. L.; Brust, M.; Nylander, T. *Langmuir* **2006**, *22*, 3294-3299.

(31) Brewer, S. H.; Glomm, W. R.; Johnson, M. C.; Knag, M. K.; Franzen, S. *Langmuir* **2005**, *21*, 9303-9307.

(32) For silver atoms: Mpourmpakis, G.; Vlachos, D. G. *Langmuir* **2008**, *24*, 7465-7473.

(33) Tsuruoka, T.; Furukawa, S.; Takashima, Y.; Yoshida, K.; Isoda, S.; Kitagawa, S. *Angew. Chem. Int. Ed.* **2009**, *48*, 4739-4743.

(34) Scherb, C.; Schödel, A.; Bein, T. *Angew. Chem. Int. Ed.* **2008**, *47*, 5777-5779.

(35) Polte, J.; Ahner, T. T.; Delissen, F.; Sokolov, S.; Emmerling, F.; Thünemann, A. F.; Kraehnert, R. *J. Am. Chem. Soc.* **2010**, *132*, 1296-1301.

(36) Kumar, S.; Gandhi, K. S.; Kumar, R. *Ind. Eng. Chem. Res.* **2007**, *46*, 3128-3136.

(37) Pong, B.-K.; Elim, H. I.; Chong, J.-X.; Ji, W.; Trout, B. L.; Lee, J.-Y. *J. Phys. Chem. C* **2007**, *111*, 6281-6287.

(38) Xia, H.; Bai, S.; Hartmann, J.; Wang, D. *Langmuir* **2010**, *26*, 3585-3589.

(39) Yao, T.; Sun, Z.; Li, Y.; Pan, Z.; Wei, H.; Xie, Y.; Nomura, M.; Niwa, Y.; Yan, W.; Wu, Z.; Jiang, Y.; Liu, Q.; Wei, S. *J. Amer. Chem. Soc.* **2010**, *132*, 7696-7701.

(40) For citrate-stabilized AgNPs: Redmond, P. L.; Wu, X.; Brus, L. *J. Phys. Chem. C* **2007**, *111*, 8942-8947.

(41) Zhou, X.; Xu, W.; Liu, G.; Panda, D.; Chen, P. *J. Am. Chem. Soc.* **2010**, *132*, 138-146.

(42) Xu, W.; Kong, J. S.; Yeh, Y.-T.; Chen, P. *Nat. Mater.* **2008**, *7*, 992-996.

(43) Zhang, S.; Leem, G.; Srisombat, L.-O.; Lee, T. R. *J. Am. Chem. Soc.* **2008**, *130*, 113-120.

(44) Weisbecker, C. S.; Merritt, M. V.; Whitesides, G. M. *Langmuir* **1996**, *12*, 3763-3772.

(45) Lin, S.-Y.; Tsai, Y.-T.; Chen, C.-C.; Lin, C.-M.; Chen, C.-H. *J. Phys. Chem. B* **2004**, *108*, 2134-2139.

(46) Bellino, M. G.; Calvo, E. J.; Gordillo, G. *Phys. Chem. Chem. Phys.* **2004**, *6*, 424-428.

(47) Hoefling, M.; Iori, F.; Corni, S.; Gottschalk, K.-E. *ChemPhysChem* **2010**, *11*, 1763-1767.

(48) Calzolari, A.; Cicero, G.; Cavazzoni, C.; Di Felice, R.; Catellani, A.; Corni, S. *J. Am. Chem. Soc.* **2010**, *132*, 4790-4795.

(49) Forster, M.; Dyer, M. S.; Persson, M.; Raval, R. *J. Am. Chem. Soc.* **2009**, *131*, 10173-10181.

(50) Barlow, S. M.; Kitching, K. J.; Haq, S.; Richardson, N. V. *Surf. Sci.* **1998**, *401*, 322-335.

(51) Liedberg, B.; Lundström, I.; Wu, C. R.; Salaneck, W. R. *J. Colloid Interface Sci.* **1985**, *108*, 123-132.

(52) Heinz, H.; Farmer, B. L.; Pandey, R. B.; Slocik, J. M.; Patnaik, S. S.; Pachter, R.; Naik, R. R. *J. Am. Chem. Soc.* **2009**, *131*, 9704-9714.

(53) So, C. R.; Tamerler, C.; Sarikaya, M. *Angew. Chem. Int. Ed.* **2009**, *48*, 5174-5177.

(54) Forster, M.; Dyer, M. S.; Persson, M.; Raval, R. *Angew. Chem. Int. Ed.* **2010**, *49*, 2344-2348.

(55) Ghiringhelli, L. M.; Delle Site, L. *J. Am. Chem. Soc.* **2008**, *130*, 2634-2638.

(56) Suh, J. S.; Kim, J. *J. Raman Spectrosc.* **1998**, *29*, 143-148.

(57) Li, Z.; Han, B.; Wan, L. J.; Wandlowski, Th. *Langmuir* **2005**, *21*, 6915-6928.

(58) Su, G.-J.; Zhang, H.-M.; Wan, L.-J.; Bai, C.-L.; Wandlowski, Th. *J. Phys. Chem. B* **2004**, *108*, 1931-1937.

(59) Langner, A.; Tait, S. L.; Lin, N.; Chandrasekar, R.; Ruben, M.; Kern, K. *Angew. Chem. Int. Ed.* **2008**, *47*, 8835-8838.

(60) Li, W.-H.; Haiss, W.; Floate, S.; Nichols, R. *Langmuir* **1999**, *15*, 4875-4883.

(61) Imae, T.; Torii, H. *J. Phys. Chem. B* **2000**, *104*, 9218-9224.

(62) Tomba, G.; Ciacchi, L. C.; De Vita, A. *Adv. Mater.* **2009**, *21*, 1055-1066.

(63) Teobaldi, G.; Zerbetto, F. *J. Phys. Chem. C* **2007**, *111*, 13879-13885.

(64) Nichols, R. J.; Burgess, I.; Young, K. L.; Zamlynny, V.; Lipkowski, J. *J Electroanal. Chem.* **2004**, *563*, 33-39.

(65) Floate, S.; Hosseini, M.; Arshadi, M. R.; Ritson, D.; Young, K. L.; Nichols, R. J. *J. Electroanal. Chem.* **2003**, *542*, 67-74.

(66) Lin, Y.; Pan, G.-B.; Su, G.-J.; Fang, X.-H.; Wan, L.-J.; Bai, C.-L. *Langmuir* **2003**, *19*, 10000-10003.

(67) Phambu, N. *Appl. Spectrosc.* **2002**, *56*, 756-761.

(68) (a) Awatani, T.; Dobson, K. D.; McQuillan, A. J.; Ohtani, B.; Uosaki, K. *Chem. Lett.* **1998**, 849-850. (b) Ekström, G. N.; McQuillan, A. J. *J. Phys. Chem. B* **1999**, *103*, 10562-10565.

(69) Zhang, R.-H.; Hong, Q.-M.; Yang, J.-M.; Zhang, H.-L.; Blackburnb, M.; Zhou, Z.-H. *Inorg. Chim. Acta* **2009**, *362*, 2643-2649.

(70) Gilbert, T. W.; Newman, L.; Klotz, P. *Anal. Chem.* **1968**, *40*, 2123-2130.

(71) Melson, G. A.; Figgis, B. N., Editors, *Transition Metal Chemistry*; Marcel Dekker, Inc.: New York, 1982.

(72) Mastropaolo, D. *Inorg. Chem.* **1976**, *15*, 1444-1449.

(73) Linic, S.; Barteau, M. A. *J. Am. Chem. Soc.* **2002**, *124*, 310-317.

(74) Capote, A. J.; Madix, R. J. *J. Am. Chem. Soc.* **1998**, *111*, 3570-3577.

(75) Liu, X.; Xu, B.; Haubrich, J.; Madix, R. J.; Friend, C. M. *J. Am. Chem. Soc.* **2009**, *131*, 5757-5759.

(76) Stacchiola, D.; Burkholder, L.; Zheng, T.; Weinert, M.; Tysoe, W. T. *J. Phys. Chem. B* **2005**, *109*, 851-856.

(77) Gong, J.; Flaherty, D. W.; Ojifinni, R. A.; White, J. M.; Mullins, C. B. *J. Phys. Chem. C* **2008**, *112*, 5501-5509.

(78) Jones, G. S.; Marrikakis, M.; Barteau, M. A.; Vohs, J. M. *J. Am. Chem. Soc.* **1998**, *120*, 3196-3204.

(79) Linic, S.; Medlin, J. W.; Barteau, M. A. *Langmuir* **2002**, *18*, 5197-5204.

(80) Camplin, J. P.; McCash, E. M. *Surf. Sci.* **1996**, *360*, 229-241.

(81) Lee, I.; Zaera, F. *J. Phys. Chem. B* **2005**, *109*, 12920-12926.

(82) Dai, Q.; Gellman, A. J. *Surf. Sci.* **1991**, *257*, 103-112.

(83) Stacchiola, D.; Burkholder, L.; Tysoe, W. T. *J. Am. Chem. Soc.* **2002**, *124*, 8984-8989.

(84) Camplin, J. P.; McCash, E. M. *J. Chem. Soc., Faraday Trans.* **1996**, *92*, 4695-4699.

(85) Khan, M. A. S.; Sen, A.; Ganguly, B. *CrystEngComm*, **2009**, *11*, 2660-2667.

(86) Wang, K.; Rangel, N. L.; Kundu, S.; Sotelo, J. C.; Tovar, R. M.; Seminario, J. M.; Liang, H. *J. Am. Chem. Soc.* **2009**, *131*, 10447-10451.

(87) Mpourmpakis, G.; Vlachos, D. G. *Phys. Rev. Lett.* **2009**, *102*, 155505.

(88) Delgado, J. M.; Blanco, R.; Orts, J. M.; Pérez, J. M.; Rodes, A. *Electrochim. Acta* **2010**, *55*, 2055-2064.

(89) Glusker, J. P. *Acc. Chem. Res.* **1980**, *13*, 345-352.

(90) Munro, C. H.; Smith, W. E.; Garner, M.; Clarkson, J.; White, P. C. *Langmuir* **1995**, *11*, 3712-3720.

(91) Lee, Z.; Jeon, K.-J.; Dato, A.; Erni, R.; Richardson, T. J.; Frenklach, M.; Radmilovic, V. *Nano Lett.* **2009**, *9*, 3365-3369.

(92) Nuzzo, R. G.; Zegarski, B. R.; Dubois, L. H. *J. Amer. Chem. Soc.* **1987**, *109*, 733-740.

(93) Liu, X.; Atwater, M.; Wang, J.; Huo, Q. *Colloids Surf., B* **2007**, *58*, 3-7.

(94) Yamamoto, S.; Watarai, H. *Langmuir* **2006**, *22*, 6562-6569.

(95) Berger, T.; Delgado, J. M.; Lana-Villarreal, T.; Rodes, A.; Gómez, R. *Langmuir* **2008**, *24*, 14035-14041.

(96) IR analysis indicated that this peak is the water bending vibration. However, it was assigned to be an asymmetric stretching vibration of carboxylate groups: Wulandari, P.; Nagahiro, T.; Michioka, K.; Tamada, K.; Ishibsshi, K.-I.; Kimura, Y.; Niwano, M. *Chem. Lett.* **2008**, *37*, 888-889.

(97) Sato, Y.; Noda, H.; Mizutani, F.; Yamakata, A.; Osawa, M. *Anal. Chem.* **2004**, *76*, 5564-5569.

(98) Wan, L.-J.; Terashima, M.; Noda, H.; Osawa, M. *J. Phys. Chem. B* **2000**, *104*, 3563-3569.

(99) Mirklin, G. T.; He, L.-T.; Griffiths, P. R. *Appl. Spectrosc.* **1999**, *53*, 1448-1453.

(100) Arnold, R.; Azzam, W.; Terfort, A.; Wöll, C. *Langmuir* **2002**, *18*, 3980-3992.

(101) Ikezawa, Y.; Sawamura, S. *Electrochim. Acta* **2009**, *54*, 2360-2366.

(102) Schmeiβer, D.; Böhme, O.; Yfantis, A.; Heller, T.; Batchelor, D. R.; Lundstrom, I.; Spetz, A. L. *Phys. Rev. Lett.* **1999**, *83*, 380-382.

(103) Osawa, M.; Ataka, K.-I.; Yoshii, K.; Nishikawa, Y. *Appl. Spectrosc.* **1993**, *47*, 1497-1502.

(104) Baia, M.; Toderas, F.; Baia, L.; Maniu, D.; Astilean, S. *ChemPhysChem* **2009**, *10*, 1106-1111.

(105) Huo, S.-J.; Li, Q.-X.; Yan, Y.-G.; Chen, Y.; Cai, W.-B.; Xu, Q.-J.; Osawa, M. *J. Phys. Chem. B* **2005**, *109*, 15985-15991.

(106) Devlin, J. P.; Consani, K. *J. Phys. Chem.* **1981**, *85*, 2597-2598.

(107) Tautz, F. S.; Eremtchenko, M.; Schaefer, J. A.; Sokolowski, M.; Shklover, V.; Umbach, E. *Phys. Rev. B* **2002**, *65*, 125405.

(108) Priebe, A.; Pucci, A.; Otto, A. *J. Phys. Chem. B* **2006**, *110*, 1673-1679.

(109) Skibbe, O.; Binder, M.; Otto, A.; Pucci, A. *J. Chem. Phys.* **2008**, *128*, 194703.

(110) Hein, M.; Dumas, P.; Sinther, M.; Priebe, A.; Lilie, P.; Bruckbauer, A.; Pucci, A.; Otto, A. *Surf. Sci.* **2006**, *600*, 1017-1025.

(111) Cabaniss, S. E.; Leenheer, J. A.; McVey, I. F. *Spectrochim. Acta, Part A* **1998**, *54*, 449-458.

(112) Diewok, J.; Ayora-Cañada, M. J.; Lendl, B. *Anal. Chem.* **2002**, *74*, 4944-4954.

(113) Ayora-Cañada, M. J.; Lendl, B. *Vib. Spectrosc.* **2000**, *24*, 297-306.

(114) Max, J.-J.; Chapados, C. *J. Phys. Chem. A* **2004**, *108*, 3324-3337.

(115) Lindegren, M.; Loring, J. S.; Persson, P. *Langmuir* **2009**, *25*, 10639-10647.

(116) Lackovic, K.; Johnson, B. B.; Angove, M. J.; Wells, J. D. *J. Colloid Interface Sci.* **2003**, *267*, 49-59.

(117) Fischer, A.; Palladino, G. *Acta Cryst. E.* **2003**, *59*, m1080-m1082.

(118) Nara, M.; Torii, H.; Tasumi, M. *J. Phys. Chem.* **1996**, *100*, 19812-19817.

(119) Berná, A.; Delgado, J. M.; Orts, J. M.; Rodes, A.; Feliu, J. M. *Electrochim. Acta* **2008**, *53*, 2309-2321.

(120) Delgado, J. M.; Berná, A.; Orts, J. M.; Rodes, A.; Feliu, J. M. *J. Phys. Chem. C* **2007**, *111*, 9943-9952.

(121) Ataka, K.-I.; Yotsuyanagi, T.; Osawa, M. *J. Phys. Chem.* **1996**, *100*, 10664-10672.

(122) Han, B.; Li, Z.; Pronkin, S.; Wandlowski, Th. *Can. J. Chem.* **2004**, *82*, 1481-1494.

(123) Delgado, J. M.; Orts, J. M.; Rodes, A. *Langmuir* **2005**, *21*, 8809-8816.

(124) Ataka, K.-I.; Osawa, M. *Langmuir* **1998**, *14*, 951-959.

(125) Wandlowski, Th.; Ataka, K.; Pronkin, S.; Diesing, D. *Electrochim. Acta* **2004**, *49*, 1233-1247.

(126) Noda, H.; Wan, L.-J.; Osawa, M. *Phys. Chem. Chem. Phys.* **2001**, *3*, 3336-3342.

(127) Max, J.-J.; Chapados, C. *J. Phys. Chem. A* **2002**, *106*, 6452-6461.

(128) Espinoza, C.; Szczepanski, J.; Vala, M.; Polfer, N. C. *J. Phys. Chem. A* **2010**, *114*, 5919-5927.

(129) Norén, K.; Loring, J. S.; Persson, P. *J. Colloid Interface Sci.* **2008**, *319*, 416-428.

(130) Barth, A.; Zscherp, C. *Q. Rev. Biophys.* **2002**, *35*, 369-430.

(131) Jäger, F.; Fahmy, K.; Sakmar, T. P.; Siebert, F. *Biochemistry* **1994**, *33*, 10878-10882.

(132) Caswell, K. K.; Bender, C. M.; Murphy, C. J. *Nano Lett.* **2003**, *3*, 667-669.

(133) Zhang, Y.; Gao, X.; Weaver, M. J. *J. Phys. Chem.* **1993**, *97*, 8656-8663.

(134) Bieri, M.; Bürgi, T. *Langmuir* **2005**, *21*, 1354-1363.

(135) Williams, J.; Haq, S.; Raval, R. *Surf. Sci.* **1996**, *368*, 303-309.

(136) Olson, A. L.; Cai, S.; Herdendorf, T. J. Miziorko, H. M.; Sem, D. S. *J. Am. Chem. Soc.* **2010**, *132*, 2102-2103.

(137) Ohe, C.; Ando, H.; Sato, N.; Urai, Y.; Yamamoto, M.; Itoh, K. *J. Phys. Chem. B* **1999**, *103*, 435-444.

(138) Du, X.; Liang, Y. *J. Phys. Chem. B* **2004**, *108*, 5666-5670.

(139) Zhang, H.; Zhao, H.; Jiang, Y.-Q.; Hou, S.-Y.; Zhou, Z.-H.; Wan, H.-L. Inorg. *Chim. Acta* **2003**, *351*, 311-318.

(140) Barnard, A. S.; Young, N. P.; Kirkland, A. I.; van Huis, M. A.; Xu, H. *ACS Nano* **2009**, *3*, 1431-1436.

(141) Rodes, A.; Pastor, E.; Iwasita, T. *J. Electroanal. Chem.* **1994**, *376*, 109-118.

(142) Delgado, J. M.; Blanco, R.; Orts, J. M.; Pérez, J. M.; Rodes, A. *J. Phys. Chem. C* **2009**, *113*, 989-1000.

(143) Clausen, M.; Öhman, L.-O.; Persson, P. *J. Inorg. Biochem.* **2005**, *99*, 716-726.

(144) Zhou, Z.-H.; Hou, S.-Y.; Wan, H.-L. *Dalton Trans.* **2004**, 1393-1399.

(145) Zhou. Z.-H.; Wan, H.-L.; Tsai, K.-R. *Inorg. Chem.* **2000**, *39*, 59-64.

(146) Allara, D. L.; Nuzzo, R. G. *Langmuir* **1985**, *1*, 52-66.

(147) Dote, J. L.; Mowery, R. L. *J. Phys. Chem.* **1988**, *92*, 1571-1575.

(148) Matzapetakis, M.; Raptopoulou, C. P.; Tsohos, A.; Papaefthymiou, V.; Moon, N.; Salifoglou, A. *J. Am. Chem. Soc.* **1998**, *120*, 13266-13267.

(149) Canning, N. D. S.; Madix, R. J. *J. Phys. Chem.* **1984**, *88*, 2437-2446.

(150) Zeleňák, V.; Vargová, Z.; Györyová, K. *Spectrochim. Acta, Part A* **2007**, *66*, 262-272.

(151) Tao, Y.-T. *J. Am. Chem. Soc.* **1993**, *115*, 4350-4358.

(152) Dubois, L. H.; Zegarski, B. R.; Nuzzo, R. G. *Langmuir* **1986**, *2*, 412-417.

(153) SERS data: (a) Siiman, O.; Bumm, L. A.; Callaghan, R.; Blatchford, C. G.; Kerker, M. *J. Phys. Chem.* **1983**, *87*, 1014-1023. (b) Kerker, M.; Siiman, O.; Bumm, L. A.; Wnag, D.-S. *Appl. Opt.* **1980**, *19*, 3253-3255.

(154) Seo, Y. U.; Lee, S. J.; Kim, K. *J. Phys. Chem. B* **2004**, *108*, 4000-4007.

(155) Dobson, K. D.; McQuillan, A. *J. Spectrochim. Acta, Part A* **1999**, *55*, 1395-1405.

(156) Uznanski, P.; Bryszewska, E. *J. Mater. Sci.* **2010**, *45*, 1547-1552.

(157) Smith, E. L.; Alves, C. A.; Anderegg, J. W.; Porter, M. D. *Langmuir* **1992**, *8*, 2707-2714.

(158) Lin, S.-Y.; Chen, C.-H.; Chan, Y.-C.; Lin, C.-M.; Chen, H.-W. *J. Phys. Chem. B* **2001**, *105*, 4951-4955.

(159) Tao, Y.-T.; Lin, W.-L.; Hietpas, G. D.; Allara, D. L. *J. Phys. Chem. B* **1997**, *101*, 9732-9740.

(160) Bessonov, A. A.; Baidina, I. A.; Morozova, N. B.; Semyannikov, P. P.; Trubin, S. V.; Gelfond, N. V.; Igumenov, I. K. *J. Struct. Chem.* **2007**, *48*, 282-288.

(161) Huerta, F.; Mele, C.; Bozzini, B.; Morallón, E. *J. Electroanal. Chem.* **2004**, *569*, 53-60.

(162) Zhang, Z.; Yoshida, N.; Imae, T.; Xue, Q.; Bai, M.; Jiang, J.; Liu, Z. *J. Colloid Interface Sci.* **2001**, *243*, 382-387.

(163) Corrigan, D. S.; Krauskopf, E. K.; Rice, L. M.; Wieckowski, A.; Weaver, M. J. *J. Phys. Chem.* **1988**, *92*, 1596-1601.

(164) Zhang, Z.; Imae, T. *Nano Lett.* **2001**, *1*, 241-243.

(165) Schlotter, N. E.; Porter, M. D.; Bright, T. B.; Allara, D. L. *Chem. Phys. Lett.* **1986**, *132*, 93-97.

(166) Wells, M.; Dermody, D. L.; Yang, H. C.; Kim, T.; Crooks, R. M. *Langmuir* **1996**, *12*, 1989-1996.

(167) Kakihana, M.; Nagumo, T.; Okamoto, M.; Kakihana, H. *J. Phys. Chem.* **1987**, *91*, 6128-6136.

(168) Huang, X.; Jiang, S.; Liu, M. *J. Phys. Chem. B* **2005**, *109*, 114-119.

(169) Nakamoto, K. *Infrared and Raman Spectra of Inorganic and Coordination Compounds*; John Wiley & Sons: New York, 1986.

(170) Abelev, E.; Starosvetsky, D.; Ein-Eli, Y. *Langmuir* **2007**, *23*, 11281-11288.

(171) Preisenberger, M.; Schier, A.; Schmidbaur, H. *J. Chem. Soc., Dalton Trans.* **1999**, 1645-1650.

(172) Jones, P. G. *Acta Cryst.* **1984**, *C40*, 1320-1322.

(173) Jones, P. G. *Acta Cryst.* **1984**, *C40*, 804-805.

(174) Puddephatt, R. J. *Chem. Soc. Rev.* **2008**, *37*, 2012-2027.

(175) Grodzicki, A.; Lakomska, I.; Piszczek, P.; Szymańska, I.; Szłyk, E. *Coord. Chem. Rev.* **2005**, *249*, 2232-2258.

(176) Jiang, W.; Pan, H.; Cai, Y.; Tao, J.; Liu, P. Xu, X.; Tang, R. *Langmuir* **2008**, *24*, 12446-12451.

(177) Kumar, P. P.; Kalinichev, A. G.; Kirkpatrick, R. J. *J. Phys. Chem. B* **2006**, *110*, 3841-3844.

(178) Peng, C. S.; Jones, K. C.; Tokmakoff, A. *J. Am. Chem. Soc.* **2011**, *133*, 15650-15660.

(179) Wang, S.; Yao, H.; Sato, S.; Kimura, K. *J. Am. Chem. Soc.* **2004**, *126*, 7438-7439.

(180) Gerken, J. B.; Badger, C.; Bisbee, C.; Gardner, S.; Qi, Y.; Vilá, V. D.; Roberts, J. D. *J. Phys. Org. Chem.* **2008**, *21*, 193-197.

(181) Wang, D.; Nap, R. J.; Lagzi, I.; Kowalczyk, B.; Han, S.; Grzybowski, B. A.; Szleifer, I. *J. Amer. Chem. Soc.* **2011**, *133*, 2192-2197.

(182) Kakiuchi, T.; Iida, M.; Imabayashi, S.-i.; Niki, K. *Langmuir* **2000**, *16*, 5397-5401.

(183) Ivanov, M. R.; Bednar, H. R.; Haes, A. J. *ACS Nano* **2009**, *3*, 386-394.

(184) Hu, K.; Bard, A. J. *Langmuir* **1997**, *13*, 5114-5119.

(185) van der Vegte, E. W.; Hadziioannou, G. *J. Phys. Chem. B* **1997**, *101*, 9563-9569.

(186) Creager, S. E.; Clarke, J. *Langmuir* **1994**, *10*, 3675-3683.

(187) Young, A. G.; Green, D. P.; McQuillan, A. J. *Langmuir* **2006**, *22*, 11106-11112.

(188) Simard, J.; Briggs, C.; Boal, A. K.; Rotello, V. M. *Chem. Commun.* **2000**, 1943-1944.

(189) Zhou, Z.-H.; Deng, Y.-F.; Cao, Z.-X.; Zhang, R.-H.; Chow, Y. L. *Inorg. Chem.* **2005**, *44*, 6912-6914.

(190) Rosendahl, S. M.; Burgess, I. J. *Electrochim. Acta* **2008**, *53*, 6759-6767.

(191) Zheng, W.; Maye, M. M.; Leibowitz, F. L.; Zhong, C. J. *Analyst* **2000**, *125*, 17-20.

(192) Tao, Y.-T.; Hietpas, G. D.; Allara, D. L. *J. Am. Chem. Soc.* **1996**, *118*, 6724-6735.

(193) Deng, Y.-F.; Zhou, Z.-H.; Wan, H.-L. *Inorg. Chem.* **2004**, *43*, 6266-6273.

(194) Matzapetakis, M.; Karligiano, N.; Bino, A.; Dakanali, M.; Raptopoulou, C. P.; Tangoulis, V. Terzis, A.; Giapintzakis, J.; Salifoglou, A. *Inorg. Chem.* **2000**, *39*, 4044-4051.

(195) Zhang, J.; Demetriou, A.; Welinder, A. C.; Albrecht, T.; Nichols, R. J.; Ulstrup, J. *Chem. Phys.* **2005**, *319*, 210-221.

(196) Bootharaju, M. S.; Pradeep, T. *J. Phys. Chem. C* **2010**, *114*, 8328-8336.

(197) Matzapetakis, M.; Kourgiantakis, M.; Dakanali, M.; Raptopoulou, C. P.; Terzis, A.; Lakatos, A.; Kiss, T.; Banyai, I.; Iordanidis, L.; Mavromoustakos, T.; Salifoglou, A. *Inorg. Chem.* **2001**, *40*, 1734-1744.

(198) Li, D.-M.; Cui, L.-F.; Xing, Y.-H.; Xu, J.-Q.; Yu, J.-H.; Wang, T.-G.; Jia, H.-Q.; Hu, N.-H. *J. Mol. Sturct.* **2007**, *832*, 138-145.

(199) Takuma, M.; Ohki, Y.; Tatsumi, K. *Organometallics* **2005**, *24*, 1344-1347.

(200) Pasilis, S. P.; Pemberton, J. E. *Inorg. Chem.* **2003**, *42*, 6793-6800.

(201) Zhou, Z.-H.; Deng, Y.-F.; Jiang, Y.-Q.; Wan, H.-L.; Ng, S.-W. *Dalton Trans.* **2003**, 2636-2638.

(202) Deng, Y.-F.; Zhang, H.-L.; Hong, Q.-M.; Weng, W.-Z.; Wan, H.-L.; Zhou, Z.-H. *J. Solid State Chem.* **2007**, *180*, 3152-3159.

(203) Kefalas, E. T.; Panagiotidis, P.; Raptopoulou, C. P.; Terzis, A.; Mavromoustakos, T.; Salifoglou, A. *Inorg. Chem.* **2005**, *44*, 2596-2605.

(204) Panagiotidis, P.; Kefalas, E. T.; Raptopoulou, C. P.; Terzis, A.; Mavromoustakos, T.; Salifoglou, A. *Inorg. Chim. Acta* **2008**, *361*, 2210-2224.

(205) Kaliva, M.; Gabriel, C.; Raptopoulou, C. P.; Terzis, A.; Salifoglou, A. *Inorg. Chim. Acta* **2008**, *361*, 2631-2640.

(206) Deng, Y.-F.; Zhou, Z.-H. *J. Coord. Chem.* **2009**, *62*, 1484-1491.

(207) Guo, Y.; Lü, J.; Li, Y.; Wang, E.; Lu, Y.; Xu, X.; Xu, L. *J. Mol. Struct.* **2006**, *782*, 44-48.

(208) Rousseau, R.; Dietrich, G.; Krückeberg, S.; Lützenkirchen, K.; Max, D.; Schweikhard, L.; Walther, C. *Chem. Phys. Lett.* **1998**, *295*, 41-46 .

(209) Knickelbein, M. B.; Koretsky, G. M. *J. Phys. Chem. A* **1998**, *102*, 580-586.

(210) Dietrich, G.; Krückeberg, S.; Lützenkirchen, K.; Schweikhard, L.; Walther, C. *J. Chem. Phys.* **2000**, *112*, 752-760.

(211) Koretsky, G. M.; Knickelbein, M. B.; Rousseau, R.; Marx, D. *J. Phys. Chem. A* **2001**, *105*, 11197-11203.

(212) Li, Y.-C.; Yang, C.-L.; Sun, M.-Y.; Li, X.-X.; An, Y.-P.; Wang, M.-S.; Ma, X.-G.; Wang, D.-H. *J. Phys. Chem. A* **2009**, *113*, 1353-1359.

(213) Rousseau, R.; Marx, D. *J. Chem. Phys.* **2000**, *112*, 761-769.

(214) A X-H···Au type hydrogen boning has been reported: (a) Kryachko, E. S.; Remacle, F. *Nano Lett.*, **2005**, *5*, 735-739. (b) Kryachko, E. S. *J. Mol. Struct.* **2008**, *880*, 23-30

(215) Chesalov, Y. A.; Chernobay, G. B; Boldyreva, E. V. *J. Struct. Chem.* **2008**, *49*, 627-638.

(216) Patron, L.; Carp, O.; Mindru, I.; Marinescu, G.; Segal, E. *J. Therm. Anal. Calorim.* **2003**, *72*, 281-288.

(217) Cornell, R. M.; Schindler, P. W. *Colloid. Polym. Sci.* **1980**, *258*, 1171-1175.

(218) Rush, P. E.; Oliver, J. D.; Simpson, G. D.; Carlisle, G. O. *J. Inorg. Nucl. Chem.* **1975**, *37*, 1393-1395.

(219) Young, A. G.; Green, D. P.; McQuillan, A. J. *Langmuir* **2007**, *23*, 12923-12931.

(220) Nuzzo, R. G.; Dubois, L. H.; Allara, D. L. *J. Am. Chem. Soc.* **1990**, *112*, 559-569.

(221) Rousseau, R.; Dietrich, G.; Krückeberg, S.; Lützenkirchen, K.; Max, D.; Schweikhard, L.; Walther, C. *Chem. Phys. Lett.* **1998**, *295*, 41-46.

(222) Sarmah, S.; Dass, N. N. *J. Therm. Anal.* **1998**, *54*, 913-920.

(223) Ha, J.; Yoon, T. H.; Wang, Y.; Musgrave, C. B.; Brown, G. E. *Langmuir* **2008**, *24*, 6683-6692.

(224) Parikh, A. N.; Gillmor, S. D.; Beers, J. D.; Beardmore, K. M.; Cutts, R. W.; Swanson, B. I. *J. Phys. Chem. B* **1999**, *103*, 2850-2861.

(225) Kluth, G. J.; Carraro, C.; Maboudian, R. *Phys. Rev. B* **1999**, *59*, R10449-R10452.

(226) Travert, J.; Lavalley, J. C.; Chenery, D. *Spectrochim. Acta* **1979**, *35A*, 291-299.

(227) (a) Quinan, J. R.; Wiberely, S. E. *Anal. Chem.* **1954**, *11*, 1762-1764. (b) Quinan, J. R.; Wiberely, S. E. *J. Chem. Phys.* **1953**, *21*, 1896-1897.

(228) Controversial δ(OH) assignments at higher wavenumbers including ref. 82 : (a) Florián, J.; Leszczynski, J.; Johnson, B. G.; Goodman, L. *Mol. Phys.* **1997**, *91*, 439-447. (b) Falk, M.; Whalley, E. *J. Chem. Phys.* **1961**, *34*, 1554-1568. (c) Carmona, P.; Molina, M.; Aboitiz, N.; Vicent, C. *Biopolym.* **2002**, *67*, 20-25. (d) Silverstein, R. M.; Webster, F. X. *Spectrometric Identification of Organic Compounds* 6th Ed.; John Wiley & Sons, Inc.: New York, 1998, pp 90- . (e) Nyquist, R. A. *Spectrochim. Acta* **1971**, *27A*, 2513-2523.

(229) (a) Wu, G.; Stacchiola, D.; Kaltchev, M.; Tysoe, W. T. *Surf. Sci.* **2000**, *463*, 81-92. (b) Wyn-Jones, E.; Orville-Thomas, W. J. *J. Mol. Struct.* **1967**, *1*, 79-89. (c) Oomens, J.; Steill, J. D.; Redlich, B. *J. Am. Chem. Soc.* **2009**, *131*, 4310-4319.

(230) Controversial assignments for the 1175/1145 cm^{-1} peaks including ref. 83 and 84: Stacchiola, D.; Burkholder, L.; Tysoe, W. T. *J. Mol. Cat. A* **2004**, *216*, 215-221.

(231) Larsen, O. F. A.; Woutersen, S. *J. Chem. Phys.* **2004**, *121*, 12143-12145.

(232) Chen, A.; Lipkowski, J. *J. Phys. Chem. B* **1999**, *103*, 682-691.

(233) Wang, X.; Andrews, L. *J. Phys. Chem. A* **2007**, *111*, 1860-1868.

(234) Avramopoulos, A.; Papadopoulos, M. G.; Sadlej, A. J. *Chem. Phys. Lett.* **2003**, *370*, 765-769.

(235) Bardet, L. *Spectrochim. Acta* **1985**, *41A*, 1477-1483.

(236) Hadži, D.; Sheppard, N. *Proc. Royal Soc. London* **1953**, *216*, 247-266.

(237) Weltner, W. *J. Am. Chem. Soc.* **1955**, *77*, 3941-3950.

(238) Bougeard, D. *Spectrochim. Acta* **1988**, *44A*, 1281-1286.

(239) Green, J. H. S. *Spectrochim. Acta* **1977**, *33A*, 575-581.

(240) Bratož, S.; Hadži, D.; Sheppard, N. *Spectrochim. Acta* **1956**, *8*, 249-261.

(241) Bootharaju, M. S.; Pradeep, T. *J. Phys. Chem. C* **2010**, *114*, 8323-8336.

(242) Tseng, R. J.; Tsai, C.; Ma, L.; Ouyang, J.; Ozkan, C. S.; Yang, Y. *Nat. Nanotech.* **2006**, *1*, 72-77.

(243) May, C. J.; Canavan, H. E.; Castner, D. G. *Anal. Chem.* **2004**, *76*, 1114-1122.

(244) Schulz, K. H.; Cox, D. F. *J. Phys. Chem.* **1993**, *97*, 647-655.

(245) Briggs, D.; Beamson, G. *Anal. Chem.* **1992**, *64*, 1729-1736.

(246) Tielens, F.; Humbolt, V.; Pradier, C.-M.; Calatayud, M.; Illas, F. *Langmuir* **2009**, *25*, 9980-9985.

(247) Burns, F. C.; Swalen, J. D. *J. Phys. Chem.* **1982**, *86*, 5123-5127.

(248) Sastry, M.; Ganguly, P. *J. Phys. Chem. A* **1998**, *102*, 697-702.

(249) Han, S. W.; Joo, S. W.; Ha, T. H.; Kim, Y.; Kim, K. *J. Phys. Chem. B* **2000**, *104*, 11987-11995.

(250) Schulz, K. H.; Cox, D. F. *J. Phys. Chem.* **1992**, *96*, 7394-7398.

(251) Dmitriev, A.; Spillmann, H.; Stepanow, S.; Strunskus, T.; Wöll, C.; Seitsonen, A. P.; Lingenfelder, M.; Lin, N.; Barth, J. V.; Kern, K. *ChemPhysChem* **2006**, *7*, 2197-2204.

(252) Zhang, P.; Sham, T. K. *Phys. Rev. Lett.* **2003**, *90*, 245502.

(253) Chesneau, F.; Zhao, J.; Shen, C.; Buck, M.; Zharnikov, M. *J. Phys. Chem. C* **2010**, *114*, 7112-7119.

(254) Tanaka, A.; Takeda, Y.; Imamura, M.; Sato, S. *Phys. Rev. B* **2003**, *68*, 195415.

(255) Heister, K.; Zharnikov, M.; Grunze, M.; Johansson, L. S. O. *J. Phys. Chem. B* **2001**, *105*, 4058-4061.

(256) Zhang, Q.; Li, N.; Goebl, J.; Lu, Z.; Yin, Y. *J. Am. Chem. Soc.* **2011**, *133*, 18931-18939.

(257) Sosibo, N. M.; Mdluli, P. S.; Mashazi, P. N.; Dyan, B.; Revaprasadu, N.; Nyokong, T.; Tshikhudo, R. T.; Skepu, A.; van der Lingen, E. *J. Mol. Struct.* **2011**, *1006*, 494-501.

(258) Martin, R. B. *J. Phys. Chem.* **1961**, *65*, 2053-2055.

(259) Pearce, K. N.; Creamer, L. K. *Aust. J. Chem.* **1975**, *28*, 2409-2415.

(260) For crystal structures: (a) Glusker, J. P.; van der Helm, D.; Love, W. E.; Dornberg, M. L.; Patterson, A. L. *J. Am. Chem. Soc.* **1960**, *82*, 2964-2965. (b) Glusker, J. P.; van der Helm, D.; Love, W. E.; Dornberg, M. L.; Minkin, J. A.; Johnson, C. K.; Patterson, A. L. *Acta Cryst.* **1965**, *19*, 561-572. (c) Andrade, L. C. R. *Z. Kristallogr.* **2002**, *NCS 217*, 537-538. (d) Tobón-Zapata, G. E.; Piro, O. E.; Etcheverry, S. B.; Baran, E. J. *Z. Anorg. Allg. Chem.* **1998**, *624*, 721-724.

(261) For the terminal ionization: (a) Loewenstein, A.; Roberts, J. D. *J. Am. Chem. Soc.* **1960**, *82*, 2705-2710. (b) Smith, G.; Wermuth, U. D.; White, J. M. *Acta Crystallogr., Sect. E: Struct. Rep. Online* **2007**, *63*, 02890.

(262) Paik, W.-k.; Han, S.; Shin, W.; Kim, Y. *Langmuir* **2003**, *19*, 4211-4216.

(263) Rodrígez-González, B; Mulvaney, P.; Liz-Marzán, L. M. *Z. Phys. Chem.* **2007**, *221*, 415-426.

(264) Ojea-Jiménez, I.; Romero, F. M.; Bastús, N. G.; Puntes, V. *J. Phys. Chem. C* **2010**, *114*, 1800-1804.

(265) Herlinger, A. W.; Wenhold, S. L.; Long, T. V. *J. Am. Chem. Soc.* **1970**, *92*, 6474-6481.

(266) Iwamoto, T.; Shriver, D. F. *Inorg. Chem.* **1971**, *10*, 2428-2432.

(267) Xu, C.; Goodman, D. W. *J. Phys. Chem.* **1996**, *100*, 1753-1760.

(268) Seshadri, K.; Atre, S. V.; Tao, Y.-T.; Lee, M.-T.; Allara, D. L. *J. Am. Chem. Soc.* **1997**, *119*, 4698-4711.

(269) Hwang, Y. S.; Lenhart, J. J. *Langmuir* **2008**, *24*, 13934-13943.

(270) NMR studies: (a)Agarwal, V.; Linser, R.; Fink, U.; Faelber, K.; Reif, B. *J. Am. Chem. Soc.* **2010**, *132*, 3187-3195. (b) Sigala, P. A.; Caaveiro, J. M. M.; Ringe, D.; Petsko, G. A.; Herschlag, D. *Biochemistry* **2009**, *48*, 6932-6939. (c) Tolstoy, P. M.; Koeppe, B.; Denisov, G. S.; Limbach, H.-H. *Angew. Chem. Int. Ed.* **2009**, *48*, 5745-5747.

(271) Govor, L. V.; Bauer, G. H.; Reiter, G.; Parisi, J. *Phys. Rev. B* **2010**, *82*, 155437.

(272) Lahann, J.; Mitragotri, S.; Tran, T.-N.; Kaido, H.; Sundaram, J.; Choi, I. S.; Hoffer, S.; Somorjai, G. A.; Langer, R. *Science* **2003**, *299*, 371-374.

(273) Tarakeshwar, P.; Manogaran, S. *Spectrochim. Acta* **1994**, *50A*, 2327-2343.

(274) Petroski, J.; El-Sayed, M. A. *J. Phys. Chem. A* **2003**, *107*, 8371-8375.

(275) Garcia, A. R.; de Barros, R. B.; Lourenço, J. P; Ilharco, L. M. *J. Phys. Chem. A* **2008**, *112*, 8280-8287.

(276) Inomata, Y.; Takeuchi, T.; Moriwaki, T. *Bull. Chem. Soc. Jpn* **1976**, *49*, 1568-1572.

(277) Baran, E. J. *Spectrochim. Acta, Part A* **2007**, *66*, 114-117.

(278) Kincaid, J.; Nakamoto, K. *Spectrochim. Acta* **1976**, *32A*, 277-283.

(279) Heinen, M.; Jusys, Z.; Behm, R. J. *J. Phys. Chem. C* **2010**, *114*, 9850-9864.

(280) Xu, B.; Madix, R. J.; Friend, C. M. *J. Amer. Chem. Soc.* **2010**, *132*, 16571-16580.

(281) There may be a charge transfer process between citrate and the metal surface.

(282) Willey, T. M.; Vance, A. L.; Bostedt, C.; van Buuren, T.; Meulenberg, R. W.; Terminello, L. J.; Fadley, C. S. *Langmuir* **2004**, *20*, 4939-4944.

(283) Kelley, A. T.; Ngunjiri, J. N.; Serem, W. K.; Lawrence, S. O.; Yu, J.-J.; Crowe, W. E.; Garno, J. C. *Langmuir* **2010**, *26*, 3040-3049.

(284) Pawsey, S.; McCormick, M.; De Paul, S.; Graf, R.; Lee, Y. S.; Reven, L.; Spiess, H. W. *J. Am. Chem. Soc.* **2003**, *125*, 4174-4184.

(285) Nair, A. S.; Kimura, K. *Phys. Chem. Chem. Phys.* **2009**, *11*, 9346-9350.

(286) Sun, L.; Kepley, L. J. Crooks, R. M. *Langmuir* **1992**, *8*, 2101-2103.

(287) Park, J.-W.; Shumaker-Parry, J. S. "Strong Resistance of Cooridnated Carboxylates to Desorption on Metal Nanoparticles under Thiol Treatment due to Intermolecular Interactions". *manuscript in preparation.*

(288) Silverstein, R. M.; Webster, F. X. *Spectrometric Identification of. Organic Compounds* 6th Ed. 1998, John Wiley & Sons, Inc., p 89.

(289) Mizukami, M.; Moteki, M.; Kurihara, K. *J. Amer. Chem. Soc.* **2002**, *124*, 12889-12897.

(290) Cézard, C.; Rice, C. A.; Suhm, M. A. *J. Phys. Chem. A* **2006**, *110*, 9839-9848.

(291) Alemán, C.; Casanovas, J.; Zanuy, D.; Hall, H. K. *J. Org. Chem.* **2005**, *70*, 2950-2956.

(292) Martin, D. S.; Cole, R. J.; Haq, S. *Surf. Sci.* **2003**, *539*, 171-181.

(293) Kawaguchi, S.; Kitano, T.; Ito, K. *Macromolecules* **1991**, *24*, 6030-6036.

(294) Doan, V.; Köppe, R.; Kasai, P. H. *J. Am. Chem. Soc.* **1997**, *119*, 9810-9815.

(295) Lee, H. M.; Kumar, A.; Kołaski, M.; Kim, D. Y.; Lee, E. C.; Min, S. K.; Park, M.; Choi, Y. C.; Kim, K. S. *Phys. Chem. Chem. Phys.* **2010**, *12*, 6278-6287.

(296) Nikoobakht, B.; El-Sayed, M. A. *Langmuir* **2001**, *17*, 6368-6374.

(297) Personal conversation with Professor Wilson Ho at the Physics Department of the University of California, Irvine.

(298) Smerieri, M.; Vattuone, L.; Costa, D.; Tielens, F.; Savio, L. *Langmuir* **2010**, *26*, 7208-7215.

(299) Personal conversation with Dr. Igor Lyubinetsky at Pacific Northwest National Laboratory (Richland, WA).

(300) Mathews, D. M.; Sheets, R. W. *J. Chem. Soc. A* **1969**, 2203-2206.

(301) Gao, Q.; Hemminger, J. C. *Surf. Sci.* **1991**, *248*, 45-56.

(302) Jeffrey, G. A. *An Introduction to Hydrogen Bonding*; Oxford University Press: New York, 1997; p 56.

(303) Cooper, E.; Leggett, G. J. *Langmuir* **1999**, *15*, 1024-1032.

(304) Chen, F.; Li, X.; Hihath, J.; Huang, Z.; Tao, N. *J. Am. Chem. Soc.* **2006**, *128*, 15874-15881.

(305) Hermse, C. G. M.; van Bavel, A. P.; Jansen, A. P. J.; Barbosa, L. A. M. M.; Sautet, P.; van Santen, R. A. *J. Phys. Chem. B* **2004**, *108*, 11035-11043.

(306) Ulman, A. *Chem. Rev.* **1996**, *96*, 1533-1554.

(307) Bulou, H.; Goyhenex, C. *Phys. Rev. B* **2002**, *65*, 045407.

(308) Barth, J. V.; Brune, H.; Ertl, G.; Behm, R. J. *Phys. Rev. B* **1990**, *42*, 9307-9318.

(309) Ulman, A.; Eilers, J. E.; Tillman, N. *Langmuir* **1989**, *5*, 1147-1152.

(310) Leveiller, F.; Jacquemain, D.; Lahav, M.; Leiserowitz, L.; Deutsch, M.; Kjaer, K.; Als-Nielsen, J. *Science* **1991**, *252*, 1532-1536.

(311) Schwartz, D. K.; Garnaes, J.; Viswanathan, R.; Zasadzinski, J. A. N. *Science* **1992**, *257*, 508-511.

(312) Schwartz, D. K.; Viswanathan, R.; Garnaes, J.; Zasadzinski, J. A. N. *J. Amer. Chem. Soc.* **1993**, *115*, 7374-7380.

(313) Smerieri, M.; Vattuone, L.; Kravchuk, T.; Costa, D.; Savio, L. *Langmuir* **2011**, *27*, 2393-2404.

(314) Li, J.-L.; Car, R.; Tang, C.; Wingreen, N. S. *Proc. Natl. Acad. Sci. U.S.A.* **2007**, *104*, 2626-2630.

(315) Giersig, M.; Mulvaney, P. *Langmuir* **1993**, *9*, 3408-3413.

(316) Dibbern, E. M.; Toublan, F. J.-J.; Suslick, K. S. *J. Am. Chem. Soc.* **2006**, *128*, 6540-6541.

(317) Tolstoy, P. M.; Schah-Mohammedi, P.; Smirnov, S. N.; Golubev, N. S.; Denisov, G. S.; Limbach, H.-H. *J. Am. Chem. Soc.* **2004**, *126*, 5621-5634.

(318) Braga, D.; Novoa, J. J.; Grepioni, F. *New J. Chem.* **2001**, *25*, 226-230.

(319) Cassidy, C. S.; Reinhardt, L. A.; Cleland, W. W.; Frey, P. A. *J. Chem. Soc., Perkin Trans. 2* **1999**, 635-641.

(320) Iwai, H.; Egawa, C. *Langmuir* **2010**, *26*, 2294-2300.

(321) Wall, J. F.; Grieser, F.; Zukoski, C. F. *J. Chem. Soc., Faraday Trans.* **1997**, *93*, 4017-4020.

(322) Groen, H.; Roberts, K. J. *J. Phys. Chem. B* **2001**, *105*, 10723-10730.

(323) Frey, P. A.; Whitt, S. A.; Tobin, J. B. *Science* **1994**, *264*, 1927-1930.

(324) Payer, D.; Comisso, A.; Dmitriev, A.; Strunskus, T.; Lin, N.; Wöll, C.; DeVita, A.; Barth, J. V.; Kern, K. *Chem. Eur. J.* **2007**, *13*, 3900-3906.

(325) Schrier, E. E.; Pottle, M.; Scheraga, H. A. *J. Am. Chem. Soc.* **1964**, *84*, 3444-3449.

(326) Chen, J.; Brooks, C. L., III; Scheraga, H. A. *J. Phys. Chem. B* **2008**, *112*, 242-249.

(327) Nishi, N.; Nakabayashi, T.; Kosugi, K. *J. Phys. Chem. A* **1999**, *103*, 10851-10858.

(328) Pašalić, H.; Tunega, D.; Aquino, A. J. A.; Haberhauer, G.; Gerzabek, M. H.; Lischka, H. *Phys. Chem. Chem. Phys.* **2012**, *14*, 4162-4170.

(329) Chocholoušová, J.; Vacek, J.; Hobza, P. *J. Phys. Chem. A* **2003**, *107*, 3086-3092.

(330) Jiang, L.; Wang, W.; Fuchs, H.; Chi, L. *Small* **2009**, *5*, 2819-2822.

(331) Yang, Y.; Wang, C. *Chem. Soc. Rev.* **2009**, *38*, 2576-2589.

(332) Nuzzo, R. G.; Bubois, L. H.; Allara, D. L. *J. Am. Chem. Soc.* **1990**, *112*, 558-569.

(333) Feyer, V.; Plekan, O.; Tsud, N.; Cháb, V.; Matolín, V.; Prince, K. C. *Langmuir* **2010**, *26*, 8606-8613.

(334) Wang, J.-g.; Selloni, A. *J. Phys. Chem. C* **2009**, *113*, 8895-8900.

(335) Lyubinetsky, I.; Deskins, N. A.; Du, Y.; Vestergaard, E. K.; Kim, D. J.; Dupuis, M. *Phys. Chem. Chem. Phys.* **2010**, *12*, 5986-5992.

(336) Mateo-Martí, E.; Rogrero,C.; Gonzalez, C.; Sobrado, J. M.; de Andrés, P. L.; Martin-Gago, J. A. *Langmuir* **2010**, *26*, 4113-4118.

(337) Kan, C.; Zhu, X.; Wang, G. *J. Phys. Chem. B* **2006**, *110*, 4651-4656.

(338) (a) Barnard, A. S. *J. Phys. Chem. B* **2006**, *110*, 24498-24504. (b) Wang, Z. L.; Mohamed, M. B.; El-Sayed, M. A. *Surf. Sci.* **1999**, *440*, L809-L814. (c) Wang, B.; Liu, M.; Wang, Y.; Chen, X. *J. Phys. Chem. C* **2011**, *115*, 11374-11381. (d) Long, N. N.; Vu, L. V.; Kiem, C. D.; Doanh, S. C.; Nguyet, C. T.; Hang, P. T.; Thien, N. D.; Quynh, L. M. *J. Phys. Conf. Ser.* **2009**, *187*, 012026.

(339) Roth, C.; Passerone, D.; Merz, L.; Parschau, M.; Ernst, K.-H. *J. Phys. Chem. C* **2011**, *115*, 1240-1247.

(340) Zeng, J.; Zheng, Y.; Rycenga, M.; Tao, J.; Li, Z.-Y.; Zhang, Q.; Zhu, Y.; Xia, Y. *J. Amer. Chem. Soc.* **2010**, *132*, 8552-8553.

(341) Dretschkow, Th.; Dakkouri, A. S.; Wandlowski, Th. *Langmuir* **1997**, *13*, 2843-2856.

(342) Brown, K. R.; Walter, D. G.; Natan, M. J. *Chem. Mater.* **2000**, *12*, 306-313.

(343) Jana, N. R.; Gearheart, L.; Murphy, C. J. *Adv. Mater.* **2001**, *13*, 1389-1393.

(344) Johnson, C. J.; Dujardin, E.; Davis, S. A.; Murphy, C. J.; Mann, S. *J. Mater. Chem.* **2002**, *12*, 1765-1770.

(345) Kuo, C.-H.; Huang, M. H. *Langmuir* **2005**, *21*, 2012-2016.

(346) Kuo, C.-H.; Chiang, T.-F.; Chen, L.-J.; Huang, M. H. *Langmuir* **2004**, *20*, 7820-7824.

(347) Ah, C. S.; Yun, Y. J.; Park, H. J.; Kim, W.-J.; Ha, D. H.; Yun, W. S. *Chem. Mater.* **2005**, *17*, 5558-5561.

(348) Zou, X.; Ying, E.; Dong, S. *Nanotechnology* **2006**, *17*, 4758-4764.

(349) Zhao, L.; Jiang, D.; Cai, Y.; Ji, X.; Xie, R.; Yang, W. *Nanoscale* **2012**, *4*, 5071-5076.

(350) Brust, M.; Bethell, D.; Schiffrin, D. J.; Kiely, C. J. *Adv. Mater.* **1995**, *7*, 795-797.

(351) Wallner, A.; Jafri, S. H. M.; Blom, T.; Gogoll, A.; Leifer, K.; Baumgartner, J.; Ottosson, H. *Langmuir* **2011**, *27*, 9057-9067.

(352) Franke, A.; Pehlke, E. *Phys. Rev. B* **2010**, *81*, 075409.

(353) Hussain, I.; Brust, M.; Barauskas, J.; Cooper, A. I. *Langmuir* **2009**, *25*, 1934-1939.

(354) Li, S.-S.; Northrop, B. H.; Yuan, Q.-H.; Wan, L.-J.; Stang, P. J. *Acc. Chem. Res.* **2009**, *42*, 249-259.

(355) Lackinger, M.; Heckl, W. M. *Langmuir* **2009**, *25*, 11307-11321.

(356) Iski, E. V.; Tierney, H. L.; Jewell, A. D.; Sykes, E. C. H. *Chem. Eur. J.* **2011**, *17*, 7205-7212.

(357) Teugels, L. G.; Avila-Bront, L. G.; Sibener, S. J. *J. Phys. Chem. C* **2011**, *115*, 2826-2834.

(358) Parschau, M.; Romer, S.; Ernst, K.-H. *J. Amer. Chem. Soc.* **2004**, *126*, 15398-15399.

(359) Haq, S.; Liu, N.; Humblot, V.; Jansen, A. P. J.; Raval, R. *Nat. Chem.* **2009**, *1*, 409-414.

(360) De Cat, I.; Gobbo, C.; Van Averbeke, B.; Lazzaroni, R.; De Feyter, S.; van Esch, J. *J. Am. Chem. Soc.* **2011**, *133*, 20942-20950.

(361) Naitabdi, A.; Humblot, V. *Appl. Phys. Lett.* **2010**, *97*, 223112.

(362) Nelson, E. M.; Rothberg, L. J. *Langmuir* **2011**, *27*, 1770-1777.

(363) Rostek, A.; Mahl, D.; Epple, M. *J. Nanopart. Res.* **2011**, *13*, 4809-4814.

(364) Coppage, R.; Slocik, J. M.; Briggs, B. D.; Frenkel. A. I.; Heinz, H.; Naik, R. R.; Knecht, M. R. *J. Am. Chem. Soc.* **2011**, *133*, 12346-12349.

(365) Lee, P. C.; Msisel, D. *J. Phys. Chem.* **1982**, *86*, 3391-3395.

(366) Lin, C.-S.; Khan, M. R.; Lin, S. D. *J. Colloid Interface Sci.* **2005**, *287*, 366-369.

(367) Lin, C.-S.; Khan, M. R.; Lin, S. D. *J. Colloid Interface Sci.* **2006**, *299*, 678-685.

(368) Turkevich, J.; Kim, G. *Science* **1970**, *169*, 873-879.

(369) Abdulla-Al-Mamun, Md.; Kusumoto, Y.; Muruganandham, M. *Mater. Lett.* **2009**, *63*, 2007-2009.

(370) Kiely, C. J. *Faraday Discuss.* **2004**, *125*, 409-414.

(371) Li, M.; Johnson, S.; Guo, H.; Dujardin, E.; Mann, S. *Adv. Funct. Mater.***2011**, *21*, 851-859.

(372) Tang, Z. Y.; Kotov, N. A.; Giersig, M. *Science* **2002**, *297*, 237-240.

(373) Blanton, S. A.; Leheny, R. L.; Hines, M. A.; Guyot-Sionnest, P. *Phys. Rev. Lett.* **1997**, *79*, 865-868.

(374) Shim, M.; Guyot-Sionnest, P. *J. Chem. Phys.* **1999**, *111*, 6955-6964.

(375) Link, S.; El-Sayed, M. A. *J. Phys. Chem. B* **1999**, *103*, 4212-4217.

(376) Klar, T.; Perner, M.; Grosse, S.; von Plessen, G.; Spirkl, W.; Feldmann, J. *Phys. Rev. Lett.* **1998**, *80*, 4249-4252.

(377) Bosbach, J.; Hendrich, C.; Stietz, F.; Vartanyan, T.; Träger, F. *Phys. Rev. Lett.* **2002**, *89*, 257404.

(378) Boeker, A.; Lin, Y.; Chiapperini, K.; Horowitz, R.; Thompson, M.; Carreon, V.; Xu, T.; Abetz, C.; Skaff, H.; Dinsmore, A. D.; Emrick, T.; Russell, T. P. *Nat. Mater.* **2004**, *3*, 302-306.

(379) (a) Korgel, B. A.; Fitzmaurice, D. *Adv. Mater.* **1998**, *10*, 661-665. (b) Giersig, M.; Pastoriza-Santos, I.; Liz-Marzán, L. M. *J. Mater. Chem.* **2004**, *14*, 607-610.

(380) (a) Jackson, A. M.; Myerson, J. W.; Stellacci, F. *Nat. Mater.* **2004**, *3*, 330-336. (b) Jadzinsky, P. D.; Calero, G.; Ackerson, C. J.; Bushnell, D. A.; Kornberg, R. D. *Science* **2007**, *318*, 430-433.

(381) Takesue, M.; Tomura, T.; Yamada, M.; Hata, K.; Kuwanmoto, S.; Yonezawa, T. *J. Am. Chem. Soc.* **2011**, *133*, 14164-14167.

(382) Sinyagin, A. Y.; Belov, A.; Tang, Z.; Kotov, N. A. *J. Phys. Chem. B* **2006**, *110*, 7500-7507.

(383) Ren. Y.; Iimura, K.-I.; Kato, T. *Langmuir* **2001**, *17*, 2688-2693.

(384) CH_2 bending modes at 1430 - 1458 cm^{-1} for aliphatic dicarboxylates on metal oxides: see ref. 155.

(385) CH_2 bending: see ref. 187.

(386) CH_2 wagging mode: see ref. 187.

(387) CH_2 twisting mode: see ref. 187.

(388) ν(C-C): see ref. 277.

(389) Huo, Z.; Tsung, C.-k.; Huang, W.; Zhang, X.; Yang, P. *Nano Lett.* **2008**, *8*, 2041-2044.

(390) Mikhlin, Y.; Likhatski, M.; Karacharov, A.; Zaikovski, V.; Krylov, A. *Phys. Chem. Chem. Phys.* **2009**, *11*, 5445-5454.

(391) Szczerba, W.; Riesemeier, H.; Thünemann, A. F. *Anal. Bioanal. Chem.* **2010**, *398*, 1967-1972.

(392) Miller, J. T.; Kropf, A. J.; Zha, Y.; Regalbuto, J. R.; Delannoy, L.; Louis, C.; Bus, E.; van Bokhoven, J. A. *J. Cat.* **2006**, *240*, 222-234.

CHAPTER 3

STRONG RESISTANCE OF COORDINATED CARBOXYLATES TO DESORPTION ON METAL NANOPARTICLES UNDER THIOL TREATMENT DUE TO INTERMOLECULAR INTERACTIONS

3.1 Introduction

Citrate-stabilized gold nanoparticles (AuNPs) are commonly used as the foundational materials for many AuNP-based studies.[1] The synthesis of citrate-stabilized AuNPs (citrate-AuNPs) was developed by Turkevich and co-workers,[2] and further developed by Frens.[3] In this method, citrate molecules reduce Au^{3+} ions to Au atoms and stabilize the colloidal AuNPs (i.e., typically 10 – 100 nm in diameter) which are formed. Generally, the metallic core size of AuNPs defines the electronic[4] and optical properties[5,6] whereas the ligand shell, i.e., citrate and other ligands such as thiol[7] and phosphine,[8] governs the chemical properties including solubility,[9] surface charge,[10] interparticle interactions,[11,12] molecule-particle interactions,[13] surface chemical reactivity,[14] and intracellular activity.[15] Due to the critical role of surface organic layers, much effort is put into modifying the surface functional groups to tailor the chemical properties of AuNPs. The most commonly used approach for surface modification is to exchange the ligands initially adsorbed on NP surfaces with another type of incoming ligand. Because thiols have a strong affinity for metals such as Au and Ag and form organized self-assembled

monolayers (SAM) on planar Au[16,17] and Ag surfaces,[18,19] ω-terminated thiols are often used for the formation of robust ligand shells on metal NPs.[20,21]

One of the most common ligand exchange processes used for citrate-AuNPs is the replacement of citrate molecules with functionalized thiols. For the most part, the approach to this exchange is typically presented in a rather simple manner based on the assumption that the thiol molecules spontaneously displace the citrates leading to a completely thiolate-functionalized nanoparticle.[20] Although ligand exchange between thiols and phosphines on the surfaces of small gold nanoclusters has been investigated[22-24] in a systematic manner, the citrate-to-thiol ligand exchange for larger nanoparticles has not been studied in detail despite the wide use of this process. The dearth of research on the citrate-to-thiol exchange probably originates from the relatively large core size of citrate-stabilized AuNPs causing 1) NP aggregation during addition of thiols, preventing ^{1}H-NMR studies, 2) low amounts of molecules making surface analysis challenging, 3) the complexity involved with functional groups such as hydroxyl[25,26] and carboxylic acids[27 - 29] coordinating with the gold surface, and 4) challenges in interpreting spectroscopy data to understand the conformation and surface coverage of the adsorbed citrate. To my knowledge, there is no reported study providing direct detection of coordinated citrate species displaced by thiol at a metal surface. A few researchers have discussed issues related to incomplete displacement of the adsorbed citrate on Au or AgNPs,[30 , 31] and point out the difficulty in replacing citrates by thiols[32] or biomolecules.[33,34] Until now, however, there have been abundant examples of reports relying on the assumption of complete displacement of the adsorbed citrates by thiols. Ligand exchange of citrate-capped metal nanoparticles typically is the first step for a large variety of studies related to the chemical and biological properties of AuNPs

including ligand surface coverage,[35,36] particle stability,[37-41] linker conjugation on NP surfaces,[9,13,37, 42 - 50] particle-molecule interactions,[13, 51] particle-ion interactions,[52] and biological/medical applications[47,53-57] as well as for silver nanoparticles.[58,59] Remaining citrate molecules impact the NP surface chemistry due to the hydroxyl/carboxyl groups and influence properties such as intracellular activity.[60,61] The significant and broad impact motivates the need for a more detailed understanding of the citrate-to-thiol ligand exchange.

Statements about facile ligand exchange of thiolates for citrate molecules on AuNPs[20,62,63] are primarily based on the difference in energy between Au-S[64,65] (~40 kcal/mol) and Au-carboxylate[27] (~2 kcal/mol) interactions, but other factors in addition to thermodynamics impact the ligand exchange process, including kinetic, electronic, steric, chelating, and solvent effects.[66] Interestingly, early postulations of citrate displacement by thiols[43,67] are not supported by the referenced article.[68] In the [ref. 68], the authors mainly discussed the adsorption of pyridine on copper colloids and observed the complete displacement of the adsorbed pyridine by thiophenol based on the disappearance of a pyridine peak at 1010 cm^{-1} in the surface-enhanced Raman scattering (SERS) spectra. As opposed to the citrate desorption process highlighted in the articles,[43,67] displacement of adsorbed citrate by pyridine was not discussed at all. Overall, it seems that the spontaneous displacement of citrates adsorbed on AuNPs by incoming thiols is generally accepted as a fact.

One of the simple tests for thiol-citrate exchange has been NP aggregation studies based on UV-Visible spectroscopy,[20] in that the aggregation is used to follow the adsorption of thiols on AuNPs, and this has become a representative protocol to monitor replacement of adsorbed citrates on metal NPs.[69, 70] This method provides a highly

qualitative approach to assess ligand exchange. The colorimetric assay based on a UV-visible absorption measurement, suggested by Whitesides and co-workers,[20] is associated with the assumption[67] that the displacement of the negatively-charged surface ions, e.g. citrate molecules, causes AuNP aggregation due to the loss of electrostatic repulsion and colloidal NP stability in solution. It is reasonable that anion adsorption on citrate-AuNPs produces the electrical charge of the NPs.[71] In this assumption, however, the propensity of desorption between citrates and other anions (Cl^-) is not considered, and the possibility of the coadsorption of thiols with preadsorbed surface citrates is neglected. Recently, the surface coverage by adsorbed citrate species on AuNPs was estimated to be ~30 % (see Chapter 2).[72] In addition to the citrate, there is evidence of coordinated chloride (Cl^-) ions. It can be suggested that rather than only citrate displacement, coadsorption of thiols with citrates may occur during the ligand exchange reaction. The resulting reduction in the electrostatic repulsion[73] can then lead to aggregation of the AuNPs after thiol addition. The observed decrease in surface potential after thiol addition[74] does not necessarily mean that surface citrates have been displaced by thiols. In this regard, Dagastine and Grieser[75] observed decreased surface charge on a planar silver surface with adsorbed citrates during addition of amines, and charge neutralization was proposed as one of the possible mechanisms[1] for the surface potential drop. The thiol adsorption may cause a decline in the negative charge on the surface, either by displacing surface Cl^-, reducing the pH of the solution, or shielding the surface citrate physically, resulting in the long-range van der Waals attractions between the thiolate layers dominating the surface properties leading to aggregation. The NP aggregation-based approach is an indirect

[1]The other proposed mechanism is the replacement of citrate.
Larson, I.; Chan, D. Y. C.; Drummond, C. J.; Grieser, F. *Langmuir* **1997**, *13*, 2429-2431.

method of studying the replacement of adsorbed citrate by incoming thiols, and to probe citrate directly by IR and XPS spectroscopic methods is attempted.

Herein, the ligand exchange of citrate-stabilized AuNPs (~39 nm in diameter) by incoming thiols is presented. The primary question to be addressed for this study is whether the surface citrate on AuNPs is displaced by incoming thiols. A kinetic study of the ligand exchange is out of the scope these investigations. Ligand-exchange reactions proceeded while preventing aggregation of AuNPs and keeping the surfaces of the NPs fully accessible for the exchange. Based on FT-IR (Fourier transform-infrared) and XPS (X-ray photoelectron spectroscopy) data for AuNPs after thiol addition, displacement of surface Cl^- as well as coadsorption of thiols and citrates are discussed. The ratio between the amounts of surface citrates and coadsorbed thiolates was quantitatively determined by XPS analysis. Contributions from the thermodynamic factor of the metal-organic bond strength and other factors including steric hindrance, chelating effects, and intermolecular interactions between surface citrates are assessed in order to explain the strong adsorption of citrate molecules on AuNPs.

3.2 Experiments

3.2.1 Materials

All chemicals were used without further purification unless otherwise stated. Tetrachloroaurate ($HAuCl_4 \cdot 3H_2O$), trisodium citrate ($Na_3C_6H_5O_7 \cdot 2H_2O$), 1-butanethiol (99%), 1-hexanethiol (95%), 1-heptanethiol (98%), 1-octanethiol (98.5%), 1-decanethiol (96%), 1-dodecanethiol (98%), 1-hexadecanethiol (92%), 4-mercapto-1-butanol (95%), 6-mercapto-1-hexanol (97%), 11-mercapto-1-undecanol (97%), 3-mercaptopropionic acid (99%), 6-mercaptohexanoic acid (90%), 11-mercaptoundecanoic acid (95%), 16-

mercaptohexadecanoic acid (90%), 4-mercaptobenzoic acid (90%), 2-aminoethanethiol (98%, Fluka, Switzerland), 4-aminothiophenol (97%), 4-mercaptopyridine (95%), (11-mercaptoundecyl)tetra(ethylene glycol) (95%, $HS(CH_2)_{11}(OCH_2CH_2)_4OH$) were purchased from Sigma-Aldrich. 16-hydroxy-1-hexadecanethiol (99%), 11-amino-1-undecanethiol (99%, hydrochloride), 4-nitrothiophenol (99%), 11-mercaptoundecyl trifluoroacetate (99%), 11-mercaptoundecanamide (99%), and methoxy-capped tetra(ethylene glycol) undecanethiol (99%, $HS(CH_2)_{11}(OCH_2CH_2)_4OCH_3$) were obtained from Asemblon (Redmond, WA). Benzyl mercaptan (96%) and ethyl 2-mercaptoacetate (97%) were purchased from Avocado Research Chemicals Ltd. (Heysham, Lancs, UK). Ethanol (EtOH, 200 proof, Pharmco-Aaper or Decon Labs) and sodium hydroxide (NaOH, Mallinckrodt Chemicals) were obtained from aforementioned companies. Water was used after purification (Barnstead Nanopure Diamond UV-UF, 17.8 MΩ/cm). All glassware was washed with aqua-regia (3:1, HCl/HNO_3) to remove gold particles and organic contaminants. Glassware contaminated heavily with organic materials and silicon wafers (Silicon Inc.) were cleaned with piranha solution (5:1, H_2SO_4/30% H_2O_2). *Caution! The piranha and aqua-regia solutions are highly corrosive and mixing the solution is very exothermic. It should be handled with extreme care and appropriate safety precautions.* The aqua-regia or piranha treated glassware was rinsed copiously with water and dried in an oven at 120 ^oC at least for 2 h.

3.2.2 Citrate-AuNP synthesis

AuNPs were synthesized using the Frens method.[3] Briefly, $HAuCl_4 \cdot 3H_2O$ (0.0232 g) was dissolved in water (200 mL), and $Na_3Citrate \cdot 2H_2O$ (0.0227 g) was dissolved in water (1 mL) and added to the boiling gold salt solution all at once with stirring. Heating

continued for additional an additional hour, and the resulting AuNP solution was cooled to room temperature with continuous stirring. The final AuNPs exhibit an average diameter of 39 nm with ~25% deviation and display an absorption maximum (λ_{max}) at 535 nm.

3.2.3 Addition of thiol solutions to citrate-AuNPs for ligand exchange

Typically, 10 mL of the 39-nm AuNP solution were centrifuged once and the resulting supernatant solution was discarded. The rest of the centrifuged AuNPs (final volume < 50 μL) was added to freshly prepared 10 mL of 1 mM ethanolic thiol solution, and then sonicated for dispersion. The added thiol amount is estimated to be more than 270 molar equivalents for monolayer formation on AuNPs (see the Appendix). The reaction mixture was left at room temperature for more than 2 h without stirring no matter how fast the NPs aggregated. To ensure completion of the reaction, a ligand exchange reaction with NO_2-Ph-SH proceeded at 40 ^{o}C for 3 d. The functionalized AuNPs were centrifuged and dispersed in ethanol three times to remove displaced citrates and excess thiols present in solution. The resultant ~100 μL-emulsion of AuNPs was used to prepare samples for IR and XPS analyses.

3.2.4 Adsorption isotherm of thiol on AuNPs

To study the early stages of adsorption of thiols on citrate-AuNPs, ligand exchange reactions were performed, similar to the protocol described above but using different thiol concentrations. With addition of a small amount of thiol ($0.25 < \chi < 2.00$, for a monolayer coverage, $\chi = 1.00$), fractional surface area smaller than the entire surface of AuNPs can be functionalized. An error in functionalized surface area due to the deviation

of particle diameter was ignored. AuNP loss during centrifugation was corrected by measuring the absorbance. Into ~3 mL of redispersed AuNP solution in ethanol, 0.225 mL ($\chi = 0.25$) , 0.300 mL ($\chi = 0.67$), 0.375 mL ($\chi = 0.42$), 0.450 mL ($\chi = 0.50$), 0.675 mL ($\chi = 0.75$), 0.900 mL ($\chi = 1.00$), 1.350 mL ($\chi = 1.50$), 1.800 mL ($\chi = 2.00$) of 1.5×10^{-5} M of 4-nitrobenzenethiol ethanolic solution were added, respectively. The final volume of each solution was adjusted to 5.0 mL (absorbance = 1.00 in 5 mL of final solutions), and the resultant solution was left at room temperature for 72 h.

3.2.5 Deprotonation of citrate carboxylic groups adsorbed on AuNPs

The pH was adjusted in order to control the protonation of the carboxylic acid group of the citrates adsorbed on the AuNPs. Centrifuged citrate-AuNPs were dispersed into water adjusted to pH ~10. The centrifugation/dispersion step in the pH 10 water was repeated three times. Irreversibly aggregated AuNPs were discarded during the centrifugation before addition of thiol.

3.2.6 UV-Vis absorption spectroscopy

Absorbance of citrate-AuNP solution was collected for a spectral range of 400 - 800 nm using a PerkinElmer Lambda 19 UV/vis/NIR spectrophotometer.

3.2.7 Attenuated total reflectance infrared spectroscopy (ATR-IR)

A PerkinElmer Spectrum 100 FT-IR spectrometer equipped with a MIRacle ATR (ZnSe crystal, PIKE Technologies) accessory was used. Centrifuged AuNP solution was transferred onto the crystal and dried with nitrogen gas. Spectra were collected at 4000 - 550 cm^{-1} after ethanol in samples had evaporated. ATR spectra were not corrected.

3.2.8 Transmission FTIR spectroscopy

The concentrated AuNPs were spread on a KBr IR card (International Crystal Laboratories, NJ) and dried with nitrogen gas. Spectra were collected using a PerkinElemer Spectrum 100 FT-IR spectrometer. Background correction was performed for samples of pH ~11 to subtract the spectrum of dried NaOH solution.

3.2.9 X-ray photoelectron spectroscopy (XPS)

X-ray photoelectron spectra were collected using a monochromatic Al Kα source (1486.6 eV) with a power of 144 W on a Kratos Axis Ultra DLD instrument (Chestnut Ridge, NY) and a 300 × 700 μm spot size. A drop-cast film of the functionalized AuNPs was prepared on silicon wafers, and good coverage of AuNP film was identified by the absence of Si peaks. Survey spectra were recorded with the pass energy of 160 eV (1 eV steps, 200 ms dwell), and high-resolution spectra at energy ranges of interest were recorded with a pass energy of 40 eV (0.1 eV, 400 ms dwell). The base pressure was 2×10^{-9} Torr. The incidence angle of the incoming X-ray was 54.7^{o}, and the electron take-off angle was 90^{o}. The binding energies shifted by substrate charging were corrected by referencing the C 1s peak of adventitious carbon to 284.8 eV. The background was subtracted by Shirely's method, which was used as a baseline for determining peak areas. Spectra were fitted using Gaussian/Lorentzian type functions.

3.2.10 Synthesis of citrate-stabilized silver nanoparticles (AgNPs)

AgNPs were synthesized according to a method in literature.[76,77] Briefly, 27 mg of $AgNO_3$ was dissolved in 150 mL water (1.0 mM), and the solution was refluxed. With vigorous stirring, 61.7 mg of $Na_3Citrate{\cdot}2H_2O$ in 6 mL water was added to the silver ion

solution (35 mM, 1% by weight). A milky yellow-greenish solution was obtained, and the pH was measured as ~6.6. The samples for ATR-IR, transmission IR, and XPS were prepared by the same methods used for AuNPs.

3.3 Results and discussion

3.3.1 Spectroscopy investigation of adsorption of alkanethiols on citrate-stabilized AuNPs

Spectroscopy analysis is used to investigate the extent of citrate displacement from citrate-AuNPs in the presence of alkanethiols. Generally, in the literature complete replacement of surface citrates on AuNPs by thiols is assumed. Often this is confirmed based on aggregation of NPs in solution upon addition of thiols. While the negatively-charged citrate-stabilized AuNPs resist aggregation due to the electrostatic repulsion between adjacent NPs, the adsorption of thiols on the AuNPs reduces the magnitude of the electric potential in the double layer on AuNPs and induces attraction. Spectroscopic approaches were used to investigate the displacement of citrate by thiols using methyl-terminated alkanethiol. This thiol was chosen because it induces NP aggregation which is often used to determine citrate displacement and the presence of the methyl group of the thiol does not interfere in identification of the carboxylic acid and hydroxyl groups of citrate in IR and XPS analysis. Figure 3.1 presents UV-Vis absorbance spectra exhibiting the typical red shift of the localized surface plasmon resonance (LSPR) of AuNPs by adding excess amounts (1 mM ethanolic solution) of 11-undecanethiol (CH_3-C_{11}-SH) into a solution of citrate-stabilized AuNPs, due to plasmon coupling in the NP aggregates. The UV-vis method for NP aggregation is an indirect method of studying the replacement

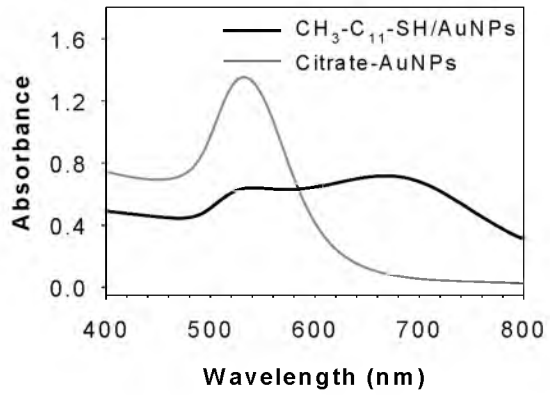

Figure 3.1. UV-visible absorbance spectra of citrate-AuNP solution as prepared (grey spectrum) and after addition of CH_3-C_{11}-SH into citrate-AuNP solution (black spectrum). The red shift of CH_3-C_{11}-SH/AuNPs displays the typical AuNP aggregation upon the thiol addition. λ_{max} = 532 nm for citrate-AuNP solution.

of adsorbed citrate by incoming thiols, and citrate was probed directly by IR and XPS spectroscopic methods.

Remaining surface citrate on AuNPs was characterized after the proceeded ligand-exchange reaction by using spectral signatures unique to the adsorbed citrate species in IR and XPS. First, a characteristic peak of the COOH hydrogen bond appearing at 1704 cm^{-1} was monitored after addition of 11-undecanethiol (CH_3-C_{11}-SH) (the dotted line in Figure 3.2A), which is assigned to a cyclic COOH dimer.[78-80] Another COOH hydrogen bond peak (shoulder) at 1734 cm^{-1} as an acyclic COOH dimer also was observed.[79,81,82] These peaks of the COOH hydrogen bonds are evidence of interactions between surface citrate species rather than citrates entrapped in alkanethiolate layers after being desorbed from the surface. It is unlikely that replaced citrates, possessing one hydroxyl and three carboxyl groups, are trapped in the hydrophobic SAMs of the alkanethiolate after being replaced from the AuNP surface. Individual citrate molecule interactions with the terminal methyl groups of the alkanethiols do not play a significant role in solution since

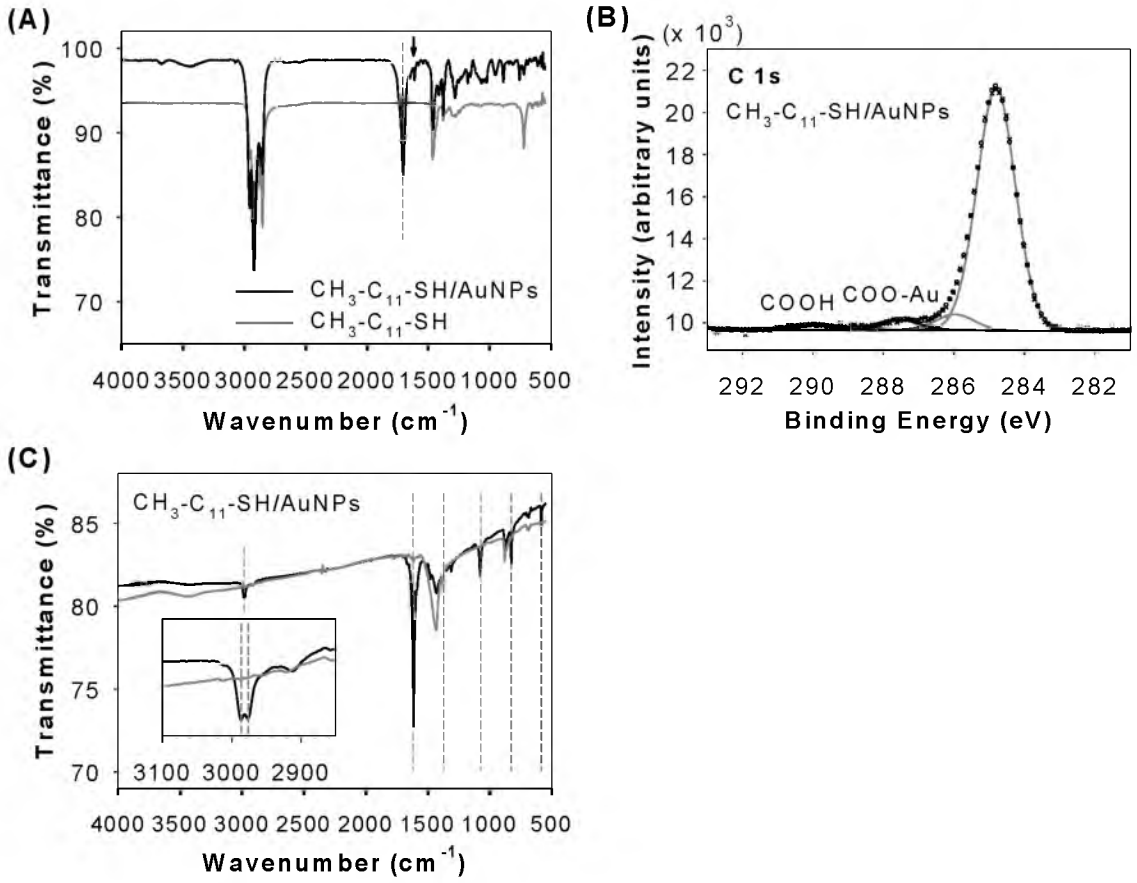

Figure 3.2. IR and XPS spectra indicative of coordinated citrate species remaining on AuNPs after addition of undecanethiol (H_3C-C_{11}-SH). (A) ATR-IR spectrum of AuNPs exhibits the characteristic ν(C=O) of hydrogen bonded -COOH groups at 1704 cm^{-1} (dotted line) along with $\nu_{asy}(COO^-)$ of surface coordinated COO-Au at 1611 cm^{-1} (arrowed). (B) XPS C 1s spectrum of AuNPs shows coordinated $\underline{C}OO^-$ on Au surfaces at 287.6 eV. (C) Transmission IR spectra display the unique IR band enhancement of surface citrate appearing when pH > ~11. The dotted lines are a guide for the peaks. The peak intensities are diminished (grey spectrum) after drying the sample on the IR card.

van der Waals attraction in ethanol is known to be very weak.[83] The existence of the surface citrate is further supported by detection of gold-carboxylate coordination. A characteristic asymmetric COO^- stretching vibration ($\nu_{asy}(COO)$) of a η^1-COO-Au coordinate (monodentate) to Au atoms via one of the carboxylate oxygen atoms was observed, which is not observed for sodium citrate and citric acid not associated with a surface. This $\nu_{asy}(COO)$ of the COO-Au coordinate appears at 1611 cm^{-1} as a small, but

sharp band (arrowed in Figure 3.2A). (The H/D exchange experiments indicated that this peak of 1611 cm^{-1} was not associated with possible low-barrier hydrogen bonds of COO···H···OOC configurations, because the peak did not shift upon deuteration. See Section 2.3.8. in Chapter 2.) Thus, the COOH associated peaks originate from the carboxylic acid groups of the adsorbed citrate, and this is direct evidence of incomplete displacement of citrate by the alkanethiols under typical experiment conditions of ligand exchange reactions. The concentration of the thiol solution was 1 mM, which is ~270 times larger than that needed to saturate the AuNP surfaces (see the Appendix).

This stability behavior of the AuNPs with other thiols was examined. ATR-IR spectra of ligand exchange reactions by other kinds of thiols that *cause NP aggregation* in 1 mM ethanolic solution, including ω-terminated alkanethiols including CH_3-C_n-SH (n = 5, 15), OH-C_n-SH (n = 4, 6, 11, 16), COOH-C_n-SH (n = 2, 5, 10, 15), NH_2-C_n-SH (n = 2, 11), $CONH_2$-C_{11}-SH, OH-EG_4-C_{11}-SH, CH_3CH_2OCO-C_1-SH, and arylthiols including benzyl mercaptan (CH_3CH_2-Ph-SH), 4-mercaptobenzoic acid (COOH-Ph-SH), 4-aminobenzenthiol (NH_2-Ph-SH), 4-mercaptopyridine (Py-SH) are presented in the Appendix. Spectra of COOH-terminated alkanethiolate functionalized AuNPs are omitted due to the presence of the same carboxylic group as citrate. Most of the IR spectra exhibit the characteristic COOH hydrogen bond peak at 1704 or 1734 cm^{-1}. For CH_3CH_2OCO-C_1-SH functionalized AuNPs, an asymmetric COO^- stretching vibration of the η^2-COO-Au coordinate (bidentate) is observed at ~1550 cm^{-1} (see the ATR-IR spectrum of ethyl 2-mercaptoacetate functionalized citrate-AuNPs in the Appendix). IR spectra of the thiols possessing C=O functionality, such as amide and acetate, are overlapped at the C=O stretching of the citrate carboxylic groups, but the distinct COOH hydrogen bonds are characteristic of the citrate carboxylic groups. From the IR studies, it was tentatively

concluded that surface citrates adsorbed on AuNPs are not displaced completely by incoming thiols, even after ligand exchange reactions were carried out using a large excess of thiols.

XPS analysis also provided evidence of remaining surface citrate after the addition of 11-undecanethiol (H_3C-C_{11}-SH). In the C 1s binding energy, two peaks of the carboxylate group from surface citrate were detected (Figure 3.2B; see the XPS C 1s spectrum of citrate-AuNPs as prepared in the Appendix). One peak is due to the gold-coordinated carboxylate (COO-Au) at 287.6 eV,[84-87] and the other is the free carboxylic group (COOH) at 289.4 eV.[88,89,ii] The strong peak at 284.8 eV is associated with the long alkyl chain of the thiol, and the peak at ~286 eV is attributed to carbon contaminants (hydroxyhydrocarbons) from air on the silicon substrate[90] although citrate –CH_2– and –COH are located at ~286 eV. Therefore, the presence of the carboxylate carbon in the C 1s region also demonstrates the surface citrate is not completely displaced by the thiol.

It also was speculated that the remaining surface citrates would exhibit unique vibrational peaks from the surface coordination of the free carboxylate group at pH > ~11. In the previous studies, it was demonstrated that at this high pH uncoordinated COO^- groups of surface citrates bind to the surface, leading to uniquely enhanced vibrational bands.[72] Briefly, the shift of ν(C-H) to higher frequencies at 2986/2977 cm^{-1} stems from strain in the citrate backbone due to pseudo-ring formation on the surface, and the ν_{asy}(COO) and ν_{sym}(COO) of the monodentate COO-Au coordinate appear at 1611 and 1371 cm^{-1}, respectively. The peak at 1078 cm^{-1} is assigned to ν(C-O) of the hydroxyl

[ii]Those peaks can be assigned to be carboxylate (287.6 eV) and protonated carboxyl groups (289.4 eV), respectively, but the acidic condition upon addition of thiols can exclude the presence of unbound carboxylate groups. 1) Lin, N.; Payer, D.; Dmitriev, A.; Strunskus, T.; Wöll, C.; Barth, J. V.; Kern, K. *Angew. Chem.* **2005**, *117*, 1512-1515. 2) Payer, D.; Comisso, A.; Dmitriev, A.; Strunskus, T.; Lin, N.; Wöll, C.; DeVita, A.; Barth, J. V.; Kern, K. *Chem. Eur. J.* **2007**, *13*, 3900-3906.

group whereas the 825 and 583 cm^{-1} are attributed to an in-plane COO^- scissoring and an in-plane COO^- rocking vibration, respectively. The characteristic IR peaks of surface citrates under the basic condition for H_3C-C_{11}-SH functionalized citrate-AuNPs were observed (Figure 3.2C) and those frequencies were used as additional evidence of remaining surface citrates. As a result, it was demonstrated that the adsorbed citrate molecules are not displaced spontaneously by addition of excess amounts of alkylthiol.

By detecting the remaining citrate in the aggregated AuNPs, it was demonstrated that the NP aggregation-based assay[20,69,70] is not plausible to determine quantitatively the replacement of citrate for the studies of ligand exchange reactions. The thiol-induced aggregation of citrate-stabilized AuNPs only indicates the adsorption of thiols on the NP surface, not necessarily the complete displacement of citrate. Even addition of a quarter molar equivalent amount of the added alkanethiol, which is not sufficient to functionalize the entire surface area of the AuNPs, caused aggregation of AuNPs (data not shown, but purple color indicative of ~39-nm AuNP aggregation was observed.). In addition, the NP aggregation, followed by possible blockage of the surface of individual AuNPs, may inhibit the citrate-to-thiol exchange reaction from proceeding to completion.[32] Thus, it cannot be conclude from the proceeded ligand exchange experiments whether thiols can replace the adsorbed citrate completely. Taking into account the limit of the ligand exchange under NP aggregation, the ligand exchange reactions were further investigated using other types of thiols that resist aggregation of NPs upon surface adsorption.

3.3.2 Investigation of exchange reactions at the surface of dispersed AuNPs

While investigating the ligand exchange reactions of various thiols with different lengths and functionalities, several thiols that prevent NPs from aggregating were found.

The thiols include 11-mercanptoundecyl trifluoromethylacetate (CF_3COO-C_{11}-SH), 4-nitrobenzenthiol (NO_2-Ph-SH), and CH_3O-EG_4-C_{11}-SH in ethanolic solution (Figure 3.3; see UV-Vis spectra of functionalized AuNPs in the Appendix). It also was found that COOH-C_2-SH and ethyl mercaptoacetate (CH_3CH_2OCO-C_1-SH) stabilize NPs, but the reaction media required is water. In these investigations, the potential role of NP aggregation and possible blocking of the citrate-capped NP surface during ligand exchange reactions are eliminated, which could contribute to observations of residual citrate. Investigating ligand exchange using dispersed NPs ensures that the surfaces are fully accessible during the exchange reaction. Ligand exchange reactions were performed for the five NP-aggregation-preventing thiols to investigate whether the surface citrate molecules are spontaneously replaced by the thiols when there is no aggregation and thus full access to the surface of the NPs.

Figure 3.4 shows XPS C 1s and IR data after the addition of 11-mercanptoundecyl trifluoromethylacetate (CF_3COO-C_{11}-SH). Unfortunately, IR spectra of CF_3COO-C_{11}-SH functionalized AuNPs and the pure thiol overlap in the carboxylic group stretching window, and thus spectral data are not informative about the presence of surface citrate

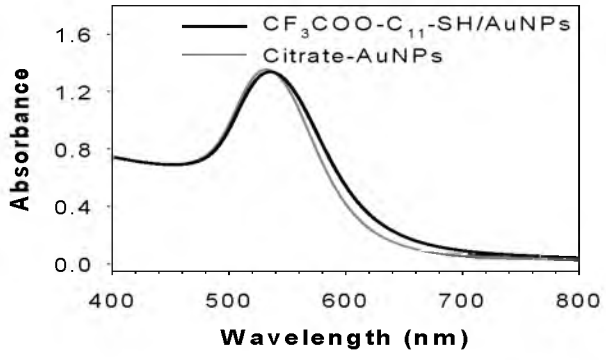

Figure 3.3. UV-Vis absorbance of CF_3COO-C_{11}-SH functionalized AuNPs. This shows little aggregation of NPs during addition of the thiol. λ_{max} = 532 nm for citrate-AuNPs.

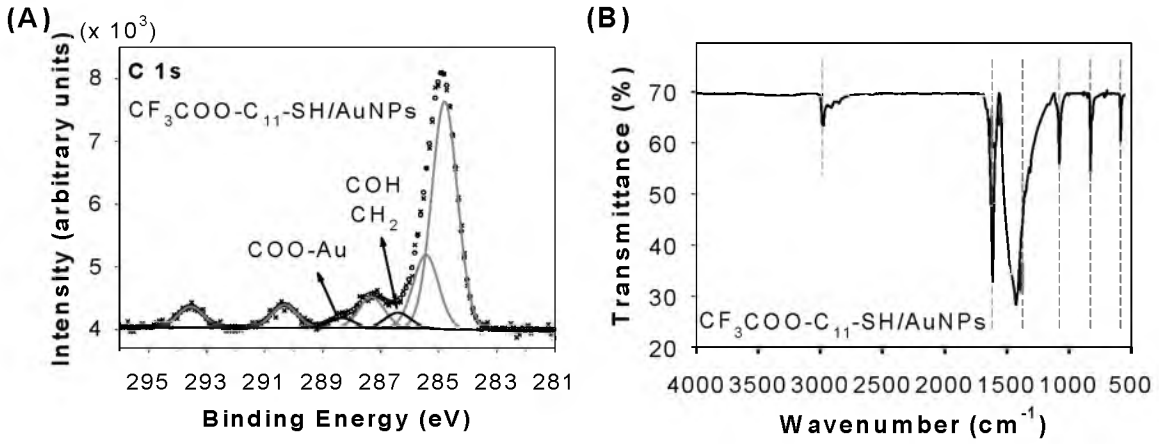

Figure 3.4. XPS and IR spectra of remaining surface citrate on AuNPs after addition of $CF_3COO\text{-}C_{11}\text{-}SH$ that does not cause NP aggregation. (A) XPS C 1s region shows the coordinated COO-Au at 288.3 eV and citrate COH/CH_2 at 286.5 eV. (B) IR band enhancement of surface citrate on AuNPs also appears when pH > ~11 (dotted lines).

(see the ATR-IR spectrum of 11-mercaptoundecyl trifluoromethylacetate functionalized citrate-AuNPs in the Appendix). For the XPS data, the major peaks of the thiol C 1s were assigned to the β-carbon at 285.4 eV, the α-carbon at 287.1 eV, the carbonyl carbon at 290.1 eV, and the fluorinated carbon at 293.2 eV,[91] which is consistent with the result in this study. The contribution from surface citrate is shown by the peaks located at 286.5 eV (COH/CH_2) and 288.3 eV (COO-Au). The other results, from the ligand exchange reactions with nitrobenzenthiol in EtOH, $CH_3O\text{-}EG_4\text{-}C_{11}\text{-}SH$ in EtOH, $COOH\text{-}C_2\text{-}SH$ in water, and ethyl mercaptoacetate in water, also confirm the surface citrate is still present (see UV-Vis absorbance and IR spectra in the Appendix). The functionalized AuNPs under solution conditions of pH > ~11 exhibit the enhanced unique IR bands through coordination of the free citrate carboxylate to AuNP surfaces (Figure 3.4B), as was discussed above, verifying the presence of surface citrate after the ligand exchange reaction with excess $CF_3COO\text{-}C_{11}\text{-}SH$.

One possible reason for observation of citrate is nonuniform thiolate adsorption on

the AuNP surfaces, rather than formation of a close-packed monolayers. It is known that methyl-terminated alkanethiols with fewer than six carbons form a relatively disordered layer on gold clusters, [92] and usually more than ten carbons without bulky terminal groups are required for the formation of a stable SAM on a planar gold surface. [93] 11-mercaptoundecyl trifluoromethylacetate, COOH-C_2-SH and ethyl mercaptoacetate do not meet this requirement for well-ordered SAM formation, which may result in the incomplete displacement of the adsorbed citrate. However, in the case of CH_3O-EG_4-C_{11}-SH, it should form a stable SAM on a planar gold surface. This indicates that the potential for ordered SAM formation is not related to the displacement of citrate. Therefore, the replacement of the adsorbed citrate is irrelevant to the effect of incoming thiols, and the incomplete displacement of surface citrates with thiols is likely primarily due to the nature of the coordination of citrate on the AuNP surface.

The ligand exchange reaction also was investigated over a prolonged time (72 h) and elevated temperature (40 ^{o}C). These experimental parameters were adopted from the thiol-to-amine ligand exchange on Au nanocrystals, where the increased time (72 h) and temperature (40 ^{o}C) leads to the completion of the exchange reaction. [94] 4-nitrobenzenethiol for the incoming ligand was chosen from among the aggregation-preventing thiols since there is no overlap in the region of the ν(C=O) vibration in the IR analysis. After proceeding with the exchange reaction, the ν(C=O) vibration at 1764 cm^{-1} was still observed, which is attributed to a free carboxylic acid of the surface citrate (Figure 3.5; see the entire spectral region in the Appendix). The coordinated carboxylate groups of the surface citrate probably transformed to a physisorbed state under the high thiol concentration (1 mM). The peak at 1662 cm^{-1} is correlated to peaks at 1442 and 1283 cm^{-1}, and this is probably the physisorbed carboxylic acid species coordinating to

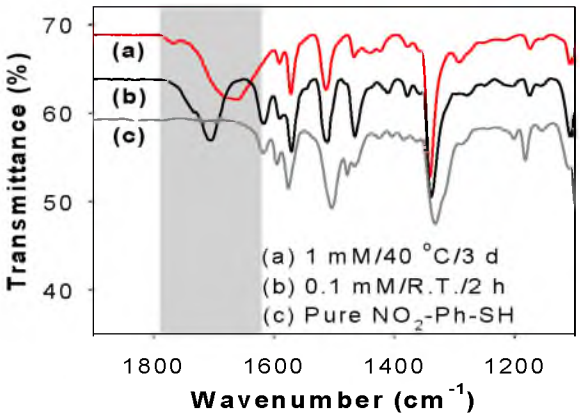

Figure 3.5. ATR-IR spectra of the citrate-to-thiolate exchange reaction on citrate-AuNPs with using 4-nitrobenzenthiol (NO_2-Ph-SH) in ethanol. The vibrational peak of citrate carboxylic group still remains (grey background region) under (a) high temperature and long incubation time and (b) common reaction conditions. (c) Pure nitrobenzenethiol is shown for comparison.

Au atoms through lone pair electrons of the carbonyl oxygen. Those peaks are not related to the possible reduced species of the nitrobenzene to aminobenzene,[95] which is evidenced by IR spectrum of 4-aminobenzenethiol functionalized AuNPs. It seems that the nitro group of the thiol promotes stabilization of the physisorbed COOH.[96] The molar equivalents of the added thiols (~270) are more than that for the complete phosphine-to-thiol exchange.[23] Even under the higher temperature (40 °C) and longer reaction time (3 d), the surface citrate on AuNPs was resistant to complete citrate-to-thiolate exchange. Therefore, it was concluded that facile ligand-exchange reactions of citrate-AuNPs with incoming thiol does not occur as was observed under common conditions in ethanol.

3.3.3 Chloride displacement by incoming thiols

Displacement of surface chloride upon treatment of ethanolic thiol solutions was investigated. Although chloride ions contribute to the overall electrostatic repulsion of citrate-stabilized AuNPs,[71,97] those ions generally are neglected in the ligand-exchange

reactions. The displacement of citrate ions by thiols has been considered. For the phosphine-to-thiol exchange reaction on small gold nanoparticles, surface chloride ions have been shown to be completely displaced.[23] The XPS analysis also demonstrates the clear disappearance of the surface chloride by the ethanolic thiol solution[iii] (Figure 3.6). The chloride ions on AuNP surfaces appear at ~270 eV for Cl 2s and at ~200 eV for Cl 2p.[98] Upon addition of the ethanolic solution of CH_3-C_{11}-SH to citrate-AuNPs, those Cl peaks disappear, indicating the entire replacement of surface chloride ions due to high sensitivity of the XPS signal. Therefore, the displaced negatively-charged species on AuNPs primarily is the chloride ions, and this can be the main reason for the decrease in surface charge of citrate-AuNPs. Citrate-AuNPs dispersed in ethanol exhibit a large negative zeta potential,[99] and displacement of chloride ions by ethanol does not cause NP aggregation. In fact, short range repulsive forces of the citrate layer protect AuNPs sterically to stabilize the NP dispersion,[71,97, 100] together with the negative surface potential. Van der Waals attractions between thiolate layers overcome electrostatic and

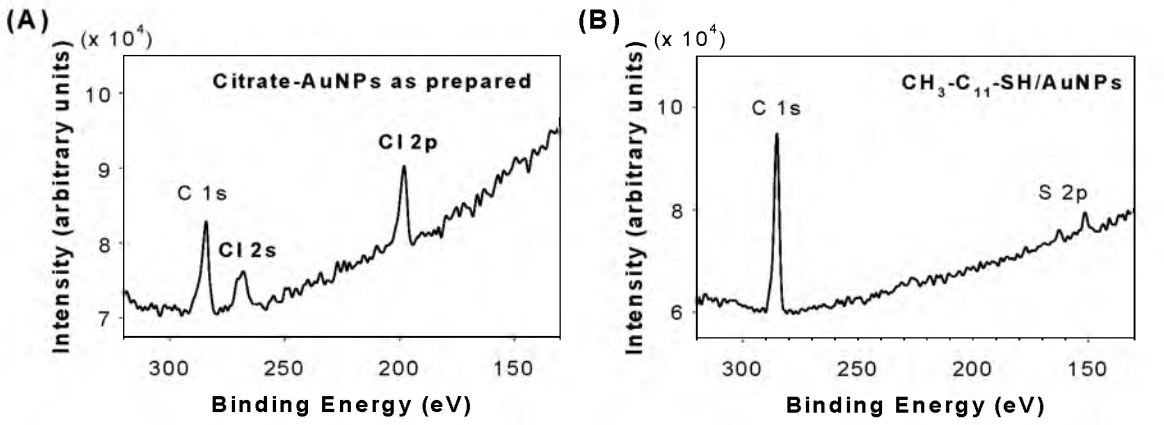

Figure 3.6. XPS Cl 1s spectra of citrate-AuNPs (A) before and (B) after functionalization by 1-dodecanethiol. Surface chloride ions on citrate-AuNPs are displaced in the ethanolic thiol solution.

[iii]The XPS analysis in another study showed that surface Cl^- ions are displaced by ethanol itself.

steric repulsions of citrate layers inducing NP aggregation.

3.3.4 Adsorption isotherm of arylthiols for determination of available surface area in the presence of surface citrates

The absorption of arylthiols on citrate-AuNPs was studied. The unique spectral signatures provide an opportunity for a more quantitative assessment of the thiolate adsorption and citrate displacement processes. The adsorption also can be followed over time since arylthiols do not organize quickly on a Au surface. An adsorption isotherm for Py-SH adsorption on citrate-AuNPs was measured using ATR-IR spectroscopy. The characteristic vibrations of the pyridine ring vibration[101-103] at 1609/1575/708 cm^{-1} were monitored, and intensities of the vibrational band at 1609 cm^{-1} were used for the amount of adsorbed Py-SH (Figure 3.7A; see other frequency regions in the Appendix). The

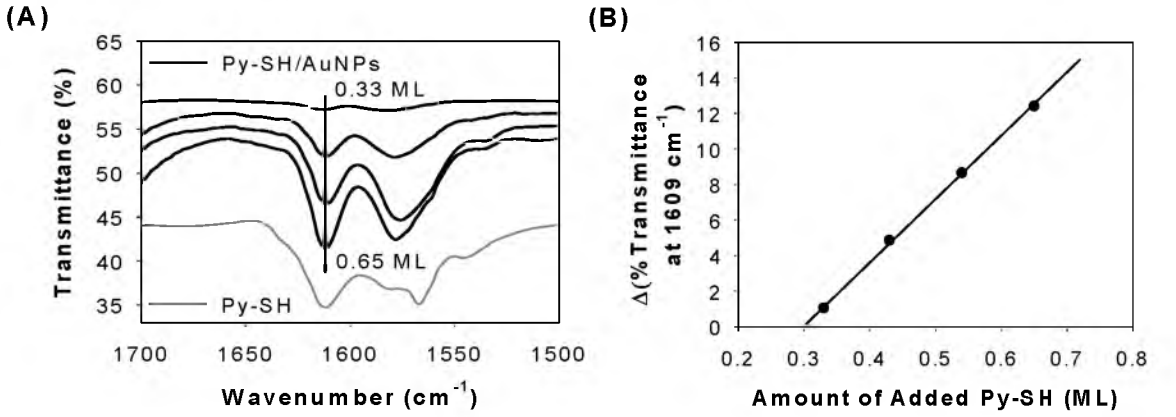

Figure 3.7. Adsorption isotherm for Py-SH adsorption on citrate-AuNPs. (A) ATR-IR spectra of Py-SH functionalized citrate-AuNPs with varied thiol amounts, showing the dependence of intensities of the pyridine ring vibration at 1609 cm^{-1} on the thiol amounts. The thiol amounts added to AuNP solutions are 0.65, 0.54, 0.43, and 0.33 ML, respectively. (B) Relationship of the amounts between added thiols (Py-SH) to the AuNP solution and adsorbed thiols on the AuNP surface. The transmittance difference at 1609 cm^{-1} represents the amount of adsorbed pyridine thiolates.

amounts of the arylthiol added to citrate-AuNP solutions were 0.33, 0.43, 0.54, and 0.65 ML compared to a monolayer coverage on the AuNP surface. Analysis of the IR spectra shows a linear relationship between the amount of adsorbed thiolate and the thiol concentration in solution (Figure 3.7B). From the plot of the adsorption isotherm, it also was found that the signal loss of the Py-SH vibration frequency was about 0.3 ML. To minimize possible desorption of the arylthiol during the centrifugation and redispersion step, the functionalized AuNP solution was centrifuged once without further purification. The repeated sonication and centrifugation in the purification step cause temperature to be elevated, which may affect the nonordering of the thiolates. The final volume after one cycle of centrifugation is less than 100 μL, and it is very minute compared to 5 mL of the initial volume, and thus the amount of left-over thiols in the final centrifuged solution is negligible. In the IR data, there is a possibility of overestimating the thiols compared to other surface adsorbed species without purification due to admolecules,[104] but the saturation feature should be shown even with a shift of the saturation point. For determination of the adsorbed thiolate amounts, the surface coverage of the benzenethiol was chosen to be 4.3×10^{14} thiols/cm^2,[iv] which was estimated by STM image of the molecule on a planar gold surface.[105]

The adsorption of pyridine thiols (Py-SH) on citrate-AuNPs was investigated quantitatively by XPS analysis (Figure 3.8). In this study, amounts of the thiol were determined by XPS peak areas, and the peak areas of S 2p and N 1s were obtained as characteristic of Py-SH. These peak areas of Py-SH were compared with those of C 1s,

---

[iv] Another value of the benzenthiol coverage on Au(111) in literature is 6.3×10^{14} thiols/cm^2 that was estimated by XPS, but with the smaller value we may not miss the transition to saturation.
For the larger surface coverage, see: Whelan, C. M.; Smyth, M. R.; Barnes, C. J. *Langmuir* **1999**, *15*, 116-126. For a smaller coverage of benzenethiol (3.3×10^{14} thiols/cm^2), see: Whelan, C. M.; Barnes, C. J.; Walker, C. G. H.; Brown, N. M. D. *Surf. Sci.* **1999**, *425*, 195-211.

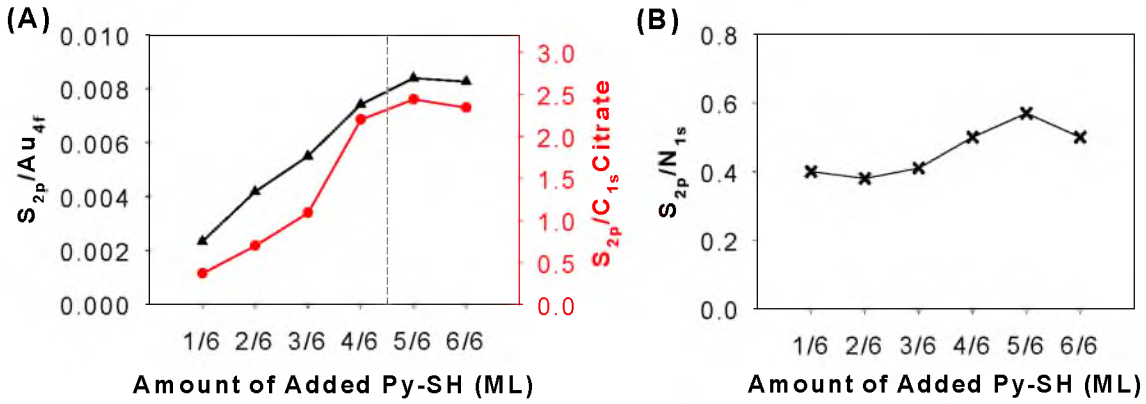

Figure 3.8. Relative amounts of Py-SH adsorbed on citrate-AuNP surfaces as change of added amounts to the AuNP solution, determined by XPS peak areas. (A) Ratios of the peak areas of S 2p based on citrate C 1s at 288 eV (●) and Au 4f at 84.0 eV (▲) were plotted for Py-SH coverages, respectively. The dotted line indicates coverage saturation at ~0.75 ML. (B) Ratios of the peak areas of S 2p and N 1s are constant regardless of Py-SH coverages, which show the accuracy of amount determination by XPS peak areas.

assigned to be primarily due to citrate, at 288 eV and Au 4f at 84.0 eV. The amounts of the added thiol to the AuNP solutions were varied from 1/6 to 1 ML based on a monolayer coverage on the entire AuNP surface. In Figure 3.8A, the ratios of the peak areas between S 2p of Py-SH and C 1s of citrate at 288 eV as well as S 2p and Au 4f are plotted, respectively. The ratios of S_{2p}/Au_{4f} increase as the amounts of added Py-SH increase up to ~5/6 ML, showing a linear relationship between the amount of adsorbed thiolate and the thiol concentration in solution. This indicates that the thiols are adsorbed on the AuNP surfaces from the solution until all available areas of the AuNP surface are occupied, which is consistent with the spontaneous adsorption of thiols on a gold surface. The plot of S_{2p}/C_{1s} also shows the similar adsorption isotherm as that of S_{2p}/Au_{4f}. Both plots illustrate a saturation of Py-SH on citrate-AuNPs. Saturation of the thiol adsorption on the AuNP surface is defined when 2/3 - 1 ML of the thiol was added. Note that the minimum amount of adsorbate to functionalize the whole surface of the AuNPs is 1 ML

when the sorption equilibrium on the surface is strongly favored. Adsorption saturation prior to 1 ML suggests some of the AuNP surfaces are already occupied by citrate molecules. The adsorption saturation can be set at 4.5/6 ML (i.e., 0.75 ML), but this value is likely overestimated due to possible interactions of pyridine with carboxylic groups[106] of surface citrate. In Figure 3.8B, ratios of S 2p and N 1s of Py-SH were plotted for each coverage, and the resulting constant ratios show an independence of the XPS intensities of Py-SH thiol regardless of the thiol coverages as expected. This supports that the determination of the amount of adsorbed thiolate by XPS peak areas is very accurate.

The adsorption of another kind of arylthiols (NO_2-Ph-SH) on citrate-AuNPs also was investigated using ATR-IR spectroscopy. 4-nitrobenzene thiol (NO_2-Ph-SH) was chosen for this surface titration, because it does not cause citrate-AuNP aggregation irrespective of concentration up to 1 mM and 3 d of the reaction time. The reaction solution was left at room temperature for 72 h since it has been reported that thiolate adsorption with the given amount is saturated within 72 h.[107] The intensity of the $\nu_{sym}(NO_2)$ vibration at 1336 cm^{-1} was monitored from ATR measurements as the amount of added thiol was increased from a quarter (χ = 1/4) up to two fractional surface coverage (χ = 2.0) (Figure 3.9A; see the entire spectral region at 4000 - 550 cm^{-1} in the Appendix). The C=O stretching vibration by hydrogen bonds between the citrate carboxylic groups and the C-H stretching vibrations[v] around 2900 cm^{-1} from the adsorbed ethanol are observed beyond the saturation point. Figure 3.9B shows the adsorption isotherm of NO_2-Ph-SH on citrate-stabilized AuNPs using IR analysis. Taking into account the presence of surface citrate and ethanol, combined with the possible admolecules due to skipping the purification step and the adsorption equilibrium in solution, the saturation point at χ = ~1.0 implies

[v]The C-H stretching of a benzene ring is above 3000 cm^{-1}.

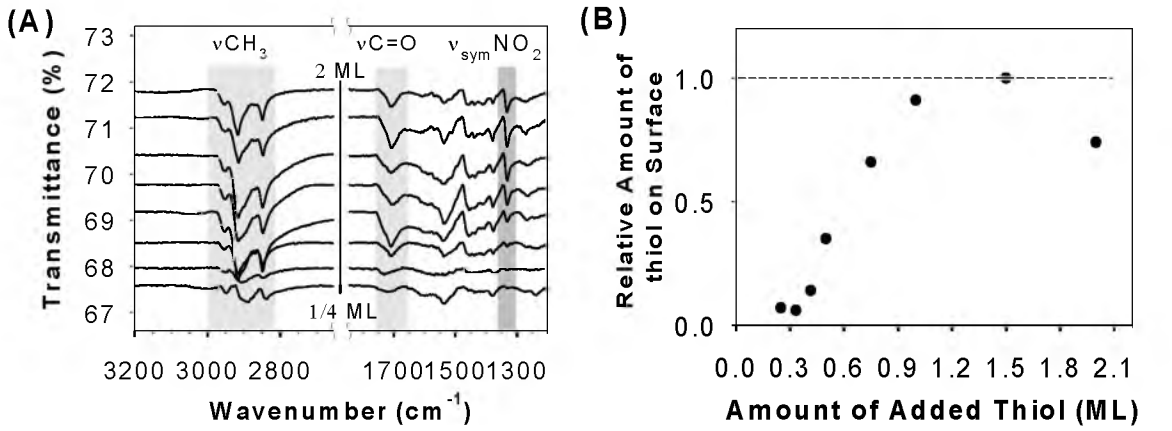

Figure 3.9. Adsorption isotherm of NO_2-Ph-SH on citrate-AuNPs. (A) ATR-IR spectra of the AuNPs functionalized by varied amounts of NO_2-Ph-SH (1/4 - 2 ML). Note that adsorbed ethanol and surface citrate are still present, which are characterized by $\nu(CH_3)$ and $\nu(C=O)$ vibrations, respectively (faint grey backgrounds). (B) Relative amounts of NO_2-Ph-SH adsorbed on AuNP surfaces as change of added amounts to the AuNP solution, determined by IR peak intensities of $\nu_{sym}(NO_2)$ vibrations (dark grey background in A). The dotted line was arbitrarily set at the maximum coverage.

that the arylthiolate cannot be occupying the entire AuNP surface. This adsorption isotherm also verifies the remaining surface citrate upon thiol treatment. Analysis of the surface saturation by XPS has not been attempted since the nitro group (N 1s at ~405 eV) is reduced to the amine group (N 1s at ~400 eV) under the XPS beam.[108] Zachariah and co-workers measured the layer thickness of 11-mercaptoundecanoic acid adsorbed on citrate-stabilized AuNPs, which is 35 % less than the predicted value, and they speculated that the thiolate layer on AuNPs is less dense than the well-packed SAMs.[36] This observation can be explained by lower surface coverage of the adsorbed thiolate than expected due to partial occupation of AuNP surfaces by citrate.

3.3.5 Local phase separation between the surface citrate and adsorbed alkanethiolate during coadsorption

The addition of thiols to the citrate-AuNP solution resulted in the coadsorption of thiols with the surface citrates. While arylthiolate adsorption provides the semi-quantitative IR signals for determination of void areas on the surface, alkanethiolate adsorption can offer additional information about the nature of the coadsorption process due to possible formation of phase-separated regions through van der Waals attractions of the hydrocarbon chains. Related to the surface coverage as discussed above, similar results with alkanethiols (CH_3-C_{11}-SH and HO-C_{11}-SH) and arylthiols (NO_2-Ph-SH and Py-SH) were obtained (see transmission IR spectra of thiol functionalized citrate-AuNPs with varied thiol amounts in the Appendix). The critical amount of thiols for the saturated layer coverage varies slightly with functionalities and types of thiols, but a value less than 0.65 ML is consistent over different thiols. Two unique aspects from alkanethiolate adsorption were observed. While the amounts of added thiols increased gradually, the intensities of IR bands of ω-terminated alkanethiolates grew significantly around the saturation point of 0.65 ML into the monolayer-like feature, which can be distinguished by the characteristic C-H stretching vibrations at 2917/2850 cm^{-1}. For example, the intensity of C-H stretching peaks of OH-C_{11}-SH thiols at 2917 and 2850 cm^{-1} dramatically increased when the amounts of added thiols increased from 0.33 to 0.65 ML (Figure 3.10A; see the entire spectral region in the Appendix). Although the thiol amounts increased to 1.3, 2.6, and 5.2 ML, the amplitude of the C-H stretching bands did not increase further. This can be explained by a cooperative adsorption of the alkanethiol before the alkanethiolate layers were well-organized for far less than a monolayer coverage (~0.65 ML), which also implies possible interactions of the alkanethiolates with

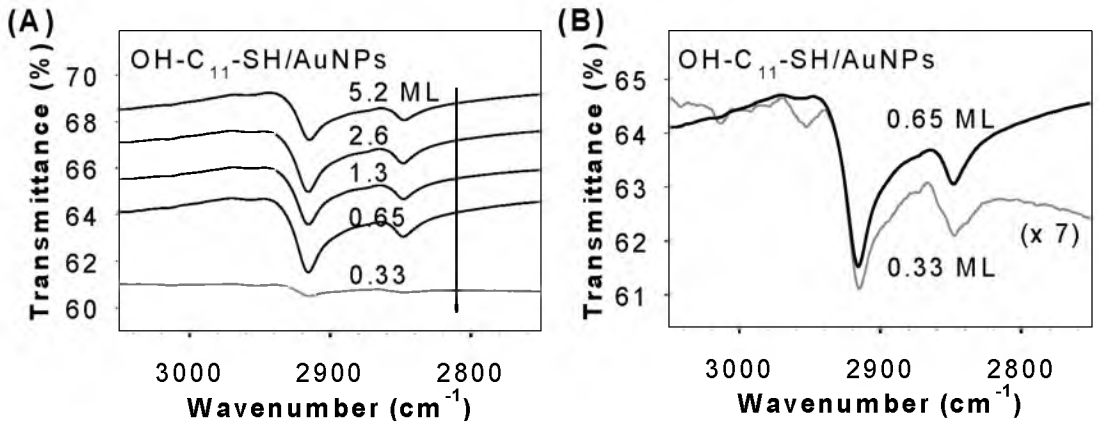

Figure 3.10. Transmission IR spectra in the region of the C-H stretching vibrations for citrate-AuNPs functionalized by varied amounts of OH-C_{11}-SH. (A) Adsorption saturation of the thiol appears prior to ~0.65 ML, which indicates the presence of remaining adsorbates on the AuNP surface. (B) The similar positions of the C-H stretching vibrations regardless of surface coverage.

preadsorbed citrate. Arylthiols did not show the dramatic change of IR band intensities including the C-H stretching region due to a lack of strong intermolecular interactions. Due to the cooperative nature and possible configuration change of the alkanethiolate adsorption,[109] the absolute amount of the adsorbed alkanethiolate cannot be linearly correlated with the intensity profile of the C-H vibrations. The adsorption states, i.e., physisorbed/chemisorbed and lying-down/upright configurations, likely change near the saturation point. Prior to the coverage saturation, the relatively weak intensity of the C-H stretching vibrations probably originates from loss of the majority of the weakly physisorbed thiol during purification steps.

Consequently, there is evidence indicating the presence of cooperatively adsorbed region[110] of alkanethiolates on the citrate-AuNP surface. To explain the above ligand exchange results, which indicate the cooperativity of adsorbed alkanethiols prior to the saturation point of less than a monolayer coverage, phase-separated regions of thiolate and citrate in nanometer-scale domains on a AuNP (111) surface are proposed, based on

the organized citrate layer on AuNPs[72] and the proposed CH_3-C_9-SH monolayer on a 2-D Au surface[111] (Figure 3.11). This coadsorbed layer cannot be called homogeneous since there is no direct chemical interaction between the two different types of molecules. Assuming that surface citrate is not desorbed, three alkanethiolates can interact with maximum van der Waals interaction of the hydrocarbon chains and without being interrupted by adsorbed citrates (Figure 3.11A). This ligand layer consists of two adsorbed and one free citrate species for each group of three alkanethiolates, which leads to the 1:1.5 ratio between adsorbed citrate species and alkanethiolates. With loss of half of the free citrate species, however, up to eight alkanethiolates can bind to the surface for every five surface citrates (four coordinated plus one free citrate species) (Figure 3.11B). This produces the 1:2 ratio between adsorbed citrate species and alkanethiolates. The local phase-separated layer accounts for the partial displacement of citrate by thiol.

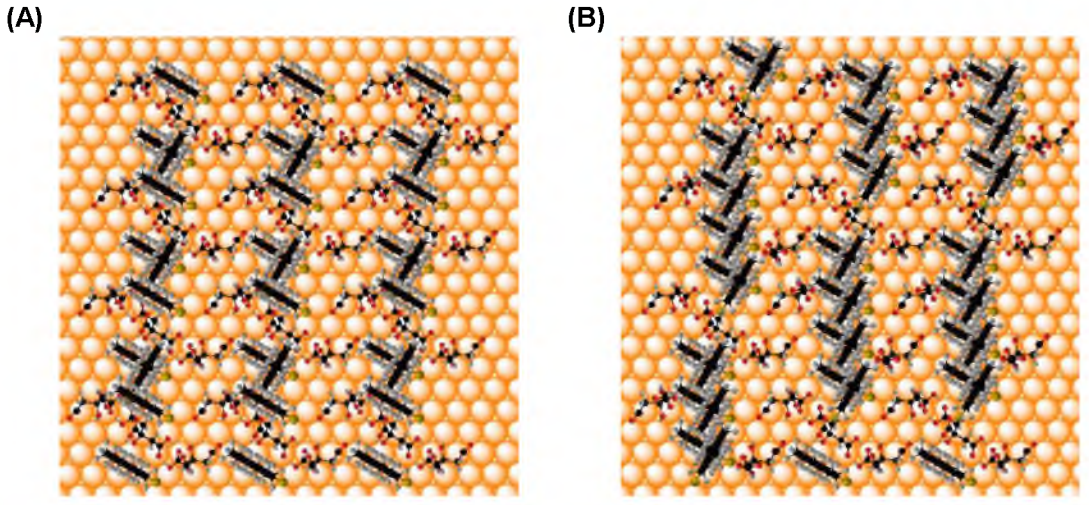

Figure 3.11. Phase-separated citrate and thiolate (CH_3-C_9-SH) layer on AuNP (111) surface at nanometer-scale domains. Surface gold atoms (orange spheres) on a gold (111) surface are illustrated as a space-filling model whereas citrate and alkanethiolate molecules are depicted as a ball-and-stick model. Note that there are eight alkanethiolates in a local SAM, which results in loss of half free citrate species.

Therefore, the formation of the alkanethiolate layer, combined with the organized citrate layer,[72] indicates that the surface layer may be composed of a stable and phase-separated ligand layer at the nanometer-scale domain on AuNPs. The surface coverage by alkanethiolates can be estimated to be 33.3 – 44.4% on the AuNP (111) surface, compared to the entire monolayer coverage (see the comparison of surface coverage of alkanethiolates on a surface of citrate-AuNPs in the Appendix).

Since the pattern of the citrate assembly on (100) and (110) surfaces is identical to that on the (111) surface (see Section 2.3.9 in Chapter 2), a similar surface coverage by alkanethiolates is expected for (100) and (110) surfaces of the AuNPs. The shape of large-sized AuNPs (> 10 nm) is typically a truncated octahedron which the majority of the AuNP surface consists of (111), (100), and (110) surfaces (see Section 2.3.9 in Chapter 2). Thus, the surface of citrate-AuNPs can be considered to be those surfaces, and the effect of edge and vertex sites is likely negligible. Also, surface defects are expected to be very minor due to the crystalline nature of the AuNPs.

The other unique aspect of the alkanethiolate adsorption is that not only the intensities of the C-H stretching vibrations increased significantly around the saturation coverage at 0.65 ML, but also the shapes and positions of the C-H stretching vibrations are almost identical through all ML-amount samples (Figure 3.10B). This strongly implies the local assembly formation of the adsorbed alkanethiolate is identical regardless of overall surface coverages. The adsorption state of the alkanethiolate layer observed by IR does not change, but the population of the layer shows dependence on the amount of added alkanethiol. The model of citrate adsorption on AuNP surfaces also is used to interpret this observation (Figure 3.12). When the amount of added alkanethiols is not enough to functionalize void areas other than the surface citrates, the alkanethiols of physisorbed

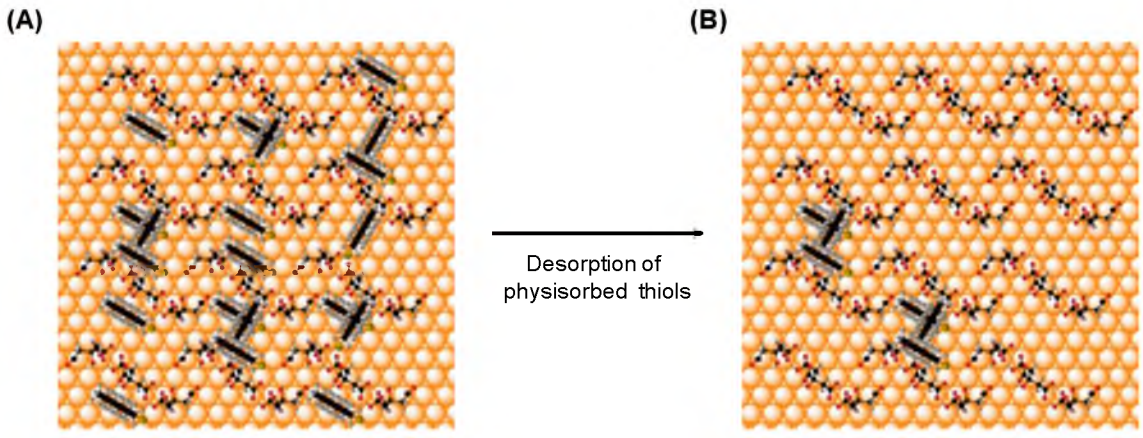

Figure 3.12. Proposed adsorption configurations of alkanethiolates (CH_3-C_9-S-) on AuNP (111) surface prior to saturation. (A) The network of surface citrates allow for intermolecular interactions between no more than three thiolate molecules. (B) Presumably physisorbed thiolates with one or two molecules are desorbed from the surface, and only the domains with three thiolate molecules remains due to feasible intermolecular interactions and subsequent transformation to chemisorbed state.

states are likely desorbed from the nanometer-scale local domains due to lack of intermolecular interactions during purification steps through centrifugation/redispersion. Figure 3.12A illustrates random adsorption of alkanethiols at the local domain on AuNP (111) surface. Using one of the models (Configuration A in Figure 3.11), it is assumed that three alkanethiol (CH_3-C_9-SH) molecules are required for relatively strong chemisorption and formation of the stable thiolate-layers in one domain. Only local domains with three alkanethiol molecules adsorbed remain after the purification step, and one or two alkanethiolate molecules at other domains are desorbed due to lack of intermolecular interactions and consequent failure for transformation into the chemisorbed state (Figure 3.12B). This results in the same thiolate-layer formation at all domains with surface citrates, but the population of the thiolate-layer is far less than after saturation (Figure 3.11A), which is consistent with the IR data in Figure 3.10. Using the other model of alkanethiolate adsorption (Configurtion B in Figure 3.11) will result in a

different number of alkanethiolates required for transformation to the chemisorbed state. It is known that ordering of short-chain alkanethiols and arylthiols become favorable in the presence of preadsorbed molecules due to potential interactions between the two different adsorbates for the layer formation.[112,113] The existence of other absorbates, i.e., citrates in this study, probably promotes the formation of the alkanethiolate layers even with several thiolate molecules on the surface. Due to intermolecular interactions with the surface citrates, adsorbed alkanethiolates exhibit the ordered monolayer feature even less than a monolayer coverage. It is also known that ω-terminated alkanethiolates can form a phase-separated microscopic SAM on a gold surface.[114]

The phase-separated SAMs on AuNPs with perfluorinated and nonfluorinated alkanethiolates have been demonstrated.[115] The route for the phase separation in this literature is different from that for the thiolate-citrate layer with preadsorbed citrate species, but favorable interactions between homo-ligands are required for both phase-separated SAMs. The former is governed by hydrophobicity, but the latter is driven by hydrogen bonds[116] of the citrate carboxylic acids and van der Waals interaction of the alkanethiolates. Au-thiolate species may be mobile on the surface for maximum van der Waals interactions between the hydrocarbon chains[117-119] in the framework of the self-assembled layer of citrate formed mainly by hydrogen bonds of the COOH groups as the surface citrates likely diffuse on the surface.

3.3.6 Quantitative determination of surface coverage between citrates and thiolates by XPS analyses

The fractional surface coverage of thiolates after addition of thiols was estimated, using the XPS C 1s spectrum for COOH-C_2-SH/AuNPs. Due to the detection limit

challenges NMR[22] is not the appropriate technique to monitor the fractional changes of the adsorbed citrate species. Since the chain length of the thiol (mercaptopropionic acid) is comparable with that of citrate (hydroxypropane tricarboxylic acid), the intensities of electrons ejected from carbons for both adsorbates, i.e., citrate and COOH-C_2-SH, can be assumed to be identical. It also was assumed that possible intensity deviations due to NP curvature effect[120] were cancelled out through signal being averaged over the sample area which is large compared to the individual NPs. Direct determination of adsorbate amounts by the C/Au atomic ratio, which is valid for a planar 2-D surface, cannot be used for the spherical AuNPs, but the relative amounts of each adsorbate can be directly estimated by the relative C 1s intensities between COO-Au and COOH. Given the ratio of the XPS C 1s peak area of COO-Au and COOH of 1:2.9 (see the XPS C 1s spectrum of 3-mercaptopropionic acid functionalized citrate-AunPs in the Appendix) and the ratio of COO-Au and COOH species per citrate trimer unit (i.e., two coordinated and one free citrates) to be 4:5, the ratio of the citrate trimer and thiolates becomes 1:6.6,[vi] which results in the 1:2.2 ratio of the surface citrate and thiolate. The surfaces of AuNPs are still adsorbed by large amounts of citrate (surface coverage of ~31 % by adsorbed citrate species). When the ratio of COO-Au and COOH species per citrate trimer unit changes from 4:5 to 3:6 (i.e., a terminal COO^- from one of the two adsorbed citrate species turns to be unbound and involve hydrogen bonds with COOH formation), which is suggested by the direct hydrogen bond formation between adsorbed citrates,[72] the ratio of the surface citrates and thiolates is 1:0.9. However, this approach dependent upon the analysis of the concentrations of two adsorbed species was not confirmative to determine

[vi]Given the amount ratio of citrate trimer (x) and thiol (y); COO-Au : COOH = 1:2.9 = 4x:(5x + y), which results in y = 6.6x.

the surface coverages due to unknown XPS signal-to-concentration response from the surface citrate as mentioned above.

A new method of a quantitative analysis was developed for determination of surface coverage of citrates and alkanethiolates. This method is based on plotting concentration ratios of citrates and alkanethiolates with varied alkanethiol lengths, assuming that thecitrate concentration is fixed. The concentrations were determined using peak areas of XPS C 1s, which characteristic C 1s of citrates at 288 eV and C 1s of alkanethiolates at 284.8 eV were used for the peak areas and thus the concentrations of the adsorbed molecules (Figure 3.13). This plot shows the results as the length of the alkanethiolates was increased systematically from 4 carbons to 12 carbons under saturated conditions of surface adsorption. The slope directly indicates the ratio of amounts of citrates and thiolates adsorbed on the AuNP surfaces (Figure 3.13A). For example, if the slope (C_{1s}thiol/C_{1s}citrate) is 1, the ratio of amounts is citrate:thiolate = 1:1. If the slope is 2, the ratio of amounts is citrate:thiolate = 1:2. This function of the peak area ratio with respect to the alkanethiolate length provides an ease of XPS quantitation for the determination of surface coverage on NP surfaces whereas adsorption isotherm[121] is so subtle that it can cause a significant error and many XPS parameters[122] are usually required for quantitative analysis on rough surfaces. In the plot, the obtained slope is ~1.7, and the amount ratio can be concluded to citrate:thiolate = 1:1.7. [vii] This result is consistent with the models of the alkanethiolate adsorption on Au(111) in Figure 3.11, which the ratio of the number of adsorbed molecules in the unit cell (adsorbed citrate:alkanethiolate) is 1.5 (Figure 3.11A) - 2.0 (Figure 3.11B). Therefore, the coverage density of alkylthiolates

[vii]The coverage densities of surface citrate on (110) and (100) surfaces, which are the most populated facets together with the (111) surface for large AuNPs, are similar to that on the (111) surface. See Section 2.3.9 Citrate polymeric chains as building blocks on other facets of the AuNPs in Chapter 2.

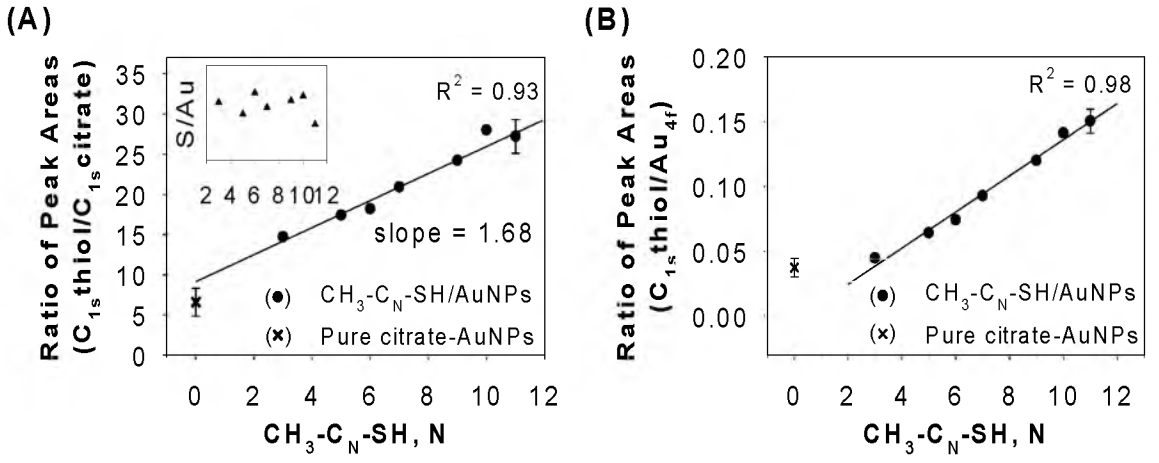

Figure 3.13. Adsorption ratio between adsorbed citrate and alkanethiolate on AuNPs, determined by XPS analysis. (A) Plot of ratios of C 1s peak area between adsorbed citrates and alkanethiolates with respect to the length of hydrocarbon. The slope (1.68) directly represents the adsorption ratio. Inset in (A) shows constant ratios of peak areas between S 2p and Au 4f, which indicate consistent surface coverage by the alkanethiolates regardless of the hydrocarbon length. (B) Plot of ratios of C 1s peak area at 284.8 eV with respect to the length of alkanethiolates, which exhibits a linear dependence of the hydrocarbon length.

determined from the XPS analysis in this study is 1.9 thiolates/nm^2 (3.4 thiolates/1.79 nm^2 = 1.9 thiolates/nm^2; 3.4 alkanethiolates adsorbed in the unit cell area of 1.79 nm^2). This value is ~42% smaller compared to the coverage of the close-packed SAM of alkanethiolates on a planar gold surface (4.5 thiolates/nm^2)[111] and in good agreement with the thiolate density on citrate-AuNPs determined by the fluorescamine-based assay (1.63 thiolates/nm^2).[123] The surface coverage by different alkanethiolates on AuNP surfaces is constant, evidenced by constant ratios of the peak areas between S 2p and Au 4f regardless of the chain length of the alkanethiolate (inset, Figure 3.13A). The linear plot of ratios of peak areas from thiolate C1s at 284.8 eV and Au 4f at 84.0 eV show a linear dependence of the length of alkanethiolate, which indicates error of the C1s peak area from adventitious carbons is consistent through the samples (Figure 3.13B). Adsorption

of adventitious carbons could be considered as a systematic error, and thus the ratios from the peak area of the alkanethiolate C 1s at 284.8 eV are still appropriate. In addition, the ratio-based analyses of peak areas in the XPS studies can compensate the possible effect of photoelectron attenuation[124,125] in the XPS intensity resulted from thick organic layers, although this effect may be negligible due to the loosely-packed layer of alkanethiolates on AuNPs.

3.3.7 Origin of the strong adsorption of citrates on AuNP surfaces

The preconception for the easy displacement of adsorbed citrate by thiol is based on the difference in the chemisorption energy on a Au surface. The typical chemisorption energy of thiolates (Au-S) is about 40 kcal/mol whereas that of carboxylates (Au-OOC) is about 2 kcal/mol. Due to the strong energy of the Au-S bond, incoming thiols are believed to replace the adsorbed citrates spontaneously. For the phosphine-to-thiol exchange, Hutchison and co-workers demonstrated complete displacement of the adsorbed triphenylphosphine (PPh_3) by incoming thiols using NMR spectroscopy.[23,126] The labile Au-P bond is exchanged by the strong Au-S bond since Au-P bond is weaker than Au-S bond. Adsorption enthalpy of trialkylphosphine on Au is ~30 kcal/mol,[127,128] and computed free energy of adsorption of single PPh_3 molecules on a Au(111) surface is ~15 kcal/mol.[129] Unlike the monodentate phosphine ligand, however, the chelate effect can play a critical role in adsorption strength of the polydentate citrate on a surface. It is known that the SAMs from chelating dithiolates are more stable than that from normal thiolates,[39,130-132] and chelating dithiocarbamate[viii] exhibits resistance to displacement by other alkanethiols.[133] Citrate adsorption on AuNP surfaces was characterized as

[viii] Electronic resonant effect also plays a role in the binding stability.

coordinating through one of the terminal and the central carboxylate groups. This chelate effect is partially responsible for resistance to desorption of the surface citrate on AuNPs.

Not only the chelating coordination by two carboxylate groups, but also the intermolecular interactions between surface citrates play an important role in the strong adsorption of citrate. It is hypothesized that surface citrates form an organized network through hydrogen bonds of the free terminal carboxylic acid groups and van der Waals attraction between citrate CH_2 fragments. Although the surface coverage of adsorbed citrate species on AuNPs is ~31%, and thus ~69% of the potentially vacant surface is sufficient for ligand exchange, the intermolecular interactions of surface citrates do not allow individual citrates to be spontaneously desorbed from the surface. The strength of hydrogen bonds of carboxylic acid groups between adjacent citrates are remarkable (total ~14 kcal/mol; ~7 kcal/mol per bond of carboxylic acid dimers at room temperature)[134-137] compared to the single carboxylate-Au interaction (~2 kcal/mol).[27] Additionally, van der Waals attraction between two CH_2 moieties can be 1.4 - 1.8 kcal/mol[138] (0.8 kcal/mol as a lower limit, determined for alkanethiolates on gold[ix] surfaces[139]). Although the adsorption energy of single citrate molecules on a Au(111) surface is very weak (~8.5 kcal/mol computed in dilute aqueous solution at pH = 7),[129] the intermolecular interactions can significantly contribute to overall adsorption energy (14 + 0.8 kcal/mol as a lower limt), resulting in the total energy of adsorption of ~23.3 kcal/mol (14 + 0.8 + 8.5 kcal/mol). Moreover, the entropy gain from the network of citrate self-assembly likely contributes to the adsorption energy in an additive manner and increases the barrier for desorption. Thus, a facile citrate-to-thiol ligand exchange does not necessarily occur due to

[ix]On Ag(111), the hydrophobic interactions and intermolecular forces between hydrocarbon chains is ~1.0 kcal/mol per CH_2: Hatchett, D. W.; Uibel, R. H.; Stevenson, K. J.; Harris, J. M.; White, H. S. *J. Am. Chem. Soc.* **1998**, *120*, 1062-1069.

enthalpy/entropy gains from the intermolecular interactions. The well-known assumption regarding the citrate displacement based on the weak gold-carboxylate interaction fails to predict the exchange behavior of surface citrate with thiolate ligands.

The surface citrates also influence the physisorption of thiols. The strong energy of the Au-S bond on chemisorption is achieved by following a physisorbed state on the surface. [104] In the physisorption process, van der Waals attractions are dominant, and a favorable physisorption eventually leads to chemisorption.[104] However, the surface citrates may diminish the physisorption of thiol by hampering van der Waals interaction of thiols and by isolating the physisorbed thiols. The model of the citrate organization on the AuNP surface may suggest that maximum number of thiolates involved in van der Waals interaction is only eight alkanethiolates (Figure 3.11). The chemisorption of thiolate on the AuNP surface possessing surface citrate is not as favorable as on a planar 2-D surface in absence of preadsorbed molecules and is not strong enough to overcome the energy barrier for desorption of the interconnected surface citrates. Nonetheless, the adsorption of thiols on AuNPs results in a stable ligand layer with citrate. On the other hand, thiolate adsorption can also influence the Au-carboxylate interaction of adsorbed citrate. A physisorbed carboxylic acid on the AuNP surface was detected, probably due to proton transfer from thiol to coordinated carboxylate species in the acidic condition upon addition of thiols. When 4-nitrobenzenthiols are adsorbed on citrate-stabilized AuNP surface, new peaks appear at 1662, 1425, and 1283 cm^{-1}. The binding of carboxylic acid by the carbonyl oxygen (on Au surface[27]) on a copper surface shows characteristic symmetric/asymmetric $\nu(C=O)_{COOH}$ vibraions at 1662 and 1283 cm^{-1}. It was demonstrated using ^{1}H-NMR where free oleic acid donated the carboxylic acid proton to coordinated oleate on CdSe quantum dots.[140] The transformation of the binding state

between physisorption by the carbonyl oxygen and chemisorption by the carboxylate oxygen(s) seems to have low activation energy on AuNP surfaces. Nonetheless, the change of adsorption states of the Au-COO(H) does not alter the desorption behavior upon thiol addition. The network of citrate organization due to intermolecular interactions disturbs the adsorption of incoming thiols.

The effect of electrostatics on the adsorption/desorption events on citrate-AuNPs also was assessed in this study. It has been reported by Song and Murray that ligand exchange is dependent on electric charge of metal cores for gold clusters.[141] They found that the ligand exchange between adsorbed and incoming thiols is accelerated by positively charging the gold clusters due to probable increase the polarity of Au-S bond and results in enhancement of the bond lability for the ligand exchange. This may be related to reductive desorption and oxidative adsorption of thiols on metal surfaces. In this study it is attempted to correlate the surface potential of citrate-AuNPs with desorption of the surface citrates and oxidative adsorption[109,142] of thiols. The surface charge of the electric double layer of as-prepared citrate-AuNPs is negative, i.e., zeta-potential between -33 mV and -43 mV for AuNPs used in this study (39 nm ± ~20%).[143] Expectedly, the surface potential drop toward 0 mV would likely cause the polarity of the Au-OOC bond to decrease and thus make the coordinated carboxylate group less labile. Decreased zeta-potential of citrate-AuNPs upon thiolate adsorption would hamper citrate desorption from the surface of AuNPs under electrostatic effects. For 39-nm citrate-AuNPs exhibiting the zetal potential of -40 mV, particle charge $(q)^{x}$ is 6.7×10^{-19} C and thus 4.2 e.[144] Although zeta-potential of bare gold films exhibit a drastic change as a function of pH,[145] that of citrate-AuNPs show a little fluctuation from -40 mV at pH 5 - 12 before reaching the

[x] $q = 4\pi\varepsilon r\xi$ (ε: permittivity of water, r: radius of the particle, ξ: zeta potential)

isoelectric point at around pH 4.5 and subsequent aggregation in solution.[33] Thus, H^+ presumably generated by thiolate formation and OH^- ions do not have a significant influence on the electric double layer of the citrate/Au interface for AuNPs. This also implies a robust interface through citrate/Au interactions. It was reported that the zeta-potential of negatively-charged citrate-AuNPs became less negative when thiols with neutral functional groups were adsorbed on AuNPs.[143] Therefore, citrate desorption with thiolate adsorption would be hindered by the adverse electrostatic effect on citrate-AuNPs, which is consistent with experimental observations in this study. Nonetheless, the charging effect on citrate desorption may not be influential, because the metal-molecule interaction is very weak compared to the intermolecular interactions between citrate molecules adsorbed on the AuNP surfaces. Even if citrates were desorbed from surfaces, they probably would remain on the surface without dissolving into solution[146] due to the strong intermolecular interactions. In addition, a noticeable change of the metal oxidation state after the thiolate functionalization was not observed for citrate-AuNPs. The ratio of XPS peak areas of Au 4f for Au(I)/Au(0) is constant at ~0.1 despite the thiolate adsorption. The change of zeta potential on the thiolate adsorption above is probably due to NP aggregation through van der Waal interactions between the thiolate layers, rather than change of electrostatics on the metal/organic interface of dispersed NPs.

The chemisorbed thiolates and adsorbed citrates lead to the formation of coadsorbed ligands on AuNPs. It is expected further that ligand exchange of thiol in the coadsorbed layer is very slow due to steric hinderance from the adsorbed ligands. Murray and co-workers found that most of the ligand exchange reactions between adsorbed and incoming thiols on gold clusters occur fast at vertex and edge sites whereas the exchange

reactions on terrace sites are very slow.[147] The thiol-to-thiol exchange on Au nanocrystals is explained by an associated mechanism[22,141,147,148] on vertex and edge sites and a dissociative pathway on terrace sites.[149] Taking into consideration the high ratio of terrace sites on the large AuNPs in this study the citrate-to-thiolate exchange probably follows a dissociative pathway. In this case, the rate-determining step is desorption of the surface citrate, and this is expected to be very slow due to the stable layer formation between the thiolate and the surface citrate. The steric hindrance of the coadsorbed ligand layer may hamper the approach of incoming thiols onto the Au surface,[149] and the entrapped citrate layer by thiolate, especially for long ω-terminated alkanethiolates, may prohibit desorption of citrate. The steric effect is known to resist incorporation of incoming species on a metal surface from solution.[94,150,151] Even polynuclear iron(III)-citrate complexes exhibit slower dissociation of citrate by incoming ligands than di- or trinuclear species due to the steric effect.[152-154] It is obvious that the citrate exchange on metal surfaces is not kinetically favorable compared to metal ions. Difficulty in citrate desorption from the AuNP surface is more pronounced on the stable thiolate-citrate ligand layer. As demonstrated above, thermodynamics of the citrate adsorption is very favorable, and citrate desorption in the resultant ligand layer may not happen at all by other thiols. If any, the partial exchange reaction probably occurs at vertex and edge sites. Hampered ligand exchange on terrace sites on AuNPs is responsible for the partial displacement of citrate.

3.3.8 Challenges in formation of thiol-based organic layers on AuNP surfaces

The steric and chelating effects and the prevented transformation of thiols to the chemisorbed state derive from the intermolecular interactions of the hydrogen bonds

between surface citrates. In general, intermolecular interactions between adsorbed molecules on metal surfaces have been considered to be of secondary importance. Recent explorations for robust organic layers on metal surfaces have been focused on how single functional groups can tightly coordinate to the surfaces. This is the main reason for the wide use of the thiol-based layer in nanotechnology. Alternatively, it can be suggested that a molecular layer on metal surfaces with weakly coordinated functional groups including carboxylate and possibly hydroxyl, phosphine or phosphate groups can be as effective as the thiol-based organic layer when intermolecular interaction between the weakly-binding groups are properly manipulated. The carboxylate or phosphate-based molecules may be even superior to the popular thiol compounds that are potentially oxidized to sulfate under some conditions and desorb from surfaces.[155] Sophisticated molecular design for both surface anchoring groups and laterally interacting moieties must be required for this approach, and a pH effect is expected to be critical. The suggested approach of incorporating strong intermolecular hydrogen bonds can open avenues for exploring methodologies towards formation of a robust organic layer on surfaces using the low-cost,[xi] nonoxidizing carboxylate or phosphate compounds.

3.4 Conclusion

Ligand exchange reactions of citrate-AuNPs by incoming thiols were studied by IR and XPS analyses. It has been assumed that surface citrates are displaced spontaneously by addition of thiol molecules on gold surfaces due to the formation of strong Au-S bond at the expense of weak Au-COO interaction, but quantitative spectroscopic evidence of

[xi]For example, 5 g of CH_3-C_{11}-SH (purity 98%) costs $58.90 whereas 25 g of CH_3-C_9-COOH (purity 98%) costs $22.80 (Sigma-Aldrich, May 2012), which the carboxylic acid is much cheaper than the alkanethiol with comparable molecular length.

citrate desorption has not been presented in the literature. The IR and XPS analyses in this study indicate that citrates adsorbed on AuNPs are not replaced significantly by thiols, and the thiolates are coadsorbed with the adsorbed citrates on the surface. With the direct spectroscopic evidence of residual citrates, the typical assumption of spontaneous citrate desorption in ligand exchange reactions with thiols has been challenged. Evidence indicates that surface chloride ions are actually displaced leading to a decrease in negatively-charged surface potential of citrate-AuNPs. The coverage ratio between citrate and alkanethiolate adsorbed on the surface of AuNPs is 1:1.7, which was determined by the XPS analysis. This surface coverage is in good agreement with the coadsorption configuration based on the model of the self-assembled layer of citrate molecules (1:1.5 - 2.0). The thermodynamic factor of the bond strength does not play a critical role in the ligand exchange reaction on AuNP surfaces. Steric and chelating effects of adsorbed citrates combined with strong intermolecular hydrogen bonds result in the strong resistance of citrate desorption and replacement by thiols. A less influential physisorption state of thiols also contributes to the incomplete citrate desorption. The residual citrate can have significant effects on studies and applications using citrate-AuNP, including surface charge, NP assembly, coupling reactions on an organic layer, and NP cellular activity. This study may facilitate investigations of carboxylate-based SAMs as an alternative for surface functionalization of metal NPs.

3.5 Appendix: Strong resistance of coordinated carboxylate to desorption on metal nanoparticles under thiol treatment due to intermolecular interactions

3.5.1 Calculations for amounts of thiols to be quantitatively added to AuNP solution

For the partial functionalization of AuNPs by thiols, the stoichiometric amounts of thiols were calculated based on surface area of a 35-nm AuNP (3.85×10^{-11} cm^2), surface coverage of alkanethiolates (4.8×10^{14} molecules/cm^2),[65] measured absorbance (A = 1.33), and extinction coefficient for 34.5-nm citrate-AuNPs ($\varepsilon = 6.1 \times 10^9$ $M^{-1}cm^{-1}$).[xii] For example, 50 μL of 0.38 mM 1-dodecanethiol solution in ethanol was added to 10 mL of redispersed citrate-AuNPs in ethanol, obtained from being centrifuged once with 10 mL of as-prepared citrate-AuNP solution.

To figure out the number of AuNPs in a solution of 10-mL citrate-stabilized AuNPs:

$$A = \varepsilon cl$$

$$1.33 = (6.1 \times 10^9\ M^{-1}cm^{-1})\cdot c\cdot(1\ cm)$$

where $\varepsilon = 6.1 \times 10^9\ M^{-1}cm^{-1}$ and A = 1.33, and thus

$$c = 2.1 \times 10^{-10}\ M$$

For a 10-mL AuNP solution,

The number of NPs in moles

$= MV$

$= (2.1 \times 10^{-10}\ M)\cdot(0.01\ L)$

$= 2.1 \times 10^{-12}$ moles $\rightarrow 1.3 \times 10^{12}$ NPs

Surface area of a 35-nm ideal spherical NP,

[xii] Liu, X.; Atwater, M.; Wang, J.; Huo, Q. *Colloids Surf., B* **2007**, *58*, 3-7.

$4\pi r^2$

$= 4\pi(35/2 \times 10^{-7}\ cm)^2$

$= 3.8 \times 10^{-11}\ cm^2$

Total surface areas of 1.3×10^{12} NPs in the 10-mL AuNP solution,

$(1.3 \times 10^{12}\ NPs)\cdot(3.8 \times 10^{-11}\ cm^2/NP) = 4.9\ cm^2$

Alkanethiolate surface density on Au(111) surface, 4.5×10^{14}molecuels/cm^2[xiii]

The total number of thiols needed to fully functionalize the entire AuNP surfaces,

$(4.9\ cm^2)\cdot(4.5 \times 10^{14}molecuels/cm^2) = 2.2 \times 10^{16}$ thiols $\rightarrow 3.7 \times 10^{-8}$ moles

Therefore, a 10 mL of 3.7×10^{-6} M thiol solution is needed to functionalize a 10-mL AuNP solution for a monolayer coverage.

Since the typical concentration of thiol solutions is 1.0 mM, $(1.0 \times 10^{-3}\ M)/(3.7 \times 10^{-6}\ M)$ = 270, so 270-ML of thiols are added.

[xiii] Love, J. C.; Estroff, L. A.; Kriebel, J. K.; Nuzzo, R. G.; Whitesides, G. M. *Chem. Rev.* **2005**, *105*, 1103-1169.

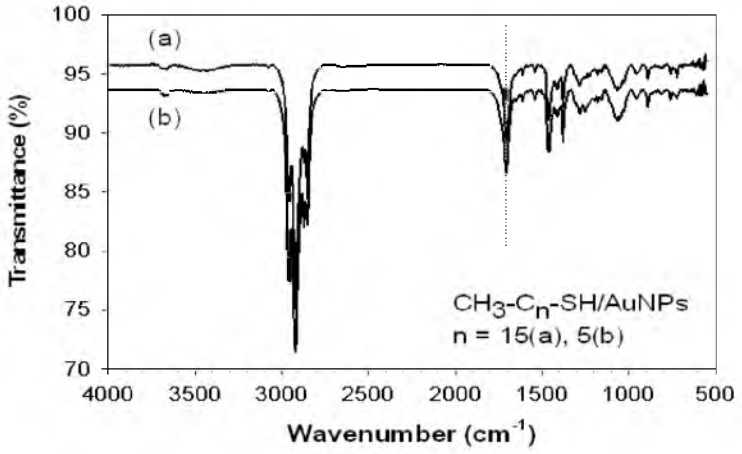

Figure 3.14. ATR-IR spectra of 1-hexanethiolate and 1-hexadecanethiolate functionalized citrate-AuNPs. The strong hydrogen bond peak of citrate carboxylic groups appears at 1704 cm^{-1} (dotted line). The peak at ~1611 and ~1540 cm^{-1} is the asymmetric COO stretching vibration of η^1-COO-Au and η^2-COO-Au, respectively. This verifies the presence of surface coordinated citrate.

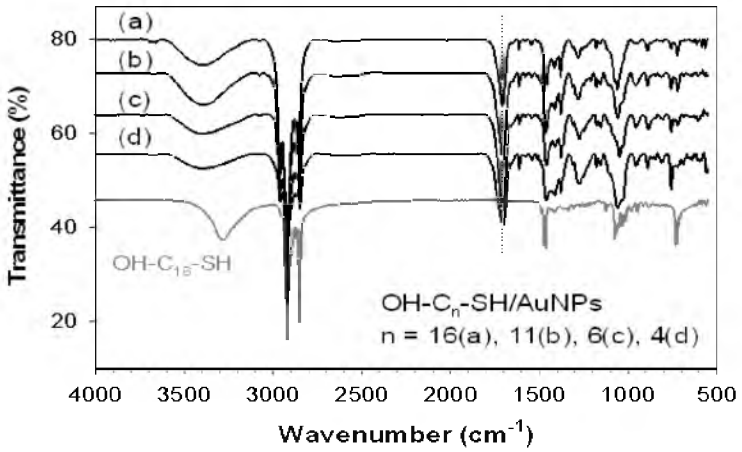

Figure 3.15. ATR-IR spectra of 4-mercapto-1-butanol, 6-mercapto-1-hexanol, 11-mercapto-1-undecanol, and 16-mercapto-1-hexadecanol functionalized citrate-AuNPs. The strong hydrogen bond peak of citrate carboxylic groups appears at 1704 cm^{-1} (dotted line). The peak at ~1611 and ~1540 cm^{-1} is the asymmetric COO stretching vibration of η^1-COO-Au and η^2-COO-A, respectively. This verifies the presence of surface coordinated citrate. (Pure OH-terminated alkanethiols for n = 6 and 4 show a small peak at 1700 cm^{-1}, but this is an impurity. Spectra are not shown.)

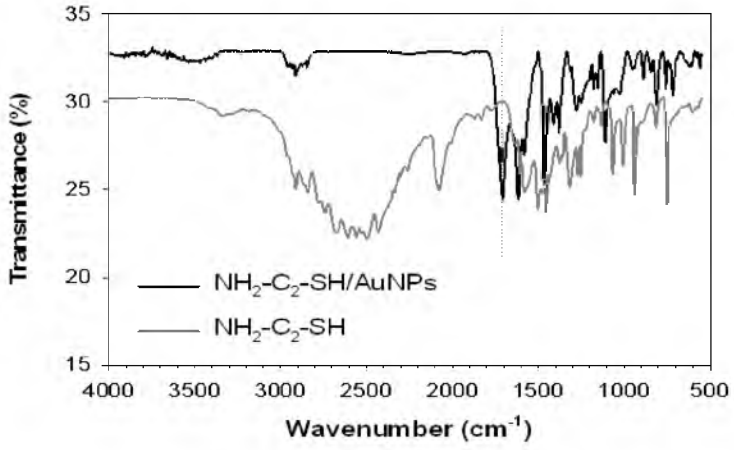

Figure 3.16. ATR-IR spectrum of 2-aminoethanethiolate functionalized citrate-AuNPs. The strong hydrogen bond peak of citrate carboxylic groups appears at 1704 cm^{-1} (dotted line).

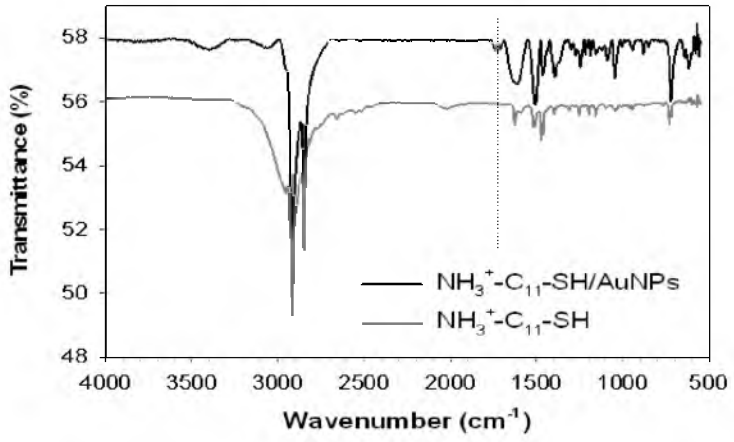

Figure 3.17. ATR-IR spectrum of 11-amino-1-undecanethiolate functionalized citrate-AuNPs. The strong hydrogen bond peak of citrate carboxylic groups appears at 1734 cm^{-1} (dotted line).

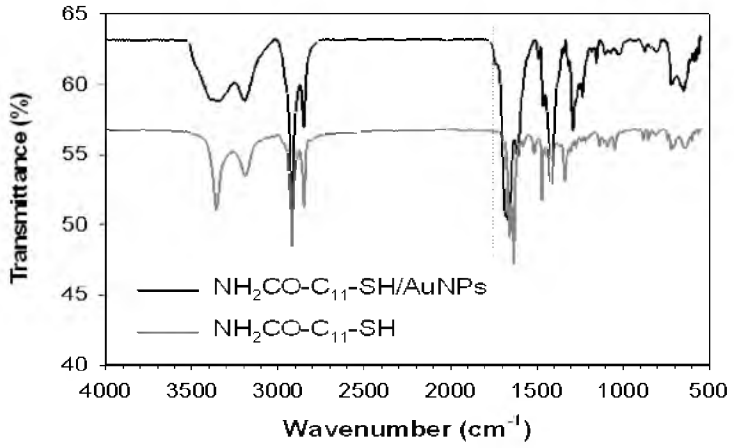

Figure 3.18. ATR-IR spectrum of 11-mercaptoundecanamide functionalized citrate-AuNPs. The strong hydrogen bond peak of citrate carboxylic groups appears at ~1700 cm^{-1}, which is overlapped with ν(C=O) vibration of the thiolate amide group, but the other hydrogen bonded COOH peak of surface citrate displays at 1734 cm^{-1} (dotted line).

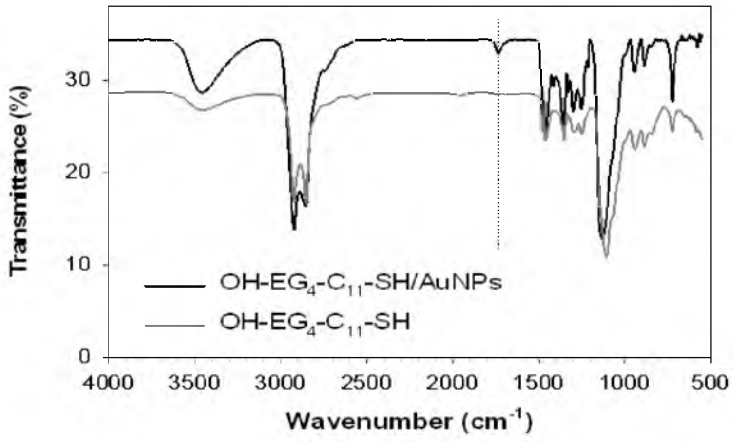

Figure 3.19. ATR-IR spectrum of (11-mercaptoundecyl)tetra(ethylene glycol) functionalized citrate-AuNPs. The hydrogen bond peak of citrate carboxylic groups appears at 1734 cm^{-1} (dotted line).

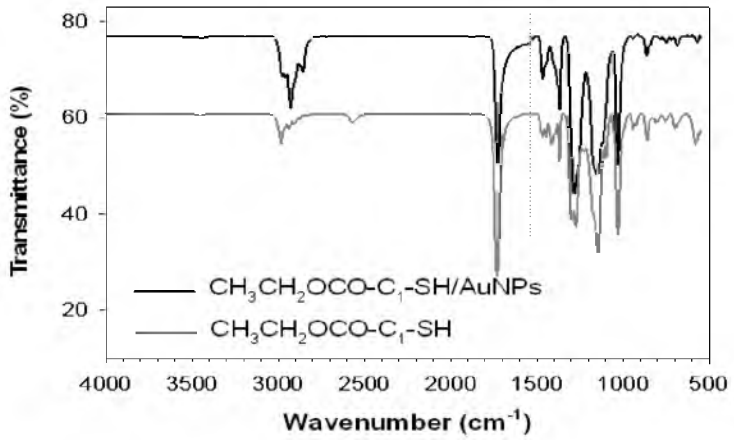

Figure 3.20. ATR-IR spectrum of ethyl 2-mercaptoacetate functionalized citrate-AuNPs. The strong hydrogen bond peak of citrate carboxylic groups appears at ~1734 cm^{-1}, which is overlapped with ν(C=O) vibration of the thiolate carbonyl group, but the asymmetric COO stretching vibration of bidentate COO-Au displays at ~1550 cm^{-1} (dotted line).

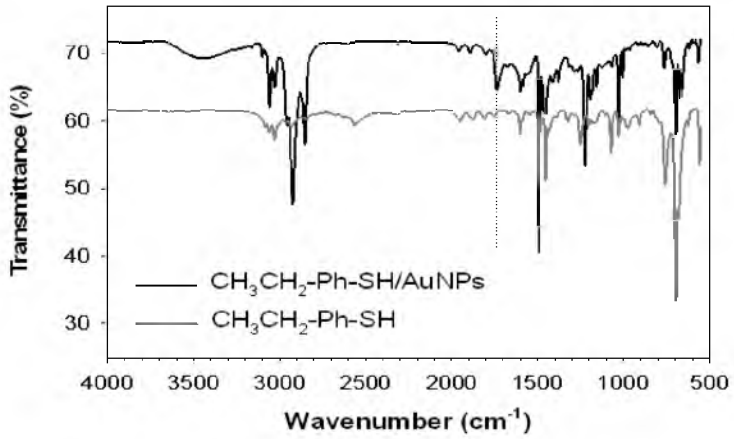

Figure 3.21. ATR-IR spectrum of benzyl mercaptan functionalized citrate-AuNPs. The hydrogen bond peak of citrate carboxylic groups at 1704 cm^{-1} is weak, but the other hydrogen bonded COOH peak of surface citrate displays at 1734 cm^{-1} (dotted line).

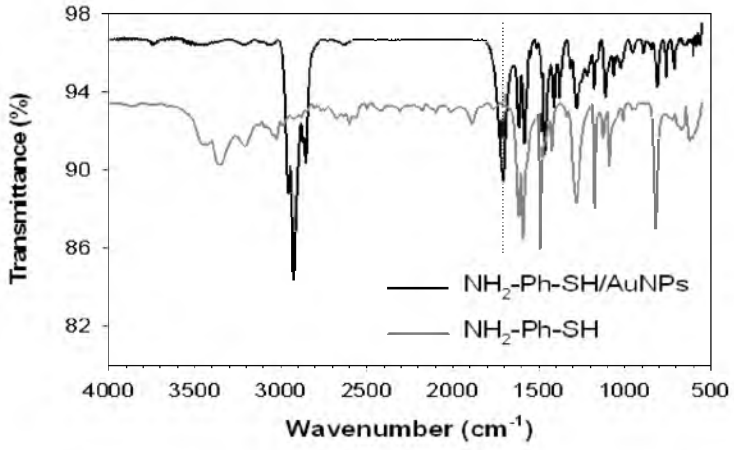

Figure 3.22. ATR-IR spectrum of 4-aminothiophenol functionalized citrate-AuNPs. The hydrogen bond peak of citrate carboxylic groups appears at 1701 cm^{-1} (dotted line).

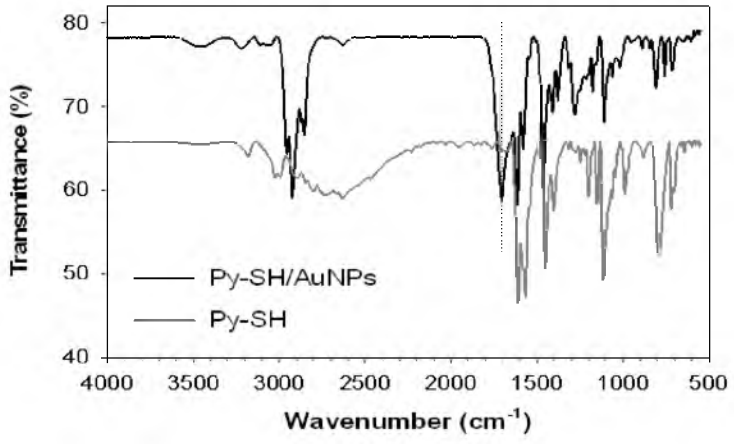

Figure 3.23. ATR-IR spectrum of 4-mercaptopyridine functionalized citrate-AuNPs. The hydrogen bond peak of citrate carboxylic groups appears at 1701 cm^{-1} (dotted line).

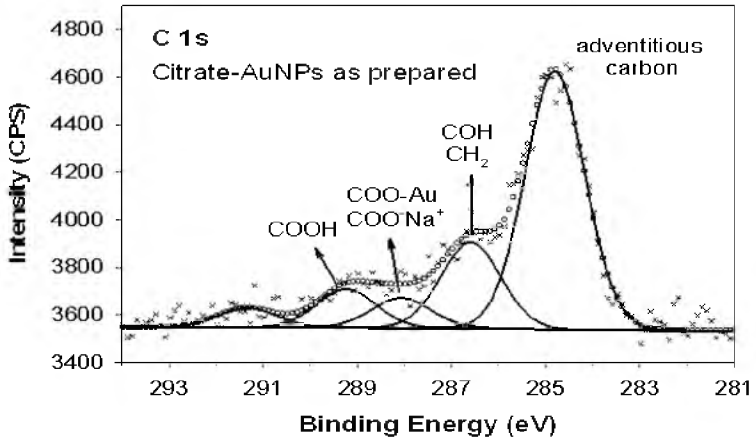

Figure 3.24. XPS C 1s spectrum of citrate-AuNPs as prepared. From the previous studies, COO-Au is located at 287.6 eV whereas the $COO^{-}Na^{+}$ of pure sodium citrate at 288.2 eV.

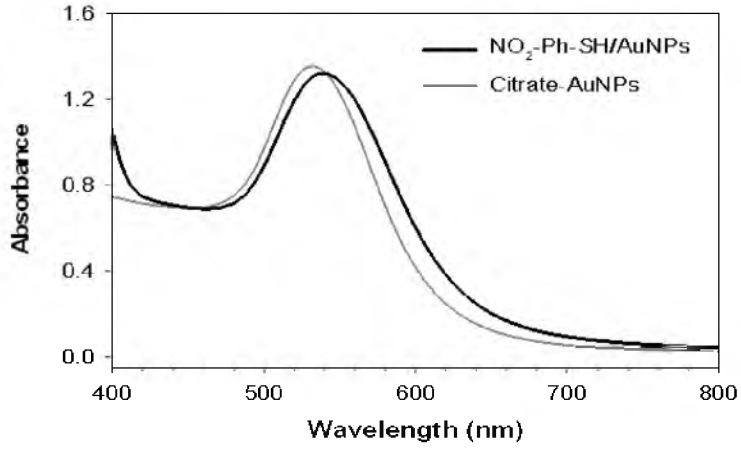

Figure 3.25. UV-Vis absorbance of 4-nitrobenzenethiolate functionalized citrate-AuNPs. This shows little aggregation of NPs. λ_{max} = 532 nm for citrate-AuNPs.

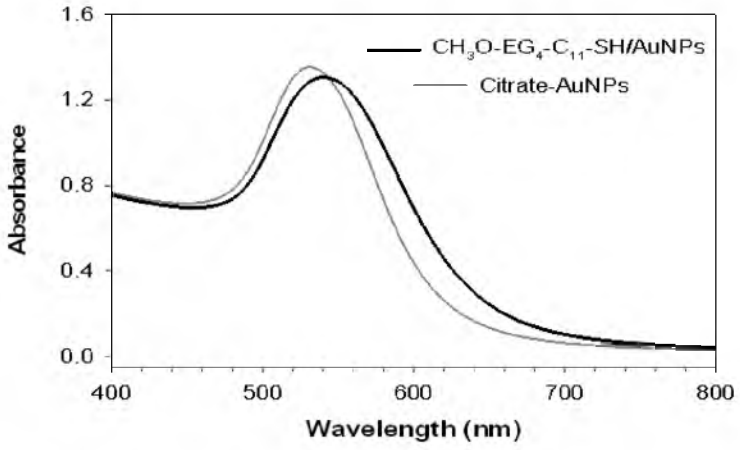

Figure 3.26. UV-Vis absorbance of methoxy-capped tetra(ethylene glycol) undecanethiolate functionalized citrate-AuNPs. This shows little aggregation of NPs. λ_{max} = 532 nm for citrate-AuNPs.

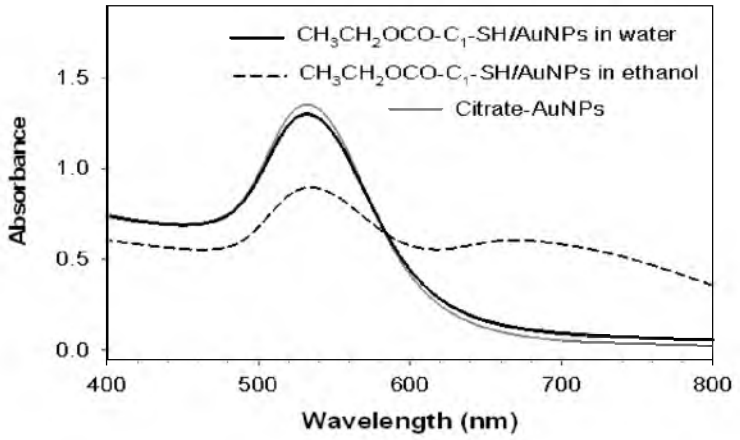

Figure 3.27. UV-Vis spectra of ethyl 2-mercaptoacetate functionalized citrate-AuNPs in water and ethanol. These show a solvent-dependent aggregation of NPs. λ_{max} = 532 nm for citrate-AuNPs.

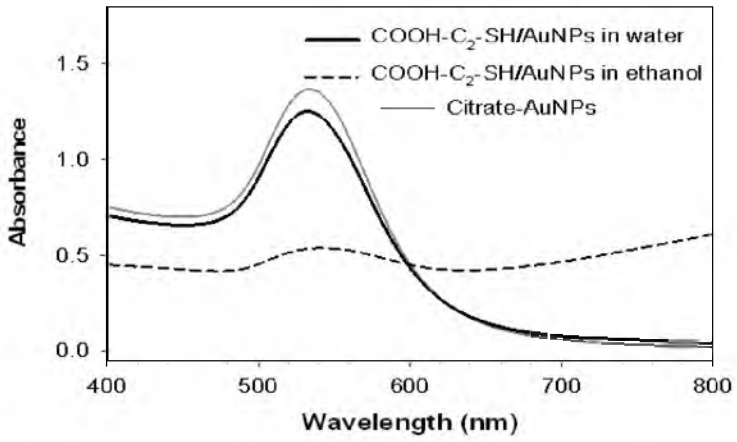

Figure 3.28. UV-Vis spectra of 3-mercaptopropionic acid functionalized citrate-AuNPs in water and ethanol. These show a solvent-dependent aggregation of NPs. λ_{max} = 532 nm for citrate-AuNPs.

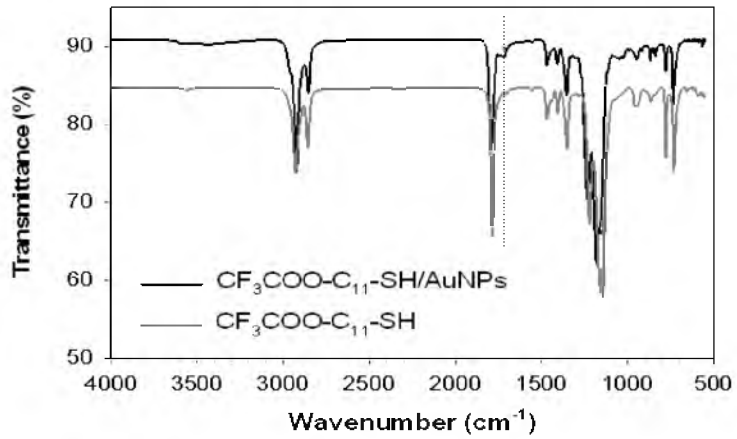

Figure 3.29. ATR-IR spectrum of 11-mercanptoundecyl trifluoromethylacetate functionalized citrate-AuNPs. Distinct features of surface citrate are overlapped with the pure thiol (ν(C=O) at ~1730 cm^{-1}, dotted line), which cannot be used to determine the remaining surface citrate.

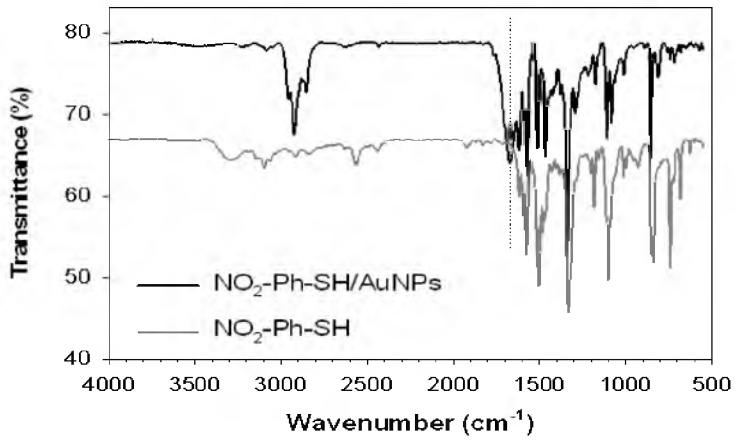

Figure 3.30. ATR-IR spectrum of 4-nitrobenzenthiolate functionalized citrate-AuNPs. The peak at ~1660 cm^{-1} is assigned to physisorbed carboxylic groups of surface citrate (dotted line).

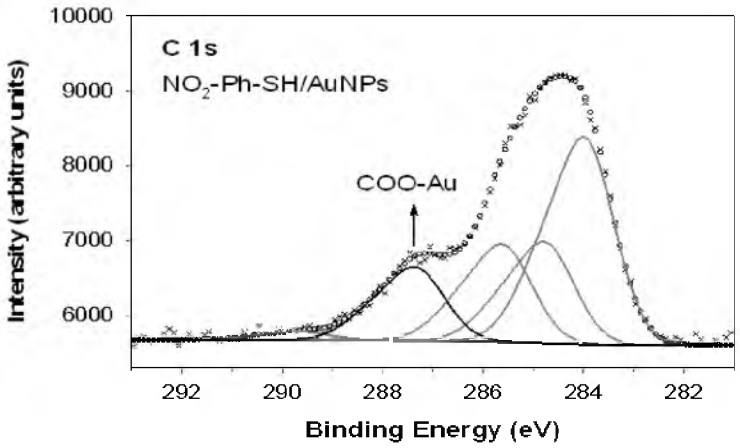

Figure 3.31. XPS C1s spectrum of 4-nitrobenzenthiolate functionalized citrate-AuNPs. The peak at ~ 287.5 eV results from the COO-Au species.

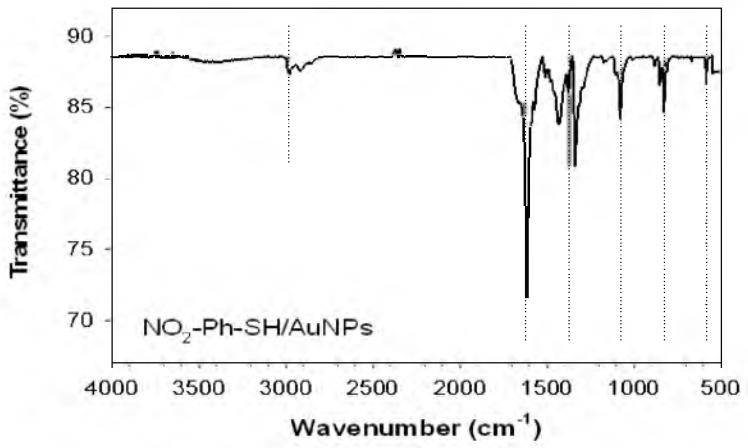

Figure 3.32. Transmission IR spectrum of 4-nitrobenzenthiolate functionalized citrate-AuNPs when pH ~11. The peaks (dotted lines) are generated when the terminal free carboxylate group binds to the AuNP surface, which verifies the presence of surface citrate.

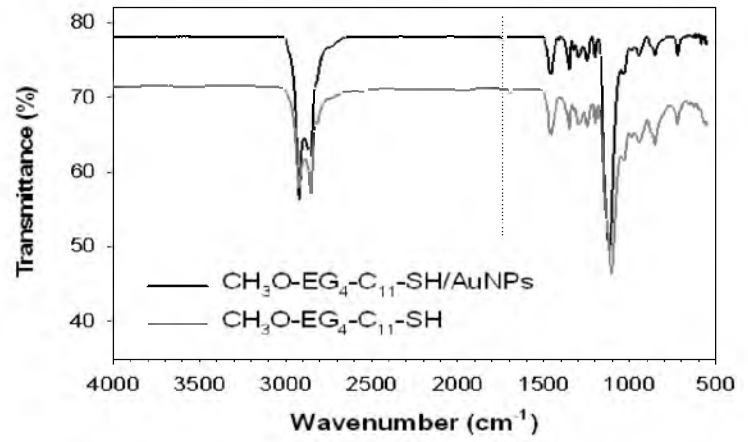

Figure 3.33. ATR-IR spectrum of methoxy-capped tetra(ethylene glycol) undecanethiolate functionalized citrate-AuNPs. The hydrogen bond peak of citrate carboxylic groups appears at 1734 cm^{-1} (dotted line).

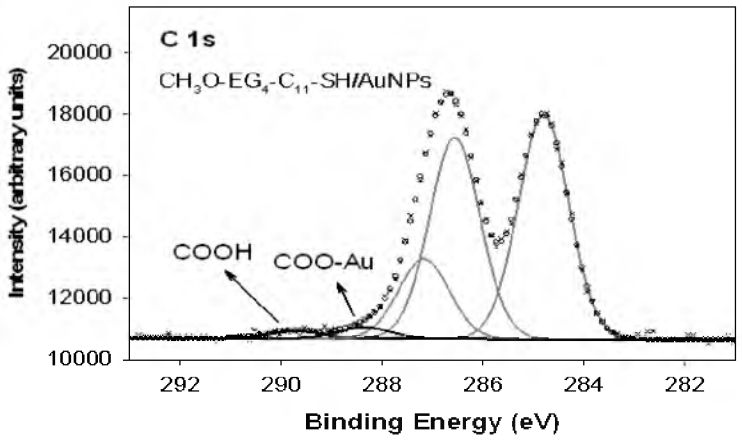

Figure 3.34. XPS C1s spectrum of methoxy-capped tetra(ethylene glycol) undecanethiolate functionalized citrate-AuNPs. The peak at ~287.5 eV results from the COO-Au species.

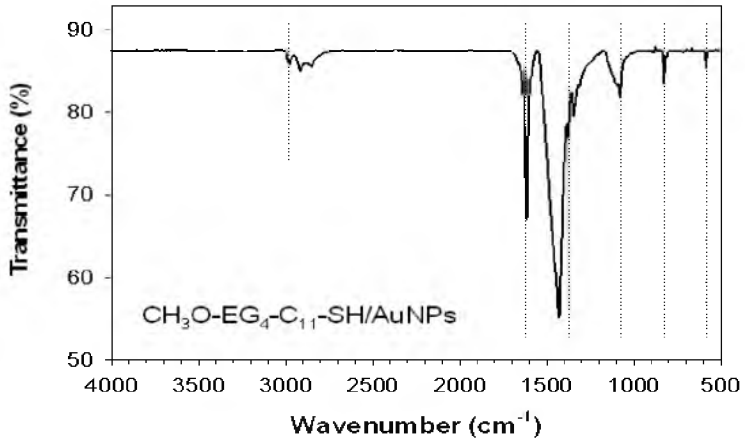

Figure 3.35. Transmission IR spectrum of methoxy-capped tetra(ethylene glycol) undecanethiolate functionalized citrate-AuNPs when pH ~11. The peaks (dotted lines) are generated when the terminal free carboxylate group binds to the AuNP surface, which verifies the presence of surface citrate.

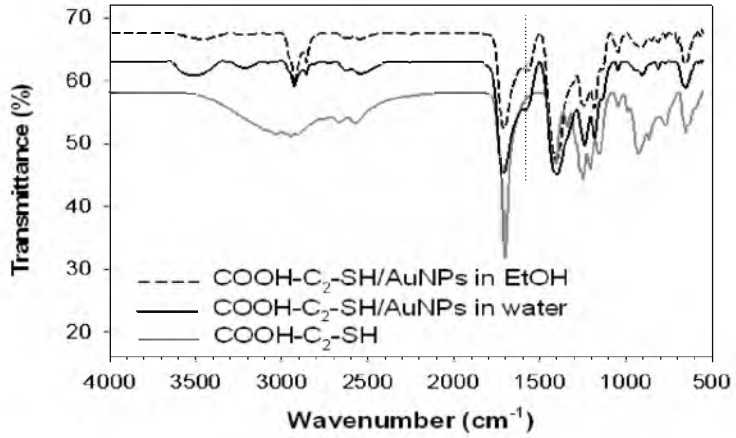

Figure 3.36. ATR-IR spectra of 3-mercaptopropionic acid functionalized citrate-AuNPs in ethanol and water. The hydrogen bond peak of citrate carboxylic groups is overlapped with that from thiolate carboxylic acid, but the asymmetric stretching vibration of COO-Au of surface citrate appears at ~1580 cm^{-1} (dotted line). Most of free carboxylic groups are protonated.

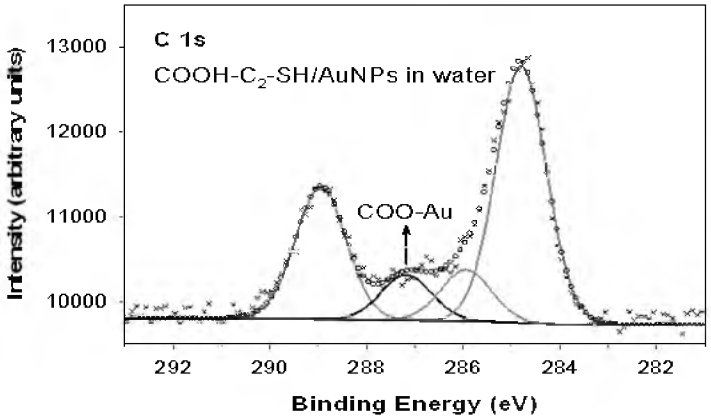

Figure 3.37. XPS C1s spectrum of 3-mercaptopropionic acid functionalized citrate-AuNPs. The peak at ~287.5 eV results from the COO-Au species. For 11-mercaptoundecanoic acid, the carbonyl carbon: 289.2 eV, α-carbon: 286.2 eV.[88,156]

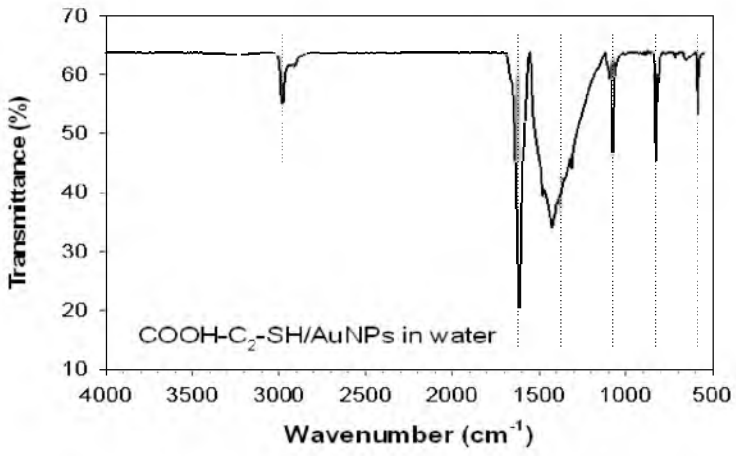

Figure 3.38. Transmission IR spectrum of 3-mercaptopropionic acid functionalized citrate-AuNPs when pH ~11. The peaks (dotted lines) are generated when the terminal free carboxylate group binds to the AuNP surface, which verifies the presence of surface citrate.

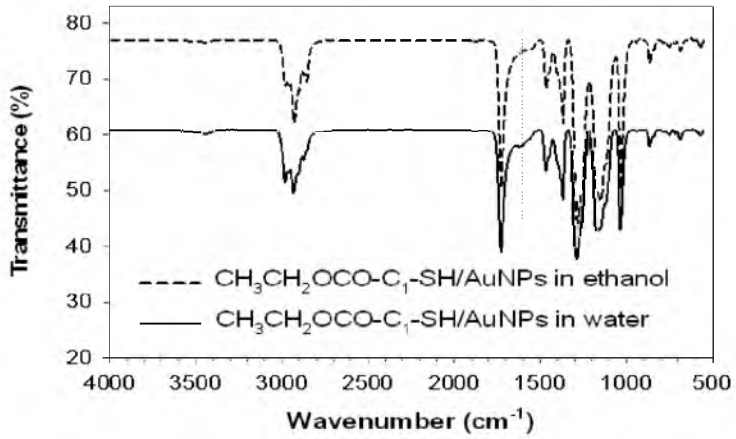

Figure 3.39. ATR-IR spectra of ethyl 2-mercaptoacetate functionalized citrate-AuNPs in ethanol and water. The hydrogen bond peak of citrate carboxylic groups is overlapped with that from thiolate carbonyl group, but the asymmetric stretching vibration of COO-Au of surface citrate appears at ~1600 cm^{-1} (dotted line).

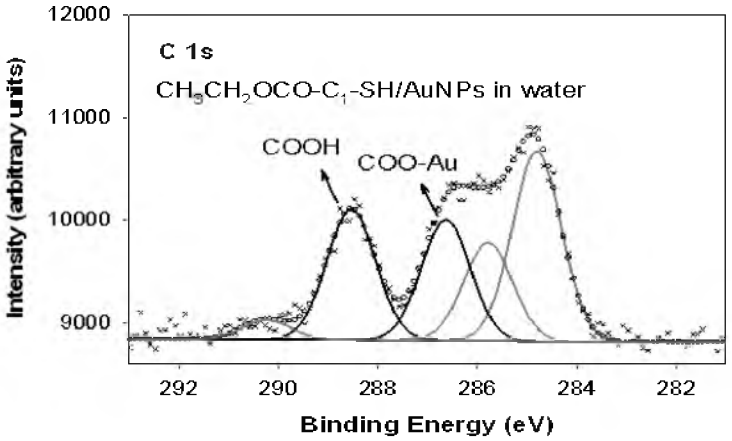

Figure 3.40. XPS C1s spectrum of ethyl 2-mercaptoacetate functionalized citrate-AuNPs. The peaks at ~287.5 and ~288.5 eV can be assigned to the COO-Au species and free carboxylic acid groups of citrate, respectively. Those peaks are overlapped with those of the α-carbon and carbonyl carbons of the thiolate.[89]

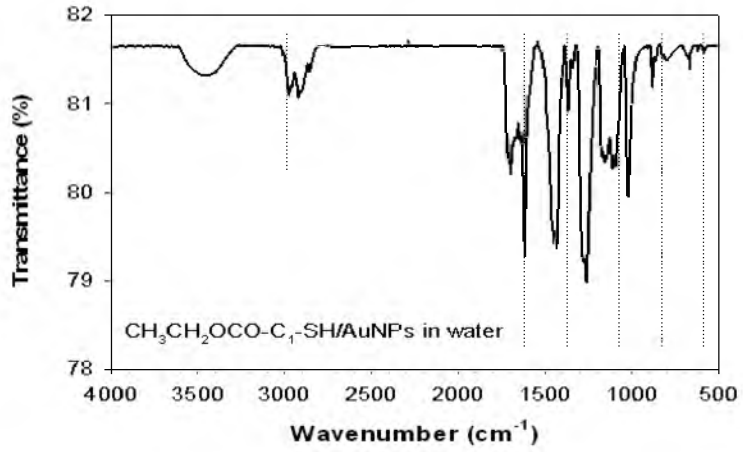

Figure 3.41. Transmission IR spectrum of ethyl 2-mercaptoacetate functionalized citrate-AuNPs when pH ~11. The peaks (dotted lines) are generated when the terminal free carboxylate group binds to the AuNP surface, which verifies the presence of surface citrate.

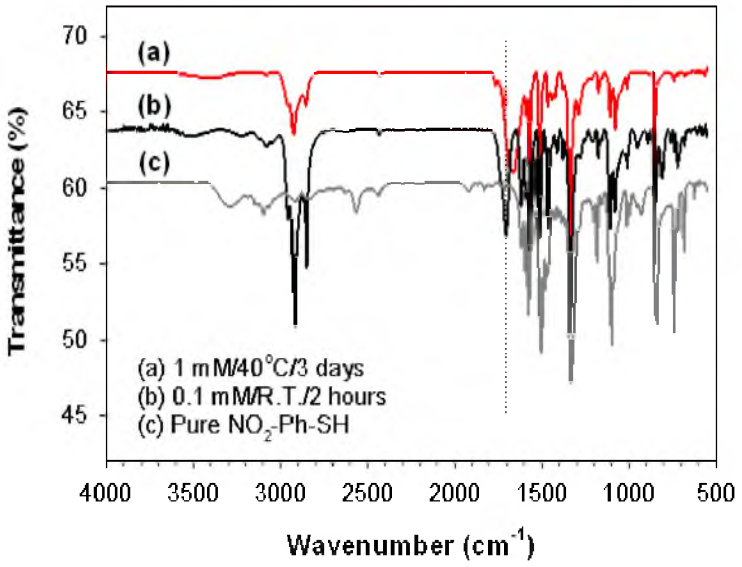

Figure 3.42. ATR-IR spectra of 4-nitobenzenthiolate functionalized citrate-AuNPs in different conditions. Thiol concentration, temperature, and incubation time for the functionalization are shown. The COOH peak is present (dotted line) after functionalization. This verifies the presence of remaining surface citrate.

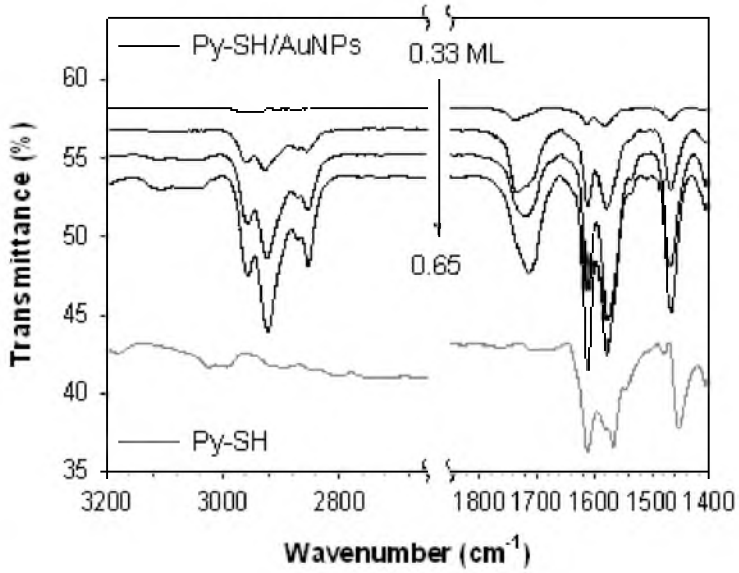

Figure 3.43. ATR-IR spectra of Py-SH functionalized citrate-AuNPs with varied thiol amounts. The thiol amounts added to AuNP solutions are 0.65, 0.54, 0.43, and 0.33 ML, respectively.

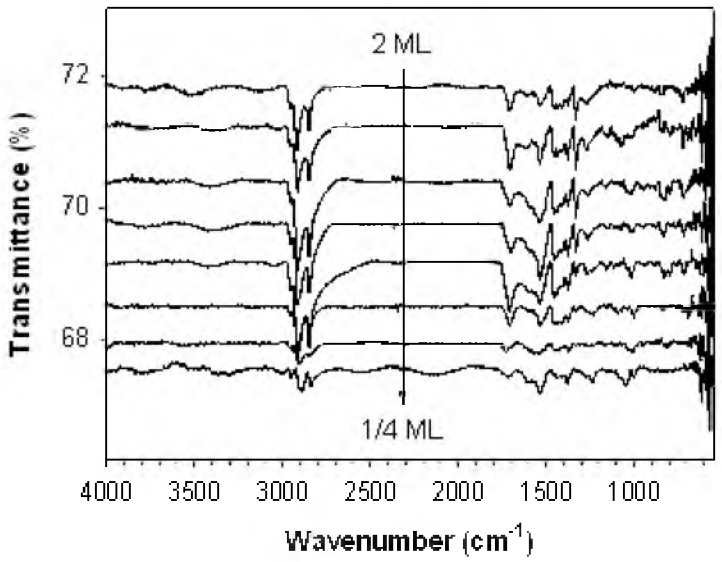

Figure 3.44. ATR-IR spectra of NO_2-Ph-SH functionalized citrate-AuNPs with varied thiol amounts. There is saturation of the peak intensities of $\nu_{sym}(NO_2)$ at 1336 cm^{-1}. The thiol amounts added to AuNP solutions are 2, 3/2, 1, 3/4, 1/2, 5/12, 1/3, and 1/4 ML to cover the factional surface area on AuNPs.

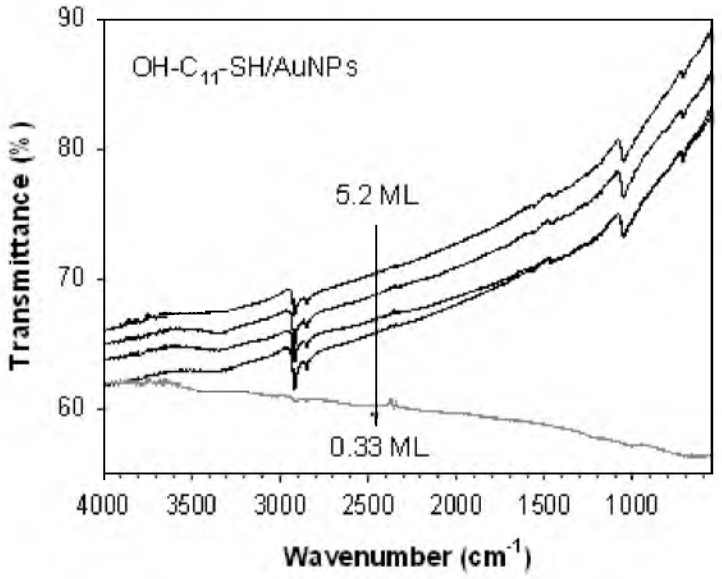

Figure 3.45. Transmission IR spectra of 11-mercapto-1-undecanol functionalized citrate-AuNPs with varied thiol amounts. These show saturation of the peak intensities. The thiol amounts added to AuNP solutions are 5.2, 2.6, 1.3, 0.65, and 0.33 ML to cover the factional surface area on AuNPs.

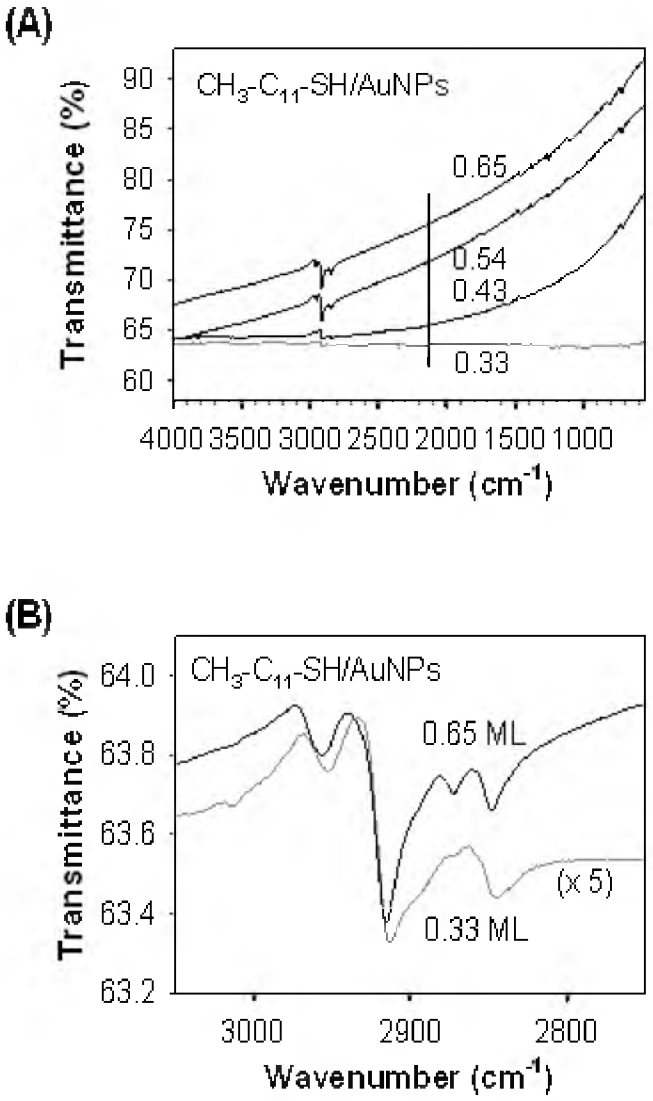

Figure 3.46. Transmission IR spectra of 1-dodecanethiolate functionalized citrate-AuNPs with varied thiol amounts. (A) Spectra show saturation of the peak intensities prior to ~0.65 ML. The thiol amounts added to AuNP solutions are 0.65, 0.54, 0.43, and 0.33 ML to cover the factional surface area on AuNPs. (B) The similar positions of $\nu(C\text{-}H)_{CH_2}$ vibrations appear at 2917/2848 cm^{-1} regardless of surface coverage.

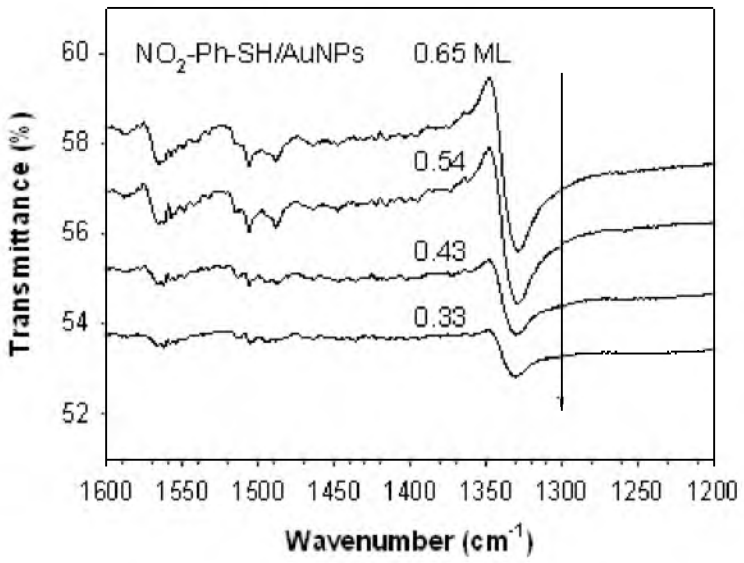

Figure 3.47. Transmission IR spectra of NO_2-Ph-SH functionalized citrate-AuNPs with varied thiol amounts. Spectra show saturation of the peak intensities of $\nu_{sym}(NO_2)$ at 1336 cm^{-1}.

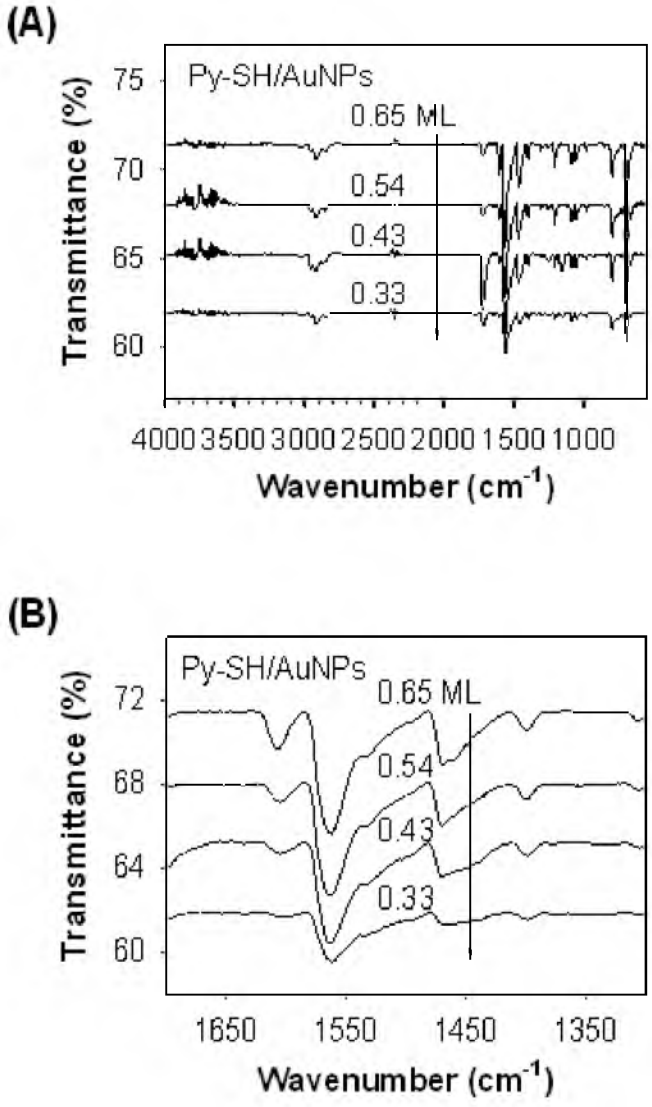

Figure 3.48. Transmission IR spectra of 4-mercaptopyridine functionalized citrate-AuNPs with varied thiol amounts. (A) The thiol amounts added to AuNP solutions are 0.65, 0.54, 0.43, and 0.33 ML to cover the factional surface area on AuNPs. (B) Spectra show saturation of the peak intensities of Py-SH prior to ~0.65 ML.

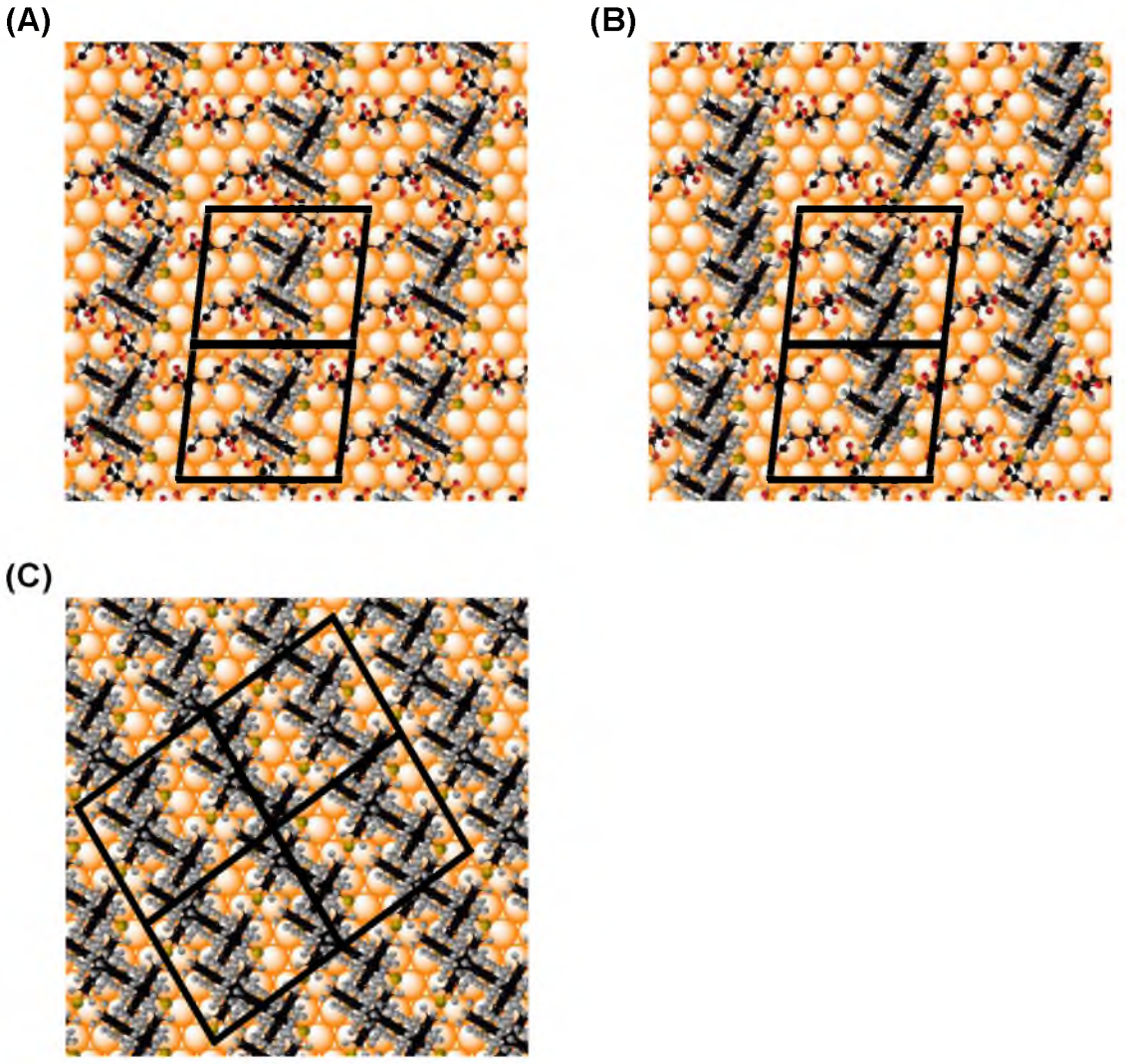

Figure 3.49. Comparison of possible configurations of adsorbed alkanethiolates (CH_3-C_9-S-) on a (111) surface of citrate-AuNPs (A and B) with the ideal monolayer on a bare (111) surface (C). Each parallelogram represents a unit cell (area: 179 $Å^2$), and in (C) it was rotated to the direction of the alkanethiolate organization. The numbers of alkanethiolates in unit cells are 6 thiolates/(2 × 179 $Å^2$) for (A), 8 thiolates/(2 × 179 $Å^2$) for (B), and 36 thiolates/(4 × 179 $Å^2$) for (C), which result in 33.3%, 44.4%, and 100% coverage by alkanethiolates, respectively.

3.6 References

(1) Daniel, M.-C.; Astruc, D. *Chem. Rev.* **2004**, *104*, 293-346.

(2) Turkevich, J.; Stevenson, P. C.; Hillier, J. *Discuss. Faraday Soc.* **1951**, 55-75.

(3) Frens, G. *Nature Phys. Sci.* **1973**, *241*, 20-22.

(4) Hostetler, M. J.; Wingate, J. E.; Zhong, C.-J.; Harris, J. E.; Vachet, R. W.; Clark, M. R.; Londono, J. D.; Green, S. J.; Stokes, J. J.; Wignall, G. D.; Glish, G. L.; Porter, M. D.; Evans, N. D.; Murray, R. W. *Langmuir* **1998**, *14*, 17-30.

(5) Kreibig, U.; Vollmer, M. *Optical Properties of Metal Clusters*; Springer: Berlin, Germany, 1995.

(6) Links, S.; El-Sayed, M. A. *Annu. Rev. Phys. Chem.* **2003**, *54*, 331-366.

(7) Brust, M.; Walker, M.; Bethell, D.; Schiffrin, D. J.; Whyman, R. *J. Chem. Soc., Chem. Commun.* **1994**, 801-802.

(8) Schmid, G.; Pfeil, R.; Boese, R.; Brandermann, F.; Meyer, S.; Calis, G. H. M.; Van der Velden, J. W. A. *Chem. Ber.* **1981**, *114*, 3634-3642.

(9) Xie, H.; Tkachenko, A. G. Glomm, W. R.; Ryan, J. A.; Brennaman, M. K.; Papanikolas, J. M.; Franzen, S.; Feldheim, D. L. *Anal. Chem.* **2003**, *75*, 5797-5805.

(10) Kalsin, A. M.; Fialkowski, M.; Paszewski, M.; Smoukov, S. K.; Bishop, K. J. M.; Grzybowski, B. A. *Science* **2006**, *312*, 420-424.

(11) (a) Sardar, R.; Heap, T. B.; Shumaker-Parry, J. S. *J. Am. Chem. Soc.* **2007**, *129*, 5356-5357. (b) Sardar, R.; Shumaker-Parry, J. S. *Nano Lett.* **2008**, *8*, 731-736.

(12) (a) Mirkin, C. A.; Letsinger, R. L.; Mucic, R. C.; Storhoff, J. J. *Nature* **1996**, *382*, 607-609. (b) Alivisatos, A. P.; Johnsson, K. P.; Peng, X.; Wilson, T. E.; Loweth, C. J.; Bruchez, M. P., Jr.; Schultz, P. G. *Nature* **1996**, *382*, 609-611.

(13) Gourishankar, A.; Shukla, S.; Ganesh, K. N.; Sastry, M. *J. Am. Chem. Soc.* **2004**, *126*, 13186-13187.

(14) Saha, K.; Agasti, S. S.; Kim, C.; Li, X.; Rotello, V. M. *Chem. Rev.* **2012**, *112*, 2739-2779.

(15) Mahmoudi, M.; Azadmanesh, K.; Shokrgozar, M. A.; Journeay, W. S.; Laurent, S. *Chem. Rev.* **2011**, *111*, 3407-3432.

(16) Nuzzo, R. G.; Allara, D. L. *J. Am. Chem. Soc.* **1983**, *105*, 4481-4483.

(17) Porter, M. D.; Bright, T. B.; Allara, D. L.; Chidsey, C. E. D. *J. Am. Chem. Soc.* **1987**, *109*, 3559-3568.

(18) Sandroff, C. J.; Garoff, S.; Leung, K. P. *Chem. Phys. Lett.* **1983**, *96*, 547-551.

(19) Bryant, M. A.; Pemberton, J. E. *J. Am. Chem. Soc.* **1991**, *113*, 3629-3637.

(20) Weisbecker, C. S.; Merritt, M. V.; Whitesides, G. M. *Langmuir* **1996**, *12*, 3763-3772.

(21) Grabar, K. C.; Allison, K. J.; Baker, B. E.; Bright, R. M.; Brown, K. R.; Freeman, R. G.; Fox, A. P.; Keating, C. D.; Musick, M. D.; Natan, M. J. *Langmuir* **1996**, *12*, 2353-2361.

(22) Guo, R.; Song, Y.; Wang, G.; Murray, R. W. *J. Am. Chem. Soc.* **2005**, *127*, 2752-2757.

(23) Woehrle, G. H.; Brown, L. O.; Hutchison, J. E. *J. Am. Chem. Soc.* **2005**, *127*, 2172-2183.

(24) Ionita, P.; Caragheorgheopol, A.; Gilbert, B. C.; Chechik, V. *J. Am. Chem. Soc.* **2002**, *124*, 9048-9049.

(25) Xu, B.; Madix, R. J.; Friend, C. M. *J. Am. Chem. Soc.*, **2010**, *132*, 16571-16580.

(26) Xu, B.; Haubrich, J.; Baker, T. A.; Kaxiras, E.; Friend, C. M. *J. Phys. Chem. C* **2011**, *115*, 3703-3708.

(27) Chen, F.; Li, X.; Hihath, J.; Huang, Z.; Tao, N. *J. Am. Chem. Soc.* **2006**, *128*, 15874-15881.

(28) Wang, J.-g.; Selloni, A. *J. Phys. Chem. C* **2009**, *113*, 8895-8900.

(29) Noda, H.; Wan, L.-J.; Osawa, M. *Phys. Chem. Chem. Phys.* **2001**, *3*, 3336-3342.

(30) Dahl, J. A.; Maddux, B. L. S.; Hutchison, J. E. *Chem. Rev.* **2007**, *107*, 2228-2269.

(31) Lohse, S. E.; Dahl, J. A.; Hutchison, J. *Langmuir* **2010**, *26*, 7504-7511.

(32) Huang, T.; Nallathamby, P. D.; Xu, X.-H. N. *J. Am. Chem. Soc.* **2008**, *130*, 17095-17105.

(33) Brewer, S. H.; Glomm, W. R.; Johnson, M. C.; Knag, M. K.; Franzen, S. *Langmuir* **2005**, *21*, 9303-9307.

(34) Su, X.; Kanjanawarut, R. *ACS Nano* **2009**, *3*, 2751-2759.

(35) Hill, H. D.; Millstone, J. E.; Banholzer, M. J.; Mirkin, C. A. *ACS Nano* **2009**, *3*, 418-424.

(36) Tsai, D-H.; Zangmeister, R. A.; Pease III, L. F.; Tarlov, M. J.; Zachariah, M. R. *Langmuir* **2008**, *24*, 8483-8490.

(37) Storhoff, J. J.; Elghanian, R.; Mirkin, C. A.; Letsinger, R. L. *Langmuir* **2002**, *18*, 6666-6670.

(38) Lin, S.-Y.; Tsai, Y.-T.; Chen, C.-C.; Lin, C.-M.; Chen, C.-H. *J. Phys. Chem. B* **2004**, *108*, 2134-2139.

(39) Zhang, S.; Leem, G.; Srisombat, L.-O.; Lee, T. R. *J. Am. Chem. Soc.* **2008**, *130*, 113-120.

(40) Ivanov, M.; Bednar, H. R.; Haes, A. J. *ACS Nano* **2009**, *3*, 386-394.

(41) Rouhana, L. L.; Jaber, J. A.; Schlenoff, J. B. *Langmuir* **2007**, *23*, 12799-12801.

(42) Demers, L. M.; Mirkin, C. A.; Mucic, R. C.; Reynolds, R. A.; Letsinger, R. L.; Elghanian, R.; Viswanadham, G. *Anal. Chem.* **2000**, *72*, 5535-5541.

(43) Gearheart, L. A.; Ploehn, H. J.; Murphy, C. J. *J. Phys. Chem. B* **2001**, *105*, 12609-12615.

(44) Lèvy, R.; Thanh, N. T. K.; Doty, R. C.; Hussain, I.; Nichols, R. J.; Schiffrin, D. J.; Brust, M.; Fernig, D. G. *J. Am. Chem. Soc.* **2004**, *126*, 10076-10084.

(45) Choi, Y.; Park, Y.; Kang, T.; Lee, L. P. *Nat. Nanotechnol.* **2009**, *4*, 742-746.

(46) Cárdenas, M.; Barauskas, J.; Schillén, K.; Brennan, J. L.; Brust, M.; Nylander, T. *Langmuir* **2006**, *22*, 3294-3299.

(47) Katz, E.; Willner, I. *Angew. Chem. Int. Ed.* **2004**, *43*, 6042-6108.

(48) Sato, T.; Brown, D.; Johnson, B. F. G. *Chem. Commun.* **1997**, 1007-1008.

(49) Baranov, D.; Kadnikova, E. N. *J. Mater. Chem.* **2011**, *21*, 6152-6157.

(50) Yang, J.; Lee, J. Y.; Ying, J. Y. *Chem. Soc. Rev.* **2011**, *40*, 1672-1696.

(51) Bellino, M. G.; Calvo, E. J.; Gordillo, G. *Phys. Chem. Chem. Phys.* **2004**, *6*, 424-428.

(52) Yu, C.-J.; Tseng, W.-L. *Langmuir* **2008**, *24*, 12717-12722.

(53) El-Sayed, I. H.; Huang, X.; El-Sayed, M. A. *Nano Lett.* **2005**, *5*, 829-834.

(54) Jain, P. K.; El-Sayed, I. H.; El-Sayed, M. A. *Nano Today* **2007**, *2*, 18-29.

(55) El-Sayed, I. H.; Huang, X.; El-Sayed, M. A. *Cancer Lett.* **2006**, *128*, 2115-2120.

(56) Grainger, D. W.; Castner, D. G. *Adv. Mater.* **2008**, *20*, 867-877.

(57) Graham, D.; Faulds, K. *Chem. Soc. Rev.* **2008**, *37*, 1042-1051.

(58) Faulds, K.; Littleford, R. E.; Graham, D.; Dent, G.; Smith, W. E. *Anal. Chem.* **2004**, *76*, 592-598.

(59) Vidal, B. C., Jr.; Deivaraj, T. C.; Yang, J.; Too, H.-P.; Chow, G.-M.; Gan, L. M.; Lee, J. Y. *New J. Chem.* **2005**, *29*, 812-816.

(60) Schaefer, J.; Jiang, H.; Ransome, A. E.; Kappock, T. J. *Biochemistry* **2007**, *46*, 9507-9512.

(61) Glusker, J. P. *Acc. Chem. Res.* **1980**, *13*, 345-352.

(62) Giersig, M.; Mulvaney, P. *Langmuir* **1993**, *9*, 3408-3413.

(63) Jang, S.; Park, J.; Shin, S.; Yoon, C.; Choi, B. K.; Gong, M.-s.; Joo, S.-W. *Langmuir* **2004**, *20*, 1922-1927.

(64) Ulman, A. *Chem. Rev.* **1996**, *96*, 1533-1554.

(65) Nuzzo, R. G.; Zegarski, B. R.; Dubois, L. H. *J. Am. Chem. Soc.* **1987**, *109*, 733-740.

(66) Huheey, J. E.; Keiter, E. A.; Keiter, R. L. *Inorganic Chemistry - Principles of Structure and Reactivity*, 4th Ed.; Harper Collins College Publishers: New York, 1993.

(67) Weitz, D. A.; Oliveria, M. *Phys. Rev. Lett.* **1984**, *52*, 1433-1436.

(68) Creighton, J. A.; Alvarez, M. S.; Weitz, D. A.; Garoff, S.; Kim, M. W. *J. Phys. Chem.* **1983**, *87*, 4793-4799.

(69) Mayya, K. S.; Patil, V.; Sastry, M. *Langmuir* **1997**, *13*, 3944-3947.

(70) Newman, J. D. S.; MacCrehan, W. A. *Langmuir* **2009**, *25*, 8993-8998.

(71) Biggs, S.; Mulvaney, P.; Zukoski, C. F.; Grieser, F. *J. Am. Chem. Soc.* **1994**, *116*, 9150-9157.

(72) Park, J.-W.; Shumaker-Parry, J. S. Conformation of Citrate Molecules Adsorbed on Gold Nanoparticles, *manuscript in preparation.*

(73) Wilcoxon, J. P.; Martin, J. E.; Schaefer, D. W. *Phys. Rev. A* **1989**, *39*, 2675-2688.

(74) Zhang, H.; He, H.-X.; Wang, J.; Liu, Z.-F. *Langmuir* **2000**, *16*, 4554-4557.

(75) Dagastine, R. R.; Grieser, F. *Langmuir* **2004**, *20*, 6742-6747.

(76) Yamamoto, S.; Watarai, H. *Langmuir* **2006**, *22*, 6562-6569.

(77) Redmond, P. L.; Wu, X.; Brus, L. *J. Phys. Chem. C* **2007**, *111*, 8942-8947.

(78) Rosendahl, S. M.; Burgess, I. J. *Electrochim. Acta* **2008**, *53*, 6759-6767.

(79) Arnold, R.; Azzam, W.; Terfort, A.; Wöll, C. *Langmuir* **2002**, *18*, 3980-3992.

(80) Tao, Y.-T.; Hietpas, G. D.; Allara, D. L. *J. Am. Chem. Soc.* **1996**, *118*, 6724-6735.

(81) Sun, L.; Kepley, L. J. Crooks, R. M. *Langmuir* **1992**, *8*, 2101-2103.

(82) Du, X.; Liang, Y. *J. Phys. Chem. B* **2004**, *108*, 5666-5670.

(83) Matsunaga, M.; Aizenberg, M.; Aizenberg, J. *J. Am. Chem. Soc.* **2011**, *133*, 5545-5553.

(84) Burns, F. C.; Swalen, J. D. *J. Phys. Chem.* **1982**, *86*, 5123-5127.

(85) Sastry, M.; Ganguly, P. *J. Phys. Chem. A* **1998**, *102*, 697-702.

(86) Han, S. W.; Joo, S. W.; Ha, T. H.; Kim, Y.; Kim, K. *J. Phys. Chem. B* **2000**, *104*, 11987-11995.

(87) Schulz, K. H.; Cox, D. F. *J. Phys. Chem.* **1992**, *96*, 7394-7398.

(88) Tielens, F.; Humbolt, V.; Pradier, C.-M.; Calatayud, M.; Illas, F. *Langmuir* **2009**, *25*, 9980-9985.

(89) Bain, C. D.; Troughton, E. B.; Tao, Y.-T.; Evall, J.; Whitesides, G. M.; Nuzzo, R. G. *J. Am. Chem. Soc.* **1989**, *111*, 321-335.

(90) Zhang, Z.; Wu, Y. *Langmuir* **2010**, *26*, 9214-9223.

(91) Whittle, T.; Leggett, G. J. *Langmuir* **2009**, *25*, 9182-9188.

(92) Hostetler, M. J.; Strokes, J. J.; Murray, R. W. *Langmuir* **1996**, *12*, 3604-3612.

(93) Bain, C. D.; Evall, J.; Whitesides, G. M. *J. Am. Chem. Soc.* **1989**, *111*, 7155-7164.

(94) Templeton, A. C.; Hostetler, M. J.; Kraft, C. T.; Murray, R. W. *J. Am. Chem. Soc.* **1998**, *120*, 1906-1911.

(95) Kim, K.; Lee, I.; Lee, S. J. *Chem. Phys. Lett.* **2003**, *377*, 201-204.

(96) For hydrogen bonds of nitro groups: (a) Laurence, C.; Graton, J.; Berthelot, M.; Besseau, F.; Le Questel, J.-Y.; Luçon, M.; Quvrard, C.; Planchat, A.; Renault, E. *J. Org. Chem.* **2010**, *75*, 4105-4123. (b) Allen, F. H.; Baalham, C. A.; Lommerse, J. P. M.; Raithby, P. R.; Sparr, E. *Acta Crystallogr., Sect. B: Struct. Sci.* **1997**, *53*, 1017-1024.

(97) Rodrígez-González, B; Mulvaney, P.; Liz-Marzán, L. M. *Z. Phys. Chem.* **2007**, *221*, 415-426.

(98) Shchukarev, A.; Boily, J.-F.; Felmy, A. R. *J. Phys. Chem. C* **2007**, *111*, 18307-18316.

(99) Palleau, E.; Sangeetha, N. M.; Ressier, L. *Nanotechnology* **2011**, *22*, 325603.

(100) Wagener, P.; Schwenke, A.; Barcikowski, S. *Langmuir* **2012**, *28*, 6132-6140.

(101) Baldwin, J. A.; Vlčková, B.; Andrews, M. P.; Butler, I. S. *Langmuir* **1997**, *13*, 3744-3751.

(102) Zhang, H.-L.; Evans, S. D.; Henderson, J. R.; Miles, R. E.; Shen, T. H. *J. Phys. Chem. B* **2003**, *107*, 6087-6095.

(103) Liu, J.; Stratmann, L.; Krakert, S.; Kind, M.; Olbrich, F.; Terfort, A.; Wöll, C. *J. Electron. Spectrosc. Relat. Phenom.* **2009**, *172*, 120-127.

(104) Schreiber, F. *Prog. Surf. Sci.* **2000**, *65*, 151-256.

(105) Wan, L.-J.; Terashima, M.; Noda, H.; Osawa, M. *J. Phys. Chem. B* **2000**, *104*, 3563-3569.

(106) Steiner, T. *Angew. Chem. Int. Ed.* **2002**, *41*, 48-76.

(107) Kassam, A.; Bremner, G.; Clark, B.; Ulibarri, G.; Lennox, R. B. *J. Am. Chem. Soc.* **2006**, *128*, 3476-3477.

(108) Mendes, P. M.; Chen, Y.; Palmer, R. E.; Nikitin, K.; Fitzmaurice, D.; Preece, J. A. *J. Phys. Condens. Matter* **2003**, *15*, S3047-S3063.

(109) Hatchett, D. W.; Stevenson, K. J.; Lacy, W. B.; Harris, J. M.; White, H. S. *J. Am. Chem. Soc.* **1997**, *119*, 6596-6606.

(110) Jin, W.; Dougherty, D. B.; Cullen, W. G.; Robey, S.; Reutt-Robey, J. E. *Langmuir* **2009**, *25*, 9857-9862.

(111) Love, J. C.; Estroff, L. A.; Kriebel, J. K.; Nuzzo, R. G.; Whitesides, G. M. *Chem. Rev.* **2005**, *105*, 1103-1169.

(112) Gyarfas, B. J.; Wiggins, B.; Zosel, M.; Hipps, K. W. *Langmuir* **2005**, *21*, 919-923.

(113) Kang, H.; Lee, H.; Kang, Y.; Hara, M.; Noh, J. *Chem. Commun.* **2008**, 5197-5199.

(114) Stranick, S. J.; Parikh, A. N.; Tao, Y.-T.; Allara, D. L.; Weiss, P. S. *J. Phys. Chem.* **1994**, *98*, 7636-7646.

(115) Gentilini, C.; Franchi, P.; Mileo, E. Polizzi, S.; Lucarini, M.; Pasquato, L. *Angew. Chem. Int. Ed.* **2009**, *48*, 3060-3064.

(116) Hai, N. T. M.; Van der Auweraer, M.; Müllen, K.; De Feyter, S. *J. Phys. Chem. C* **2009**, *113*, 11567-11574.

(117) Yu, M.; Bovet, N.; Satterley, C. J.; Bengió, S.; Lovelock, K. R. J.; Milligan, P. K.; Jones, R. G.; Woodruff, D. P.; Dhanak, V. *Phys. Rev. Lett.* **2006**, *97*, 166102.

(118) Maksymovych, P.; Sorescu, D. C.; Yates, J. T., Jr. *Phys. Rev. Lett.* **2006**, *97*, 146103.

(119) Kautz, N. A.; Kandel, S. A. *J. Am. Chem. Soc.* **2008**, *130*, 6908-6909.

(120) Techance, S. D.; Gamble, L. J.; Castner, D. G. *J. Phys. Chem. C* **2011**, *115*, 9432-9441.

(121) Ernstsson, M.; Claesson, P. M.; Shao, S. Y. *Surf. Interface Anal.* **1999**, *27*, 915-929.

(122) Fulghum, J. E.; Linton, R. W. *Surf. Interface Anal.* **1988**, *13*, 186-192.

(123) Xia, X.; Yang, M.; Wang, Y.; Zheng, Y.; Li, Q.; Chen, J.; Xia, Y. *ACS Nano* **2012**, *6*, 512-522.

(124) Bain, C. D.; Whitesides, G. M. *J. Phys. Chem.* **1989**, *93*, 1670-1673.

(125) Laibinis, P. E.; Whitesides, G. M.; Allara, D. L.; Tao, Y.-T.; Parikh, A. N.; Nuzzo, R. G. *J. Am. Chem. Soc.* **1991**, *113*, 7152-7167.

(126) Woehrle, G. H.; Hutchison, J. E. *Inorg. Chem.* **2005**, *44*, 6149-6158.

(127) Jewell, A. D.; Tierney, H. L.; Sykes, E. C. H. *Phys. Rev. B* **2010**, *82*, 205401.

(128) Jewell, A. D.; Sykes, E. C. H.; Kyriakou, G. *ACS Nano* **2012**, *6*, 3545-3552.

(129) Feng, J.; Pandey, R. B.; Berry, R. J.; Farmer, B. L.; Naik, R. R.; Heinz, H. *Soft Matter* **2011**, *7*, 2113-2120.

(130) Black, A. J.; Wooster, T. T.; Geiger, W. E.; Paddon-Row, M. N. J. *Am. Chem. Soc.* **1993**, *115*, 7924-7925.

(131) Garg, N.; Lee, T. R. *Langmuir* **1998**, *14*, 3815-3819.

(132) Shon, Y.-S.; Lee, T. R. *Langmuir* **1999**, *15*, 1136-1140.

(133) Zhao, Y.; Pérez-Segarra, W.; Shi, Q.; Wei, A. *J. Am. Chem. Soc.* **2005**, *127*, 7328-7329.

(134) Mathews, D. M.; Sheets, R. W. *J. Chem. Soc. A*, **1969**, 2203-2206.

(135) Gao, Q.; Hemminger, J. C. *Surf Sci.* **1991**, *248*, 45-56.

(136) Jeffrey, G. A. *An Introduction to Hydrogen Bonding*; Oxford University Press: New York, 1997; p 56.

(137) Cooper, E.; Leggett, G. J. *Langmuir* **1999**, *15*, 1024-1032.

(138) Dubios, L. H.; Nuzzo, R. G. *Annu. Rev. Phys. Chem.* **1992**, *43*, 437-463.

(139) Nuzzo, R. G.; Bubois, L. H.; Allara, D. L. *J. Am. Chem. Soc.* **1990**, *112*, 558-569.

(140) Fritzinger, B.;Capek, R. K.; Lambert, K.; Martins, J. C.; Hens, Z. *J. Am. Chem. Soc.* **2010**, *132*, 10195-10201.

(141) Song, Y.; Murray, R. W. *J. Am. Chem. Soc.* **2002**, *124*, 7096-7102.

(142) Walczak, M. M.; Popenoe, D. D.; Deinhammer, R. S.; Lamp, B. D.; Chung, C.; Porter, M. D. *Langmuir* **1991**, *7*, 2687-2693.

(143) Kim, T.; Lee, K.; Gong, M.-s.; Joo, S. W. *Langmuir* **2005**, *21*, 9524-9528.

(144) Wang, Y.; Weinstock, I. A. *Dalton Trans.* **2010**, *39*, 6143-6152.

(145) Giesbers, M.; Kleijn, J. M.; Stuart, M. A. C. *J. Colloid Interface Sci.* **2002**, *248*, 88-95.

(146) Kakiuchi, T.; Usui, H.; Hobara, D.; Yamamoto, M. *Langmuir* **2002**, *18*, 5231-5238.

(147) Hostetler, M. J.; Templeton, A. C.; Murray, R. W. *Langmuir* **1999**, *15*, 3782-3789.

(148) (a) Song, Y.; Huang, T.; Murray, R. W. *J. Am. Chem. Soc.* **2003**, *125*, 11694-11701. (b) Donkers, R. L.; Song, Y.; Murray, R. W. *Langmuir* **2004**, *20*, 4703-4707.

(149) Caragheorgheopol, A.; Chechik, V. *Phys. Chem. Chem. Phys.* **2008**, *10*, 5029-5041.

(150) Paulini, R.; Frankamp, B. L.; Rotello, V. M. *Langmuir* **2002**, *18*, 2368-2373.

(151) Kwon, Y.; Mrksich, M. *J. Am. Chem. Soc.* **2002**, *124*, 806-812.

(152) Gautier-Luneau, I.; Merle, C.; Phanon, D.; Lebrun, C.; Biaso, F.; Serratrice, G.; Pierre, J.-L. *Chem. Eur. J.* **2005**, *11*, 2207-2219.

(153) Faller, B.; Nick, H. *J. Am. Chem. Soc.* **1994**, *116*, 3860-3865.

(154) Ito, H.; Fujii, M.; Masago, Y.; Yoshimura, C.; Waite, T. D.; Omura, T. *J. Phys. Chem. A* **2011**, *115*, 5371-5379.

(155) Vericat, C.; Vela, M. E.; Benitez, G.; Carro, P.; Salvarezza, R. C. *Chem. Soc. Rev.* **2010**, *39*, 1805-1834.

(156) Tielens, F.; Costa, D.; Humblot, V.; Pradier, C.-M. *J. Phys. Chem. C* **2008**, *112*, 182-190.

CHAPTER 4

DIRECTING RAMAN PROBE MOLECULES INTO JUNCTIONS OF GOLD NANOPARTICLE DIMERS BY ASYMMETRIC FUNCTIONALIZATION

4.1 Introduction

Assemblies of noble metal nanoparticles (NPs) give rise to localized electromagnetic (EM) field enhancements in NP junctions by coupling of localized surface plasmons (LSPs). This EM field enhanced region is often called a *hot spot*.[1,2] While the types, shapes, and sizes of metal NPs mainly govern the optical properties of NP assemblies,[3] the local optical behavior can be tuned by controlling interparticle spacing at a molecular level (< 2 nm) with use of the ligands.[4,5] This is an advantage over control of spacing in NP arrays or pairs fabricated by lithographic techniques including nanosphere and electron-beam lithographies, for which routine production of a sub-10-nm gap is challenging.[6] In general, there are two ways to produce NP assemblies, through either electrostatic- or molecular linker-based approaches.[7] The former relies on controlling the kinetics of NP aggregation whereas the latter utilizes linker molecules such as DNA and organic molecules.

Due to the strong electric field enhancement at hot spots, NP assemblies including dimers, trimers, and 1-D chains have been utilized as plasmonic nanomaterials[8,9] especially for surface-enhanced Raman scattering (SERS) applications.[10] Many SERS studies have been based on random NP aggregates which often result in irreproducible

SERS responses from the uncontrollable distribution[11] and/or the minute population[12] of hot spots, which hamper systematic studies. In this regard, gold and silver NP dimers have been investigated as SERS platforms, due to the generation of enhanced SERS signals from molecules located in the junction hot spot.[12-18] A challenge of using NP assemblies in SERS studies is the rational attachment of Raman probe molecules at hot spot interfaces which are well-defined in terms of the location and surface coverage of Raman probes as well as the gap spacing. Probe placement is especially important because of the strong influence of the local fields on SERS enhancements. Since there is a large field gradient around a hot spot, the magnitude of the EM fields change from the edges to the center positions within the NP junctions.[19] As a result, Raman molecules may not be enhanced equally around the NP surface,[15] and the distribution of the EM fields must be correlated with the location of Raman probes. Therefore, it is important to place Raman probes precisely in a well-defined position even in a single assembly[11] for fundamental aspects and quantitative analyses in SERS studies including single molecule SERS (SM-SERS).[20]

In addition to controlling the location of Raman probes in NP assemblies, the surface coverage of the probes also should be considered carefully. For most of the NP assembly-based SERS studies, Raman probe molecules are assumed to form a monolayer on individual NP surfaces,[15] and then the NPs are assembled through kinetically controlled aggregation. However, the uniform monolayer coverage for each nanoparticle is an assumption, and this is prone to errors in determining SERS enhancements. Moreover, the composition of the surface organic layer (single layer, multilayer, low surface coverage, etc.) is directly related to the estimate of interparticle spacing that is a very sensitive factor in the EM field enhancement. Recently, a centrifugation method was used

to prepare dimers and other assemblies, and then the NP assemblies were encapsulated with dielectric materials including silica[13,14,21,22] or polymers[15] in order to stabilize assembly morphologies. In this method, however, the interparticle spacing was determined based on the assumption of the monolayer coverage of Raman probes on NP surfaces,[15] but high resolution transmission electron microscope (TEM) measurements indicated nonuniform interparticle spacing with variations up to ~1 nm.[13] This may suggest the multilayer formation of Raman probes. Xia and coworkers have obtained SERS exclusively from hot spots of silver nanocube dimers,[11] but the correlation between the SERS from the hot spots and the interfacial structure with well-defined gap spacing and estimated number of the Raman probe molecules has not been investigated. Without detailed characterization of the organic layers present on the NP assemblies, quantitative determination of SERS signal enhancements is challenging.

In order to control experiments for the SERS enhancement at the NP hot spot it is desirable to utilize asymmetrically functionalized metal NPs providing formation of well-defined assembly junctions. Previously, it was demonstrated that the asymmetric AuNPs acted as building blocks for NP assemblies including dimers[23] and 1-D chains.[24] This approach allows for controlled functionalization in a spatially-localized region of individual NPs. The asymmetrically-functionalized NPs are assembled in solution through covalent bond formation[25] or attractive interactions between spatially localized ligands present on different particles. During the NP assembly process, target molecules are exclusively adsorbed in this NP region where field enhancements are expected leading to SERS from hot spots generated by the junction formation. Direct correlation between single particle morphologies and SERS responses has been made primarily using single particle measurements,[11-14,17,18,26] but ensemble measurement approaches can also

be used to investigate the assembly-SERS relationship,[15,16,27] when a controlled assembly process is used. This asymmetric functionalization approach offers structural reproducibility of NP dimers producing well-defined and controlled hot-spot junctions, which can be used as a robust SERS-active nanostructure for SERS studies.[28]

Herein, a SERS study of AuNP dimers with Raman probes precisely placed in the hot spots using the asymmetric functionalization approach is presented. A linear relationship between SERS intensities and dimer formation yields was observed, which experimentally demonstrate the role of hot spots in generating SERS. In this study, scanning electron microscope (SEM) analysis indicates the formations of AuNP dimers are more than about 70% among NP assemblies on glass substrates where the SERS responses are measured at the same substrates. While the averages of dimer formations and SERS intensities follow a linear relationship, the extent of the standard deviation of the dimer yield and SERS intensities also exhibit a dependency of the dimer population at the given analytical areas for SEM and SERS measurements. It is demonstrated the ensemble Raman measurements reflect the hot-spot-generating SERS from AuNP dimers.

4.2 Experiments

4.2.1 Materials

All chemicals were used without further purification. Gold chloride trihydrate ($HAuCl_4 \cdot 3H_2O$, ACS grade), sodium citrate tribasic dihydrate ($Na_3C_6H_5O_7 \cdot 2H_2O$, 99%), 11-mercapto-1-undecanol ($HSCH_2(CH_2)_9CH_2OH$, $C_{11}OH$, 97%), 6-mercapto-1-hexanol ($HSCH_2(CH_2)_4CH_2OH$, 97%), and 3-aminopropyltriethoxysilane (99%) were purchased from Sigma Aldrich. 4-nitrobenzenethiol (SH-Ph-NO_2, NBT, 99%), 11-amino-1-undecanethiol hydrochloride ($HSCH_2(CH_2)_9CH_2NH_2 \cdot HCl$, 99%), 16-hydroxy-1-

hexadecanethiol ($HSCH_2(CH_2)_{14}CH_2OH$, 99%) were purchased from Asemblon (Redmond, WA). Ethanol (200 Proof) was obtained from Decon Labs (King of Prussia, PA). Microscope cover glass (22 mm × 22 mm, 1.5 mm thick) was obtained from Fisher or VWR. Water was used after purification (Barnstead Nanopure Diamond UV-UF, 17.8 MΩ/cm). All glassware was cleaned using aqua-regia (3:1, HCl/HNO_3), rinsed thoroughly with nanopure water, and then dried at 120 ºC in an oven for at least 2 h. *Caution! The aqua-regia solution is highly corrosive and mixing the solution is very exothermic. It should be handled with extreme care and appropriate safety precautions.*

4.2.2 Synthesis of asymmetrically functionalized gold nanoparticles

Citrate-stabilized gold nanoparticles were synthesized using Frens' method[29] by combining gold chloride trihydrate (0.02282g), sodium citrate tribasic dihydrate (0.02235g), and 200 mL of nanopure water. The size of AuNPs is 39 nm (± 25%) in diameter, and the typical absorbance is 1.33 at λ_{max} = 534 nm. The solution of the resulting 39-nm AuNPs was added to a jar containing an aminosilane-functionalized cover glass that was prepared using published methods,[23,30] and then the jar was kept at room temperature for 1 d. The AuNPs were coated on both sides of the cover glass. The cover glass with immobilized AuNPs was rinsed by pouring copious amount of nanopure water directly into the glass. Once the excess AuNPs were removed, ethanol was gradually added to the water-containing jar to minimize the effect of heat on the immobilized AuNPs during solvent mixing. The resultant cover glass with the immobilized citrate-stabilized AuNPs is stable in ethanol without NP aggregation or detachment. For typical asymmetric functionalization, one cover glass was immersed and kept in 1 mM ethanolic solution of 11-amino-1-undecanethiol for 2 h. The partially

functionalized AuNPs were released from the cover glass by sonication in 5 mL ethanol and the region of the surface previously in contact with the substrate was functionalized by immersion in 50 μL of 2 mM 11-mercapto-1-undecanol solution (equivalent to maximum 30 ML (monolayer) coverage on the spatially localized surface area) and various amounts (50 μL, 100 μL, 200 μL, 400 μL) of 1 mM 4-nitrobenzenethiol (NBT) solution (15 to 120 ML coverage on the spatially localized surface area, respectively). One ML coverage is defined as the surface coverage of molecules adsorbed on a gold surface (see ref. 50). Five mL of 1 mM NBT solution were used to prepare aggregated NPs. The resultant AuNP solution was left at room temperature for 2 h.

4.2.3 Determination of the AuNP surface area and the number of AuNPs immobilized on the cover glass

An average surface area of 4800 nm^2 for the AuNPs was estimated based on a sphere with diameter of 39 nm. It is assumed that 10% of the total surface was in contact with the silane layer (the spatially localized surface area, 480 nm^2), which was used to estimate area of coverage of the secondary thiols used to functionalize this region. The number of AuNPs released from both sides of one cover glass (22 mm × 22 mm) was determined by measuring the AuNP absorbance using UV-Visible spectroscopy and using the published extinction value for 31-nm AuNPs.[31,32] The typical absorbance was 0.2 for 5 mL of the AuNP solution. Using the extinction coefficient of 31-nm AuNPs ($\varepsilon = 4.7 \times 10^9\ M^{-1}cm^{-1}$ at 524 nm)[32] and Beer's law, the number of AuNPs per cover glass was estimated as 1.2×10^{12}. As additional check on this approximation, the number density of AuNPs on the cover glass surface was estimated by counting the immobilized AuNPs from SEM images. The surface density of 31-nm AuNPs on the silanized cover

glass was 9 NPs/(100 nm × 100 nm). Using this density, the number of particles expected to be in solution after being released from the cover glass was 8.7×10^{11}. The number of AuNPs obtained by UV-visible measurement and SEM image analysis are in good agreement (~1×10^{12} AuNPs). Similarly, the number of 39-nm AuNPs per cover glass is expected to be ~1×10^{12}, which was used in determining the amounts of secondary thiols for the asymmetric functionalization process.

4.2.4 UV-Vis absorption spectroscopy

Absorbance spectra of AuNP solutions were collected at 400 - 800 nm using a PerkinElmer Lambda 19 UV/vis/NIR spectrophotometer.

4.2.5 Attenuated total internal reflectance (ATR) FTIR spectroscopy

A PerkinElmer Spectrum 100 FT-IR spectrometer equipped with a MIRacle ATR (ZnSe crystal, PIKE Technologies) accessory was used. A concentrated AuNP solution prepared by centrifugation was drop cast on the crystal and dried with nitrogen gas. Spectra were collected at 4000 – 550 cm^{-1} with a resolution of 4 cm^{-1}. The spectra were background-corrected, and then normalized based on the peak at 2917 cm^{-1}. Peak deconvolution of symmetric NO_2 stretching vibrations of NBT was performed with a Gaussian function using OriginPro 8 (OriginLab Corp).

4.2.6 Sample preparation for SEM and SERS studies

Spin coating was used to obtain a homogenous distribution of AuNPs over the surface of the cover glass substrates. In this process, 1 mL of the AuNP solution was drop cast on the cover glass and rotated at 3000 rpm. For each AuNP-coated cover glass sample,

SERS measurements were made and the particles were analyzed using SEM. For normal Raman measurements of NBT without AuNPs, aqueous NBT solution was placed on a glass cover slip and was allowed to dry. The actual weight of NBT on the substrate was obtained by subtracting the weight of the cover glass itself from that of the glass substrate with NBT. A spot of dried NBT was 7.5 mm in diameter and the actual weight of the dried NBT was 0.04 (± 50%) mg.

4.2.7 Scanning electron microscopy (SEM)

A field emission scanning electron microscope (NanoNova 630, FEI) was used to analyze and count the number of AuNP assemblies. Ten SEM images of areas of 3.75 μm × 3.75 μm were obtained from each substrate. The numbers of total individual AuNPs in the determination of dimer formation yields are 437, 587, 618, and 950 for the substrates of 15, 30, 60, and 120 ML NBT coverage, respectively, and the standard deviations from the samples were normalized based on 600 NPs.[33]

4.2.8 Raman scattering spectroscopy

For collecting Raman scattering spectra, a DXR Raman microscope (ThermoFisher Scientific, Madison, WI) equipped with a 633-nm laser and a 10× objective (NA 0.25) was used. The laser power was 5 mW. Spectra were collected at 3200 – 100 cm^{-1} with a resolution of 5.3 - 8.8 cm^{-1}. A broad peak over 3000 cm^{-1} originates from substrate fluorescence with inconsistent intensity. Each spectrum was obtained by 5 scans with a 2-s exposure per scan. The estimated lateral beam size is ~6 μm in diameter which is close to the expected value based on company reported specifications (7 μm) with the given

laser wavelength and the numerical aperture of the objective.[i] For SERS measurements, a map with an area of 2000 μm × 2000 μm consists of 16 spectra, obtained periodically with a regular interval. The numbers of maps are 3 for 15 ML, 7 for 30 ML, 5 for 60 ML, and 4 for 120 ML samples. SERS intensities are determined for the symmetric stretching of the nitro group ($\nu_{sym}NO_2$) at 1336 cm^{-1}. Spectra without the NO_2 stretching intensity were not included in SERS analysis. For normal Raman measurements of dried NBT on glass substrate, 10 maps with 16 spectra were obtained.

4.2.9 Transmission electron microscopy (TEM)

Interparticle spacing of AuNP dimers was determined from images generated by TEM (Tecnai T-12, FEI) at 120 KV accelerating voltage. One drop of AuNP solution was placed on a 150-mesh Formvar-coated copper grid (Ted Pella, Inc) and left to dry. The gap distance was analyzed by measuring interparticle distances at the minimum point of separation for 79 AuNP dimers in the TEM images using Scion Image Beta 4.02 software.

4.3 Results and discussion

4.3.1 Formation of AuNP dimers by asymmetric functionalization

AuNPs (~40 nm in diameter) were prepared, and 4-nitrobenzenethiol (NBT) along with HS-C_{11}-OH were incorporated in a spatially localized patch on the surface of the particles using the asymmetric functionalization process developed by Shumaker-Parry

[i]The measured 532-nm laser spot size was compared with a 50× objective (NA 0.75) to the theoretical value in order to find a conversion factor for the DXR Raman microscope (Zhu, L.; Cai, T.; Huang, J.; Stringfellow, T. C.; Wall, M.; Yu, L. *J. Phys. Chem. B* **2011**, *115*, 5849-5855).
The measured lateral resolution: 0.84 μm.
Theoretical spatial resolution (Rayleigh formula): 0.61λ/NA = (0.61 × 532 nm)/0.75 = 0.43 μm.
Laser spot diameter: 2 × (Spatial resolution)
The estimated resolution of the 633-nm laser spot size with a 10× objective (NA 0.25) = (0.61 × 633 nm)/0.25 = 1.54 μm, so the estimated spot size is 2 × 1.54 μm × 0.84μm/0.43μm = 6.0 μm.

and co-workers (Figure 4.1; see also Figure 1.4 in Chapter 1).[23] The NBT serves as a Raman probe and the HS-C_{11}-OH induces dimer formation between AuNPs through hydrogen bonding between HS-C_{11}-OH molecules spatially localized on two different particles. Thus, the NBT, also present in the spatially localized patch, then becomes directed to the AuNP gap upon dimer formation. A surface templating process is used to achieve the spatial localization of the ligands on the asymmetrically functionalized AuNPs. Briefly, a silane-functionalized glass substrate masks the surface of immobilized citrate-stabilized AuNPs, making contact with the silane layer by electrostatic interactions. During initial thiol treatment, the ligands adsorb on the nanoparticle, except on the region of the nanoparticle in contact with the substrate. This relatively small surface region of the AuNP, which the small surface regions are called *reactive surfaces*, becomes a reactive site for AuNP dimer formation after the second thiol functionalization, and the functional groups of the second thiols are responsible for assembling the asymmetric NPs through covalent bond formation[23-25] or noncovalent interactions.

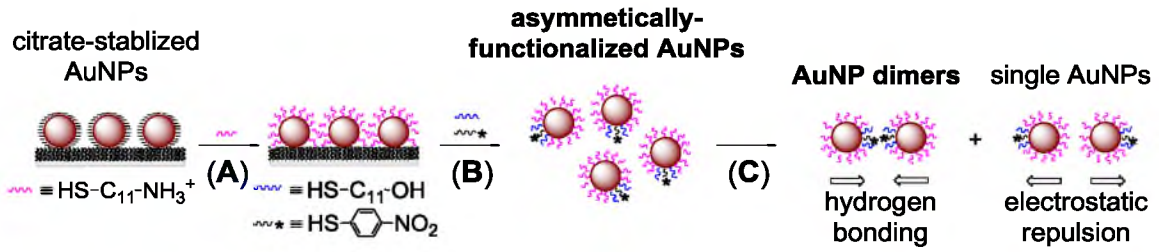

Figure 4.1. Steps to form AuNP dimers with Raman probe molecules directed to the AuNP assembly gap or hot spots. The process is based on producing asymmetrically functionalized AuNPs prepared using a silanized glass substrate to mask a region of the AuNP surface (Step A). Raman probes (HS-Ph-NO_2) are incorporated in that masked region along with dimer-inducing molecules (Step B). For this study, the asymmetrically functionalized AuNPs are induced to form AuNP dimers by hydrogen bond formation between hydroxyl-terminated linkers (Step C). Positively-charged surface layers (pink ligands) prevent randomly oriented dimer formation.

Sonication of the glass substrate covered with the adsorbed NPs releases the particles into solution so that the reactive surface can be functionalized further with various types of thiol molecules. In the modified method in this study, positively-charged HS-C_{11}-NH_3^+ was used to functionalize the bulk of the AuNP surface area (i.e., first functionalization) because it was observed to promote AuNP stability in ethanol solution prior to the second functionalization stabilizing the particles against random aggregation, probably due to electrostatic repulsion of the positively-charged organic layer. The large surface portions are called *stabilizing surfaces*.

In the second functionalization, NBT was added as a Raman probe molecule combined with the molecular linker HS-C_{11}-OH that is known to induce AuNP assembly. The hydroxyl group interaction occurs during the drying process,[34] because the interaction between hydroxyl-terminated layers in ethanol solution is very weak.[35] In this case, however, some dimers were formed in solution, evidenced by the broader peak feature of UV-visble absorption spectra in solution (see the Appendix). A detailed investigation of the specific steps of dimer formation is outside the scope of this study, but the role of the linker in dimer formation is shown through experimental evidence. Using the asymmetrically-functionalized AuNPs, the positively-charged stabilizing surfaces likely prohibit the formation of randomly oriented dimer with stabilizing surfaces meeting to form a gap due to electrostatic repulsion. Instead, the dimer formation is directed by the presence of the patches where two particles can approach more easily through hydrogen bonds of the linkers. Gold particle assemblies through hydrogen bonds of the hydroxyl-terminated alkanethiols have been demonstrated experimentally.[34]

4.3.2 Correlation between AuNP dimers and SERS intensities

Incorporation of Raman probes in the junctions of the AuNP dimers was investigated by SERS. When Raman probes are placed in the junctions of the AuNP assemblies, a correlation between the morphology of NP assemblies and the intensity of Raman scattering is expected due to uneven local fields on surfaces of NP assemblies, i.e., hot spots in the NP junctions. When adsorption of Raman probes on AuNPs is not related to a specific location and morphology of NP assemblies, however, the Raman scattering is expected to be dependent on the amount of Raman probe. Figure 4.2A presents a summary of the SERS responses from the AuNP assemblies related to the amount of Raman probe NBT used during the asymmetric functionalization process. The NBT amount is presented as monolayer (ML) and refers to the number of NBT molecules in solution with respect to the number of NBT molecules adsorbed in a close-packed monolayer in the template region of the AuNP (approximate 10% of the surface). The intensity of the symmetric NO_2 stretching[36] at 1336 cm^{-1} was used (see the Raman scattering spectrum of AuNP dimers prepared without the second functionalization in the Appendix for verification of the peak assignment), and the intensities are averaged values from multiple measurements on each substrate. Figure 4.2B shows representative SERS spectra. Figure 4.2C and 4.2D present representative SEM images for the substrates of the AuNP dimers and random aggregates, respectively. First of all, the intensity of Raman scattering is not dependent on the amount of Raman probe used. For example, adding more NBT beyond the 30-ML coverage for the reactive surface did not produce higher SERS intensities. As the concentration of NBT increased from 2×10^{-2} mM (30-ML coverage) to 8×10^{-2} mM (120-ML coverage), the intensity of SERS decreased. Moreover, the substrate (31% AuNP dimers) prepared with 30-ML coverage amounts of

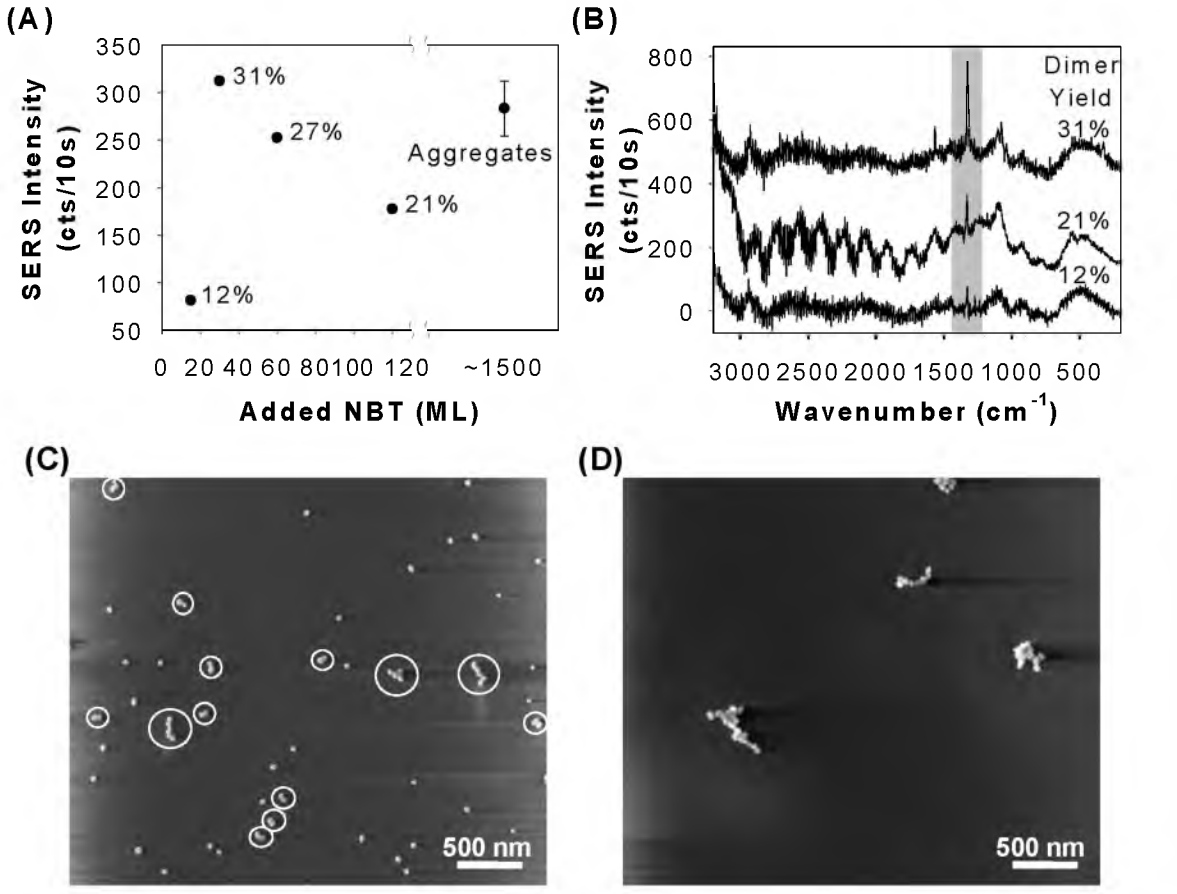

Figure 4.2. Raman spectra and SEM images of AuNPs incorporated with Raman probes. (A) SERS intensities with respect to concentrations of NBT molecules added in solution, converted to the coverage of a close-packed monolayer (ML) on the *reactive surface* of the AuNP. Dimer yields are presented. (B) Representative SERS spectra for different dimer yields. The symmetric NO_2 stretching region (1336 cm^{-1}) used for SERS intensities is highlighted. Representative SEM images for (C) AuNP dimers and (D) aggregates, respectively. The assemblies in the larger circle on (C) are counted as two dimers.

the Raman probes (2×10^{-2} mM) exhibits a slightly larger SERS signal than the substrate (AuNP aggregates) prepared with excess amounts (1 mM, ~1500-ML coverage) of the Raman probes. Additionally, the independence of NBT concentrations indicates a possible contribution from excess NBT is negligible on the intensity of Raman scattering signal. Note that the AuNP samples were prepared on glass substrates by spin-coating, and thus the amount of the excess NBT remained on NP surfaces is very minute.

Consequently, there is no positive correlation between the amount of Raman probe and the intensity of SERS.

Instead, AuNP dimer yields turned out to be correlated with the SERS intensities. As the AuNP dimer yields increased, the SERS intensities also increased (Figure 4.2A). The yield of AuNP dimers directly reflects the population of the hot spots of the AuNP dimers. This morphology-dependent SERS demonstrates that a high SERS enhancement is achieved when Raman probes are placed in the hot spot regions of the AuNP dimers. With using the limited amount of Raman probe (30-ML coverage) the asymmetric functionalization approach led to a specific placement of the Raman probes in the junction of the AuNP dimers. Under similar numbers of AuNPs involved in the SERS measurement, the AuNP dimers provide for the hot spot regions efficiently compared to the NP aggregates possessing randomly-distributed hot spots (see a representative SERS spectrum of NP aggregates in the Appendix). For the substrates prepared using the limited amounts of NBT (15 - 120 ML coverage), the dimer is the most populated among assemblies (see the distribution of dominant type of AuNP assemblies for each substrate in the Appendix) while the population of single NPs is still dominant (Figure 4.2C). Single and assembled NPs are very minor members of the particle population for the randomly aggregated NP sample (Figure 4.2D). When the dimer yields were obtained, AuNP trimers were considered as one monomer and one dimer and AuNP tetramers were counted as two dimers. High-order assemblies beyond tetramers were scarcely observed (the number of population is less than 8% among assembled NPs), and thus not included in determination of the dimer yield. It is well-known that SERS from the hot spots of NP assemblies is enhanced by a factor of up to ~10^8, compared to the normal Raman scattering without metal nanostructures. Thus, it is reasonable not to observe SERS on

single AuNPs under common experimental conditions due to the intrinsically little amount of Raman probe molecules on NP surfaces and the lack of enhanced electric field.[13,17] The AuNP dimers provide for the hot spot regions for SERS whereas single AuNPs do not exhibit enhanced electric field resulting in no detectable Raman response. Detection of Raman signals from AuNP dimers is evidence of placement of Raman probes in the junctions. Overall, it was demonstrated that the high SERS enhancements were achieved by the efficient placement of the Raman probes at the junctions of AuNP dimers.

4.3.3 Linear relationship between AuNP formation and SERS enhancement

Interestingly, a linear relationship between the SERS intensities and the dimer yields was observed within a range of 12 – 31 % dimer yield as shown in Figure 4.3A. This relationship can be explained by the population of AuNP dimers directly correlating with

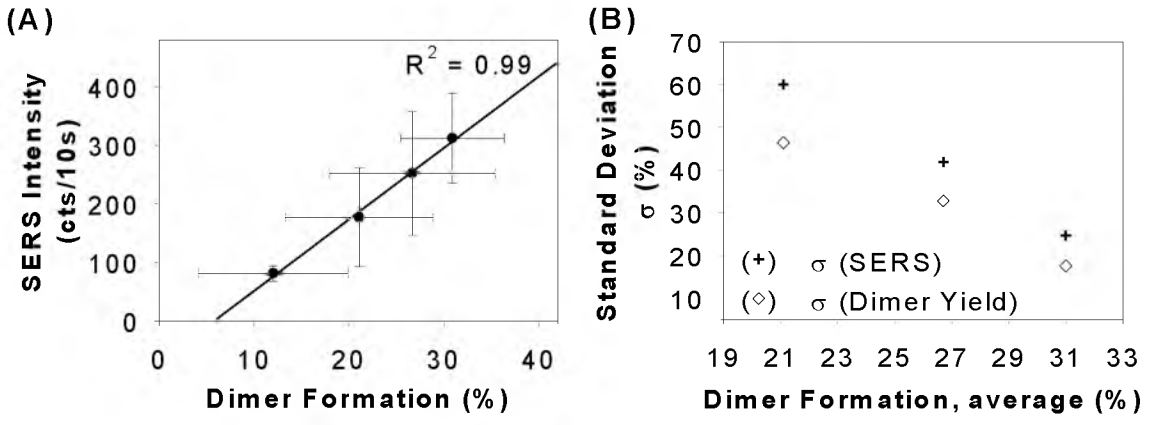

Figure 4.3. Relationship of SERS intensities as well as standard deviations of SEM and Raman scattering measurements with respect to averaged yields of dimer formation. (A) A linear relationship between averaged dimer formation and SERS intensities. Error bars represent the standard deviation of the measurements. (B) Correlation in error of SERS and dimer yield measurements with the dimer formation.

hot spot population leading to the measured SERS intensities. In addition, this provides evidence that the signal from NBT comes predominantly from the hot spots due of AuNP dimers to the strong dependence of the SERS intensity on the hot spot population. The AuNP dimers provide for the hot spot regions where the Raman signals of the probe molecules are linearly enhanced depending on the hot spot populations. The asymmetrically functionalized AuNPs were designed to place the Raman probes only at the junctions of the dimers, which was also supported by the SERS from the hot spots. In this study, the SERS intensities were ensemble-averaged from dimers, but the average SERS intensities given the dimer yields can still represent the optical property of dimers since the dimer is the dominant species to provide for hot spots. For direct correlation of the NP morphology and SERS enhancement, single particle SERS measurements can be made, but an ensemble-averaged SERS approach has been applied for dominantly populated single assemblies.[15,16,27] It was demonstrated AuNP dimers are dominant in generating SERS in this study. Moreover, the standard deviations of the SERS on each substrate are highly correlated with those of the dimer yields (Figure 4.3B). The relative standard deviations (%) are weighted values after correction based on the number of NPs. Note that the standard deviation of the 12% dimer was omitted due to the unexpectedly narrow standard deviation (16%) from four SERS spectra. Most SERS intensities from the low population of dimers were believed to disappear in the baseline with left behind a certain range of SERS intensity (70 - 100 cts/10s), which resulted in the very narrow standard deviation. In general, a standard deviation is inversely proportional to the square root of the target population. As the yield of dimers increases, the standard deviation is expected to decrease, which is consistent with the result (Figure 4.3B; see the correlation between standard deviations of SERS intensities and dimer yields as a function of a

square-root of the number of dimer yields in the Appendix). The distribution of the SERS responses is directly correlated with that of the absolute number of dimers. Therefore, this correlation demonstrates that the SERS intensities are exclusively generated from AuNP dimers.

One observation is that the fitted line in Figure 4.3A does not cross through the origin. The SERS intensity becomes null when the dimer formation is 5.8%, and the SERS intensity is minus value at 0% dimer formation (-70 cts/10s). After subtracting 5.8% from each dimer yield, the standard deviation and the square root of the dimer yield exhibit a linear relationship as predicted (see the correlation between standard deviations of SERS intensities and dimer yields after 5.8-% correction in the Appendix). This, the offset of 5.8% was considered as significant, leading to explain possible causes of deviations from an ideal plot based on the 5.8% error even though it is possible to alternatively fit the points in Figure 4.3A with including the origin as an expected point. This offset was accounted for based on three reasons. One is that a possible adsorbate orientation-dependent SERS response. It is known that the SERS signal is more enhanced when the adsorbed molecule is closer to metal surfaces.[37, 38] The possible change of NBT orientation was observed as the change of NBT amounts, probably due to physi- or chemisorbed states. Raman scattering spectra exhibit change of the peak shape of the symmetric NO_2 stretching ($\nu_{sym}NO_2$), which may be related to NBT orientation. As the amount of added NBT increases from 15-ML to 120-ML coverage, the peaks at 1335 cm^{-1} are attenuated and the peak at 1328 cm^{-1} shifts to a higher wavenumber at 1330 cm^{-1}. In addition, IR data also show the similar spectral feature of the $\nu_{sym}NO_2$ as the amount of NBT increases (see normalized spectra in the regions of the symmetric -NO_2 stretching vibration at different NBT coverages in the Appendix). The $\nu_{sym}NO_2$ band shifted from

1329 to 1340 cm^{-1} as the added amount of NBT increased from 15-ML to 120-ML coverage. This probably arises from a change in configuration of the NBT from tilting to perpendicular lying down to a more upright configuration.[39] The other reason is the error in counting the number of dimers. Definitely, the SERS enhancements in higher-order assemblies such as trimers and tetramers are not the sum from single NPs and dimers.[15] If the second reason was dominant, the stronger SERS from dimers than higher-order assemblies would be suggested,[40,41] due to negative value of the SERS intensity (-70 cts/10s) at 0% dimer yield. The last reason is the systematic error caused when determining the signal intensities. The noise level of spectra is similar to the figure (-70 cts/10s).

4.3.4 Exclusive contribution from hot spots to SERS enhancement

To correlate the SERS with assembly type was attempted by comparing ratios from two most populated assemblies, i.e., dimer and trimer (see the Appendix) as well as with amount of NBT (Figure 4.4; see Section 4.5.1 and 4.5.2 in the Appendix for calculation). In this analysis, the yield of dimer formation was converted to a weighted hot-spot population, which contributions of the SERS intensity from each hot spot of dimers and trimers were applied, based on a reported value in literature. Chen and co-workers found that the SERS intensity of each trimeric hot spot is three times as strong as each dimeric population and the averaged SERS intensity. Note that the largest population among hot spot for Au@Ag core-shell NPs,[15] and this intensity ratio (I_{dimer}/I_{trimer} = 1/3) was used in this study. Figure 4.4A presents the plot of a linear trend between this weighted hot-spot AuNP assemblies is the dimer (> 70% among dimers, trimers and tetramers; see the Appendix). The estimated NBT ratio on the reactive surface was directly determined

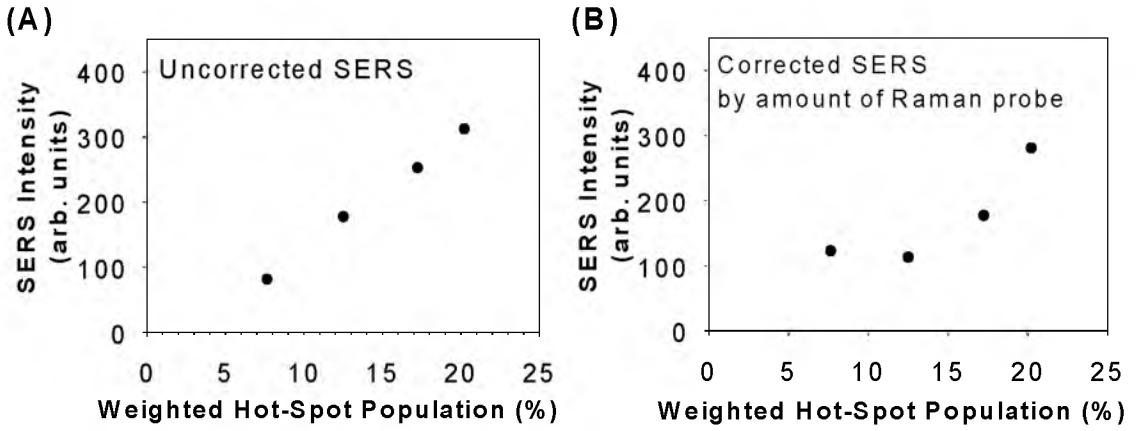

Figure 4.4. Relationship between populations of dimeric and trimeric hot-spots and SERS intensities. (A) The plot exhibits linearity before SERS intensities are corrected by estimated coverages of Raman probe at hot spots. (B) The plot is deviated from linearity when the surface coverages of Raman probe are corrected.

from the mole ratio of NBT and the linker added in solution, which are 0.33, 0.50, 0.67, and 0.80 for 15 - 120 ML, respectively (Figure 4.2A). These estimated amounts of Raman probe were used to correct SERS intensities. Trimers were considered to consist of three asymmetric NPs, and thus the number of Raman probe at a trimer was assumed to be 50-% more than that of a dimer consisting of two asymmetric NPs. With correcting the SERS intensity based on the resultant amount of Raman probe at hot spots, the plot shows a significant deviation from linearity (Figure 4.4B). The solution concentration of the Raman probe may not reflect that on NP surfaces. In addition, possible orientational change of the adsorbed NBT may affect the SERS intensity, and the intensity of the hot spot might be able to be correlated with a position of the adsorbed molecule inside the hot spot.

4.3.5 Analysis of standard deviations between SERS and dimer formation for origin of SERS enhancement

The discrepancy of the standard deviations between the SERS and the dimer formation was accounted for with different analytical areas on the SEM image and the SERS laser spot size. The analytical area for each SEM image is 14.1 μm^2 (= 3.75 μm × 3.75 μm), which is smaller than that of the focused laser spot (6.0 μm in diameter, area = 28.3 μm^2) on the substrates. The laser spot size was obtained specifically for the Raman instrument used in this study,[42] with the 633-nm laser and the 10× objective (N.A. 0.25) (see Experiments). The analytical area (A) can be directly proportional to the number (N) of dimers on the substrates. When the laser spot size was assumed to be 4.24 μm in diameter, the experimental ratio ($\sigma_{SERS}/\sigma_{Dimer\ Formation}$ = 1.0) of the standard deviations between the SERS and the dimer yield, which was obtained after correcting the 5.8%-error in the dimer formations (Figure 4.5; see discussion in Section 4.3.2 for the 5.8%-error), is the same as the calculated value ($\sigma_{SERS}/\sigma_{Dimer\ Formation} = \sqrt{N}_{Dimer\ Formation}/\sqrt{N}_{SERS} = \sqrt{A}_{Dimer\ Formation}/\sqrt{A}_{SERS} = \sqrt{14.1}\ \mu m^2/\sqrt{\pi(4.24/2)^2}\ \mu m^2 = 1.0$). With the focused laser spot of 6.0-μm in diameter, the calculated ratio ($\sigma_{SERS}/\sigma_{Dimer\ Formation} = \sqrt{N}_{Dimer\ Formation}/\sqrt{N}_{SERS} = \sqrt{A}_{Dimer\ Formation}/\sqrt{A}_{SERS} = \sqrt{14.1}\ \mu m^2/\sqrt{28.3}\ \mu m^2 = 0.71$) became 0.71, which is deviated significantly from the experimental ratio (1.0). Since a small area was probed with the smaller spot size (4.2 μm) and so likely contained a small population of dimers given the average surface coverage from SEM analysis, the standard deviation of SERS and the ratio of $\sigma_{SERS}/\sigma_{Dimer\ Formation}$ were increased. Even though the estimated size of the focused laser spot is 6.0 μm, it can be predicted that the *effective* size of the laser beam for SERS excitation is 4.24 μm. As a result, the predicted standard deviation by distribution of dimers demonstrated that the averaged SERS intensities actually represent the hot-spot-

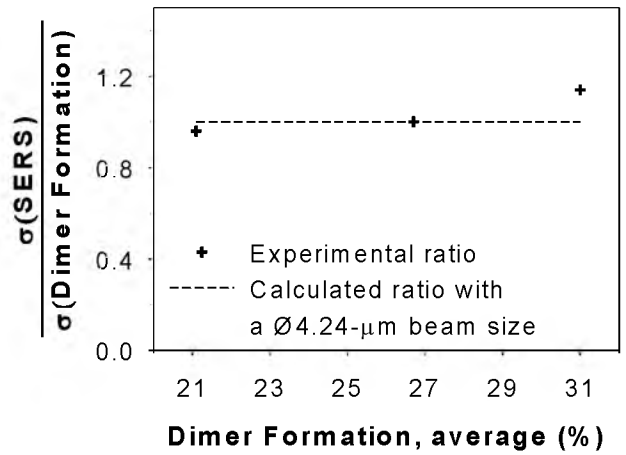

Figure 4.5. Ratio of standard deviations between SERS and SEM measurements. Standard deviations reflect the absolute number of AuNP dimers on SERS intensity measurements and AuNP dimer counts in SEM images. The laser beam size for SERS is smaller than the analytical area of the SEM image in this study, which is consistent with the relatively large standard deviation of SERS measurements. This implies that the discrepancy of standard deviations between SEM and SERS originates from the difference in the number of AuNPs for the two types of measurements. With an effective beam size of 4.24 μm, the ratio obtained from experiments is in good agreement with the predicted value.

generating SERS exclusively from AuNP dimers.

4.3.6 Alignment of asymmetric AuNPs in dimers with respect to location of Raman probe

The effect of the interparticle spacing on SERS was studied by incorporation of hydroxyl-terminated linkers with different chain lengths (Figure 4.6). Even though incorporating OH-terminated alkanethiols of different lengths also effects on the yield of dimer formation, there is a significant discrepancy of SERS intensity depending on lengths in a range of the similar yield, i.e., 8 - 15% (Figure 4.6A). When C_6-OH was used (estimated interparticle spacing: ~2.2 nm), a SERS signal was not observed regardless of the amount of NBT added. On the other hand, when C_{16}-OH was used (estimated

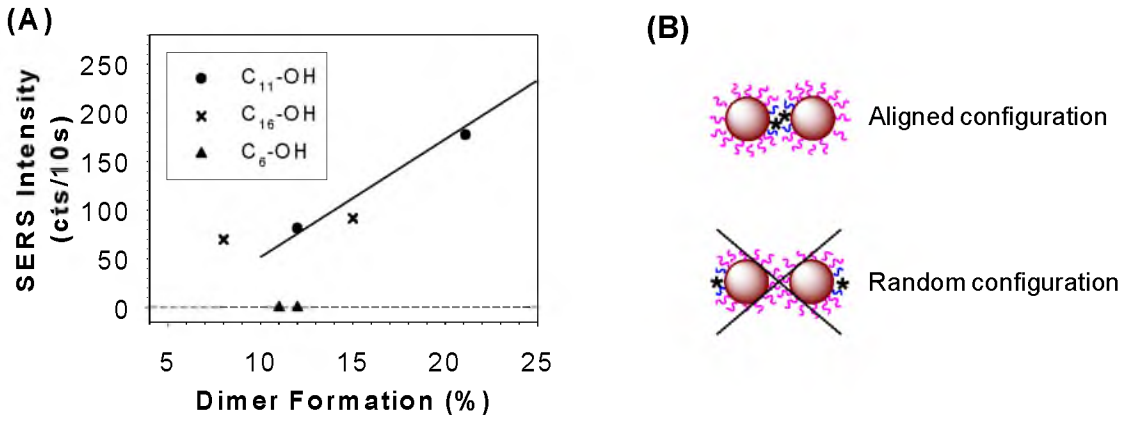

Figure 4.6. Effects of interparticle spacing in AuNP dimers on SERS enhancement, induced by change of linker lengths. (A) Comparison of SERS intensities of AuNP dimers prepared by the OH-terminated alkanethiol linkers with different hydrocarbon lengths. (B) Two representative configurations of asymmetric NPs in dimer formation. One is an aligned configuration with Raman probes (*) located at hot spots, which the linker length-dependent SERS is expected. The other is a random configuration that is independent of the hydrocarbon length of the linker. Only the aligned configuration is consistent with the experimental SERS result from AuNP dimers.

interparticle spacing: ~4.4 nm), the SERS signal was enhanced similarly to the signals generated using C_{11}-OH (see Section 4.3.7 for detailed estimation of the interparticle spacing). This observation can be explained only with an aligned configuration of the asymmetric NPs (Figure 4.6B). The OH-terminated alkanethiols adsorbed the AuNP surface in the vicinity of Raman probe induces the asymmetric NPs to be aligned, having the location of Raman probe be placed at the junction of the resultant dimer. A similar SERS response would be expected irrespective of the lengths of linkers at the given yield of dimer formation if a random configuration is dominant. The dimer formation through the positively-charged stabilizing surface (*stabilizing-to-stabilizing*) unlikely occurs due to electrostatic repulsion, which led to avoidance of SERS-inactive dimers, i.e., no Raman probe in the junction of AuNP dimers. It is well-known that the LSP of AuNP dimers changes dramatically as the particles approach an interparticle spacing of less than

2 nm.[43-45] In contrast to what is expected, the SERS enhancement decreases as the gap spacing decreases from 11-carbon chain length to 6-carbon chain while the SERS intensities from 16-carbon and 11-carbon chains are comparable. However, this trend is against calculated results in the literature where the opposite trend has been reported based on calculations.[13,16] Detailed correlation of the SERS with the gap spacing using calculation is out of scope in this study, but the potential usefulness of the AuNP dimers, fabricated by the asymmetric functionalization method, is emphasized as platforms in hot-spot generating SERS studies. Moreover, the dependency of dimer formation on the linker length supports the aligned configuration of the asymmetric NPs as a dominant species of dimers.

It was further investigated that the aligned configuration of the asymmetric NPs through the linker (configuration IA, Figure 4.7) governs the dimer formation, rather than possibly varied configurations. While the SEM images of AuNP dimers cannot distinguish the orientation of asymmetric NPs, the SERS intensities of AuNP dimers are able to address the configuration of asymmetric NPs with respect to the location of Raman probes in hot spot regions. A maximum SERS signal is expected when Raman probes of both asymmetric NPs are located at the junctions (hot spots) of AuNP dimers. Here, a control experiment was performed in absence of linkers, only using the Raman probes for the second functionalization. Interestingly, under the similar dimer yield ~21%) for both of the samples with/without linkers,[ii] the averaged SERS intensity of the dimer sample prepared with the linker is almost twice as much as the dimer sample prepared without linker. The formed dimers with and without linkers, both possessing

[ii]The percentages of dimers/trimers and ratios of added NBT/linker are 81.5%/11.1% and 4/1 for the sample prepared with linkers and 77.7%/16.0% and 2/0 for the sample prepared without linkers, respectively. The amounts of added NBT are also comparable for both samples.

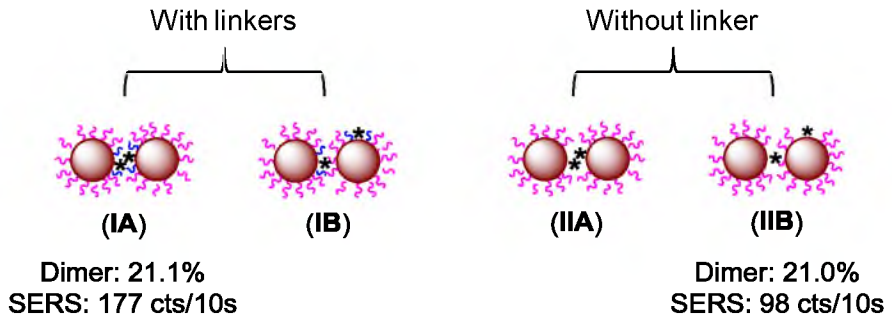

Figure 4.7. Illustration of the linker (HS-C_{11}-OH) role in the orientation of asymmetric NPs in dimers. Configurations (I) represent dimer formations with the linker (blue color) whereas configurations (II) without linker. Configurations (A) indicate aligned asymmetric NPs in dimers with respect to the location of Raman probes (*) whereas configurations (B) randomly-oriented asymmetric NPs. Note that the ratio of the approximate number of the Raman probes in the junctions (IA/IIB = 2/1) is compatible with the ratio of SERS intensities (IA/IIB = 177/98) under the same dimer yield.

21%-dimers, exhibited Raman intensities of 177 cts/10s and 98 cts/10s (see a representative Raman scattering spectrum of randomly oriented AuNP dimers in the Appendix), respectively. Due to the similar populations of hot spots, this difference in SERS intensities can be associated with different amounts of Raman probes at the hot spots.

As is illustrated in Figure 4.7, this led to the speculation that the aligned configuration (IA) is dominant when the linker is used whereas the random configuration (IIB) is dominant when the linker is absent since the amount of the Raman probe at hot spots for the aligned dimers is twice as much as the randomly-oriented dimers. The linker induces the aligned configuration of asymmetric NPs, forming configuration IA rather than configuration IB. Without linkers, however, asymmetric NPs form into configuration IIB possessing about a half amount of Raman probes at the hot spots, compared to configuration IIA. Due to electrostatic repulsion of the stabilizing layer of asymmetric NPs, dimers are formed through either both reactive surfaces (*reactive-to-reactive*,

configuration A) or only one reactive surface (*reactive-to-stabilizing*, configuration B). The former relies on hydrogen bonds of the OH-terminated linkers, and the latter likely utilizes electrostatic attraction between the positively-charged stabilizing layer and the negatively-charged carboxylate groups of remaining citrate on the reactive surface. Note that interparticle spacing for both configurations (IA and IIB) is comparable (two monolayers of C_{11}-OH thiol for IA and a monolayer of C_{11}-NH_3^+ thiol plus Ph-NO_2 thiol or surface remaining citrate for IIB). The importance of AuNP alignment for SERS intensities has been demonstrated in 1-D assemblies.[46] As a result, the correlation between the estimated amount of Raman probes at hot spots and the SERS intensity, depending on the orientation of asymmetric AuNPs, also supports the aligned dimer configuration is dominant with aid of linkers.

4.3.7 Interface of the AuNP-surface/adsorbed-molecule at hot spots

Determination of the interparticle spacing is closely related to the NP surfaces and the functionalization on the reactive surface. TEM analysis was used to estimate the interparticle gap distance, but it provides only lateral images impacting the accuracy of this determination. When a gap interface in NP assemblies is not parallel to the beam direction, the entire interface is not represented by the microscope image. Thus, this limit in TEM image analysis causes deviations in spacing determination and results in two extremes, the large spacing estimates and the appearance of a merged interface.[13] The upper limit of the measured distances probably represents the real interparticle spacing. Due to the inaccuracy of the TEM-based spacing measurement, it is important to establish well-defined interfaces of the assembly junctions, *especially for small gaps between large NPs*.

Most of all, the relatively large AuNPs and silver NPs (AgNPs) (> 10 nm in diameter) are still crystalline particles with faceted surfaces although they have been often assumed to be perfect spheres in theoretical consideration for NP-based studies. The Au or AgNPs likely interact via molecular layers at facets,[14,47] rather than at edges, due to the maximum attractive interaction on the large terrace area. It was assumed that the AuNPs in this study were ideal truncated octahedrons, consisting of eight (111) hexagons and six (100) squares,[14] as were suggested for large AuNPs (> ~20 nm in diameter).[48] The area of one hexagonal facet is 9.7% of the total surface area whereas that of one square facet is 3.7% of the total surface area. For this purposes, it is assumed the hexagon is likely the reactive surface (i.e., the spatially localized region) since the hexagon area is believed to be in contact with the silane layer in the immobilization step of the asymmetric functionalization for maximum electrostatic interaction. This leads to another important assumption in that the asymmetric AuNPs assemble into dimers through interactions between ligands adsorbed to the hexagon faceted areas for similar reasons of maximum hydrogen bond interactions of the hydroxyl linker molecules. Moreover, this assumption is practical because it is very challenging to distinguish the surface coverages of two mixed organic layers on metal NPs[49] within ~6 percent accuracy.

For the 40-nm AuNPs, the area of the reactive surface is ~480 nm^2. Based on these assumptions and the known surface coverages of benzenethiol [50] (4.3×10^{14} benzenethiols/cm^2)[iii] and alkanethiol[51] (4.5×10^{14} alkanethiols/cm^2) on a Au(111) surface, it was possible to add the linker and Raman probes quantitatively into solution, assuming that the ratio between the added amounts of thiols are the same as that adsorbed on Au

[iii]This value was obtained based on the STM analysis. The XPS determined coverage for benzenethiol is larger (6.3×10^{14} thiols/cm^2): Whelan, C. M.; Smyth, M. R.; Barnes, C. J. *Langmuir* **1999**, *15*, 116-126.

surfaces due to the similar binding energy (35 kJ/mol and -33 kJ/mol for octanethiol and NBT, respectively[39]). Although the mole ratio [linker]/([Raman-probe] + [linker]) is varied between 0.2 and 0.7 among AuNP dimer samples, the SERS intensities with estimated amounts of Raman probes could not be correlated for each AuNP dimer sample since the adsorbate coverage also influences the adsorbate geometry and thus SERS. More importantly, the added amount of the linker HS-C_{11}-OH was excess (30-ML coverage amount on the reactive surface), but a monolayer formation of the hydroxyl thiol with Raman probes was expected since a bilayer of the hydroxyl thiols does not form on Au surfaces through the hydroxyl group interaction irrespective of concentration.[52] This experimental design can prevent a multilayer linker formation on the reactive surface. In addition, the linker molecules may prohibit possible changes of the motion and orientation of Raman probes adsorbed together on a surface[53] during laser-mediated SERS measurements.

A ligand shell around each NP component was observed in the TEM image (Figure 4.8A). The contrast of the ligand layer likely results from negatively-charge gold chloride complexes[54,55] that interact with the positively-charged functional group of the amine thiol at the asymmetric functionalization step, and the gold complexes are originally adsorbed on the silane layer electrostatically during the citrate-AuNP immobilization procedure. The shell layer thickness (the distance between the center of the shell layer and the AuNP surface) is 1.9 nm (± 0.4) obtained from the given AuNP dimer, and this is close to the theoretical thickness of the layer[iv] consisting of the amine thiol and gold chloride complex (~2.0 nm). Note that the shell layer is not shown at the junction of the

[iv]ChemBio3D (CambridgeSoft) program was used to obtain the length of molecules. The Au-S bond length is 2.85 Å, and the tilted angle for aryl- and alkanethiols is 30° to normal.

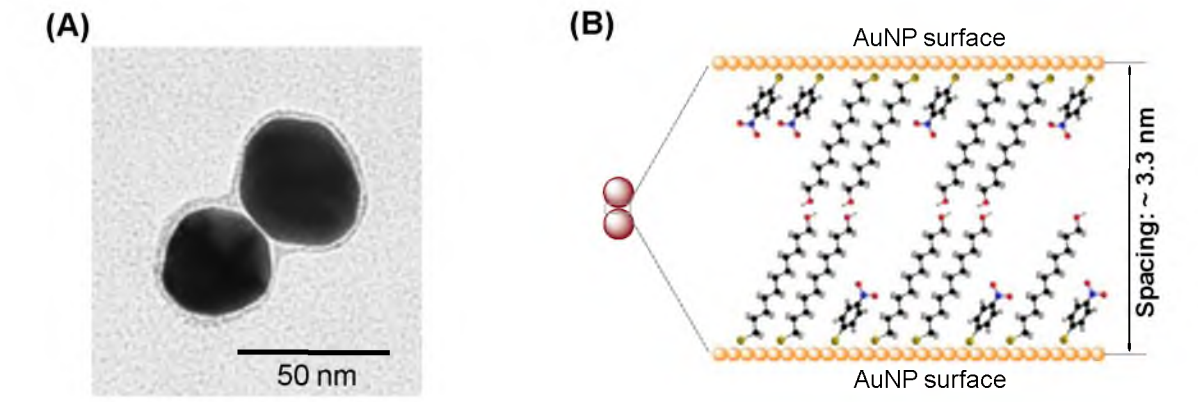

Figure 4.8. Interface of a AuNP dimer. (A) A representative TEM image of AuNP dimers, exhibiting a facet-to-facet junction. (B) Depicted junction of the AuNP dimer showing the Raman probes (HS-Ph-NO_2) and hydrogen-bonded linkers (HS-C_{11}-OH) adsorbed on different NP surfaces, which leads to determination of the junction spacing of ~3.3 nm. The interparticle spacing determined from the TEM analysis (3.0 ± 0.1 nm) is in good agreement with the calculated distance (3.3 nm).

AuNP dimer, which demonstrates the asymmetric AuNPs as the building block of the dimer. Noticeably, the AuNPs were typically assembled through a facet-to-facet binding (Figure 4.8A). Interparticle spacing of 92 AuNP dimers was measured, and the average from 4% upper limits of the measured values is 3.0 nm (±0.1) (see the distribution of measured interparticle spacing for AuNP dimers in the Appendix). This value is in good agreement with calculated spacing based on the assumption about the AuNP junction (~3.3 nm) (Figure 4.8B). The fitting of the measured gap spacing with a Gaussian distribution implies the randomness of the measured value, and thus probably suggests that the gap with respect to TEM electron beam is randomly oriented to normal.

4.3.8 Role of linker molecules in the formation of AuNP dimers

The formation of the AuNP dimer was elucidated in more detail. The added amounts of NBT were changed by 15 - 120 ML coverages while keeping the amount of hydroxyl

linker[34,56,57] to be 30 ML coverage, in order to investigate the efficiency of the dimer formations as the ratio of the two ligands were changed. The SERS and SEM images were obtained from the same glass substrates, which led to direct comparison of the SERS and the SEM image. The SEM samples were prepared after waiting for 2 h upon the second functionalization, in order to make sure that most of the added thiols can adsorb into the AuNP surfaces.[58] The broadened peaks of AuNPs in UV-Vis absorbance implied that some dimers were formed in solution (see UV-Visible absorption spectra of the solutions of asymmetric AuNPs in the Appendix). Figure 4.9 represents NP association/dissociation behaviors as change of the linker ratio in solution. As the ratio of the linker increases, the asymmetric AuNPs assemble into dimers, reaching a maximum of the mole ratio [linker]/([Raman-probe] + [linker]), χ, = ~0.5. When there are enough hydroxyl groups on the AuNP surface, the cooperative hydrogen bond through the interfacial hydroxyl groups governs the AuNP dimer formation. However, as the amounts

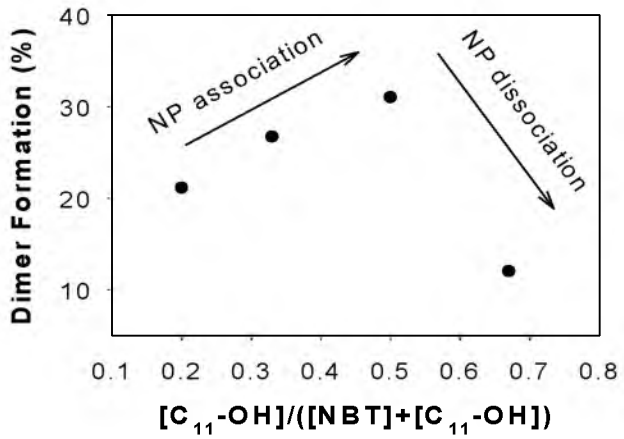

Figure 4.9. Dependence of the formation of the AuNP dimers on the amount of the linker ($HS\text{-}C_{11}\text{-}OH$) added in solution. Interactions between the linker-functionalized AuNPs are dominant prior to the linker ratio, χ = [linker]/([Raman-probe] + [linker]) = ~0.5 (NP association). As the linker amount increases further ($\chi > 0.5$), interactions of the linker-functionalized AuNPs with free linkers become dominant, and this hinders the formation of NP dimers (NP dissociation).

of the linker increases further, it prevents the dimer formation, which can be explained that the hydroxyl linker functionalized AuNPs interact with free linkers dominantly at the high concentration of the added linker molecules. Sudden change of adhesion force between hydroxyl groups depending on hydroxyl contents was reported, which the force [mN/m] was dropped drastically from 110 to 30, 30, and 10 as the hydroxyl content (%) was decreased from 100 to 75, 50, and 25.[59] The dependence of the formation of AuNP dimer on the linker concentration demonstrated the driving force of the dimer formation is the hydrogen bond between the linker hydroxyl groups.[35,60]

Considering the highest yield of the dimer formation (~31%) at χ = ~0.5 (despite the larger binding constant of alkanethiol compared to that of benzenethiol[39]), it was assumed that the surface coverage for each thiol on the reactive surface is equal. Therefore, it was concluded ~50% of the reactive surface was functionalized with the Raman probe molecule at χ = ~0.5, which ~2000[v] NBT were placed on each hot spot of the dimer. With the well-defined asymmetric functionalization method and the mechanism of the dimer formation it was eventually possible to avoid a large uncertainty in the actual number of the Raman probes, and thus to offer a much better estimate of the surface coverage.

Additionally, in the absence of the linkers, citrate accumulated at interfaces may be able to mediate the dimer formation through hydrogen bonds of carboxylic acid groups. This was evidenced by appearance of the carboxylic acid peaks in SERS spectra of AuNP dimers. The carboxylic acid peak at ~1730 cm^{-1} was observed when any thiol was not added for the second asymmetric functionalization step (see the Raman scattering spectrum of AuNP dimers prepared without the second functionalization in the

[v] 2 × (4.3NBT/nm^2 × 0.5 × 480 nm^2) = 2064; this is an upper limit since there are likely citrate molecules remaining on the surface. Also ethanol can bind to the surface.

Appendix). However, the interaction between citrate carboxylic groups remaining on the reactive surface and linker hydroxyl groups[61] may also contribute to the dimer formation.

4.3.9 Determination of SERS enhancement factor

Finally, the normalized SERS at the hot spot per AuNP dimer was calculated from ~2000 NBT. Note that the average diameter of the single NPs is 40 nm, and the interparticle spacing of the dimer is ~3.3 nm. Using a 4.2-μm laser spot size for the SERS measurements and a dimer formation yield from the substrate that produced 31% dimers as well as correcting the 5.8% random dimer configuration, it was found that one dimer produced a SERS signal of ~37 cts/10s and 3.7×10^{-4} cts/(mW·s·molecule).[vi] Normal Raman from NBT without NPs also was obtained. By obtaining unsaturated Raman intensities from solid NBT on glass substrates (see the distribution of Raman scattering intensities from pure NBT molecules in the Appendix for verifying unsaturated NBT amounts on the substrate), the normalized conventional Raman of NBT was calculated to be 2.8×10^{-10} cts/(mW·s·molecule)[vii] given the laser spot size of 4.2 μm. Therefore, the SERS enhancement factor is ~10^6 from the hot spot of the AuNP dimer. Note that the enhancement factor is a polarization-averaged value without specifically exciting hot spots parallel to the dimer axis through polarized light. The SERS enhancement factor in this study is smaller by two orders of magnitude than the value reported from other AuNP assemblies[13] that is sufficient to detect a single molecule (enhancement factors required:

[vi] Nine dimers per 14.1-μm^2 SEM image area; under the 4.2-μm laser spot size, the spot area is 14.1-μm^2; the SERS average is 312 cts/10s; 312 cts/(1-0.058)dimer = 37 cts; 37 cts/(10s·5mW·2000NBT) = 3.7×10^{-4} cts/(mW·s·molecule)

[vii] The average intensity of the normal Raman from the dried NBT is 679 cts/10s at 5 mW. In the given laser spot area (13.8 μm^2), Raman intensity per μm^2 is 49.1 cts/(10s·μm^2), and there are 3.45×10^9 NBT molecules/μm^2. Thus, the normalized conventional Raman of NBT is 49.1 cts/((5mW·10s·μm^2)·(3.45×10^9 molecules/μm^2)) = 2.8×10^{-10} cts/(mW·s·molecule).

10^8 - 10^{10}).[19] The detailed studies of the SERS enhancements from AuNP dimers with molecular geometry, change of interparticle spacing and polarization by single particle measurements are ongoing.

4.4 Conclusion

The asymmetric functionalization method was utilized to place Raman probe molecules (4-nitrobenzenethiol, NBT) in a spatially localized region of AuNPs.[62] The asymmetrically functionalized AuNPs (average diameter of individual NPs: 40 nm) form into dimers with aid of the hydroxyl-terminated alkanethiols as linker, and the localized regions with Raman probes are located at the junction of AuNP dimers. This produces SERS exclusively from the hot-spots of dimers. The orientation of the asymmetric NPs in dimers was investigated by SERS analyses, and the alignment of the asymmetric NPs was demonstrated. The plot between SERS intensities and dimer yield exhibits linearity, and this is strong evidence of the specific placement of the Raman probe at the junctions of AuNP dimers. The hydrocarbon length of the linkers affects SERS intensities, which supports the specific location of Raman probes at the junctions of AuNP dimers. With estimating the number of NBT (2000 molecules) and interparticle spacing (3.3 nm), the determined enhancement factor of SERS is 10^6. Due to the well-defined interface, the asymmetric functionalization approach can be applied to other NP-assembly-based studies including SM-SERS.

4.5 Appendix: Directing Raman probe molecules into junctions of gold nanoparticle dimers by asymmetric functionalization

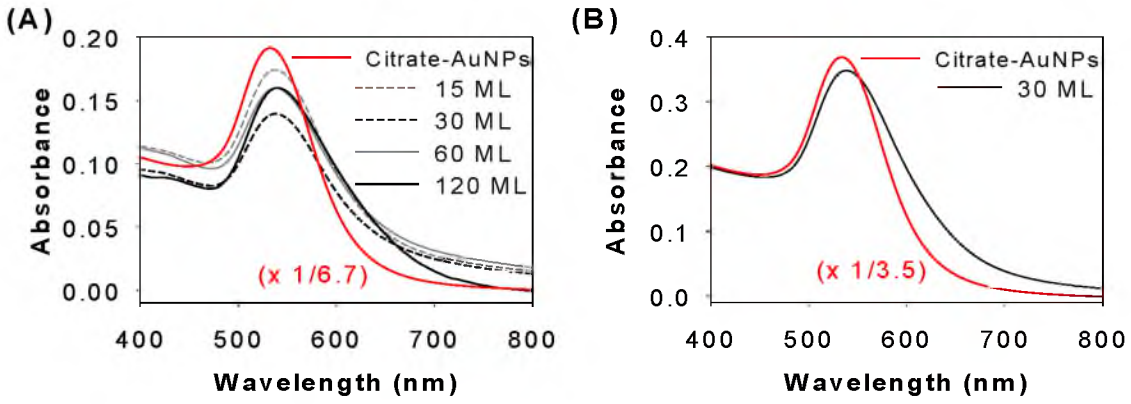

Figure 4.10. UV-Visible absorption spectra of solutions of asymmetric AuNPs with varied amount ratios of linkers. The NP solutions (A) with linkers (30 ML) and (B) without linker. The Raman probes were added for both samples, which the concentrations are represented by the numbers of monolayer (ML). Asymmetrically-functionalized AuNPs exhibit some assemblies regardless of the linker addition.

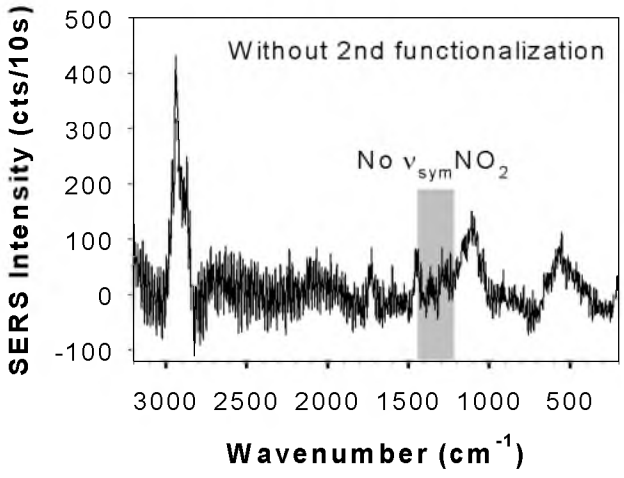

Figure 4.11. Raman scattering spectrum of AuNP dimers prepared without the second functionalization. Immobilized AuNPs on a glass substrate were released into ethanol solution by sonication without additional thiols. Note that the symmetric NO_2 stretching of 4-NBT at 1336 cm^{-1} was not observed as expected, but the νC=O stretching of carboxylic acid groups of citrate at 1730 cm^{-1} was detected.

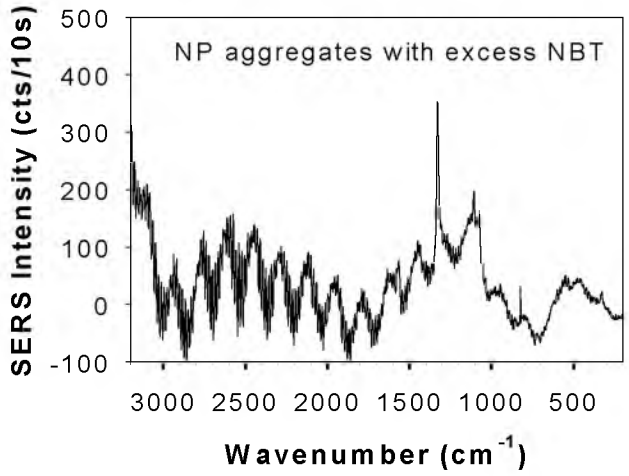

Figure 4.12. Representative Raman scattering spectrum of the NP aggregate sample.

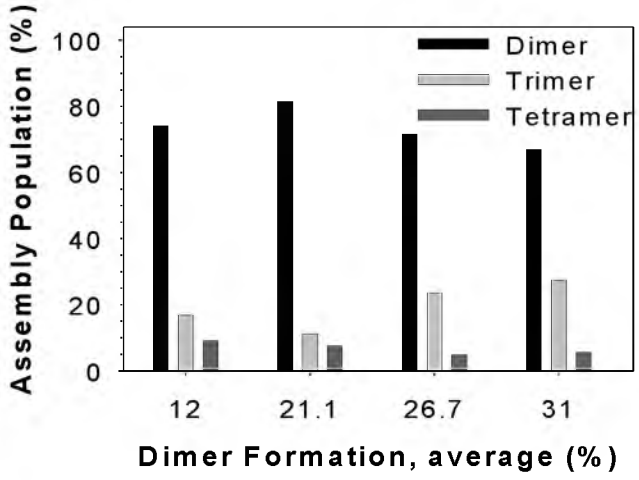

Figure 4.13. Distribution of dominant types of AuNP assemblies for each substrate. Dimers, trimers, and tetramers are the most populated types of assembly. The number of occurrence for high-order assemblies beyond tetramers is less than 8% among the whole assembled NPs. For each averaged dimer formation from 12 to 31%, the ratios of dimers/trimers are 0.742/0.169, 0.815/0.111, 0.715/0.236, and 0.700/0.275, respectively.

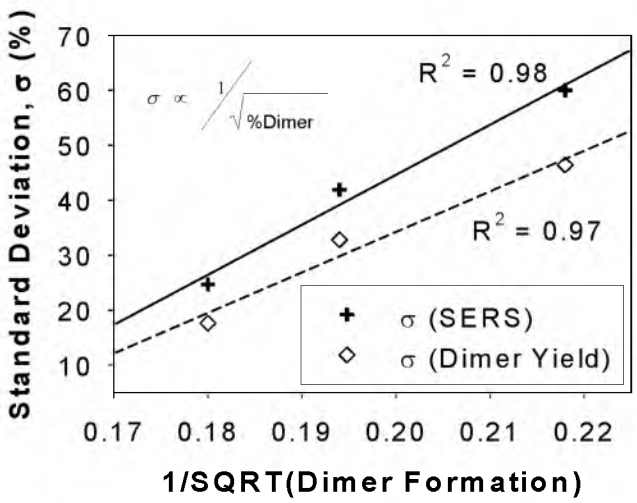

Figure 4.14. Correlation between standard deviations of SERS intensities and dimer yields as a function of a square-root of the number of dimer yields. The linearity directly reflects the SERS responses from AuNP dimers. Generally, a standard deviation is inversely proportional to a square-root of sample size.

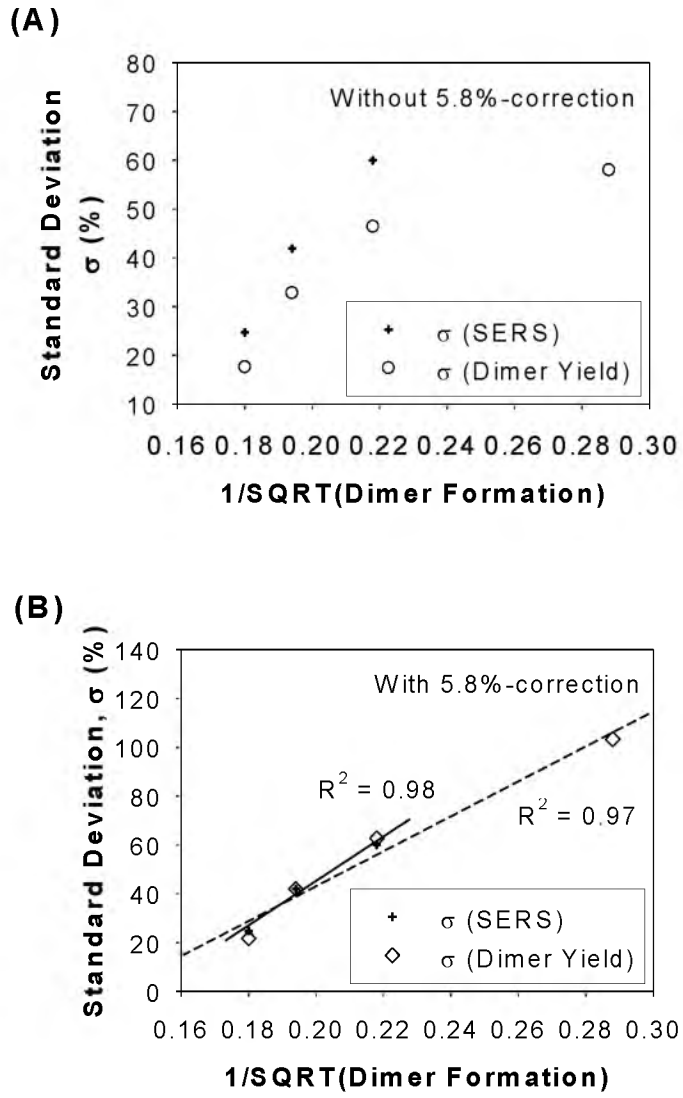

Figure 4.15. Correlation between standard deviations of SERS intensities and dimer yields as a function of a square-root of the number of dimer yields with respect to the 5.8%-correction. This percentage was subtracted from each dimer yield in correction. (A) Before correction, exhibiting a deviation from linearity for the standard deviation of dimer formation. One point at the largest 1/SQRT(Dimer formation) is dropped in Figure 4.14. (B) The linearity for the standard deviation of dimer formation was recovered after correction.

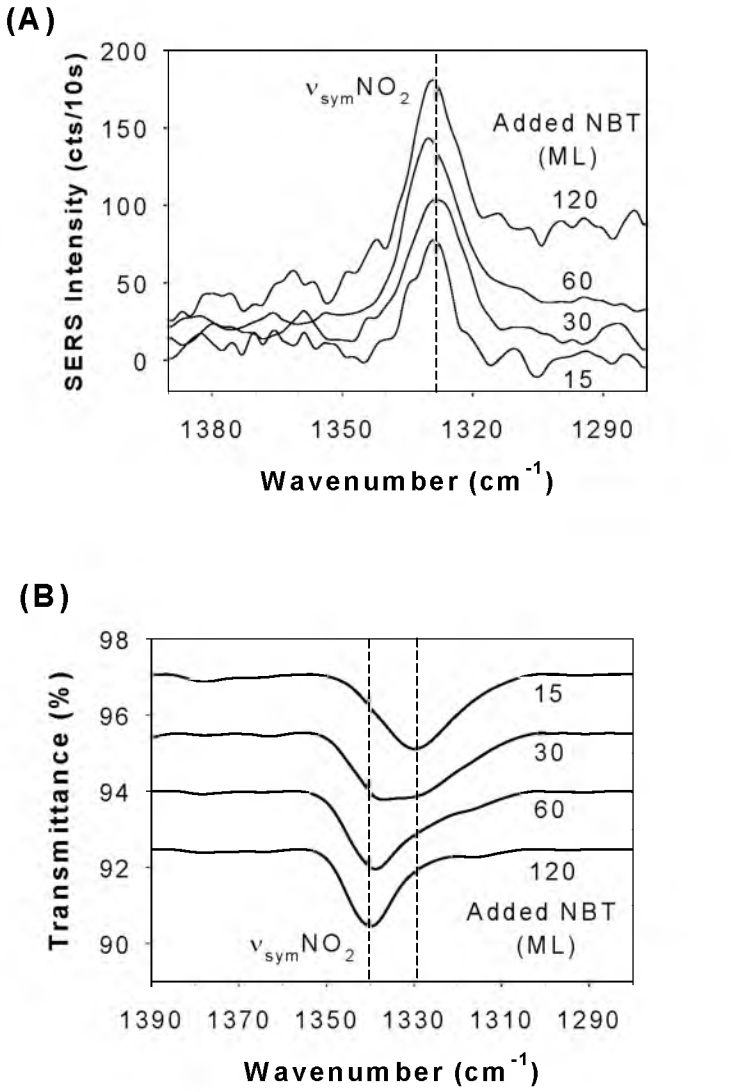

Figure 4.16. Normalized spectra in the symmetric NO_2 stretching ($\nu_{sym}NO_2$) regions at different NBT coverages. (A) Raman scattering spectra and (B) ATR-IR spectra. Dotted lines are given as guides at 1335/1328 cm^{-1} for (A) and 1329/1340 cm^{-1} for (B), which these peak shifts may indicate possible geometric changes of the adsorbed NBT with change of coverage. The IR peak areas of 1340 cm^{-1}/1329 cm^{-1} after deconvolution were 0/41.3, 11.0/38.3, 20.7/24.9, and 23.9/10.5 for 15, 30, 60, and 120-ML, respectively. IR peak shift of the asymmetric NO_2 stretching ($va_{asy}NO_2$) at 1517 cm^{-1} was not observed.

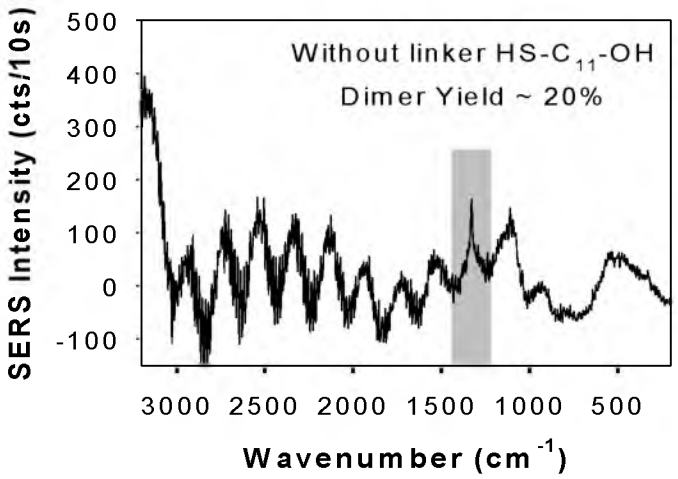

Figure 4.17. Representative Raman scattering spectrum of the randomly oriented AuNP dimers when a linker is not used.

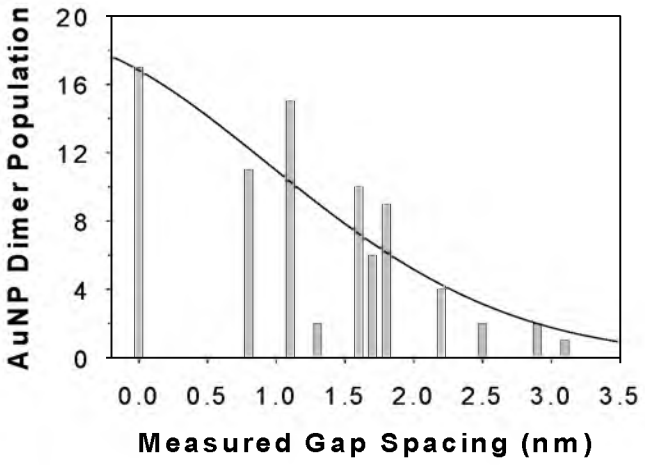

Figure 4.18. Distribution of measured interparticle spacing for all 92 AuNP dimers in TEM images from 30-ML sample. The fitted curve is Gaussian, which implies random orientation of the interparticle gap to normal in TEM imaging.

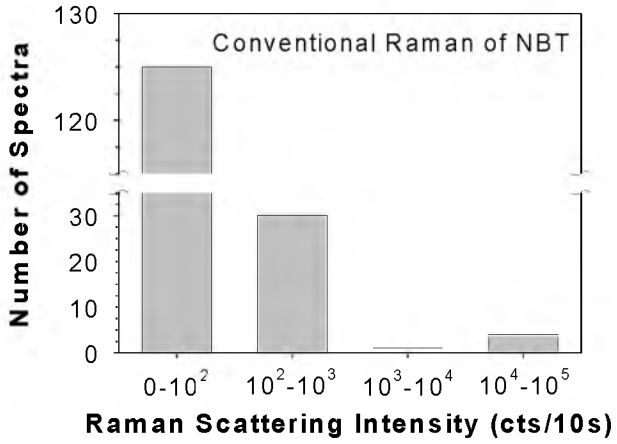

Figure 4.19. Distribution of Raman scattering intensities from pure NBT molecules. The small populations of two largest intensities, i.e., 10^3 - 10^4 and 10^4 - 10^5 cts/10s, verify that the NBT sample was not saturated in signal.

4.5.1 Weighted hot-spot population

Normalized weighted hot-spot population (%)

= (Avg. dimer yield) / [(#NP of a dimer) × (dimer population ratio) / ((#hot-spot of a dimer) × (dimeric hot-spot intensity)) + (#NP of a trimer) × (trimer population ratio) / ((#hot-spot of a trimer) × (trimeric hot-spot intensity))]

For 12-% averaged dimer formation (population rato of dimers/trimers = 0.742/0.169),

the weighted hot-spot population (%)

= (12%) / [2 × 0.742 / (1 × 1) + 3 × 0.169 / (2 × 3)] = 7.65 %

4.5.2 SERS intensity corrected by weighted hot-spot population

Unnormalized SERS intensity corrected by weighted hot-spot population

= (Avg. SERS intensity) / [(relative amount of NBT at one hot spot of a dimer) × (dimer population ratio) + (relative amount of NBT at two hot spots of a trimer) × (trimer population ratio)] / (NBT ratio)

For 12-% averaged dimer formation (averaged SERS intensity = 81.3 cts/10s, NBT ratio = 0.333),

the corrected SERS intensity at hot spots (unnormalized)

= 81.3 / [(2 × 0.742) + (3 × 0.169)] / 0.333 = 122.6 cts/10s

Avg. dimer yield (%)	Dimer ratio	Trimer ratio	Avg. SERS intensity (cts/10s)	Weighted hot-spot population (%)	Corrected SERS at hot-spots without NBT ratio	NBT ratio	Corrected SERS at hot-spots with NBT ratio
12.0	0.742	0.169	81.3	7.65	40.8	0.33	122.6
21.1	0.815	0.111	177.4	12.52	90.4	0.80	113.0
26.7	0.715	0.236	252.4	17.25	118.1	0.67	177.0
31.1	0.700	0.275	312.2	20.23	140.3	0.50	280.6

4.6 References

(1) Stockman, M. I.; Pandey, L. N.; George, T. F. *Phys. Rev. B* **1996**, *53*, 2183-2186.

(2) Aravind, P. K.; Nitzan, A.; Metiu, H. *Surf. Sci.* **1981**, *110*, 189-195.

(3) (a) Ghosh, S. K.; Pal, T. *Chem. Rev.* **2007**, *107*, 4797-4862. (b) Mayer, K. M.; Hafner, J. H. *Chem. Rev.* **2011**, *111*, 3828-3857.

(4) Kim, B.; Tripp, S. L.; Wei, A. *J. Am. Chem. Soc.* **2001**, *123*, 7955-7956.

(5) Han, L.; Luo, J.; Kariuki, N. N.; Maye, M. M.; Jones, V. W.; Zhong, C. J. *Chem. Mater.* **2003**, *15*, 29-37.

(6) Im, H.; Bantz, K. C.; Lindquist, N. C.; Haynes, C. L.; Oh, S.-H. *Nano Lett.* **2010**, *10*, 2231-2236.

(7) Romo-Herrera, J. M.; Alvarez-Puebla, R. A.; Liz-Marzán, L. M. *Nanoscale* **2011**, *3*, 1304-1315.

(8) Halas, N. J.; Lal, S.; Chang, W.-S.; Link, S.; Nordlander, P. *Chem. Rev.* **2011**, *111*, 3913-3961.

(9) Jones, M. R.; Osberg, K. D.; Macfarlane, R. J.; Langille, M. R.; Mirkin, C. A. *Chem. Rev.* **2011**, *111*, 3736-3827.

(10) Otto, A. *J. Raman Spectrosc.* **2006**, *37*, 937-947.

(11) Camargo, P. H. C.; Rycenga, M.; Au, L.; Xia, Y. *Angew. Chem. Int. Ed.* **2009**, *48*, 2180-2184.

(12) Camden, J. P.; Dieringer, J. A.; Wang, Y.; Masiello, D. J.; Marks, L. D.; Schatz, G. C.; Van Duyne, R. P. *J. Am. Chem. Soc.* **2008**, *130*, 12616-12617.

(13) Wustholz, K. L.; Henry, A.-I.; McMahon, J. M.; Freeman, R. G.; Valley, N.; Piotti, M. E.; Natan, M. J.; Schatz, G. C.; Van Duyne, R. P. *J. Am. Chem. Soc.* **2010**, *132*, 10903-10910.

(14) Li, W.; Camargo, P. H. C.; Lu, X.; Xia, Y. *Nano Lett.* **2009**, *9*, 485-490.

(15) Chen, G.; Wang, Y.; Yang, M.; Xu, J.; Goh, S. J.; Pan, M.; Chen, H. *J. Am. Chem. Soc.* **2010**, *132*, 3644-3645.

(16) Alexander, K. D.; Hampton, M. J.; Zhang, S.; Dhawan, A.; Xu, H.; Lopez, R. *J. Raman Spectrosc.* **2009**, *40*, 2171-2175.

(17) Talley, C. E.; Jackson, J. B.; Oubre, C.; Grady, N. K.; Hollars, C. W.; Lane, S. M. Huser, T. R.; Nordlander, P.; Halas, N. J. *Nano Lett.* **2005**, *5*, 1569-1574.

(18) Ringler, M.; Klar, T. A.; Schwemer, A.; Susha, A. S.; Stehr, J.; Raschke, G.; Funk, S.; Borowski, M.; Nichtl, A.; Kürzinger, K.; Phillips, R. T.; Feldmann, J. *Nano Lett.* **2007**, *7*, 2753-2757.

(19) Le Ru, E. C.; Etchegoin, P. G.; Meyer, M. *J. Chem. Phys.* **2006**, *125*, 204701.

(20) Etchegoin, P. G.; Le Ru, E. C. *Phys. Chem. Chem. Phys.* **2008**, *10*, 6079-6089.

(21) Roca, M.; Pandya, N. H.; Nath, S.; Haes, A. J. *Langmuir* **2010**, *26*, 2035-2041.

(22) Tyler, T. P.; Henry, A.-I.; Van Duyne, R. P.; Hersam, M. C. *J. Phys. Chem. Lett.* **2011**, *2*, 218-222.

(23) Sardar, R.; Heap, T. B.; Shumaker-Parry, J. S. *J. Am. Chem. Soc.* **2007**, *129*, 5356-5357.

(24) Sardar, R.; Shumaker-Parry, J. S. *Nano Lett.* **2008**, *8*, 731-736.

(25) Hofmann, A.; Schmiel, P.; Stein, B.; Graf, C. *Langmuir* **2011**, *27*, 15165-15175.

(26) Kleinman, S. L.; Ringe, E.; Valley, N.; Wustholz, K. L.; Phillips, E.; Scheidt, K. A.; Schatz, G. C.; Van Duyne, R. P. *J. Am. Chem. Soc.* **2011**, *133*, 4115-4122.

(27) Larmour, I. A.; Faulds, K.; Graham, D. *J. Phys. Chem. C* **2010**, *114*, 13249-13254.

(28) Lim, D.-K.; Jeon, K.-S.; Kim, H. M.; Nam, J.-M.; Suh, Y. D. *Nat. Mater.* **2010**, *9*, 60-67.

(29) Frens, G. *Nature Phys. Sci.* **1973**, *241*, 20-22.

(30) Nath, N.; Chilkoti, A. *Anal. Chem.* **2004**, *76*, 5370-5378.

(31) Liu, X.; Atwater, M.; Wang, J.; Huo, Q. *Colloids Surf., B* **2007**, *58*, 3-7.

(32) Mucic, R. C.; Storhoff, J. J.; Mirkin, C. A.; Letsinger, R. L. *J. Am. Chem. Soc.* **1998**, *120*, 12674-12675.

(33) Harris, D. C. *Quantitative Chemical Analysis, 5th Ed.*; W.H. Freeman & Co.: New York, 1998, pp 68-86.

(34) Matsunaga, M.; Aizenberg, M.; Aizenberg, J. *J. Am. Chem. Soc.* **2011**, *133*, 5545-5553.

(35) Sinniah, S. K.; Steel, A. B.; Miller, C. J.; Reutt-Robey, J. E. *J. Am. Chem. Soc.* **1996**, *118*, 8925-8931.

(36) Seo, Y. U.; Lee, S. J.; Kim, K. *J. Phys. Chem. B* **2004**, *108*, 4000-4007.

(37) Willets, K. A.; Van Duyne, R. P. *Annu. Rev. Phys. Chem.* **2007**, *58*, 267-297.

(38) Jiang, J.; Bosnick, K.; Maillard, M.; Brus, L. *J. Phys. Chem. B* **2003**, *107*, 9964-9972.

(39) Jakubowicz, A.; Jia, H.; Wallace, R. M.; Gnade, B. E. *Langmuir* **2005**, *21*, 950-955.

(40) Brus, L. *Acc. Chem. Res.* **2008**, *41*, 1742-1749.

(41) Tay, L.-L.; Hulse, J.; Kennedy, D.; Pezacki, J. P. *J. Phys. Chem. C* **2010**, *114*, 7356-7363.

(42) Zhu, L.; Cai, T.; Huang, J.; Stringfellow, T. C.; Wall, M.; Yu, L. *J. Phys. Chem. B* **2011**, *115*, 5849-5855.

(43) Danckwerts, M.; Novotny, L. *Phys. Rev. Lett.* **2007**, *98*, 026104.

(44) Romero, I.; Ai zpurua, J.; Bryant, G. W.; García de Abajo, F. J. *Opt. Express* **2006**, *14*, 9988-9999.

(45) Atay, T.; Song, J.-H.; Nurmikko, A. V. *Nano Lett.* **2004**, *4*, 1627-1631.

(46) Jiang, C.; Lio, W. Y.; Tsukruk, V. V. *Phys. Rev. Lett.* **2005**, *95*, 115503.

(47) Giersig, M.; Pastoriza-Santos, I.; Liz-Marzán, L. M. *J. Mater. Chem.* **2004**, *14*, 607-610.

(48) Barnard, A. S.; Young, N. P.; Kirkland, A. I.; van Huis, M. A.; Xu, H. *ACS Nano*, **2009**, *3*, 1431-1436.

(49) Yan, B.; Zhu, Z.-J.; Miranda, O. R.; Chompoosor, A.; Rotello, V. M.; Vachet, R. W. *Anal. Bioanal. Chem.* **2009**, *396*, 1025-1035.

(50) Wan, L.-J.; Terashima, M.; Noda, H.; Osawa, M. *J. Phys. Chem. B* **2000**, *104*, 3563-3569.

(51) Love, J. C.; Estroff, L. A.; Kriebel, J. K.; Nuzzo, R. G.; Whitesides, G. M. *Chem. Rev.* **2005**, *105*, 1103-1169.

(52) Kelley, A. T.; Ngunjiri, J. N.; Serem, W. K.; Lawrence, S. O.; Yu, J.-J.; Crowe, W. E.; Garno, J. C. *Langmuir* **2010**, *26*, 3040-3049.

(53) Futamata, M.; *Faraday Discuss.* **2006**, *132*, 45-61.

(54) Mikhlin, Y.; Likhatski, M.; Karacharov, A.; Zaikovski, V.; Krylov, A. *Phys. Chem. Chem. Phys.* **2009**, *11*, 5445-5454.

(55) Wang, Y.; Neyman, A.; Arkhangelsky, E.; Gitis, V.; Meshi, L.; Weinstock, I. A. *J. Am. Chem. Soc.* **2009**, *131*, 17412-17422.

(56) Li, M.; Johnson, S.; Guo, H.; Dujardin, E.; Mann, S. *Adv. Funct. Mater.* **2011**, *21*, 851-859.

(57) Lin, S.; Li, M.; Dujardin, E.; Girard, C.; Mann, S. *Adv. Mater.* **2005**, *17*, 2553-2559.

(58) Kassam, A.; Bremner, G.; Clark, B.; Ulibarri, G.; Lennox, R. B. *J. Am. Chem. Soc.* **2006**, *128*, 3476-3477.

(59) Uner, B.; Ramasubramanian, M. K.; Zauscher, S.; Kadla, J. F. *J. Appl. Polym. Sci.* **2006**, *99*, 3528-3534.

(60) Duwez, A.-S.; Poleunis, C.; Bertrand, P.; Nysten, B. *Lanmuir* **2001**, *17*, 6351-6357.

(61) Noy, A.; Vezenov, D. V.; Lieber, C. M. *Annu. Rev. Mater. Sci.* **1997**, *27*, 381-421.

(62) Park, J.-W.; Liu, A.-X.; Shumaker-Parry, J. S. "Directing Raman Probe Molecules into Junctions of Gold Nanoparticle Dimers by Asymmetric Functionalization". *manuscript in preparation.*

CHAPTER 5

POLYMER-INDUCED SYNTHESIS OF STABLE GOLD AND SILVER NANOPARTICLES AND SUBSEQUENT LIGAND EXCHANGE IN WATER*

5.1 Introduction

Metal nanoparticles, particularly gold, have received wide attention for application in photonics,[1,2] electronic and optical detection systems,[3,4] device development,[5-8] therapeutics,[9,10] and catalysis.[11,12] Due to the requirements for control of nanoparticle size and surface functionalization for this broad range of applications, different synthetic methods have been developed to generate monodisperse gold nanoparticles (AuNPs). One of the most widely-used methods is the reduction of tetrachloroaurate ions ($AuCl_4^-$) in aqueous medium using sodium citrate to generate particles with diameters typically ranging from 10 to 100 nm.[13] Although this method has good control over producing a particular particle size, it is limited to the synthesis of larger particles. The Brust method and various modifications[14-16] are useful for the generation of AuNPs having core sizes ranging from 1 to 4 nm. In the Brust method, the

*Reprinted with permission from Sardar, R.; Park, J.-W.; Shumaker-Parry, J. S. *Langmuir* **2007**, *23*, 11883-11889. Copyright 2007 American Chemical Society. The second author conducted all experimental and characterization work reported except as indicated. The author also composed the manuscript corresponding to Chapter 5. Sardar, R. carried out the TEM imaging and provided experimental design guidance. Shumaker-Parry, J. S. provided experimental design and editorial guidance.

transfer of $AuCl_4^-$ into toluene or chloroform is performed using tetraalkylammonium bromide followed by reduction with sodium borohydride in the presence of alkylthiols. Disadvantages of this method include contamination of the synthesized particles with boride[17] and potential presence of impurities introduced by the use of capping ligands which also hinder the surface modification and functionalization of particles for particular applications. A few other single-step reduction processes also were developed to generate monodisperse gold nanoparticles but these are limited to organic media.[18,19] In addition, reduction of gold salt to form AuNPs using amine-containing organic molecules has been investigated,[20-24] but most of the amine compounds used in those AuNP syntheses are soluble in only organic solvents, and the reduction reactions must take place in an organic solvent or in a biphasic system. As a result, the nanoparticles prepared using those methods are not easily dispersed in aqueous solution. To use the AuNPs in an aqueous-based or biological systems, it is necessary to functionalize the particles with ligands which facilitate phase transfer from an organic to an aqueous medium.

Alternative synthetic strategies based on using polymers as both the reducing and stabilizing agent for the generation of stable metal nanoparticles without the use of an additional stabilizing agent have been developed. The resulting nanoparticle-polymer composites have been shown to be useful in catalytic transformations[25] and could be useful for nanostructured solar cells, photonic band gap materials, storage devices, and drug delivery. Some polymers can fulfill the required dual role as a reducer and stabilizer. Examples include poly(methylhydrosiloxane),[26] poly(N-vinyl-2-pyrrolidone),[27] poly(sodium acrylate),[28] poly(ethylene oxide),[29] poly(vinyl alcohols),[30] and polyethylenimine.[31] However, even in the syntheses using those polymers, either the

reduction reaction was carried out in organic solvents or produced polydisperse nanoparticles. In both situations, the use of the nanoparticles is restricted, or at least complicated, for aqueous-based (e.g., biological) applications or applications that require monodisperse particles (e.g., electronics).

The major advantage of using a polymer as a stabilizing agent is that it can be used to tailor the nanocomposite properties and also to provide long-tem stability of the nanoparticles by preventing particle agglomeration.[32-34] To produce stable polymer-encapsulated nanoparticles, the polymer should have a coordinating group such as a thiol or amine in its backbone. Although monodisperse particles may be synthesized using a thiolated polymer, [35-38] the surface modification of those nanoparticles by nonthiolated ligands would be difficult due to the strong sulfur-gold interaction and complete displacement by even thiolated ligands would be difficult to achieve. On the other hand, an amine group has a weak interaction with metal nanoparticles and can be easily replaced by a thiolated ligand.[22]

In this context, a suitable synthetic approach is desirable where the nanoparticles could be stabilized by polymer-containing amine functional groups which can undergo ligand exchange with a variety of thiolated ligands for specific nanoparticle applications. Although poly(allylamine) (PAAm) was previously studied for its stabilizing ability,[39] the polymer's dual character both as reducing and stabilizing agent for the generation of stable metal nanoparticles has not been reported yet. In this article, we report a simple, inexpensive, single-step synthesis of gold nanoparticles using poly(allylamine) (PAAm) both as a reducing and a stabilizing agent. The polymer-nanoparticle composite synthesis was carried out in water, making the method versatile and environmentally friendly. One

of the main challenges in obtaining a useful polymer-nanoparticle composite is controlling the particle dispersion inside the polymer matrix. We show that the particle size and size dispersion can be controlled by simply varying the molar ratio of the PAAm used in the reaction. The synthesized polymer-stabilized nanoparticles are stable in water for at least a month. We demonstrate successful ligand exchange on the polymer-stabilized gold nanoparticles with a variety of ω-functionalized acid-, alcohol-, amine-, and biotin-terminated alkylthiols. The methodologies, including ligand exchange, are also applied to generate finely dispersed silver nanoparticles in aqueous solution.

5.2 Experiments

5.2.1 Materials

$HAuCl_4 \cdot 3H_2O$, $AgNO_3$, poly(allylamine) (PAAm, 20 wt. % solution in water, M_w *ca.*65,000), 16-mercaptohexadecanoic acid (MHA), 2-mercaptoethylamine (MEA), 11-mercapto-1-undecanol (MUOH) were purchased from Aldrich. Biotin-terminated tri(ethylene glycol) hexadecanethiol was obtained from ASEMBLON (Redmond, WA). All water used was purified using a NANOpure Diamond^{TM} (Barnstead, Nanopure water, 17.8 MΩ/cm). Absolute ethanol was obtained from Aapper (200 proof, Shelbyville, KY). All glassware was washed with aqua-regia (3:1, $HCl:HNO_3$) and rinsed copiously with Nanopure water. All chemicals were used as received without further purification.

5.2.2 Spectroscopy and microscopy measurements

Absorption spectra (300 nm to 800 nm) were collected using a Perkin-Elmer Lambda 19 UV/Vis/NIR spectrophotometer. Samples of polymer-stabilized NPs were taken from

the reaction vessel during synthesis and analyzed without a cooling step. A Perkin-Elmer Spectrum One FTIR Spectrometer was used for IR analysis. IR samples were prepared by dropping approximately 400 μL of sample on a PTFE (polytetrafluoroethylene) IR card (International Crystal Laboratories, NJ) and allowing it to dry in air overnight. Transmission electron microscopy (TEM) micrographs were obtained using an FEI Company Tecnai T-12 TEM operating at 100 KV accelerating voltage. For TEM analysis, each solution was centrifuged at 1000 r.p.m. for 30 min, one drop of reaction mixture was deposited on a 150-mesh formvar-coated copper grid, and excess solution was removed by wicking with filter paper to avoid particle aggregation. The particle size analysis was conducted by analyzing 200 particles in the TEM images using Scion Image Beta 4.02 Software. In Scion Image, after setting the known distance and unit, the 'Analyze Particle' parameter was used to generate a table of particle diameters. This table was then exported into Microsoft Excel 2003 for statistical analysis.

5.2.3 Preparation of the PAAm-stabilized AuNPs

Twenty mg of $HAuCl_4 \cdot 3H_2O$ (0.051 mmol) were dissolved in 190 mL of Nanopure water in a three-neck round-bottom flask. After the solution was allowed to reflux with constant stirring, 10 mL of a 0.04 M poly(allylamine) aqueous solution was added to the reaction vessel. The reaction was monitored by UV-visible spectroscopy, and the reaction was allowed to proceed until the amplitude of the absorption spectrum reached a maximum. The color of the final product solution was dark reddish purple. Once the reaction was complete, the solution was allowed to cool to room temperature and stored in a brown-glass container. The reaction procedure was repeated with varying amounts of

polymer solution as described in the 'Results and discussion' section below.

5.2.4 Preparation of the PAAm-stabilized AgNPs

Twenty mg of $AgNO_3$ (0.118 mmol) and 10 mL of 0.04 M poly(allylamine) solution were used to prepare AgNPs in 200 mL of water. The synthetic procedure was the same as that used for the synthesis of AuNPs. The product AgNP solution was yellow without noticeable precipitation during the reaction. The yellow color was detectable by eye after the reaction had proceeded for about 25 min. A stable absorption spectrum maximum was reached 24 h after the addition of PAAm.

5.2.5 Ligand exchange

The polymer-AuNPs solution was centrifuged for 30 min at 1000 r.p.m., and only clear supernatant was used in the ligand-exchange reactions. For each ligand exchange, 5 mL of the polymer-AuNPs solution was mixed with 1 mL of 1 mM thiol-ligand, and the solution was stirred for 4 h at room temperature. The solution color did not change during any of the ligand-exchange reactions. The reaction mixtures were analyzed using UV-visible absorption spectroscopy, TEM, and FTIR. Similar methodology was followed for the ligand-exchange studies of polymer-stabilized AgNPs.

5.3 Results and discussion

5.3.1 Characterization of PAAm-stabilized gold nanoparticles in water

Gold nanoparticle synthesis using PAAm as both a reducing and stabilizing agent is shown in Scheme 5.1. Approximately 4 min after the addition of polymer to an aqueous

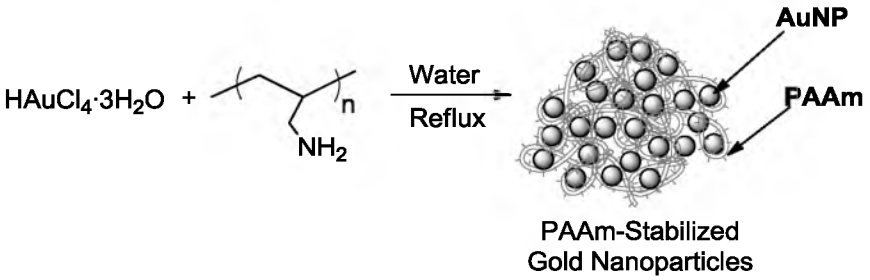

Scheme 5.1. PAAm induced synthesis and stabilization of gold nanoparticles in water

solution of $HAuCl_4 \cdot 3H_2O$, the solution turned light purple. The purple color deepened to medium purple at 10 min and at 30 min the final solution was dark reddish purple.

UV-visible absorption spectroscopy was used to monitor the AuNP synthesis at different stages. Representative spectra are shown in Figure 5.1. The light-purple solution collected at 4 min showed a broad peak maximum, λ_{max}, at 521 nm, which is characteristic for AuNPs in this size regime and dielectric environment.[40] The λ_{max} was red-shifted by 3 nm to 524 nm for the medium purple solution collected at 10 min. At the end of the reduction (~30 min), the λ_{max} for the dark reddish-purple solution was 521 nm which is a 3 nm blue shift from 524 nm for the medium purple colored solution. In a previous report,[26] a similar blue shift also was observed for polymer-stabilized silver nanoparticles. This blue shift is likely due to the dissociation of larger particles into smaller particles. In our system, at the initial stage of the reaction when small nanoparticles are formed, the particles could collide with each other to produce larger, more stable particles, leading to a red-shift in the λ_{max}. After time, those bigger particles could dissociate due to heating to form smaller-sized particles that are stabilized by the amine pendant groups on the PAAm backbone which leads to the formation of polymer-encapsulated stable nanoparticles. The mechanism of the gold reduction process can be

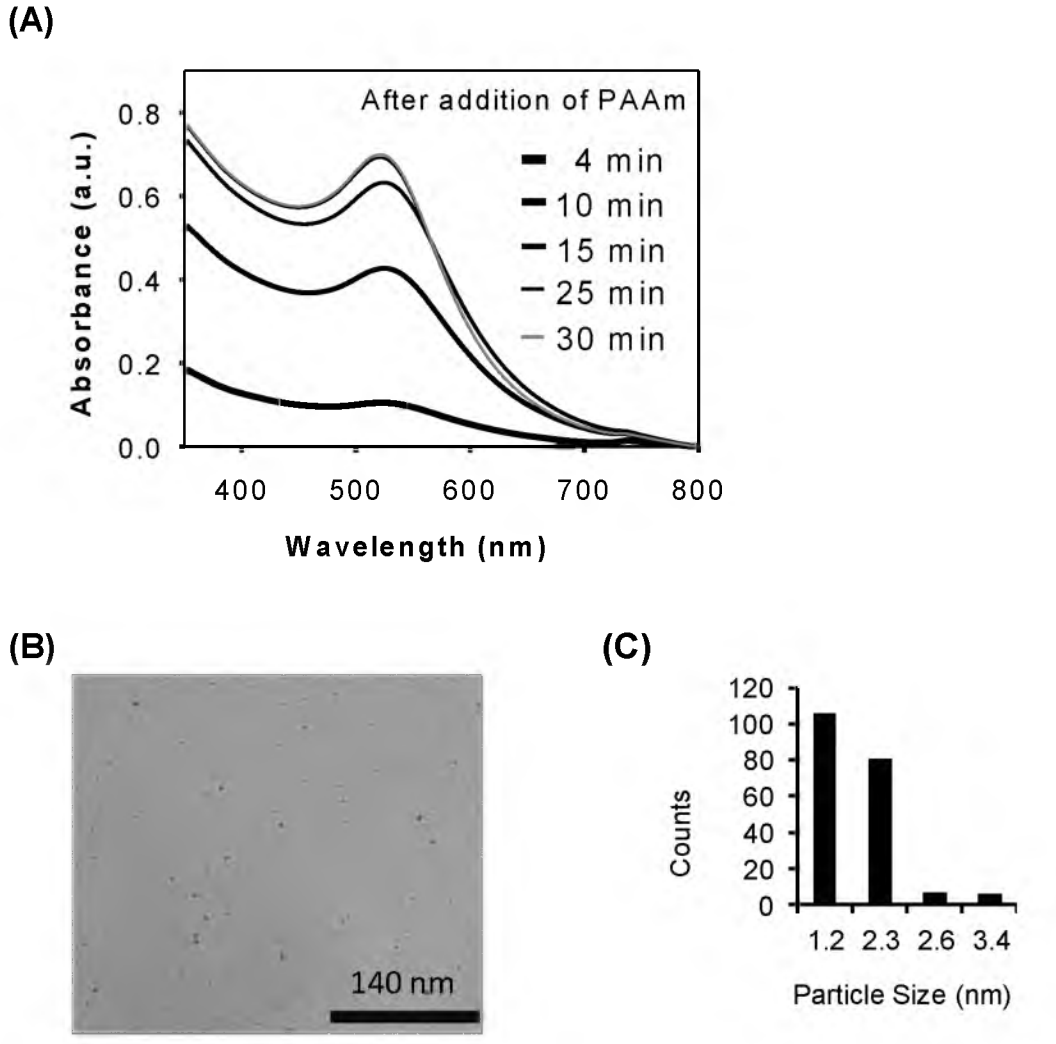

Figure 5.1. (A) UV-visible absorption spectra, (B) TEM image, and (C) the corresponding particle size analysis histogram of the gold nanoparticles.

explained by the metal ion-induced oxidation of amine to nitrile, which has been described previously.[41,42]

The final dark reddish purple AuNP solution was then analyzed by transmission electron microscopy (TEM) to determine the particle size, size distribution and morphology. The TEM analysis showed the formation of spherical gold nanoparticles with an average diameter of 1.7 ± 0.6 nm. Figure 5.1B and 5.1C present a representative

TEM image and the corresponding size histogram of the synthesized AuNPs, respectively. The polymer-encapsulated AuNPs were stable in water without additional surfactant and displayed an intense absorption peak, λ_{max}, of 522 nm without a shoulder at longer wavelengths for 40 d (see the Appendix).

We investigated the use of different PAAm concentrations (0.04 - 0.32 M) to control the particle size and size dispersion in the AuNP synthesis, shown in Table 5.1. The formation of AuNPs in the presence of different polymer concentrations was monitored by UV-visible absorption spectroscopy (see the Appendix). We observed that at higher polymer concentration the initial rate of formation of AuNPs was slower, and the reduction takes a longer time to complete. In a recent publication, Patakfalvi *et al.* reported that $NaBH_4$ reduction of silver salt took a longer time to reach completion in the presence of a higher concentration of stabilizing polymer PVP.[43] In our system, PAAm also acts as a stabilizer, and our observations correlate well with the reported result. The AuNPs also were analyzed by TEM. Representative TEM images are shown in Figure 5.2A and 5.2B. In the presence of 0.16 M and 0.32 M of PAAm, the AuNP size was 2.6 ± 0.9 and 2.2 ± 0.6 nm, respectively. These particles are larger than particles synthesized using a lower polymer concentration (e.g., 0.04 M, 1.7 ± 0.6 nm particle diameter). At the higher PAAm concentration (0.32 M) some micellar structures also were observed along with individual AuNPs. Additional experiments are underway to understand the slow formation of gold nanoparticles at higher polymer concentrations and also the effect of polymer concentration on AuNP size dispersion.

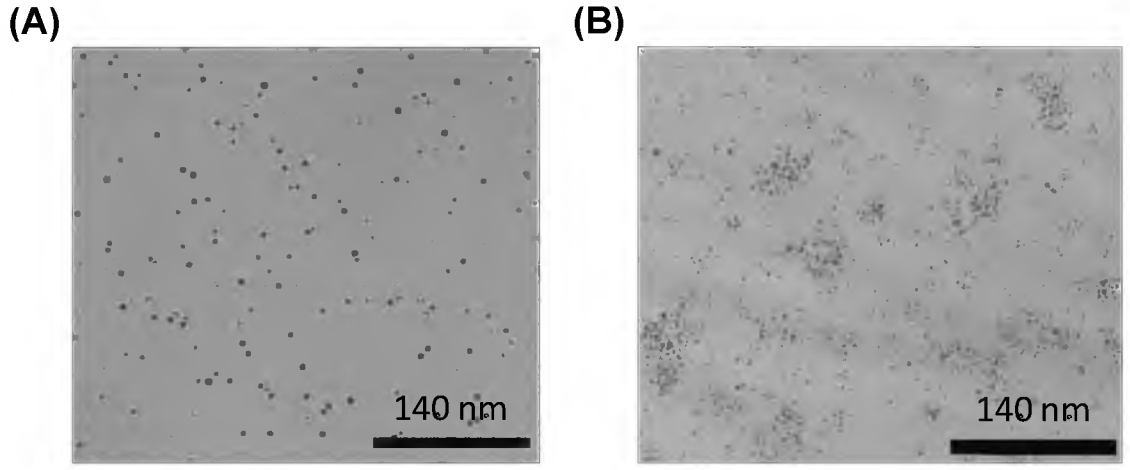

Figure 5.2. TEM images of the AuNPs synthesized using PAAm concentrations of (A) 0.16 M and (B) 0.32 M.

Table 5.1. Comparison of reaction time, UV-visible absorption maxima, and size of gold nanoparticles synthesized using different PAAm concentrations.[a]

[PAAm] (M)	Time for stable λ_{max} (min)	UV-vis maximum (λ_{max}) (nm)	Particle size (nm)[b]
0.04	30	521	1.7 (0.6)
0.08	45	515	3.0 (1.0)
0.16	80	515	2.6 (0.9)
0.32	220	513	2.2 (0.6)

[a]In each case, 200 particles were counted to determine the size and the dispersity.
[b]The number in parenthesis indicates the standard deviation.

5.3.2 Ligand-exchange study of AuNPs

Ligand-stabilized nanoparticles have been studied extensively for a variety of applications and also have been used as model systems for fundamental place-exchange reaction studies.[44-46] The place-exchange reaction is a versatile and important method for preparation of functionalized metal nanoparticles.[47-49] In this reaction, addition of ligand-protected nanoparticles to a solution of a second ligand effects partial replacement of the

protecting shell on the nanoparticle surface with the second ligand. Ligand exchange has been studied the most for thiol-protected Au nanoparticles, and the exchange mechanism for thiols with AuNPs has been studied extensively by Murray and coworkers.[50,51] Typically, the place-exchange reaction leads to a mixed ligand shell composed of the initial capping-ligand and the second ligand used in the exchange reaction. More complex ligand shells composed of more than two constituents have been formed through place-exchange reactions using either a simultaneous exchange process with a mixture of thiols in solution or in a step-wise process through sequential place-exchange reactions with different ligands. In all of these place-exchange methods, the extent of ligand exchange and the composition of the resulting ligand shell are both highly dependent on the reaction conditions (e.g., concentrations, solvent, etc.) and the ligand structure including the chain length, bulkiness of terminal group, charge, etc. [51a,b,d] In addition, some thiols used as capping ligands during synthesis are not soluble in aqueous medium and thus limit the solubility of the nanoparticles when ligand exchange with water-soluble thiols is not complete.

As mentioned earlier, the AuNPs in this study are stabilized in water by amine groups on the backbone of the PAAm. The ligand-exchange reaction of these amines with stronger surfactants such as thiolated ligands could be very beneficial to achieve controlled functionalization of the AuNPs. For example, complete displacement of the amine ligands by thiol ligands will lead to nanoparticles functionalized with a single type of ligand. In addition, a mixed ligand shell could be produced by using a mixed solution of thiols during the ligand exchange process. It is expected that the ligand composition would be dependent upon the specific ligands used and the reaction conditions. However,

the relationship between the reaction parameters and resulting ligand composition could be elucidated through experiments and applied to achieve compositional control. For this purpose, the versatility of the synthetic process using PAAm as both a reducing and a stabilizing agent was further investigated through ligand-exchange studies. Different ω-functionalized alkylthiols including 16- mercaptohexadecanoic acid (MHA), 11-mercapto-1-undecanol (MUOH), 2-mercaptoethylamine (MEA), and biotinylated alkylthiol were used for ligand-exchange reactions with the polymer-stabilized gold nanoparticles for this study according to Scheme 5.2.

Briefly, in the ligand-exchange process, 5 mL of AuNP solution (PAAm, 0.04 M) was reacted with 1 mM ethanolic solution of the thiol for 4 h with stirring at room temperature. The reaction mixture was monitored by UV-visible absorption spectroscopy and the absorption maxima (λ_{max}) varied from 524 - 529 nm depending on the ligand used (see the Appendix). For each solution, one drop of the crude product was deposited on a TEM grid to determine the morphology of the particles in the presence of different

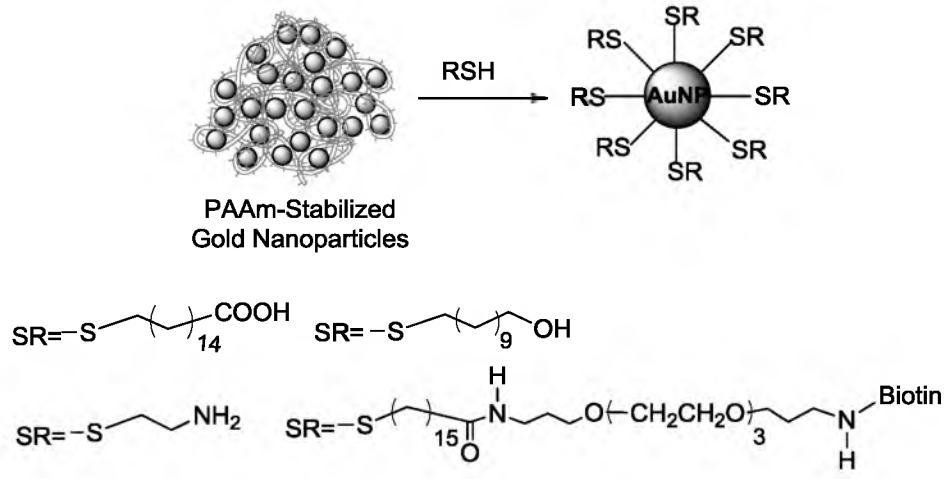

Scheme 5.2. Representation of ligand-exchange study of the polymer-stabilized AuNPs with different thiolated ligands

ligands. Figure 5.3 presents representative TEM images of the AuNPs after exchange with different ligands. Table 5.2 includes a comparison of the UV-visible absorption maxima and size of the AuNPs after the ligand-exchange reactions using different ligands. Particle size analysis presented in Table 5.2 shows that that after the ligand exchange the capped nanoparticles are larger in size compared to the original polymer-stabilized AuNPs. For example, prior to ligand exhange the average particle size was 1.7 ± 0.6 nm for the PAAm-stabilized AuNPs. After ligand exchange with MHA, the average particle size increased to 2.4 ± 0.8 nm. One reason for the formation of larger AuNPs in

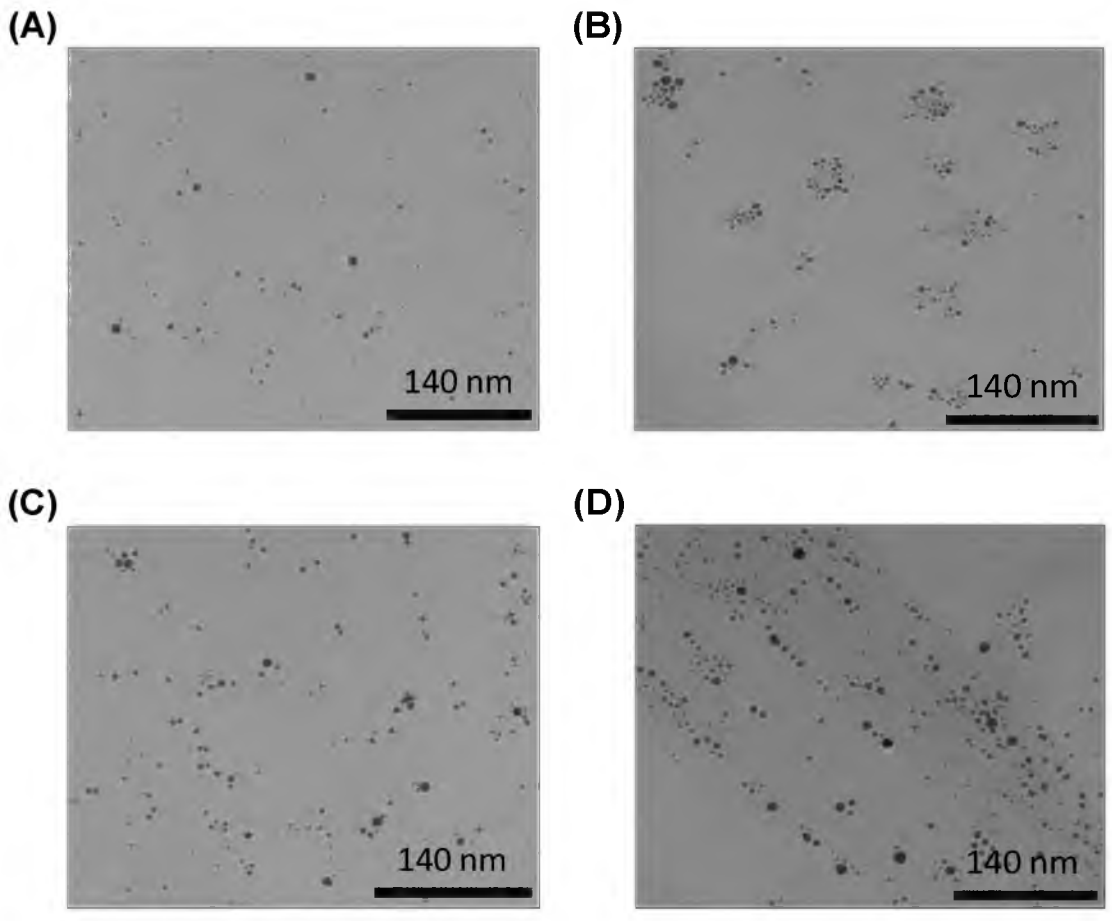

Figure 5.3. TEM images of the different thiolated ligand-stabilized gold nanoparticles. (A) MHA, (B) MUOH, (C) MHA, and (D) biotin-terminated alkylthiol.

Table 5.2. Comparison of UV-visible absorption maxima and the particle size of the gold nanoparticles in the presence of different ligand environments.[a]

Gold-Sols	UV-visible. Abs. Maxima (λ_{max}-nm)	Particle Size[b] (nm)
Au-PAAm	521	1.7 (0.6)
Au-MHA	527	2.4 (0.8)
Au-MUOH	525	2.9 (0.8)
Au-MEA	521	2.7 (0.8)
Au-Biotin	526	3.1 (1.1)

[a]In each case, 200 particles were counted to determine the size and the size dispersion.
[b]The number in parenthesis indicates the standard deviation.

the presence of thiolated ligands could be that the strong thiolated ligand replaces the polymer molecules from the nanoparticle surface and during this dynamic exchange process, small nanoclusters aggregate to form comparatively larger particles.

FTIR spectroscopy was used to investigate the ligand-exchange reaction process in more detail. The IR transmission spectra of PAAm, PAAm-stablilized AuNPs, MHA, and AuNPs capped with MHA are shown in Figure 5.4. The absorption feature at 3304 cm^{-1} in Figure 5.4a is due to the N-H stretching band[52] of the amine groups, which is not observed in the polymer-AuNPs composite indicating the coordination of amine groups with the nanoparticles.[53,40b] In the polymer-AuNPs, new strong peaks appearing at 3044 cm^{-1} and 3134 cm^{-1} are assigned to the symmetric NH_3^+ stretching bands, and 1608 cm^{-1} and 1509 cm^{-1} are attributed to the asymmetric and symmetric NH_3^+ deformation, respectively.[54] The formation of NH_3^+ is expected from the acidic condition of the final solution. One of the CH_2 stretching bands[52] of the polymer-AuNPs appears around 2930 cm^{-1} as a shoulder. A sharp strong band of CH bending[55] at 1404 cm^{-1} is characteristic of PAAm-AuNPs composites. Pure MHA shows the asymmetric and symmetric CH

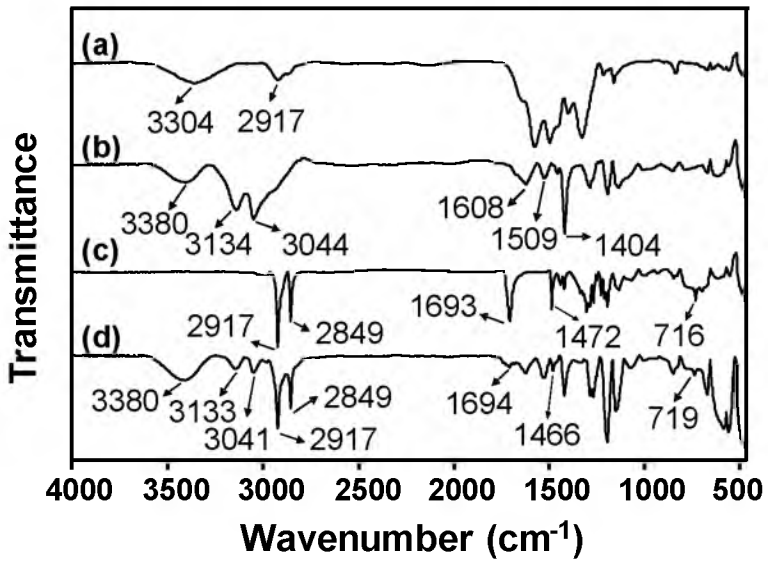

Figure 5.4. FTIR spectra of (a) pure PAAm, (b) PAAm-AuNPs composite, (c) pure MHA, and (d) MHA ligand exchange AuNPs.

stretching[56,57] at 2917 cm^{-1} and 2849 cm^{-1}, respectively, and the peak at 1693 cm^{-1} is the CO stretching band of carboxylic acid.[56] A number of vibrational bands of pure MHA after the ligand exchange disappeared, but a new peak at 1466 cm^{-1} is assigned to the CH_2 scissoring mode, which is close to reported value at 1460 cm^{-1} of the MHA SAMs (self-assembled monolayers) on gold film.[58] Noticeably, the CS stretching band of MHA[59] shifts from 716 cm^{-1} to 719 cm^{-1} due to incorporation into new surface environments of AuNPs. The absorption band at 3380 cm^{-1} in both the Figure 5.4b and d could be due to the presence of trace water in the samples.

5.3.3 Synthesis and ligand-exchange study of silver nanoparticles

Silver nanoparticles (AgNPs) are useful candidates for different applications such as sensors,[60] catalysts,[61] SERS substrates,[62] and also in biotechnology.[63] Under similar reaction conditions, the synthesis of AgNPs using PAAm as a reducing and stabilizing

agent was also investigated. The reduction process was slow, taking almost 24 h to reach a stable absorption maximum in the UV-visible spectra collected at different time points during the synthesis. After 24 h, the product AgNP solution was yellow and exhibited an intense absorption peak, λ_{max}, at ~405 nm, as shown in Figure 5.5A. We centrifuged the solution and deposited one drop of supernatant on a TEM grid for morphological analysis. A representative TEM image of the AgNPs is shown in Figure 5.5B. TEM analysis confirmed the formation of nanoparticles with an average diameter of 4.4 ± 0.9 nm.

The place-exchange reactions of the polymer-stabilized AgNPs also were investigated using previously mentioned ω-functionalized alkylthiols. In case of silver nanoparticles, we used the same protocol as described for the PAAm-stabilized AuNPs. The different ligand-stabilized AgNPs were analyzed by UV-visible absorption spectroscopy (see the Appendix). We haven't observed any substantial changes in the absorption maxima in the UV-visible absorption spectra. TEM analysis showed that the sizes of the thiol-stabilized

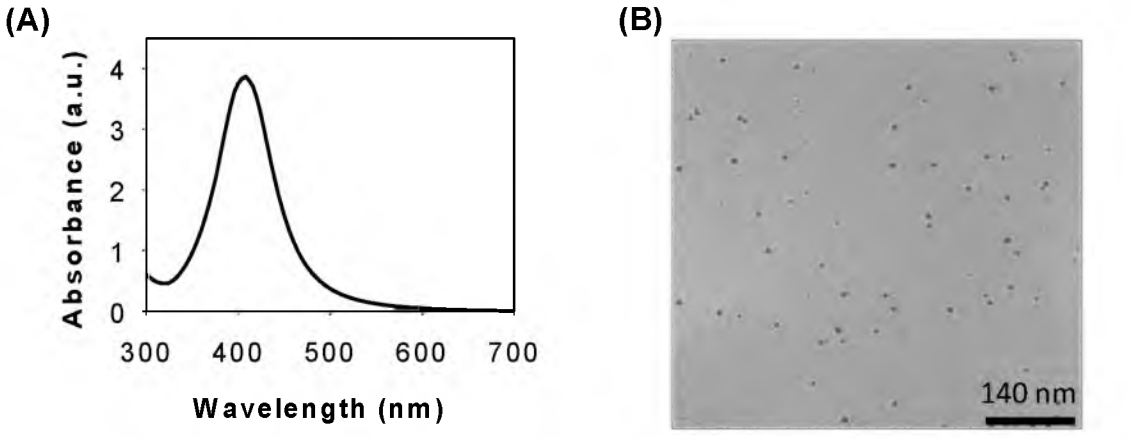

Figure 5.5. UV-visible absorption spectra (A), and a representative TEM image (B) of the synthesized AgNPs using PAAm.

silver particles were different compared to polymer-stabilized AgNPs (see the Appendix). A detailed ligand-exchange study is underway.

5.4 Conclusion

In conclusion, we have reported a facile, aqueous-phase, single-step synthesis of gold nanoparticles using poly(allylamine) as a reducing agent. The polymer acted both as a reducing as well as a stabilizing agent and the synthetic process required no additional stabilizer. The particle size can be controlled by varying the concentration of PAAm. The synthesized polymer-encapsulated gold nanoparticles showed remarkable stability in water. The polymer-stabilized gold nanoparticles underwent ligand exchange with a variety of ω-functionalized acid-, alcohol-, amine-, and biotin-terminated alkylthiols. The methodology was also successfully applied for the synthesis and functionalization of stable silver nanoparticles.

5.5 Appendix: Polymer-induced synthesis of stable gold and silver nanoparticles and subsequent ligand exchange in water

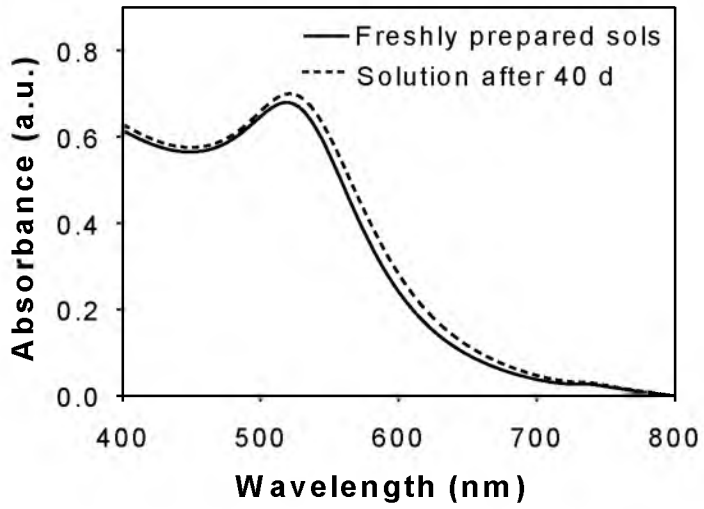

Figure 5.6. Stability of PAAm-stabilized gold nanoparticles.

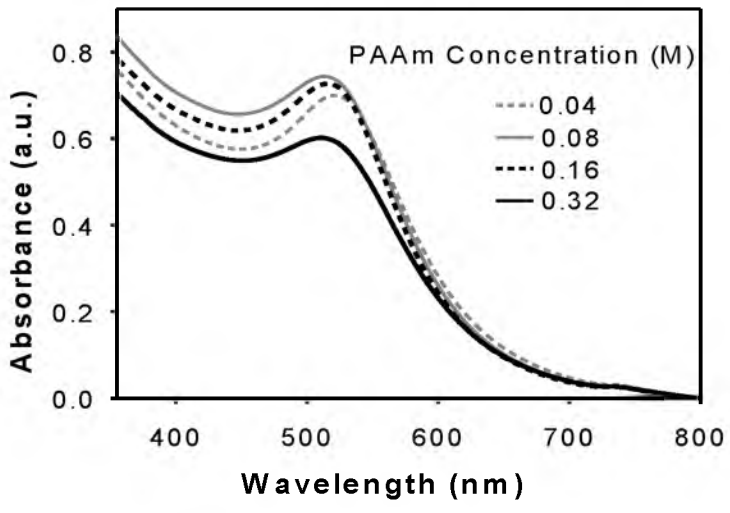

Figure 5.7. UV-visible absorption spectra of AuNPs synthesized using different PAAm concentrations.

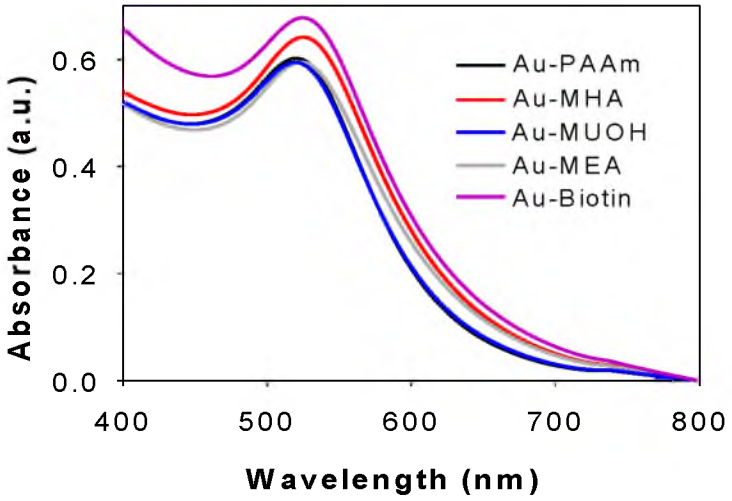

Figure 5.8 UV-visible absorption spectroscopy comparison of gold nanoparticles in different ligand environments.

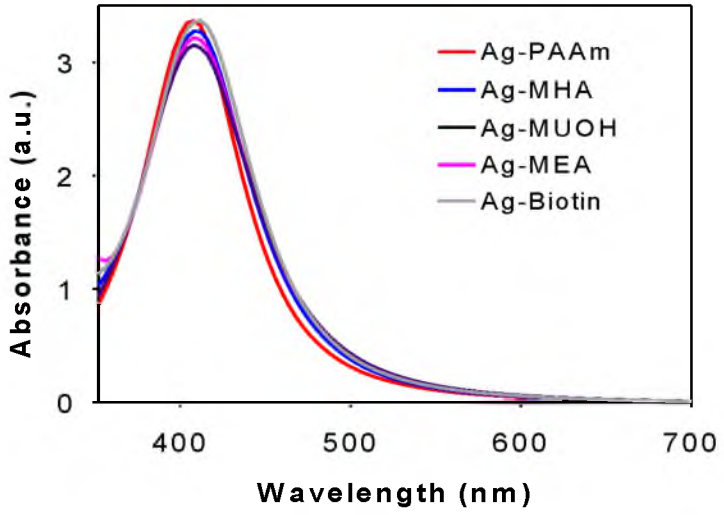

Figure 5.9. UV-visible absorption spectroscopy comparison of silver nanoparticles in different ligand environments.

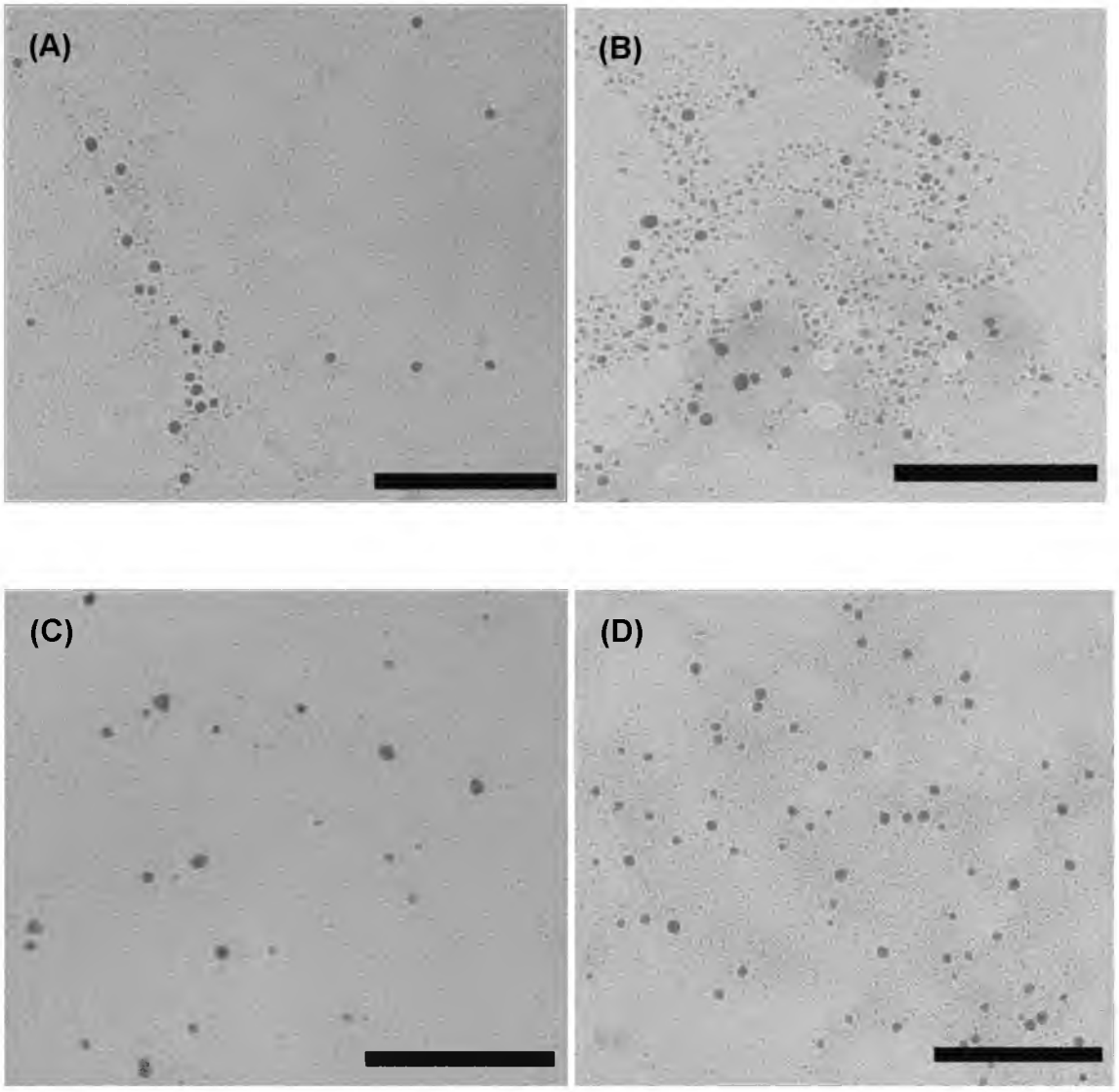

Figure 5.10. TEM images of silver nanoparticles stabilized by (A) MHA-, (B) MUOH-, (C) MEA-, and (D) biotin-terminated alkylthiols. Scale bars are 140 nm.

Table 5.3. Comparison of UV-visible absorption maxima and particle sizes of silver nanoparticles in different ligand environments.

Silver-Sols	UV-Vis. Abs. Maxima(λ_{max}) (nm)	Particle Size (nm)
Ag-PAAm	405	4.4 (0.9)
Ag-MHA	410	4.6 (1.2)
Ag-MUOH	407	3.1 (0.9)
Ag-MEA	407	4.9 (1.5)
Ag-Biotin	411	4.5 (1.0)

5.6 References

(1) Burda, C.; Chen, X.; Narayan, R.; El-Sayed, M. A. *Chem. Rev.* **2005**, *105*, 1025-1102.

(2) Thomas, K. G.; Kamat, P. V. *Acc. Chem. Res.* **2003**, *36*, 888-898.

(3) Katz, E.; Willner, I. *Angew. Chem. Int. Ed.* **2004**, *43*, 6042-6108.

(4) Taton, T. A.; Mirkin, C. A.; Letsinger, R. L. *Science* **2000**, *289*, 1757-1760.

(5) Maier, S. A.; Brongersma, M. L.; Kik, P. G.; Meltzer, S.; Requicha, A. A. G.; Atwater, H. A. *Adv. Mater.* **2001**, *13*, 1501-1505.

(6) Novak, J. P.; Brousseau, L. C.; Vance, F. W.; Johnson, R. C.; Lemon, B. I.; Hupp, J. T.; Feldheim, D. L. *J. Am. Chem. Soc.* **2000**, *122*, 12029-12030.

(7) He, L.; Musick, M. D.; Nicewarner, S. R.; Salinas, F. G.; Benkovic, S. J.; Natan, M. J.; Keating, C. D. *J. Am. Chem. Soc.* **2000**, *122*, 9071-9077.

(8) Feldheim, D. L.; Keating, C. D. *Chem. Soc. Rev.* **1998**, *27*, 1-12.

(9) Pissuwan, D.; Valenzuela, S. M.; Cortie, M. B. *TRENDS Biotech.* **2006**, *24*, 62-67.

(10) Jain, P. K.; Lee, K. S.; El-Sayed, I. H.; El-Sayed, M. A. *J. Phys. Chem. B* **2006**, *110*, 7238-7248.

(11) Tsunoyama, H.; Sakurai, H.; Negishi, Y.; Tsukuda, T. *J. Am. Chem. Soc.* **2005**, *127*, 9374-9375.

(12) Enache, D. I.; Edwards, J. K.; Landon, P.; Solsona-Espriu, B.; Carley, A. F.; Herzing, A. A.; Watanabe, M.; Kiely, C. J.; Knight, D. W.; Hutchings, G. J. *Science* **2006**, *311*, 362-365.

(13) Turkevich, J.; Stevenson, P. C.; Hillier, J. *Discuss. Faraday. Soc.* 1951, 55-75.

(14) Brust, M.; Walker , M.; Bethell, D.; Schiffrin, D. J.; Whyman, R. *J. Chem. Soc., Chem. Commun.* **1994**, 801-802.

(15) Collier, C. P.; Saykally, R. J.; Shiang, J. J.; Henrichs, S. E.; Heath, J. R. *Science* **1997**, *277*, 1978-1981.

(16) Cliffel, D. E.; Zamborini, F. P.; Gross, S. M.; Murray, R. W. *Langmuir* **2000**, *16*, 9699-9702.

(17) Bonnemann, H.; Brijoux, W.; Brinkmann, R.; Fretzen, R.; Joussen, T.; Koppler, R.; Korall, B. K.; Neiteler, P.; Richter, J. *J. Mol. Catal.* **1994**, *86*, 129-177.

(18) Jana, N. R.; Peng, X. *J. Am. Chem. Soc.* **2003**, *125*, 14280-14281.

(19) Schulz-Dobrick, M.; Sarathy, K. V.; Jasen, M. *J. Am. Chem. Soc.* **2005**, *127*, 12816-12817.

(20) Selvakannan, P. R.; Mandal, S.; Pasricha, R.; Adyanthaya, S. D.; Sastry, M. *Chem. Commun.* **2002**, 1334-1335.

(21) Kumar, P. S.; More, A. S.; Shingte, R. D.; Wadgaonkar, P. P.; Sastry, M. *Adv. Mater.* **2004**, *16*, 966-971.

(22) Hiramatsu, H.; Osterloh, F. E. *Chem. Mater.* **2004**, *16*, 2509-2511.

(23) Subramaniam, C.; Tom, R. T.; Pradeep, T. *J. Nanopart. Res.* **2005**, *7*, 209-217.

(24) Newman, J. D. S.; Blanchard, G. J. *Langmuir* **2006**, *22*, 5882-5887.

(25) (a) Chauhan, B. P. S.; Rathore, J. S. *J. Am. Chem. Soc.* **2005**, *127*, 5790-5791. (b) Chauhan, B. P. S.; Rathore, J. S. Glloxhani, N. *Appl. Organomet. Chem.* **2005**, *19*, 542-550. (c) Chauhan, B. P. S.; Rathore, J. S.; Bandoo, T. *J. Am. Chem. Soc.* **2004**, *126*, 8493-8500.

(26) Chauhan, B. P. S.; Sardar, R. *Macromolecules* **2004**, *37*, 5136-5139.

(27) Hoppe, C. E.; Lazzari, M.; Pardines-Blanco, I.; Lopez-Quintela, M. A. *Langmuir* **2006**, *22*, 7027- 7034.

(28) Hussain, I.; Brust, M.; Papworth, A. J.; Cooper, A. I. *Langmuir* **2003**, *19*, 4831-4835.

(29) Sakai, T.; Alexandridis, P. *J. Phys. Chem. B* **2005**, *109*, 7766-7777.

(30) Longenberger, L.; Mills, G. *J. Phys. Chem.* **1995**, *99*, 475-478.

(31) Chen, C. C.; Hsu, C. H.; Kuo, P. L. *Langmuir* **2007**, *23*, 6801-6806.

(32) Barnes, K. A.; Karim, A.; Douglas, J. F.; Nakatani, A. I.; Gruell, H.; Amis, E. J. *Macromolecules* **2000**, *33*, 4177-4185.

(33) Kim, B. J.; Bang, J.; Hawker, C. J.; Kramer, E. J. *Macromolecules* **2006**, *39*, 4108-4114.

(34) Balaza, A. C.; Emrick, T.; Russell, T. P. *Science* **2006**, *314*, 1107-1110.

(35) Wuelfing, W. P.; Gross, S. M.; Miles, D. T.; Murray, R. W. *J. Am. Chem. Soc.* **1998**, *120*, 12696-12697.

(36) Teranishi, T.; Kiyokawa, I.; Miyake, M. *Adv. Mater.* **1998**, *10*, 596-599.

(37) Corbierre, M. K.; Cameron, N. S.; Sutton, M.; Mochrie, S. G. J.; Lurio, L. B.; Ruhm, A.; Lennox, R. B. *J. Am. Chem. Soc.* **2001**, *123*, 10411-10412.

(38) Hussain, I.; Graham, S.; Wang, Z.; Tan, B.; Sherrington, D.; Rannard, S. P.; Cooper, A. I.; Brust, M. *J. Am. Chem. Soc.* **2005**, *127*, 16398-16399.

(39) (a)Lee, J.; Yang, B.; Li, R.; Seery, T. A. P.; Papadimitrakopoulos, F. *J. Phys. Chem. B* **2007**, *111*, 81-87.(b) El-Khoury, J. M.; Caruntu, D.; O'Connor, C. J.; Jeong, K.U.; Cheng, S. Z. D.; Hu, J. *J. Nanopart. Res.* **2007**, *9*, 959-964. (c) Hong, Y.; Sen, A. *Chem. Mater.* **2007**, *19*, 961-963.

(40) (a) Alvarez, M. M.; Khoury, J. T.; Schaaff, T. G.; Shafigullin, M. N.; Vezmar, I.; Whetten, R. L. *J. Phys. Chem. B* **1997**, *101*, 3706-3712. (b) Ding, Y.; Zhang, X.; Liu, X.; Guo, R. *Colloids and Surface A: Physicochem. Eng. Aspects* **2006**, *290*, 82-88.

(41) Clarke, T. G.; Hampson, N. A.; Lee, J. B.; Morley, J. R.; Scanlon, B. *Tetrahedron Lett.* **1968**, *54*, 5685-5688.

(42) Capdevielle, P.; Lavigne, A.; Sparfel, D.; Lafont-Baranne, J.; Cuong, N. K.; Maumy, M. *Tetrahedron Lett.* **1990**, *31*, 3305-3308.

(43) Patakfalvi, R.; Papp, S.; Dekany, I. *J. Nanopart. Res.* **2007**, *9*, 353-364.

(44) Hainfeld, J. F. *Science* **1987**, *236*, 450-453.

(45) Zhong, C. J.; Maye, M. M. *Adv. Mater.* **2001**, *13*, 1507-1511.

(46) (a) Loweth, C. J.; Caldwell, W. B.; Peng, X., Alivisatos, A. P.; Schultz, P. G. *Angew. Chem. Int. Ed.* **1999**, *38*, 1808-1812. (b) Worden, J. G.; Shaffer, A. W.; Huo, Q. *Chem. Commun.* **2004**, 518-519. (c) Sung, K. M.; Mosley, D. W.; Peelle, B. R.; Zhang, S.; Jacobson, J. M. *J. Am. Chem. Soc.* **2004**, 126, 5064-5065. (d) Kassam, A.; Bremner, G.; Clark, B.; Ulibarri, G.; Lennox, R. B. *J. Am. Chem. Soc.* **2006**, *128*, 3476-3477. (e) Warner, M. G.; Hutchison, J. E. *Nature. Mater.* **2003**, *2*, 272-277.

(47) Daniel, M. C.; Astruc, D. *Chem. Rev.* **2004**, *104*, 293-346.

(48) (a) Woehrle, G. H.; Brown, L. O.; Hutchison, J. E. *J. Am. Chem. Soc.* **2005**, *127*, 2172-2183. (b) Brown, L. O. Hutchison, J. E. *J. Am. Chem. Soc.* **1999**, *121*, 882-883. (c) Brown, L. O. Hutchison, J. E. *J. Phys. Chem. B* **2001**, *105*, 8911-8916.

(49) Thomas, K.G.; Kamat, P. V. *Acc. Chem. Res.* **2003**, *36*, 888-898.

(50) Templeton, A. C.; Wuelfing, W. P.; Murray, R. W. *Acc. Chem. Res.* **2000**, *33*, 27-36.

(51) (a) Hostetler, M. J.; Green, S. J.; Stokes, J. J.; Murray, R. W. *J. Am. Chem. Soc.* **1996**, *118*, 4212-4213. (b) Hostetler, M. J.; Templeton, A. c.; Murray, R. W. *Langmuir* **1999**, *15*, 3782-3789. (c) Templeton, A. C.; Chen, S.; Gross, S. M.; Murray, R. W. *Langmuir* **1999**, *15*, 66-76, (d) Ingram, R. S.; Hostetler, M. J.; Murray, R. W. *J. Am. Chem. Soc.* **1997**, *119*, 9175-9178. (e) Cliffel, D. E.; Zamborini, F. P.; Gross, S. M.; Murray, R. W. *Langmuir* **2000**, *16*, 9699-9702.

(52) Nyquist, R. C. *Interpreting Infrared, Raman, and Nuclear Magnetic Resonance Spectra*, Academic Press, New York, **2001**, Vol.1.

(53) (a) Kumar, A.; Mandal, S.; Selvakannan, P. R.; Pasricha, R.; Mandale, A. B.; Sastry, M. *Langmuir* **2003**, *19*, 6277-6282.

(54) (a) Calvo, E. J.; Bonazzola, C. Langmuir **2003**, 19, 5279-5286. (b) Itano, K.; Chai, J.; Rubner, M. F. *Macromolecules* **2005**, *38*, 3450-3460.

(55) Zucolotto, V.; Ferreira, M.; Cordeiro, R. M.; Constantino, C. J. L.; Balogh, D. T.; Zanatta, A. R.; Moreira, W. C.; Oliveira Jr., O. N. *J. Phys. Chem. B* **2003**, *107*, 3733 -3737.

(56) Jordon, C. E.; Frey, B. L.; Kornguth, S.; Corn, R. M. *Langmuir* **1994**, *10*, 3642-3648.

(57) Hostetler, M. J.; Stokes, J. J.; Murray, R. W. *Langmuir* **1996**, *12*, 3604-3612.

(58) Gole, A.; Orendorff, C. J.; Murphy, C. J. *Langmuir* **2004**, *20*, 7117-7122.

(59) Pang, S.; Gao, H.; Xie, S.; Yao, J.; He, S. *J. Phys. D: Appl. Phys.* **2001**, *34*, 3425-3429.

(60) Henley, A. J.; Carey, J. D.; Silva, S. R. P. *Appl. Phys. Lett.* **2006**, *89*, 183120-3.

(61) Sudrik, S. G.; Maddanimath, T.; Chaki, N.; Chavan, S. P.; Chavan, S. P.; Sonawane, H. R. Vijayamohanan. *Org. Lett.* **2003**, *5*, 2355-2358.

(62) El-Sayed, M. A. *Acc. Chem. Res.* ***2001***, *34*, 257-264.

(63) (a) Morley, K. S.; Webb, P. B.; Tokareva, N. V.; Krasnov, A. P.; Popov, V. K.; Zhang, J.; Roberts, C. J.; Howdle, S. M. *Eur. Poly. J.* **2007**, *43*, 307-314. (b) Mohan, y. M.; Lee, K.; Premkumar, t.; Geckeler, K. E. *Polymer* **2007**, *48*, 158-164. (c) Li, P.; Li, J.; Wu, C.; Wu, Q.; Li, J. *Nanotechnology* **2005**, *16*, 1912-1917.

CHAPTER 6

CONCLUDING REMARKS

6.1 Conclusions and perspectives on future research

The focus of the research in this dissertation was to investigate the interfacial chemical and physical properties and surface modification of citrate-stabilized gold nanoparticles (AuNPs) as well as to develop the syntheses and ligand-exchange of poly(allylamine)-stabilized AuNPs and silver nanoparticles (AgNPs). Surface chemistry governs the chemical phenomena of the metal NPs, and the physical properties of NPs including surface enhanced Raman scattering (SERS) can be significantly influenced by interface-related factors such as thickness of organic layers and interparticle spacing. In most nanoparticle-based research, however, the organic/metal interface has been neglected or oversimplified while the focus has been on the utilization of the metal NPs for various applications such as sensing and biological/medical imaging.

Citrate-stabilized AuNPs and AgNPs have been extensively used for nanoparticle-based studies after the development of control of the metal-core size of the NPs by the citrate reduction method. However, the citrate layers on the surface of the NPs have not been well-characterized. The nanometer-sized materials (typically, 10 – 100 nm for citrate-stabilized AuNPs) pose a particular challenge for the characterization of coordinated organic layers on the surface. Scanning tunneling microscopy (STM), the most accessible technique to characterize the molecular topology on a planar surface,

cannot routinely provide a molecular image on metal NP surfaces due to the surface curvature.[1] X-ray crystallographic analysis[2] is not accessible because of the non-uniform sizes of the prepared NPs and negligible contribution from organic molecules on the NP surface to X-ray diffraction. Nuclear magnetic resonance (NMR) is not sensitive to investigate surface organic layers on the relatively large size of metal NPs due to low concentration of the organic molecules. A single analytical technique may not be possible to provide a detailed picture of an entire structure of an organic layer on metal NPs with a size range of around 10 – 100 nm.

A variety of analytical methods for studying the citrate layer were used in this dissertation research. Those methods include Fourier transform-Infrared (FT-IR), X-ray photoelectron spectroscopy (XPS), transmission electron microscopy (TEM), STM, and simulation. Vibrational spectroscopy is still powerful for studying the structure of organic molecules adsorbed on surfaces. A fingerprinting vibrational frequency from coordinated functional groups of molecules adsorbed on metal NPs correlates with a structure of individual adsorbates, such as small organic ligands including citrate molecules. Attenuated total internal reflectance (ATR) FT-IR and transmission FT-IR were used to characterize the coordination of carboxylate and hydroxyl groups of adsorbed citrate species. In order to probe coordination of the functional groups on the surface, excess citrate layers on citrate-stabilized AuNPs (39 nm ± 20% in diameter) were removed by purifying the NPs with NaOH solution. The OH^- solution interrupts possible intermolecular interactions, i.e., hydrogen bonding, between carboxylic acid groups of surface citrate/citric acid molecules. IR data of NPs purified with D_2O/NaOD provided additional information of COOH/OH coordination due to a shift of related vibrational frequencies resulting from H/D exchange. In addition, the C1s binding energy of citrate

molecules was measured by XPS, and the coordination of COOH groups were found to be consistent with the IR data.

From the IR and XPS analyses of the purified citrate-stabilized AuNPs, the conformation of adsorbed citrate species was proposed. Citrate molecules are adsorbed on the AuNP surface through η^2-COO^- coordination of the central carboxylate group and η^1-COO^- coordination of one terminal carboxylate group with both the other terminal carboxylate group and the hydroxyl group uncoordinated. The proposed citrate conformation is similar to that proposed on AgNPs by Smith and co-workers,[3] and the bidentate coordination through the central and one of the terminal carboxylate groups of citrate on a Ag(111) surface was demonstrated by Yin and co-workers.[4] Nichols and co-workers proposed a different conformation of citrate molecules adsorbed on planar gold surfaces based on IR analysis, which only one type of COO^- stretching vibration through η^2-COO^- coordination was claimed to be present and thus all three COO^- groups of citrate bind to the surface through tridentate coordination.[5] Although the reported IR data are consistent with IR data in this study, an indication of other stretching vibrations of COO^- groups was neglected. The proposed structure of citrate molecules directly adsorbed on AuNPs is consistent with data provided by others and in this study.

IR data in this study also indicated the presence of additional citrate layers. Original citrate layers were preserved during NP purification steps through partial functionalization of NPs with about 1/2 stoichiometric amounts of methyl-terminated alkanethiols relative to a monolayer coverage on the AuNP surfaces. The alkanethiol layer prevents the NPs from irreversibly aggregating during centrifugation steps that are necessary to purify citrate-stabilized AuNPs. IR data showed the characteristic frequencies of hydrogen bonds between carboxylic acid groups and another asymmetric

stretching vibration of the central carboxylate group. Those imply the spectral feature of dangling citrate species interacting with the adsorbed species by hydrogen bonds between the terminal carboxylic acid groups, which resulted in units of citrate trimers consisting of one dangling and two adsorbed citrate molecules. Intermolecular interactions of the dangling citrate with two adsorbed citrate molecules (~28 kcal/mol for two hydrogen-bonded COOH-dimers) prevail over the metal-carboxylate interaction (~2 kcal/mol for Au-COO^- interaction), which strongly suggests a long-range ordered layer of citrate molecules on the surface of AuNPs.

TEM and STM images of citrate layers in literature were adapted and analyzed further to investigate a specific orientation of the adsorbed and dangling citrate species. A double-layer of citrate molecules on AuNPs was imaged by atomic-resolution TEM imaging and the layer spacing was measured to be 3.0 - 3.5 Å,[6] which is shorter than the allowed distance between one of the smallest organic molecules (i.e., methane) due to van der Waals repulsion (4.0 Å). The short layer spacing indicates there must be a unique orientation between dangling and adsorbed citrate molecules, which the COOH plane of hydrogen-bonding between the terminal carboxylic acid groups is oriented at an angle of about 25^o form surface. The direction of hydrogen bonded carboxylic acid groups led to determination of a specific conformation of citrate that fit the pattern of citrate adsorption on a Au(111) surface as imaged by STM.[7] Interestingly, only one type of enantiomer is consistent with the STM image of citrate molecules, which may suggest chirality of the adsorbed citrate molecules. Dangling citrate molecules should be stretched out to interact with adjacent adsorbed citrate molecules. As a result, the orientation and geometry of the citrate trimer on a Au(111) surface have been determined, which is consistent with both TEM and STM images of citrate layers on gold surfaces.

With the citrate trimers as building blocks, adsorption patterns were simulated on the Au(111) surface. This simulation is based on the geometry and position of coordinated carboxylate groups as well as the orientation of the terminal carboxylic acid groups, and it is not an outcome from energy optimization by computation. The geometry-based simulation can still provide an optimized pattern of citrate adsorption since coordination of carboxylate groups on a gold surface is governed by relative positions of polarizable oxygen atoms with respect to the bridged sites on the metal surface exhibiting high potential wells, rather than by specific surface chemistry.[8] In addition, it was demonstrated that intermolecular interactions are much stronger than the Au-carboxylate interaction for citrate adsorption on the gold surface. Thus, the geometry-based simulation without energy optimization is feasible to investigate the citrate adsorption on the gold surface.

The simulation results of the citrate adsorption on Au(111) indicate that the terminal carboxylic groups of adjacent adsorbed citrates can be hydrogen-bonded (distance: 7.0 Å) while the other terminal carboxylic groups are hydrogen-bonded with dangling citrate species. Only the central carboxylate groups of citrate molecules, which exhibit the lowest pK_a,[9] seem to be initially coordinated to the AuNP surface. This hydrogen-bonded network produces polymeric citrate chains, which further interact each other through van der Waals attraction between the CH_2 moieties (distance: 5.5 Å). Through the same intermolecular interactions as the AuNP (111) surface, the self-assembled layer of the polymeric citrate chains also are possible on AuNP (110) and (100) surfaces, which are the most populated facets in the truncated octahedron[10] of large sized AuNPs (> 10 nm in diameter) along with the (111) surface. Atomic force microscopy (AFM) force measurements for citrate layers between a AuNP and a planar gold substrate suggested a

hydrogen-bonded network consisting of dihydrogen citrate molecules ($H_2Citrate^-$).[11] The surface coverage of adsorbed citrate species without the dangling citrate molecules is 1.86×10^{-10}mol/cm^2. The conformation of citrate molecules adsorbed on AuNPs is well-organized, rather than forming an amorphous structure.[12] The citrate configuration shows a bi-layer formation, as opposed to the hypothesized multilayer,[13] and the estimated layer thickness is 6.0 - 6.5 Å.

Attention has been given to the metal core size and the role of citrate as reducing agent in syntheses and studies of citrate-stabilized AuNPs whereas the size and shape of formed particles have not been correlated with the entire citrate layer. The self-assembled layer of citrate adsorbed on AuNP surfaces is not only the first example of a proposed conformation of the organic layer on citrate-stabilized AuNPs at a molecular level, but also a possible breakthrough for investigating the stabilizing role of the citrate layer in NP-based studies including particle growth mechanisms. For example, the configuration of the polymeric citrate network on (111), (110), and (100) surfaces of AuNPs can be incorporated to understand NP growth mechanisms and the formation of isotropic shapes. The distance of the hydrogen bond between two adjacent adsorbed citrates is close to the ideal value on the (111) and (100) surfaces, but not on the (110) surface. The size match between the polymeric citrate chain and the metal surface may be a key factor for NP-stabilizing role of citrate molecules and related to development of particular NP shapes. It also was found that the molecular dimension of the polymeric citrate chains are commensurate on surfaces of silver, platinum, and palladium NPs that are stabilized by citrate molecules, but not for copper NPs. The networked citrate layer cannot shrink enough to be commensurate on the surface of copper nanoparticles, which is consistent with the instability[14] of copper NPs prepared using the citrate reduction method. The

approach to characterize the citrate layer on AuNPs in this research can be employed for other metal NPs, and this experimental evidence would suggest the conformation and stabilizing role of citrate molecules adsorbed on those metal NPs.

In addition, the chirality of the citrate layer on AuNPs may impact NP-based research. Only the R enantiomer of the adsorbed citrate species was observed on a Au(111) surface in this study. Each NP facet of the AuNPs is stabilized with only one type of citrate enantiomer. Experimental evidence of a chiral citrate layer on AuNPs may be provided using circular dichroism (CD) spectroscopy. In situ CD evaluation may be required to measure small-sized AuNPs at the nucleation period during the NP formation.[15] However, the citrate reduction method may intrinsically lead to a mixture of R- and S-enantiomeric citrate-AuNPs, and the possibility of a mixture of R- and S-citrate layers on individual AuNPs cannot be excluded. Computational simulation for small gold clusters[16] might predict the chiral adsorption of citrate molecules if the chirality of the organic layer was a consequence of the metal core.

More investigation is needed to probe the orientation of the central carboxylic acid group of the dangling citrate molecules. This would also provide the orientation of the hydroxyl group at the center position of citrate molecules. Interestingly, the achiral dangling citrate species interacts with chiral adsorbed species in the entire citrate layer. In addition, the orientation of the central carboxylic acid groups may play a critical role in interparticle interactions of citrate-AuNPs, because the central COOH groups are located at the very outer layer of the AuNPs. The optimized orientation for hydrogen bonding between the central COOH groups would make it possible for them to cooperatively interact on the surfaces of the AuNPs. However, to probe the orientation of the central COOH groups would be very challenging due to lack of known interactions with surface

ions such as Cl^- and/or Na^+. The central COOH groups of dangling citrate may be randomly oriented.

It should be noted, however, that IR data in this study provided direct evidence only for the citrate coordination, the presence of dangling citrate species and hydrogen-bonded carboxylic acid groups. Without the STM image of citrate organization on a planar Au(111) and the TEM image of the citrate layers on AuNPs, it would not possible to propose the conformation of the citrate layer. In addition, citrate adsorption on Au(100) and (110) surfaces needs to be demonstrated experimentally, possibly by STM experiments. Specific unit cell parameters of the citrate self-assembly for those surfaces were predicted in this study, which are different from that on a (111) surface. Nevertheless, this study suggested the driving forces of the intermolecular interactions are much stronger than the metal-carboxylate interaction, governing the citrate adsorption on AuNP surfaces.

Investigation of citrate desorption from AuNP surfaces demonstrated the importance of studying the organic/metal interface for metal NPs. While complete desorption of surface citrates from gold surfaces by addition of thiol molecules has been assumed, experimental evidence of desorption of citrate molecules adsorbed directly on the metal surfaces has not been reported. In most studies, a decrease in the negative-charge of citrate-stabilized AuNPs and subsequent NP aggregation in solution have been used as evidence for desorption of negatively-charged citrate molecules.[17] This assumption is based on the formation of strong Au-S bond (~40 kcal/mol)[18] compared to the relatively weak Au-carboxylate interaction (~2 kcal/mol).[19] However, intermolecular interactions between surface citrate molecules, the possibility of thiol-coadsorption, and the contribution of surface chloride ions to the negative-charge of the AuNPs are generally

neglected. From the study of the citrate conformation on AuNPs, it was demonstrated that the intermolecular interactions between citrate molecules, rather than the metal-molecule interaction, govern the adsorption of citrate on the metal surface. Also, the presence of dangling citrate species interacting with adsorbed species was demonstrated. Neither the detection of certain amounts of desorbed citrates nor the observation of NP aggregation can be conclusive evidence for citrate desorption from AuNPs. Quantitative analyses based on direct spectroscopic signals from adsorbed citrate need to be provided in the citrate-to-thiol exchange reaction.

The adsorbed citrate has characteristic IR and XPS signals due to coordination of carboxylate groups to Au surfaces. The asymmetric stretching vibration of η^1-COO^- coordination at 1611 cm^{-1} and the C 1s binding energy of Au-COO^- coordination at ~288 eV were used as spectroscopic evidence of residual citrate molecules. Other spectroscopic signals include enhanced IR peaks of citrate that appeared under high pH conditions (pH > 11), probably by coordination of all carboxylate groups to the AuNP surface, as well as hydrogen-bonded carboxylic acid groups appeared at ~1700 and ~1734 cm^{-1} as an additional indication. Those three types of characteristic spectral features of adsorbed citrate species and the IR peak of the COOH hydrogen bonds indicative of citrate interactions on AuNPs still were observed after addition of excess amounts of ω-terminated alkanethiols and arylthiols to the AuNP solution. The presence of residual citrate molecules is consistent regardless of the type and functionality of added thiol molecules as well as degree of NP aggregation in solution, elevated temperature, and prolonged reaction time (40 ^oC/3 days). Instead, complete desorption of surface chloride ions was observed due to disappearance of Cl 2s and 2p peaks in XPS spectra after addition of ethanolic alkanethiol solution. This result indicates that the

surface charge drop of citrate-AuNPs, which induces NP aggregation, originates in part from desorption of chloride ions, rather than citrate molecules. In addition, observations from the behavior of NP aggregation in ethanol itself and other thiol solutions indicate that van der Waals attraction between the coadsorbed thiol layers significantly affects the NP aggregation. It was demonstrated that citrate molecules cannot be desorbed completely from AuNPs after addition of thiol.

Semi-quantitative analyses of thiol adsorption on citrate-AuNPs were performed by adsorption isotherm studies using intensities of IR peaks from various types of thiol molecules. The intensities of the IR peaks from thiols were saturated prior to a monolayer coverage on the AuNP surface. This indicates the presence of pre-adsorbed organic species, i.e., citrate. When alkanethiol was added to the AuNPs, a cooperative feature of the development of C-H stretching vibrations was observed. The characteristic C-H stretching vibrations at 2917/2850 cm^{-1} are indicative of the ordering between the hydrocarbon chains. This unique adsorption behavior of alkanethiols was correlated with phase-separated citrate/thiol layers in nanometer-scale domains. A certain number of alkanethiol molecules is required for the thiol organization and chemisorption in the domain on the AuNP surface.

XPS analysis was used for quantitative investigation of surface coverage by citrate and thiol molecules. The ratio of the peak areas from S_{2p}/Au_{4f} was measured after the varied amounts of mercaptopyridine were added to citrate-AuNPs. The plot of S_{2p}/Au_{4f} as a function of added amounts of the thiol shows saturation of thiol adsorption prior to 5/6-monolayer coverage. Furthermore, a new XPS analysis method was developed to determine the amount ratio between surface citrates and adsorbed alkanethiols. Since XPS signals from surface citrate are very weak, experimental determination of the

surface coverage from a single type of thiol-functionalized AuNPs possesses significant experimental error. This issue was circumvented by use of varied hydrocarbon lengths of methyl-terminated alkanethiols that were adsorbed on each sample of citrate-AuNPs. The signal response from alkanethiolate under the incremented hydrocarbon lengths represents the ratio of surface coverage between citrate and alkanethiol molecules. The area ratio between the C 1s of Au-COO at 288 eV and the C 1s of the hydrocarbon at 284.8 eV ($C1s_{thiol}/C1s_{citrate}$) was plotted as a function of the hydrocarbon length. The slope of the plot was found to be 1.7, which is the ratio of the surface coverage between citrate and alkanethiol on AuNP surfaces (citrate:alkanethiol = 1:1.7). The resulting density of alkanethiol on the AuNP surface is 1.9 thiols/nm^2, and this value is in good agreement with the thiol density on citrate-AuNPs determined by the fluorescamine-based assay (1.63 thiols/nm^2).[20] The surface coverage of alkanethiol on the AuNP surface found in this study is much less than that of the close-packed SAM of alkanethiols (4.5 alkanethiols/nm^2) [21] on a planar gold surface (~42%). Interestingly, the measured alkanethiol density on AuNPs is consistent with thiol coadsorption model on gold surfaces in this study without loss of adsorbed citrate molecules. Only half of dangling citrate species seems to be detached from AuNP surfaces. Therefore, it can be concluded that most of surface citrate molecules are not desorbed from AuNPs after addition of thiols.

The main origin of the stable adsorption of surface citrate is the intermolecular interaction of hydrogen bonds between carboxylic acid groups. The bond energy per a pair of the carboxylic acid dimers is ~14 kcal/mol.[22] This is much stronger than the metal-molecule interaction (~2 kcal/mol for Au-COO). There is also van der Waals attraction between the CH_2 fragments (1.4 - 1.8 kcal/mol for $CH_2 \cdots CH_2$).[23] Overall

enthalpy and additional entropy gain from the robust network of the citrate layer is expected to overcome the strength of the Au-S bond (~40 kcal/mol). The steric hindrance from the network of the citrate layer and the chelating effect from bidendate citrate coordination are of secondary importance. The strong adsorption of the surface citrate can also have a negative effect on the chemisorption state of adsorbed thiols. Thiol molecules should be adsorbed initially on void areas in between the citrate network on the surfaces of AuNPs where the surface coverage by adsorbed citrate is only ~30%, but the intermolecular interaction between the restricted numbers of thiol molecule (3 – 8 molecules) may not be favorable enough for the initial physisorbed state to transform to the stable chemisorbed state. The environment of the formation of thiol-layer on citrate-AuNPs is quite different from a bare gold surface.

The IR data indicated the formation of the phase-separated adsorption of alkanethiolates on the surface of AuNPs. This unique adsorption of alkanethiolates was interpreted using the model of the self-assembled layer of citrate adsorbed on the Au(111) surface. STM investigation on a planar gold surface would provide supporting evidence of the coadsorption of alkanethiolates on gold surfaces where citrate molecules are pre-adsorbed. Expected results from the STM study are the image of phase-separated domains at a nanometer scale, the number of alkanethiolate molecules at each domain, and the population of dangling citrate molecules remained on the surface after addition of alkanethiols. These STM results could be compared with the model of the alkanethiolate/citrate coadsorption and also verify that citrate molecules on the gold surface are not displaced by thiol molecules.

The coadsorption of thiol molecules on citrate-AuNPs was demonstrated using IR and XPS analyses in this dissertation research. The similar experiments done for the AuNPs

can be performed for other citrate-stabilized metal NPs such as silver, platinum, and palladium NPs. Since the conformation of the citrate layer seems to be identical for all of the citrate-stabilized metal NPs, similar experimental results are expected for those NPs. Citrate molecules may not be displaced by thiol molecules, and coadsorption of thiolates on citrate-stabilized metal NPs would be likely dominant after addition of thiol molecules to the NP solution. However, the distance of the COOH hydrogen bond between two adjacent adsorbed citrates deviates from the ideal value for the surfaces of other metal NPs, which may reduce the strength of the hydrogen bonds. Under this condition, the entire citrate layer might be displaced by thiol molecules. The palladium NPs could be influenced by this effect since the atomic spacing of a Pd(111) surface is relatively smaller than the distance between the adjacent COOH groups. The extent of a displacement of citrate molecules on those metal NPs also can support the proposed conformation of the citrate layer on citrate-stabilized metal NPs.

The strong resistance of surface citrate on the AuNP surface under the addition of thiols was demonstrated. This suggests a challenge for the thiol-based organic layer on the surface of metal NPs. The assumption of the spontaneous desorption of coordinated carboxylate groups is spread across the surface and nano-science, and there have been abundant examples reported in literature based on the complete desorption of citrate molecules under the thiol treatment. The effects of the residual citrates can significantly modify or improve interpretations of experimental data when citrate-AuNPs are used as materials in the course of studies. The carboxylic and hydroxyl groups of residual citrate can affect pH in the NP-containing media and coupling reactions carried out on the outer organic layer on NPs because the functional groups, surface charge of NPs, and density of the organic layer on NPs should be considered. The residual citrate on AuNPs may

significantly influence the inter- or intracellular activity of the NPs. The other possible impact on surface science is that carboxylate-based organic layers may be superior to the popular thiol-based layer. One of the main reasons for the popularity of thiol molecules is the spontaneous adsorption on metal surfaces. However, the thiol-layer is destroyed in a short period of time (< 6 months) due to the breakage of the metal-thiolate bond via oxidation of thiol to sulfate. Note that since 1990's extensive research related to thiol molecules have been done due to the consideration of the robust thiol-layer formation on meal surfaces. Manipulation of intermolecular interactions between adsorbed molecules can be more important than the strength of metal-organic bonds. This study suggests the functionalization of the carboxylate-based layer on metal surfaces as an alternative approach for surface modification due to the cost-effective and oxidation-free functionality of carboxylate molecules.

A regional functionalization for metal NPs is a challenge for use of the resultant asymmetric particles (Janus particles) in NP assembly. The asymmetric functionalization of AuNPs has attracted a particular interest due to a localized surface plasmon (LSPR). Interparticle coupling of the localized surface plasmon resonance provides interesting optical phenomena from NP assemblies rather than isolated single NPs. It is well-known that the junction of a NP assembly is a hot-spot where a large enhancement of electromagnetic field (EM) occurs. While the asymmetrically-functionalized metal NPs have been used for NP assembly, the orientation of the individual asymmetric-NP in an assembly has not been investigated.[24] Similar NP assemblies can produce different optical responses due to possibly different orientations of asymmetric NPs. For example, surface enhanced Raman scattering (SERS) enhancement is highly dependent on the location of the adsorbed Raman probes with respect to the hot spot. The placement of

Raman probes at hot spots gives the largest SERS enhancement. Determination of the orientation of asymmetric NPs leads to accurate analyses for optical studies related to NP assembly.

The orientation of asymmetric functionalized AuNPs (diameter of individual NPs: ~ 39 nm ± 20%) and the location of Raman probes (4-nitrobenzenethol) were correlated with SERS intensity. The main goal of this study was to place the Raman probes exclusively at the junctions of AuNP dimers fabricated through the asymmetric functionalization approach,[24] while achieving higher yields of the dimer formation. Positively-charged HS-C_{11}-NH_3^+ was used to functionalize first the bulk of the AuNP surface (~90%) except the spatially localized region (~10%) where both hydroxyl-terminated alkanethiol linkers and the Raman probes were adsorbed later on AuNPs. The linkers induce the hydrogen bonds between the hydroxyl groups, leading to the attraction of the asymmetric NPs into formation of dimers. During this dimer formation, added Raman probe thiols are also adsorbed specifically in the spatially localized region. Samples of AuNP dimers were prepared on common glass slides and used to obtain SEM images of NP morphologies and SERS intensities. The resultant yield of the dimer formation is 12 – 31 % depending on the amount ratio between the linker and the Raman probe, and dimers are the most populated assemblies (≥ 70%) through all samples.

A linear relationship between the dimer yield and SERS intensity was found. This empirical result indicates the SERS intensity is linearly dependent on the population of hot-spots, which demonstrated the SERS enhancement originates from the hot-spots of the AuNP dimers. The dependence of standard deviations on the absolute number of dimers also suggests the origin of the SERS enhancement from dimers. The standard deviation of SERS measurements is larger than that of SEM measurements due to the

small beam size of the laser on a Raman instrument. The SERS intensities were further compared with AuNP-dimer samples that were prepared with a change of the linker length as well as removal of the linker. The resulting dependence of SERS on the nature of linker is consistent with the hypothesis that the linkers induce the formation of AuNPs through the spatially localized regions. Linkers create the aligned configuration of the asymmetric NPs with the adsorbed Raman probes located at the junction of dimers. Without linker, asymmetric NPs are randomly oriented in formed dimers. As a result, the orientation of the asymmetric AuNPs and the location of the Raman probe were characterized with respect to the junction of the AuNP dimer using SERS.

Since the SERS enhancement is a function of the interparticle spacing, and we characterized the interface of the junction of the AuNP dimer. The gap spacing determined from our TEM analysis is 3.0 ± 0.1 nm, and this value is in excellent agreement with our calculation for hydrogen-bonded linkers, HS-C_{11}-OH (3.3 nm). The determined SERS enhancement factor for the AuNP dimer is 10^6, based on the monolayer coverage by the Raman probe (NBT) on the spatially localized region (~2000 molecules per hot spot) and the interparticle spacing of 3.3 nm. This is smaller by two orders of magnitude for single-molecule detection.[25] The well-defined interface on AuNPs suggests the asymmetric functionalization approach can be used as a platform for SM-SERS studies.

It should be mentioned that the SERS analysis relied on AuNP dimers with a narrow range of yield (within 19%). A higher yield of the dimer formation than 31 % could not be achieved with the method of dimer preparation in this study. Another approach for AuNP dimer formation, such as the covalent-bond linkage rather than the hydrogen bond, can produce higher yields, but the experimental condition of the coupling reaction may

reduce the adsorption of adjacent Raman probe molecules. In addition, the linearity between SERS and hot-spot population deviates when the amounts of Raman probes are corrected based on concentrations in solution. However, solution concentrations may not reflect those on the NP surface, and the surface coverage by the Raman probe may be constant through samples. Also, the orientation change of the adsorbed Raman probes may occur and affect the SERS intensities.

Achievement of high yields of the dimer formation would provide high quality data utilizing the asymmetric AuNPs. Manipulation of the molecular interaction between linker molecules, which bring two asymmetric NPs together for dimer formation, is the key factor to obtain high dimer yields. Thiolated DNA molecules are good candidates for linkers, because the cooperative hydrogen bonds of DNA molecules are very strong. The interparticle spacing of dimers can be controlled by the length of DNA. The other approach to obtain more dimers is to purify dimers from single NPs and other types of NP assembly through a separation process using microfluidic devices. The microfluidic separation approach mainly relies on the sizes of NPs and the size-dependent surface charge. However, the nonuniform sizes of citrate-AuNPs used in the asymmetric functionalization approach would hamper the separation of dimers from single NPs since the size of dimers can be comparable to large single NPs. Using NPs with uniform sizes may be required in the microfluidic separation. Other NP-synthesis methods and other kinds/shapes of metal NPs would be helpful not only to obtain mono-dispersed NPs but alto to extend the asymmetric functionalization approach into formations of bimetallic hybrid dimers such as Au-Ag dimers.

One of the future research directions is a polarization-dependent study at the hot-spot interface. Single-particle investigation would be a direct method for it, but ensemble

measurements in regular arrays of organized dimers would be more effective since signals from a single dimer are very weak. A solution of NP dimers could be spread on a nanopatterned template where NP dimers can be placed in a regular direction, which generates arrays of regularly oriented dimers.[26] The polarization-dependent study would lead to the correlation of hot-spot-generating SERS with possible changes of molecular orientations at the metal surface. Those experimental results could be correlated with well-defined interfacial factors such as molecular orientations and positions in the hot spot as well as interparticle spacing at a single molecular level, which can be controlled by the asymmetric functionalization approach.

Lastly, the syntheses of smaller sizes of Au- and AgNPs (< 5nm in diameter) rather than the common citrate-stabilized Au- and AgNPs were achieved in water. The synthesis of metal NPs in aqueous media is important due to absence of organic solvent and resultant accessibility for biological applications. In this study, poly(allylamine) both reduces gold ions for NP formation and stabilizes the formed AuNPs with particle dispersion in the polymer. The assemblies of the polymer-AuNPs can be controlled by changing the solution pH.[27] This synthetic approach was also applied to the synthesis of AgNPs. The amine-to-thiol ligand exchange on the metal NPs was demonstrated by IR and TEM analyses. IR data indicate the adsorption of thiols on the metal NPs. The TEM analysis for the ligand-exchange relied on the change of the particle sizes after addition of thiols to the polymer-metal NPs, but this is indirect evidence. For a quantitative approach to provide convincing evidence of the complete amine-to-thiol exchange, future studies should employ IR spectroscopy to verify the absence of residual polymers on the surfaces of metal NPs, and XPS may provide conclusive information for the extent of the ligand exchange.

This dissertation research is an example of importance of detailed surface characterization for metal NPs. Molecular adsorption and desorption at the metal/organic interface have been mainly investigated for citrate-stabilized Au- and AgNPs as well as poly(allylamine)-stabilized Au- and AgNPs. This study focuses on the conformation of surface citrate, the interaction of surface citrate with incoming thiol molecules, the orientation of asymmetric AuNPs in dimers, and the syntheses and interactions of poly(allylamine)-functionalized Au- and AgNPs in water. The quantitative IR and XPS methods made it possible to study the molecular adsorption on metal NPs, which revealed the neglected aspects of nanoparticle-based research including understanding of the citrate layer and the significant effect of intermolecular interactions on sorption behaviors of surface citrate. The approaches and findings from the study of citrate-stabilized AuNPs can apply to other studies relating to the structure and adsorption of hydroxycarboxylic acids on metal surfaces, including amino acids. The correlation analysis in SERS signals from AuNP dimers led to the determination of orientations of asymmetric NPs in dimers with respect to the location of the Raman probe. The interfacial characterization at the junction of the AuNP dimer established the well-defined surface characteristic of the asymmetric NPs, which expands use of the asymmetric NPs toward various model systems of plasmonic nanomaterials. This dissertation research eliminated the fundamental assumptions made for citrate-stabilized Au- and AgNPs relating to the molecular adsorption of citrate and thiol molecules by detailed characterizations at the molecule/metal interface at a molecular level.

6.2 References

(1) As a rare example: Jackson, A. M.; Myerson, J. W.; Stellacci, F. *Nat. Mater.* **2004**, *3*, 330-336.

(2) Jadzinsky, P. D.; Calero, G.; Ackerson, C. J.; Bushnell, D. A.; Kornberg, R. D. *Science* **2007**, *318*, 430-433.

(3) Munro, C. H.; Smith, W. E.; Garner, M.; Clarkson, J.; White, P. C. *Langmuir* **1995**, *11*, 3712-3720.

(4) Zhang, Q.; Li, N.; Goebl, J.; Lu, Z.; Yin, Y. *J. Am. Chem. Soc.* **2011**, *133*, 18931-18939.

(5) Nichols, R. J.; Burgess, I.; Young, K. L.; Zamlynny, V.; Lipkowski, J. *J Electroanal. Chem.* **2004**, *563*, 33-39.

(6) Lee, Z.; Jeon, K.-J.; Dato, A.; Erni, R.; Richardson, T. J.; Frenklach, M.; Radmilovic, V. *Nano Lett.* **2009**, *9*, 3365-3369.

(7) Lin, Y.; Pan, G.-B.; Su, G.-J.; Fang, X.-H.; Wan, L.-J.; Bai, C.-L. *Langmuir* **2003**, *19*, 10000-10003.

(8) Feng, J.; Pandey, R. B.; Berry, R. J.; Farmer, B. L.; Naik, R. R.; Heinz, H. *Soft Matter* **2011**, *7*, 2113-2120.

(9) Pearce, K. N.; Creamer, L. K. *Aust. J. Chem.* **1975**, *28*, 2409-2415.

(10) (a) Barnard, A. S.; Young, N. P.; Kirkland, A. I.; van Huis, M. A.; Xu, H. *ACS Nano* **2009**, *3*, 1431-1436. (b) Wang, B.; Liu, M.; Wang, Y.; Chen, X. *J. Phys. Chem. C* **2011**, *115*, 11374-11381.

(11) Wall, J. F.; Grieser, F.; Zukoski, C. F. *J. Chem. Soc., Faraday Trans.* **1997**, *93*, 4017-4020.

(12) Glusker, J. P. *Acc. Chem. Res.* **1980**, *13*, 345-352.

(13) Dahl, J. A.; Maddux, B. L. S.; Hutchison, J. E. *Chem. Rev.* **2007**, *107*, 2228-2269.

(14) Abdulla-Al-Mamun, Md.; Kusumoto, Y.; Muruganandham, M. *Mater. Lett.* **2009**, *63*, 2007-2009.

(15) Polte, J.; Ahner, T. T.; Delissen, F.; Sokolov, S.; Emmerling, F.; Thünemann, A. F.; Kraehnert, R. *J. Am. Chem. Soc.* **2010**, *132*, 1296-1301.

(16) Hull, J. M.; Provorse, M. R.; Aikens, C. M. *J. Phys. Chem. A* **2012**, *116*, 5445-5452.

(17) Weisbecker, C. S.; Merritt, M. V.; Whitesides, G. M. *Langmuir* **1996**, *12*, 3763-3772.

(18) Nuzzo, R. G.; Zegarski, B. R.; Dubois, L. H. *J. Am. Chem. Soc.* **1987**, *109*, 733-740.

(19) Chen, F.; Li, X.; Hihath, J.; Huang, Z.; Tao, N. *J. Am. Chem. Soc.* **2006**, *128*, 15874-15881.

(20) Xia, X.; Yang, M.; Wang, Y.; Zheng, Y.; Li, Q.; Chen, J.; Xia, Y. *ACS Nano* **2012**, *6*, 512-522.

(21) Love, J. C.; Estroff, L. A.; Kriebel, J. K.; Nuzzo, R. G.; Whitesides, G. M. *Chem. Rev.* **2005**, *105*, 1103-1169.

(22) Jeffrey, G. A. *An Introduction to Hydrogen Bonding*; Oxford University Press: New York, 1997; p 56.

(23) Dubios, L. H.; Nuzzo, R. G. *Annu. Rev. Phys. Chem.* **1992**, *43*, 437-463.

(24) (a) Sardar, R.; Heap, T. B.; Shumaker-Parry, J. S. *J. Am. Chem. Soc.* **2007**, *129*, 5356-5357. (b) Sardar, R.; Shumaker-Parry, J. S. *Nano Lett.* **2008**, *8*, 731-736.

(25) Wustholz, K. L.; Henry, A.-I.; McMahon, J. M.; Freeman, R. G.; Valley, N.; Piotti, M. E.; Natan, M. J.; Schatz, G. C.; Van Duyne, R. P. *J. Am. Chem. Soc.* **2010**, *132*, 10903-10910.

(26) Alexander, K. D.; Hampton, M. J.; Zhang, S.; Dhawan, A.; Xu, H.; Lopez, R. *J. Raman Spectrosc.* **2009**, *40*, 2171-2175.

(27) Sardar, R.; Bjorge, N. S.; Shumaker-Parry, J. S. *Macromolecules* **2008**, *41*, 4347-4352.